UNIVERSITY OF SOUTHAMPTON

FINITE ELEMENT ANALYSIS OF A CEMENTLESS PROXIMAL FEMORAL STEM IN RELATION TO EARLY STEM STABILITY AND INTERFACE BONE STRAIN

Au Seong Wong

Doctor of Philosophy

Faculty of Engineering and Applied Science
Bioengineering Sciences Research Group

June 2003

UNIVERSITY OF SOUTHAMPTON

ABSTRACT

SCHOOL OF ENGINEERING AND APPLIED SCIENCE
BIOENGINEERING SCIENCES GROUP

Doctor of Philosophy

FINITE ELEMENT ANALYSIS OF A CEMENTLESS PROXIMAL FEMORAL STEM IN RELATION TO EARLY STEM STABILITY AND INTERFACE BONE STRAIN

by Au Seong Wong

Modern cementless hip stems rely on the initial stability as measured by micromotion at the bone-implant interface to allow bone ingrowth in order to fix the stem to the supporting bone. Many factors including stem geometry, size, surface texture, bone quality, the presence or absence of interference-fit and loading of stem influence the initial stem stability. Very little has been published on the effect of the degree of interference-fit on the initial stem stability. An excessive interference-fit may not improve the stem stability significantly but may increase the risk of femoral fracture. However, if interference-fit is too low, bone ingrowth may not occur. Published finite element studies of cementless hip stem stability have examined performance based on the model of a single femur, without examining the influence of the variation of bone quality on the initial stem micromotions. This could be an inadequate assessment, as the properties of femur are known to vary between individuals. This thesis examined a few factors influencing the initial stability of the stem, including bone quality, degree of interference-fit and the effect of viscoelastic creep of bone on the degree of interference-fit, to improve the preclinical assessment of cementless hip stem.

The adequacy of assessing stems stability using only one femoral bone property was tested by varying the bone properties systematically and examining the resultant stem stability and interface strain. Unlike previous published studies which looked at the micromotion values only, the interface strains were also examined in this thesis, because recent studies suggest that interface strain is a predictor of implant migration. Stem micromotion and interface strains were found to increase nonlinearly with the overall stiffness of the femur, which suggest that risk of fixation failure and implant migration increase with decrease of overall bone stiffness. This suggests that more predictive preclinical finite element analyses of new stem designs should be performed with multiple femurs, which span the range of the bone quality likely to be expected *in vivo*.

The effect of varying the degree of interference-fit on stem stability and interface strains was examined. Interference-fit was found to reduce significantly the micromotions of the stem, but with a diminishing reduction of micromotions with further increase in the degree of interference-fit. Strains at the interface bone and surface of the femur increase rapidly with increasing interference-fit, which increase the interface bone damage and risk of femoral fracture with decreasing benefit. The effect of bone creep on the residual stresses of bone induced by the interference-fit was also examined. The results suggest that it could be pointless to increase interference-fit beyond certain level as the creep will reduce the residual stresses to value similar to that of a lower degree of interference-fit. Stem stability was found to be influenced by the residual stresses of the femur, in particular the residual stresses generated within the cortex. Poorer quality bone was found to increase stem micromotion due to lower residual stress and poorer resistance to deformation.

This thesis has shown that the inclusion of an interference-fit does significantly improve the initial stability of a hip stem. The contribution of the cortex is significant. In order to achieve the optimal stability, a compromise needs to be achieved between the reduction in micromotion as compared to the bone strain.

To Boon Yee and Gran

For their love and patience

Table of Contents

List of Figures

List of Tables

List of Equations

List of Abbreviations and Symbols

BMU	Bone remodelling unit
BW	Body weight
PCSA	Physiological cross-sectional area
THA	Total hip arthroplasty
PMMA	Polymethymethacrylate
HA	Hydroxyapatite
CT	Computed-Tomography
HU	Hounsfield unit
DEXA	Dual-energy X-ray Absorptiometry
TB	Cancellous bone
CB	Cortical bone
SB	Subchondral bone
A, P	Anterior, posterior
S, I,	Superior, inferior
M, L	Medial, lateral
ρ	Apparent density
E	Young's modulus
G	Shear modulus
σ	Stress
$\sigma_{ultimate}$	Ultimate stress
USS	Ultimate shear stress
σ_y	Yield stress
ε_y	Yield strain
σ/E	Normalized stress
$d\varepsilon/dt$	Creep strain rate
ε_E	Equivalent strain
ε_x, ε_y, ε_z	Normal strain
γ_{xy}, γ_{yz}, γ_{xz}	Shear strain
T_f	Time to failure
$F_{residual}$	Maximum absolute residual force
$F_{reaction}$	Maximum absolute reaction force
Tol	Convergence tolerance
T	Temperature
T_{melt}	Melting temperature or denaturalisation temperature

Acknowledgement

It has been an absolutely new and rewarding experience doing a Phd. with all the up and down moments. During the most difficult periods, supports from my family and friends have been invaluable to pull me through. To my Mum and Dad, thanks for the loving care throughout my live, and Grannies, my brother and sister for their love. Friends that I have made in Southampton, who have been wonderful.

My special appreciation to my academic supervisor, Dr. Mark Taylor, who has been very supportive and generous with his time and encouragement. His suggestions and inputs into this thesis have been invaluable. Doing a PhD. with Mark was a great experience and his encouragement to his students to attend international conferences widens the outlook of a student beyond the immediate concerns of the PhD. For all these, I am very thankful to him. Beside Mark, the inputs from my co-supervisors Dr Andrew New from University of Southampton, and Dr Allan Ritchie and Dr Graham Isaac from DePuy International (Leeds, UK) are fully appreciated.

The people within the Bioengineering Sciences Group have been friendly and cooperative. Their willingness to share information and knowledge are highly appreciated. This bunch of great people makes the experience within the group easy and fun, and they are definitely the type of folks that I would like to have for my future job. Many thanks to past and present members of the group, Anna, Georges, Antonio, John, Vinu, Tom, Anne, Ching, Racheal, Neil, Johnny, Lucy, Adam, Loujaine, Mamadou, Ji Ye and Martin.

Many thanks to Gwyneth, Sue and others within the School of Engineering Sciences for various contributions during my stay in the University of Southampton.

Last but not least, I would like to acknowledge the generous funding from DePuy International (Leeds, UK) for this project.

Preface

Hip implants are mechanical devices designed to work in the body. Computational modelling of hip implants requires the knowledge of biological and mechanical behaviours of bone, and the loads at the hip joint. In Chapter 1, the biological and mechanical properties of bone are reviewed. The load at the hip joint and muscle forces acting on the femur were reviewed in Chapter 2. Chapter 3 reviews the state of the art of the cementless hip arthroplasty. The clinical performance, factors associated with implant failure and methods of preclinical assessment of cementless hip stems are reviewed. At the end of Chapter 3, the objectives of this thesis are described.

Chapter 4 describs the model of the anatomical model of the implanted proximal femur. The robustness of the model was tested by performing convergence studies for different mesh densities and analysis parameters. Appropriate values were selected to be used in later chapters to ensure accuracy of the results.

Chapter 5 examines the effect of bone quality on the stem micromotions and interface bone strains. In this chapter, the interference-fit at the bone-stem interface was not simulated.

Chapter 6 examines the effect of different degree of interference-fit on the initial stem micromotions and strains of the femur. Bone was assumed to have linear elastic behaviour in Chapter 6. However, higher degree of interference-fit was found to induce high interface strain and plastic deformation of interface bone could occur in reality. As a result, the micromotions could have been underestimated.

In Chapter 7, bone was assumed to have elastic-perfectly plastic behaviour to check if plastic behaviour of bone significantly affects the predicted micromotions and interface bone strains in Chapter 6.

In Chapter 6, bone stresses are assumed to be unchanged by stress relaxation of bone. The residual stresses in the femur could be lower due to stress relaxation of bone. If the residual stresses in the femur is not maintained for a sufficiently long period of time, then the interference-fit will be ineffective. The reduction of residual stresses may also affect the predicted micromotions and stresses of the femur. In Chapter 8, bone creep is simulated to examine the change of residual stresses of the femur induce by interference-fit with time. The effects of the change of residual stresses on micromotions are also examined.

The overall findings of this thesis are discussed in Chapter 9 and the main conclusions are presented. In Chapter 10, recommendations for future improvements are made.

Chapter 1 Bone biology and mechanical properties

1.1 Function of the skeletal system

Bone is a complex organ that performs many functions [Cowin, 2001]. It provides a rigid framework on which muscles, tendons and ligaments can be attached and transmit forces to generate motion. During movement, muscular contraction transmits force from one part of the body to another part of the body through bone. In certain regions of the body, bones join together to perform a protective function such as the rib cage, pelvis and the skull. Within these bony enclosures, our vital organs like brain, heart and lungs are protected from physical force. Bones are a reservoir for bone marrow, which is essential for production of white and red blood cells. Bones are also a reservoir of ions, in particular calcium and contribute to regulation of extracellular fluid composition particularly calcium concentration.

1.2 Anatomy of bone

Bone can be divided into two types of bone [Cowin, 2001] – cortical (compact) bone and cancellous (porous) bone. Generally, cortical bone forms the outer shell of bone. Inside the cortical bone shell are the cancellous bone and bone marrow.

A typical model of a long bone structure is shown in Figure 1.1 [Cowin, 2001]. Cortical bone generally forms the diaphyseal or shaft region of a long bone and acts to transmit load from one joint to another. It provides the bulk of the bone stiffness and strength. The two ends of a long bone are generally broader than the shaft and consist of epiphysis and metaphysis. Just under the articular surface is the epiphysis and is separated by the growth plate from the metaphysis. The inner volume of both epiphysis and metaphysis are made up of cancellous bone and the outer layer of cortical bone covers the cancellous bone. The articular surfaces at both ends of the bone are covered by a layer of cartilage. The periosteum is the membrane that covers the outer surface of the bone and endosteum covers the inner surfaces of the bone. The medullary cavity is the hollow cavity filled with marrow in the diaphyseal region of the femur.

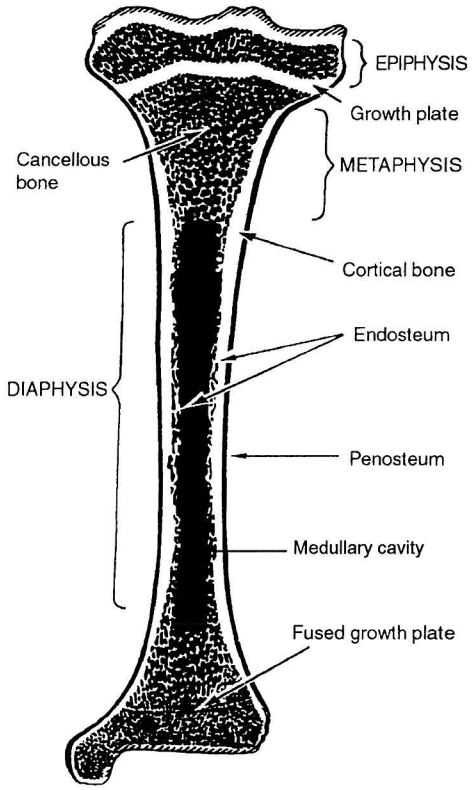

Figure 1.1 Schematic diagram of the human tibia [Cowin, 2001].

The growth plate is the region where new bone is formed during growth in childhood. Fusion of growth plate occurs when growth stops in young adulthood. The periosteum consists of outer layer of fibrous connective tissue and an inner cellular layer of undifferentiated cells. The periosteum can form bone during growth and fracture healing. The endosteum is a membrane of bone surface cells (osteoblasts, osteoclasts and bone lining cells).

1.2.1 Cortical Bone

Cortical bone forms 80% of the human skeletal system [Cowin, 2001]. This is a dense bone with macroscopic channels. Cortical bone performs most of the protective and structural function of the skeletal system. The typical structure of adult human cortical bone is shown in Figure 1.2 [Marieb, 1998]. In adult human bone, cortical bone is in the form of osteonal bone.

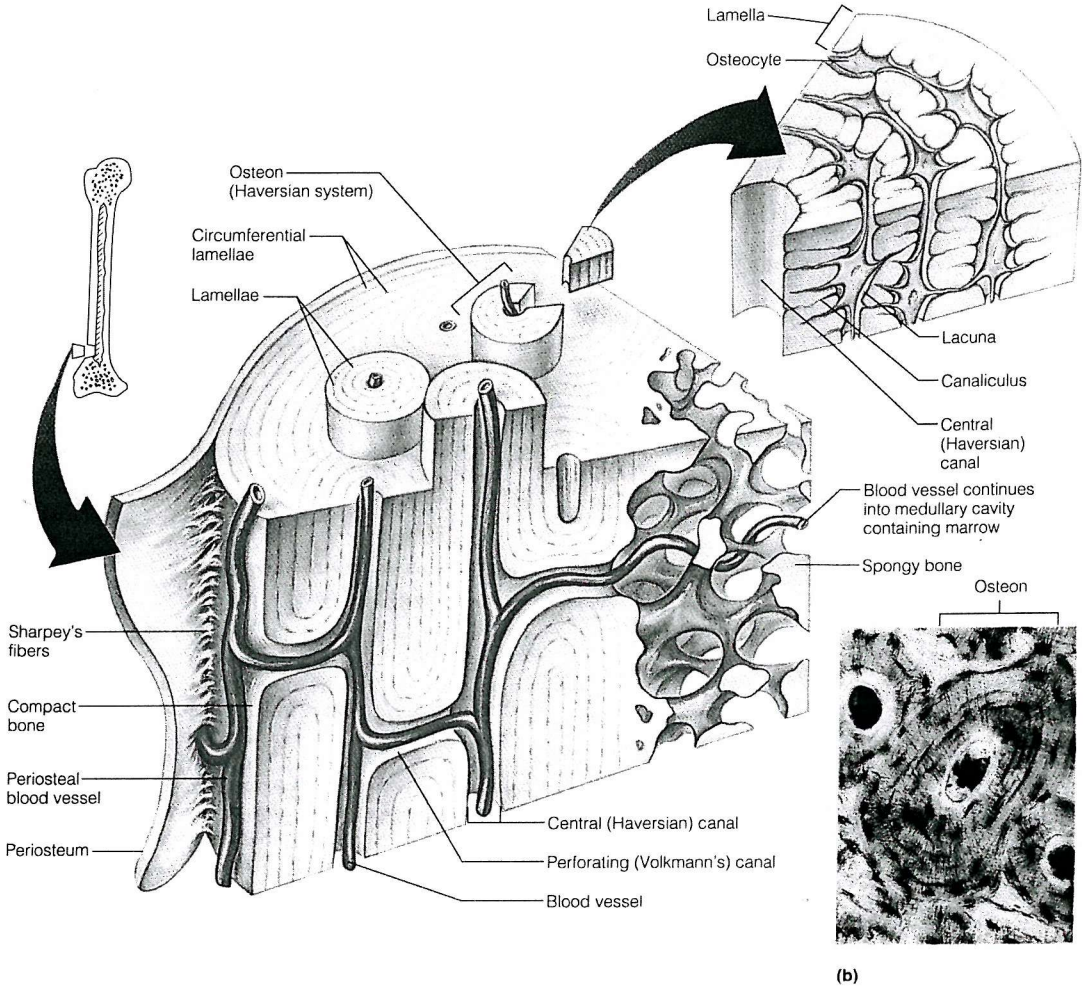

Figure 1.2 (a) Structure of cortical (b) Cross section of cortical bone showing osteon with its lacunae and canaliculi bone [Marieb, 1998].

Osteon, or Haversian system– This is the structural unit of cortical bone. An osteon is made up of concentric lamellae about 200-250 μm in diameter. It forms about two thirds of the cortical bone volume. Inside the concentric lamellae is the central canal through which runs blood vessel, lymphatic, nerves and loose connective tissue. The outer border of osteon is a layer of cement line about 1-2 μm thick, formed from mineralised matrix deficient of collagen fibres. The osteons are also inter-connected by transverse Volksmann canals.

Circumferential lamellae – Several layers of lamellae extending uninterrupted around part or all of the circumference of the inner and outer surfaces of the shaft are known as circumferential lamellae.

Interstitial lamellae – These are former osteons that have been partially resorbed. They are angular fragments that fill the gaps between functional osteons. They formed about one third of the cortical bone volume.

Lacunae – These are cavities between lamellae within an osteon and are normally filled with osteocytes.

Canaliculi – Small canals that connect lacunae together. Canaliculi that open to the extracellular fluid and bone surfaces form a network that allows transport of nutrients and metabolic products of the osteocytes.

Osteocytes – These are the most abundant bone cells in mature bone. They performed the important functions of maintaining bone mineral, detecting microdamage to initiate bone repair and detecting strain distribution to determine if changes to bone structure are necessary for bone to perform effectively.

1.2.2 Cancellous bone

20 % of the human skeleton is made up of cancellous bone [Cowin, 2001]. This is a porous bone that is formed by a lattice of large plates and rods known as trabeculae. The rod trabecular and plate trabecular is shown in Figure 1.3.

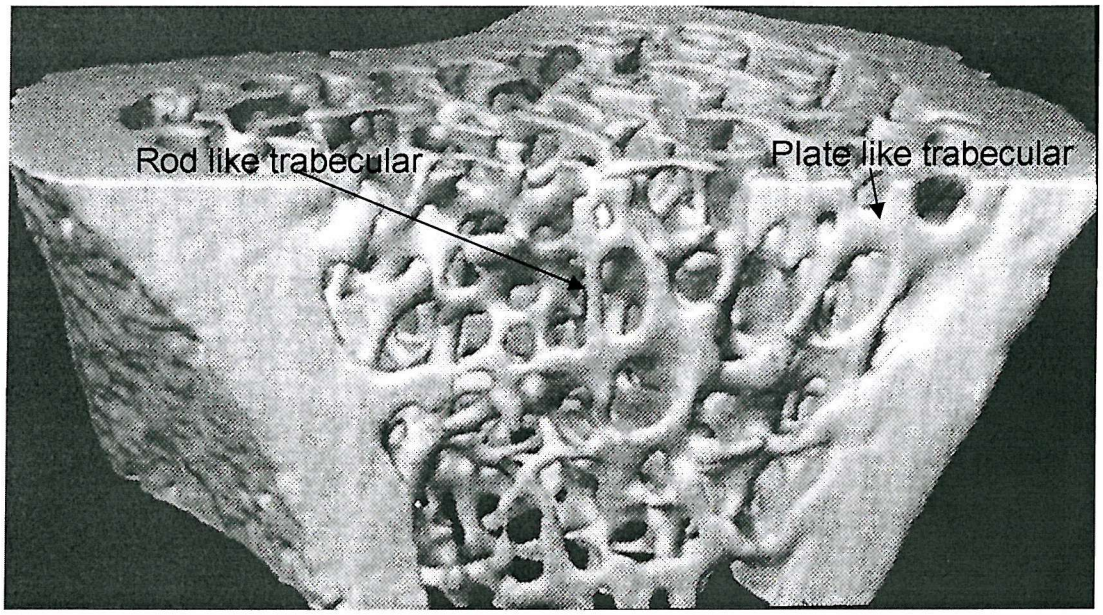

Figure 1.3 Cancellous bone. The rod and plate trabeculae can be clearly identified.

The trabeculae of adult cancellous bone consists of hemiosteon or trabecular packets and interstitial lamellar bone (Figure 1.4) [Cowin, 2001]. Hemiosteons are shaped like crescents. Like cortical bone, mature hemiosteons and interstitial lamellae are formed from lamellar bone, not woven bone. Osteocytes occupy the lacunae and nutrients are carried to the osteocytes through the canaliculi. Bone turnover in cancellous bone is much faster than in cortical bone. The surface area per unit volume of cancellous bone is about eight times that of cortical bone. Cancellous bone is involved in ion regulation of the body [Cowin, 2001].

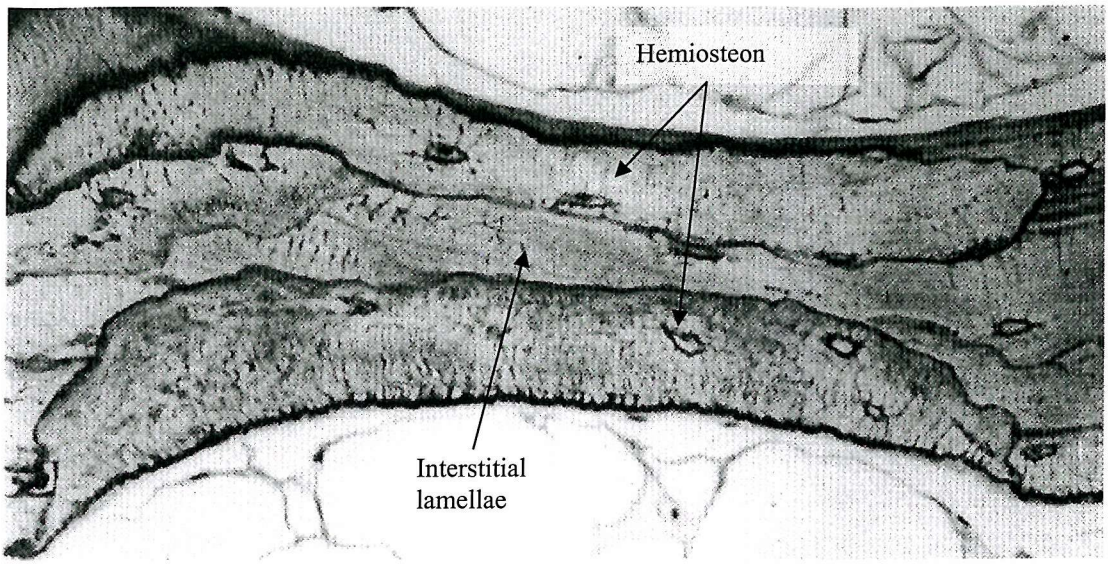

Figure 1.4 A trabecular showing two crescent-liked hemiosteon at the top and bottom. The interstitial lamellae are sandwiched between the two hemiosteon. Cement line separates the hemiosteons and interstitial lamellae. [Cowin, 2001].

1.2.3 Bone composition

Bone is made up of 65% minerals, 35% organic matrix, bone cells and water [Cowin, 2001]. The organic matrix is about 90% collagen fibres and about 10% noncollageneous proteins. The majority of the collagen fibres are type 1 collagen fibre. The function of the noncollageneous proteins is unknown.

The bone mineral which is responsible for the hardness of bone is located within and between the collagen fibres in the form of small crystals. Bone mineral consists of impure hydroxyapatite, $Ca_{10}(PO_4)_6(OH)_2$. The impurities include carbonate, citrate, magnesium, fluoride and strontium incorporated into the crystal lattice or absorbed onto crystal surface.

1.3 Functional adaptation of bone

Bone develops and changes its architecture throughout the human life span. Bone adapts its architecture to its function and this is called functional adaptation [Hernandez *et al.*, 2000; Cowin, 2001]. Functional adaptation of bone is achieved through the process of modelling and remodelling. Adaptation of bone involved the deposition and/or resorption of bone as a result of activities of bone cells called osteoclasts and osteoblasts [Hernandez *et al.*, 2000]. Osteoclasts are responsible for bone resorption while osteoblasts are responsible for bone formation [Cowin, 2001]. Modelling of bone involves only osteoclastic activity when bone is resorbed and osteoblastic activity when bone formation occurs [Hernandez *et al.*, 2000; Cowin, 2001]. Remodelling of bone on the other hand involves the combined activities of osteoclasts and osteoblasts and this is called the bone-remodelling unit (BMU) [Hernandez *et al.*, 2000]. The

BMU resorbs bone and then deposits bone. The surface of trabecular bone and Haversian canals are where bone modelling and remodelling occur [Hernandez *et al.*, 2000].

It is still not well understood what are the conditions that govern the adaptation of bone structure. Mathematical models of bone adaptation normally proposed that bone adapts to a certain equilibrium condition [Cowin and Hegedus, 1976; Beaupre *et al.*, 1990; Weinans *et al.*, 1993; Prendergast and Taylor, 1994]. The difference between the signal and the equilibrium condition drive the adaptation process. Cowin and Hegedus (1976) proposed that the difference between the actual strain and an equilibrium strain level is the adaptation stimulus. A higher value of strain will increase the apparent density of bone while a lower value of strain will reduce the apparent density. Other adaptation models based on other mechanical parameters like strain energy density [Weinans *et al.*, 1993] and equivalent stress [Beaupre *et al.*, 1990] have been proposed. Prendergast *et al.* (1994) moved away from stress/strain parameters and instead proposed that bone adaptation is controlled by a damage parameter. In this model, the damage parameter is the percentage fatigue life of the bone. The bone adapts to try to achieve the equilibrium repair rate that would give bone an equilibrium percentage of fatigue life. However, the continuous loss of bone as human ages does suggest that there may not be an equilibrium condition in bone adaptation.

The adaptation models of Beaupre *et al.* (1990) and Weinans *et al.* (1993) included both external modelling and internal remodelling of bone. External modelling refers to the change of periosteal geometry while internal remodelling refers to the change of porosity of bone (thus density). The models assumed that any adaptation stimulus switch-on both the modelling and remodelling of bone. Weinans *et al.* (1993) also proposed that there is a zone near the equilibrium condition where bone adaptation is dormant, and also the density change of bone as a result of bone adaptation does not continue below or above certain density. However, it has not been clearly define what are the actual conditions in the body that lead to internal remodelling or external modelling. It has been proposed that bone resorption happens below 100 με and modelling occurred above 1000 με and in between is the dormant zone [Frost, 1997]. This contradicted the assumption of adaptation models that any adaptation stimulus causes bone modelling and remodelling regardless of the strain magnitude.

Weinans *et al.* (1993) assumed that the stimulus to bone adaptation comes from a single simulated activity. Beaupre *et al.* (1990) assumed a daily stress stimulus, which is the summation of the adaptation stimulus from different daily activities. The stimulus signals in each bone location is based on the highest load in those particular activities from site specifics equilibrium conditions. Based on the assumption that bone adapts to highest loads. However, it has been reported that similar bone loading history that spans the strain range from 2 με to 2000 με has been measured in different animals [Fritton *et al.*, 2000]. Low strain loading was found to be more

frequent and distributed more evenly while the highest strain only occurs a few times a day and distributed less evenly. In turkey ulnae, events on the order of few microstrains occurred a few thousands times a day while events on the order of 100 με occurred about 100 times a day. This seems to contradict the proposal of Frost (1997), which in this situation should predict lost of bone mass rather than maintenance of bone mass. The respective role of low and high strain event in bone adaptation is therefore still a debate. Therefore, what should constitute a representative daily adaptation stimulus is still not very clear. The direct measurement of strain, strain energy or equivalent strain energy in comparison to an adaptation model has not been achieved. Therefore, it is not possible to say if bone adapts only to the highest load.

The positive effect of bone adaptation is that bone is able to adapt to its function even after formation of bone architecture in childhood [Cowin, 2001]. If the load is high enough to stimulate modelling of bone, modulation of bone architecture and mass can occur. Removal of microdamage, replacement of dead and hypermineralised bone can be achieved through bone remodelling to ensure bone integrity [Carter, 2000; Cowin, 2001]. On the negative side, excessive bone remodelling can perforate and remove trabeculae leading to weaker cancellous bone. Similarly, remodelling can increases cortical bone porosity and decreases cortical width, with the same effect of reducing cortical bone strength.

1.4 Mechanical properties of bone

1.4.1 Elastic modulus, yield and ultimate stress and strain of bone

1.4.1.1 Cortical bone

Cortical bone behaves like a viscoelastic material. Several investigators have noticed that the Young's modulus and ultimate strength of cortical bone have higher values if higher strain rates are applied [Burstein and Frankel, 1968; Currey, 1975; Carter and Hayes, 1976; Carter, 1977]. This means that cortical bone is stiffer and stronger when more vigorous activities are being performed. The ultimate strength and Young's modulus has been reported to be proportional to the strain rate raised to the power of 0.06 [Carter, 1977]. Physiologically, strain rates of $0.002s^{-1}$ and $0.01s^{-1}$ during walking and running have been measured *in vivo* [Lanyon *et al.*, 1975].

The Young's modulus in both compression and tension is similar and have higher values along the principal direction of the osteon than the radial and circumferential directions (since most test were conducted with specimen from the shaft of long bone, with specimens taken from the shaft wall) [Reilly and Burstein, 1975; Ashman *et al.*, 1984; Lotz *et al.*, 1991], as shown in Table 1.1. Reilly and Burstein (1975) reported that the Young's modulus of bovine cortical bone specimen in the radial and circumferential directions of the bone was isotropic, and lower than in the principal osteon direction. Ashman *et al.* (1984) measured the Young's modulus of human

cortical bone using ultrasound and reported values of 12 and 13.4 GPa in the circumferential and radial direction respectively. In the axial direction, the Young's modulus was 20 GPa. The similarity of the radial and circumferential Young's moduli measured by Ashman *et al.* (1984) support the finding that cortical bone is transversely isotropic. The ratio of transverse to axial Young's modulus is about 0.6 to 0.67 at the femoral shaft [Reilly and Burstein, 1975; Ashman *et al.*, 1984]. The anisotropy of cortical bone could also be location dependent. Lotz *et al.* (1991) reported that the diaphyseal femur has a ratio of transverse to principal Young's modulus of 0.472 and this showed greater anisotropy than the metaphyseal cortical bone with ratio of 0.56.

As shown in Table 1.1, the range of cortical bone's apparent Young's modulus in the principal orientation of the osteons in the diaphyseal femur and tibia is between 10 and 20 GPa [Reilly and Burstein, 1975; Carter *et al.*, 1981b; Ashman *et al.*, 1984; Lotz *et al.*, 1991; McCalden *et al.*, 1993; Rho *et al.*, 1993; Courtney *et al.*, 1996; Zioupos and Currey, 1998]. The Young's modulus could also be a function of location. In comparison to the measured values in the diaphyseal femur of 12.5 GPa, a lower value of about 9.6 GPa has been reported for the metaphyseal femur and this could be due to lower density as well as different architecture [Lotz *et al.*, 1991]. In the transverse direction, values between 5 and 13 GPa has been reported [Reilly and Burstein, 1975; Ashman *et al.*, 1984; Lotz *et al.*, 1991].

The ultimate strength of cortical bone is greater in compression than in tension in the principal direction of the osteon as shown in Table 1.1. The shear strength is less than both the compressive and tensile strength. The ratio of compression: tension: shear is about 3:2:1 [Reilly and Burstein, 1975; Cezayirlioglu *et al.*, 1985]. The ratio of ultimate tensile strength in the principal osteon orientation to the transverse orientation is about 2:1 [Reilly and Burstein, 1975; Lotz *et al.*, 1991]. The ultimate compressive strength is about 200 MPa in the principal osteon orientation and 133 MPa in the transverse direction [Reilly and Burstein, 1975; Cezayirlioglu *et al.*, 1985]. The ultimate tensile strength of cortical bone is in the range of 85 and 154 MPa in the principal osteon direction [Reilly and Burstein, 1975; Cezayirlioglu *et al.*, 1985; McCalden *et al.*, 1993] and about 50 MPa in the transverse direction [Reilly and Burstein, 1975; Lotz *et al.*, 1991]. Lotz *et al.* (1991) reported 28% higher ultimate tensile strength in the principal osteon direction in diaphyseal region in comparison to the metaphyseal region. The ultimate tensile strength is similar in the transverse direction in both regions. The observed differences in the principal direction and similarity in the transverse direction could be due to the differences in cortical bone architecture observed in both regions.

The ultimate tensile strain is about 4 times higher in the principal osteon orientation than in the transverse orientation of cortical bone [Reilly and Burstein, 1975], as shown in Table 1.1. The big difference between the principal and transverse direction is caused by stress concentration in the Haversian canal during transverse tensile test. Ultimate tensile strain is therefore anisotropic in cortical bone. The same study reported that the ultimate compressive strain in the principal

orientation is 1.5 times smaller than the transverse orientation, but the measurement is less certain. The stress-strain curve of cortical bone in a uniaxial test is shown in Figure 1.5. The tensile curve will stress harden until fracture occurs and the point of ultimate tensile strength is measured here. The compression curve will reach the highest stress and the curve will continue on horizontal deflection due to compaction of the fracture pieces. Reilly and Burstein (1975) measured the ultimate compressive strain at the point of highest stress. However, Reilly and Burstein (1975) suggested that impaction of fragments in compressive test made the measurement of compressive failure strain inaccurate and therefore the big differences between the transverse and principal tensile ultimate strain is not shown in the compression test. Cezayirlioglu *et al.* (1985) reported that the compressive and tensile ultimate strain in the principal direction is similar. The ultimate tensile strain is similar to Reilly and Burstein (1975)'s, but the ultimate compressive strain is higher. Yield strain from tensile test is generally smaller than 0.01 [Carter *et al.*, 1980; Courtney *et al.*, 1996] and this is much smaller than ultimate tensile strain of about 0.03 [Reilly and Burstein, 1975; Cezayirlioglu *et al.*, 1985].

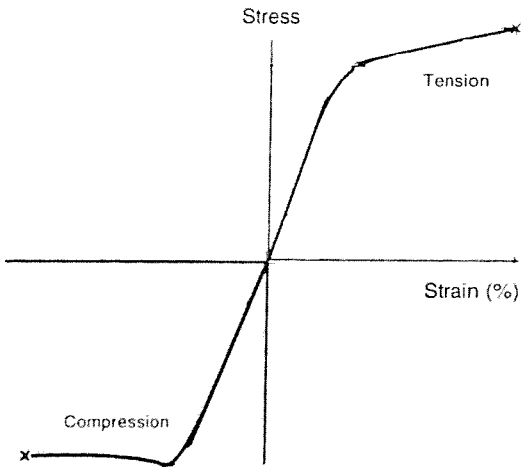

Figure 1.5 Typical linear elastic stress-strain behaviour of cortical bone. Bottom curve is the compressive behaviour of bone and top curve is the tensile behaviour of bone under static loading. [Reilly and Burstein, 1975].

Comparison between different values reported in the literature is quite difficult due to different test methods and procedures. For instance, Lotz *et al.* (1991) measured the properties of bone using 3 point bending test and reported 26% lower values for the Young's modulus of the diaphyseal femur in comparison to Reilly and Burstein (1975)'s value. In order to calculate the Young's modulus from 3 point bending test, Lotz *et al.* (1991) assumed the value of the poisson's ratio and measured the cross-sectional moment of inertia of the test specimen. Since the test specimens are thin (0.18-0.4 mm thickness), the Haversian canal can introduce up to 50% error and affects the calculated Young's modulus. Various studies have also used different strain rates during loading. For example, McCalden *et al.* (1993) used a loading rate of 0.03 εs^{-1} and Courtney *et al.* (1996) used a loading rate of 0.001 εs^{-1}. According to Carter (1977)'s relationship that

Young's modulus is proportional to strain rate raised to the power of 0.06, the differences in Young's modulus due to the different loading strain rate could be about 22%.

Author	Location and method of measurement	Modulus (Gpa) Mean ± SD Or Range	Ultimate compressive strength (Mpa) Mean ± SD Or Range	Ultimate tensile strength (Mpa) Mean ± SD Or Range	Ultimate compressive strain Mean ± SD Or Range	Ultimate tensile strain (Mpa) Mean ± SD Or Range	Other reported data
Reilly and Burstein, 1975	Femur Uniaxial test	$E_{11} = 17$ $E_{22} = 11.5$ $G = 3.28$	$\sigma_{11} = 193$ $\sigma_{22} = 133$	$\sigma_{11} = 133$ $\sigma_{22} = 51$	$\varepsilon_{u11} = 0.018$ $\varepsilon_{u22} = 0.028^{*}$	$\varepsilon_{u11} = 0.031 \pm 0.0072$ $\varepsilon_{u22} = 0.007 \pm 0.0014$	USS = 68 Mpa
Carter *et al.*, 1981b	Femur Uniaxial test	$E_{11} = 17.5 \pm 1.9$		$\sigma_{11} = 140 \pm 12$			$\sigma_{yt11} = 129 \pm 11$ MPa $\varepsilon_{yt11} = 0.0068 \pm 0.0004$
Ashman *et al.*, 1984	Femur Ultrasound	$E_{11} = 20$ $E_{22} = 13.4$ $E_{33} = 12$		-			
Cezayirlioglu *et al.*, 1985	Tibia (VII decade) Uniaxial test	-	192±6.9	154±8.7	$\varepsilon_{u11} = 0.027 \pm 0.0059$	$\varepsilon_{u11} = 0.03 \pm 0.0086$	USS = 66 8 ± 5.5 Mpa
Lotz *et al.*, 1991	Femur 3 point bending test	Diaphyseal $E_{11} = 12.5 \pm 2.1$ $E_{22} = 5.9 \pm 1.5$ Metaphyseal $E_{11} = 9.6 \pm 2.4$ $E_{22} = 5.5 \pm 1.7$		Diaphyseal $\sigma_{11} = 128 \pm 16$ $\sigma_{22} = 47 \pm 12$ Metaphyseal $\sigma_{11} = 101 \pm 25$ $\sigma_{22} = 50 \pm 25$			
McCalden *et al.*, 1993	Femur shaft Uniaxial test	$10 < E_{11} < 21$		$85 < \sigma_{11} < 122$		$0.016 < \varepsilon_{u11} < 0.036$	
Rho *et al.*, 1993	Tibia Uniaxial test Ultrasound	$E_{11} = 20.7 \pm 1.9$ $E_{11} = 18.6 \pm 3.5$					
Courtney *et al.*, 1996	Femur Tensile test	$E_{11} = 15.69 \pm 1.66$					$\varepsilon_{yt11} = 0.00378 \pm 0.00066$ $\sigma_{yt11} = 55.3 \pm 8.6$ MPa
Jepsen and Davy, 1997	Femur Torsion test	$G = 5.0 \pm 0.2$					$\varepsilon_y = 0.013 \pm 0.001$ $\varepsilon_u = 0.052 \pm 0.009$ $\sigma_y = 55.8 \pm 3.8$ MPa USS = 74.1 ± 3.2 MPa
Zioupos and Currey, 1998	Femur shaft 3 point bending test	$11 < E_{11} < 17.5$ MPa					

E – Young's modulus, G – Shear modulus, USS – Ultimate shear strength, σ - ultimate compressive or tensile strength, ε_{yt} – tensile yield strain, ε_u – ultimate strain, σ_{yt} – tensile yield stress, Subscripts $_{11}$ – in the direction of long axis bone, $_{22}$ – in the radial direction or transverse to long axis of bone in no circumferential data is specified, $_{33}$ – in the circumferential direction

* - Strain value from the 52 year male donor only.

Table 1.1 Mechanical properties of cortical bone.

1.4.1.2 Cancellous bone

The mechanical properties of cancellous bone can be treated at the apparent level or at the trabecular level. In most cancellous bone tests, the specimen consists of a block or a cylinder (some are waisted over the gauge attachment). Tests at this level treats cancellous bone at the apparent level, which assumes that cancellous bone is a continuum material and measures the properties at the specimen level. At the tissue level, the test specimen is the trabecular itself. At the apparent level, cancellous bone has lower Young's modulus (less than 3.2 GPa in Table 1.2) than cortical bone, which corresponds to the lower apparent density of cancellous bone range from 0.05 gcm^{-3} to 0.8 gcm^{-3} [Ashman, 1989; Keller, 1994] in comparison to maximum apparent density of cortical bone of about 1.9 gcm^{-3} [Lotz *et al.*, 1991]. At tissue level, the Young's modulus of trabeculae are in the order of cortical bone, although consistently smaller [Ashman *et al.*, 1984; Ashman and Rho, 1988; Turner *et al.*, 1999]. Using ultrasonic wave technique, Ashman and Rho (1988) reported that trabecular bone has a modulus about 7 GPa less than cortical bone [Ashman *et al.*, 1984]. Turner *et al.* (1999) reported smaller difference of 3 GPa using ultrasonic wave technique and 5 GPa using nanoindentation technique. The bone mineral content and material density of trabeculae are less than cortical bone and this is likely to be the reason of lower Young's modulus of trabecular bone [Ashman and Rho, 1988]. For most analytical purposes, cancellous bone is treated at the apparent level, and the discussion in this section is confined to mechanical properties of cancellous bone at the apparent level.

The stress-strain curve of cancellous bone is shown in (Figure 1.6). It is generally agreed that cancellous bone is linear-elastic with similar tensile and compressive Young's moduli [Rohl *et al.*, 1991; Keaveny *et al.*, 1994b]. However, the post-yield behaviour is different in tension and compression. In tension, trabeculae in cancellous bone break and a gap open between them. The load bearing ability stops abruptly just after ultimate strength (Figure 1.6a). In compression, there is a linear elastic region, a plateau region after the ultimate stress and followed by a region of increasing stress until fracture occurs (Figure 1.6b). In compression, the long plateau is caused by elastic buckling or plastic yield, depending on whether the yield region has rod or plate trabeculae respectively [Gibson, 1985]. When the trabeculae walls come together and are touching each other after the plateau region, there is a sharp increase in stress due to compaction until complete failure has occurred [Gibson, 1985].

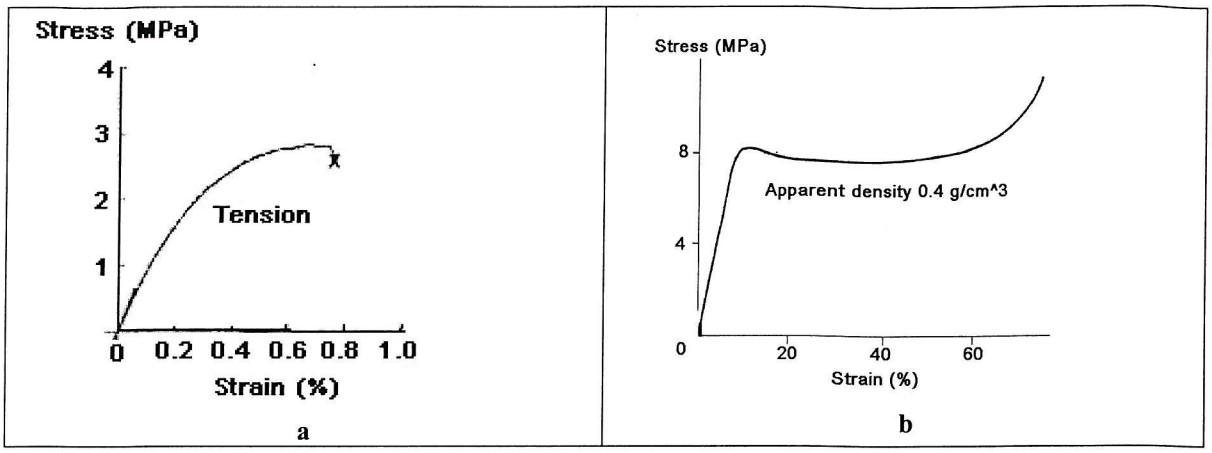

Figure 1.6 Stress-strain curve of cancellous bone [Wachtel and Keaveny, 1997]. The initial part of the curve is linear elastic in compression and tension.

Author	Location and method of measurement	Compressive apparent elastic modulus, MPa ± SD	Tensile apparent elastic modulus, MPa ± SD	Shear Modulus, MPa ± SD	Yield stress ± SD
Goldstein *et al.*, 1983	Proximal tibia Compression test	$31 \pm 18 < E_3 < 336 \pm 86$	-	-	-
Martens *et al.*, 1983	Proximal femur Uniaxial compression	Femoral head $E_1 = 900 \pm 710$ $E_2 = 811 \pm 604$ $E_3 = 403 \pm 66$ Femoral neck $E_1 = 616 \pm 707$ $E_2 = 174 \pm 84$ $E_3 = 63 \pm 7$ Intertrochanteric $E_1 = 263 \pm 170$ $E_2 = 317 \pm 293$ $E_3 = 12 \pm 6$	-	-	Femoral head $\sigma_1 = 9.3 \pm 4.5$ $\sigma_2 = 10.2 \pm 3.3$ $\sigma_3 = 4.9 \pm 1.27$ Femoral neck $\sigma_1 = 6.6 \pm 6.3$ $\sigma_2 = 2.8 \pm 1.3$ $\sigma_3 = 0.965 \pm 0.33$ Intertrochanteric $\sigma_1 = 3.6 \pm 2.3$ $\sigma_2 = 3.7 \pm 1.5$ $\sigma_3 = 0.595 \pm 0.20$
Ashman and Rho, 1988	Human femur Ultrasonic technique Femur 1 Femur 2 Femur 3	 $E_1 = 959$ $E_1 = 1780$ $E_1 = 2170$	-	-	-
Ashman, 1989	Human tibia Ultrasonic technique	$E_1 = 346.8 \pm 218$ $E_2 = 457.2 \pm 282$ $E_3 = 1107.1 \pm 634$	-	$G_{12} = 8.3 \pm 66.4$ $G_{13} = 32.6 \pm 78.1$ $G_{23} = 262.4 \pm 135$	-
Rohl *et al.*, 1991	Human tibia Uniaxial compression Uniaxial tension	$E_1 = 485 \pm 333$ $E_1 = 483 \pm 323$	-	-	-
Dalstra *et al.*, 1993	Human pelvis Uniaxial test	$E_1 = 61.6 \pm 48.2$ $E_2 = 42.4 \pm 29.1$ $E_3 = 31.0 \pm 22.5$			
Goulet *et al.*, 1994	Various bones Orthogonal compression test	$E_1 = 173 \pm 204$ $E_2 = 123 \pm 120$ $E_3 = 287 \pm 255$	-	-	$\sigma_1 = 3.31 \pm 3.14$ $\sigma_2 = 2.58 \pm 2.19$ $\sigma_3 = 4.63 \pm 3.48$
Morgan and Keaveny, 2001	Axial test Vertebra Proximal tibia Greater trochanter Femoral neck	$E_1 = 344 \pm 148$ $E_1 = 1091 \pm 634$ $E_1 = 622 \pm 302$ $E_1 = 3230 \pm 936$	$E_1 = 349 \pm 133$ $E_1 = 1068 \pm 840$ $E_1 = 597 \pm 330$ $E_1 = 2700 \pm 772$	-	-

E – Young's modulus, G_{ij} – shear modulus corresponding to shear forces in the i direction with displacements in the j direction, σ - yield stress, SD – Standard deviation, Subscripts - $_1$ = Anterior-posterior direction, $_2$ = Medial-lateral direction, $_3$ = Superior-inferior direction

Table 1.2 Mechanical properties of human cancellous bone.

Because the values are apparent Young's modulus, the apparent density of the cancellous bone specimen significantly influenced the values of apparent Young's modulus. Therefore, there is wide range of Young's moduli for cancellous bone depending on the location where the cancellous bone is taken and also the direction of load. Values ranging from as low as 12 MPa [Martens *et al.*, 1983] and as high as 3200 MPa [Morgan and Keaveny, 2001] have been reported. The range of values is summarized in Table 1.2. There are studies that showed that 60% of Young's modulus of cancellous bone can be explained by apparent density alone [Keaveny and Hayes, 1993] while accounts for structural properties of cancellous bones can explain about 90% of the measured Young's modulus [Goulet *et al.*, 1994].

Unlike cortical bone, cancellous bone exhibits a range of behaviour from isotropy to anisotropic [Martens *et al.*, 1983; Ashman, 1989; Dalstra *et al.*, 1993; Goulet *et al.*, 1994]. In weight bearing regions, principal Young's modulus is oriented in the major orientation of trabeculae and in the loading direction [Martens *et al.*, 1983; Ashman, 1989; Goulet *et al.*, 1994]. However, in nonweight bearing areas like the acetabulum, some regions have been reported to be isotropic [Dalstra *et al.*, 1993]. Certain regions like the femoral neck [Martens *et al.*, 1983] and proximal tibia [Ashman, 1989] that are uniaxially loaded has anisotropy ratio of about 3 or more while other regions like pelvis which have no direct weight bearing has lower anisotropy ratio of about 2 [Dalstra *et al.*, 1993].

Similar to apparent Young's modulus, the ultimate strength of cancellous bone is dependent on apparent density. Some studies have reported that ultimate strength is proportional to the square of apparent density [Carter and Hayes, 1977; Rice *et al.*, 1988]. There are contradicting results regarding the relative tensile and compressive ultimate strength of cancellous bone. Some studies have reported that compressive ultimate strength is greater than [Stone *et al.*, 1983; Kaplan *et al.*, 1985; Keaveny *et al.*, 1994a], equal to [Carter *et al.*, 1980] or less than [Rohl *et al.*, 1991] tensile strength. In comparison to previous studies, Keaveny *et al.* (1994a) attempt to reduce the measurement error by using waisted specimens to produce a region of uniform stress. This study reported that tensile ultimate strength is 30% lower than compressive ultimate strength, and this is similar to Kaplan's *et al.* (1985) result but less than the 60% reduction reported by Stone *et al.* (1983). However, in Stone's *et al.* (1983) study, the tensile strength was extrapolated from a failure criterion.

Early investigators reported cancellous bone strength in terms of the yield or ultimate stress, but recent evidence indicates that strain-based descriptions may be simpler and more useful. Both the yield and ultimate strain of cancellous bone has been reported to be independent of the apparent density [Turner, 1989; Rohl *et al.*, 1991; Keaveny *et al.*, 1994a]. Keaveny *et al.* (1994a) reported that both the yield and ultimate compressive strain is 30% higher than the yield and ultimate tensile strain (Table 1.3). In contrast, Rohl *et al.* (1991) reported 28% higher ultimate

tensile strain than compressive strain. Kopperdahl and Keaveny (1998) reported 8% higher tensile ultimate strain than compressive strain. Rohl's *et al.* (1991) study has excluded some tensile specimens due to fracture out of the gauge length and this may have biased the result towards tests with higher failure strain. However, both Kopperdahl and Keaveny (1998) and Keaveny *et al.* (1994a) used the same test protocol, but the former used human bone while the latter used bovine bone. It is possible that bovine cancellous bone with more plate-like trabeculae will have higher ultimate compressive strain due to stronger resistance against buckling than human bone with lower density and less plate-like trabeculae than bovine cancellous bone.

Reference	Bone type	Number	Strain, % ± SD Yield	Ultimate	Stress, Mpa ± SD Yield
Compression					
Lindahl, 1976	Human vertebral	32	6.1 ± 2.3	9.0 ± 4.5	
	Human proximal tibia	32	6.9 ± 4.5	11.6 ± 6.2	
Hansson *et al.*, 1987	Human vertebral body	231	6.0 ± 2.2	7.4 ± 2.4	
Rohl *et al.*, 1991	Human proximal tibia	15		1.11 ± 0.63	
Keaveny *et al.*, 1994a	Bovine Proximal tibia	30	1.09 ± 0.49	1.86 ± 0.49	
Kopperdahl and Keaveny, 1998	Human vertebral body	22	0.81 ± 0.06	1.45 ± 0.3	
Keaveny *et al.*, 1999	Human vertebral body	25		1.28 ± 0.29	
Morgan and Keaveny, 2001	Human vertebral body	30	0.77 ± 0.06		2.02 ± 0.92
	Human proximal tibia	15	0.73 ± 0.06		5.83 ± 3.42
	Human femur: greater trochanter	10	0.70 ± 0.05		3.21 ± 1.83
	Human femur: Neck	14	0.85 ± 0.1		17.45 ± 6.15
Tension					
Rohl *et al.*, 1991	Human proximal tibia	15		1.55 ± 0.49	
Keaveny *et al.*, 1994a	Bovine Proximal tibia	29	0.78 ± 0.04	1.37 ± 0.33	
Kopperdahl and Keaveny, 1998	Human vertebral body	22	0.78 ± 0.04	1.59 ± 0.33	
Morgan and Keaveny, 2001	Human vertebral body	31	0.70 ± 0.05		1.72 ± 0.64
	Human proximal tibia	16	0.65 ± 0.05		4.5 ± 3.14
	Human femur: greater trochanter	13	0.61 ± 0.05		2.44 ± 1.26
	Human femur: neck	13	0.61 ± 0.03		10.93 ± 3.08

SD – standard deviation

Table 1.3 Summary of cancellous bone yield strain and stress reported in the literature.

However, Kopperdahl and Keaveny (1998) suggests that tensile yield strain is independent of the apparent density but the compressive yield strain is not. The difference can be explained by the different failure mechanisms observed in tension and compression. The compressive yield strain was found to be linearly correlated to lower density cancellous bone, but independent of density for high density cancellous bone. At lower densities, the ratio of length over thickness of trabeculae should be higher for lower density cancellous bone and therefore it is more likely to fail by buckling, and therefore a decrease in density resulting in a decrease of the yield strain [Gibson, 1985]. For higher densities, trabeculae are plate like, the ratio of trabeculae length over thickness is lower and buckling effect become less significant [Gibson, 1985]. The yield strain is therefore constant. For cancellous bone loaded in tension, buckling cannot occur, and therefore the tensile

yield strain is independent of density. The different conclusion reached by Kopperdahl and Keaveny (1998) is due to the inclusion of specimens with greater range of density in comparison to Keaveny *et al.* (1994a).

Although yield or ultimate strength of cancellous bone is anisotropic [Martens *et al.*, 1983; Goulet *et al.*, 1994], the yield strain bone has been reported to be independent of direction [Chang *et al.*, 1999]. This study compared the yield strain along the principal direction of trabeculae and at an oblique angle (30-40°) using bovine bone. The measured yield strain was found to be independent of direction. The yield strain in compression is 15% higher than in tension, lower than the 30% reported in other studies but have the similar trend [Keaveny *et al.*, 1994a; Kopperdahl and Keaveny, 1998].

In contrast to previous studies on effect of apparent density on yield strain, Morgan *et al.* (2001) studied the dependence of yield strain on anatomical sites. Cancellous bone samples from the vertebral, the proximal tibia, the greater trochanter and the femoral neck were tested with an apparent density of cancellous bone range between 0.09 and 0.75 gcm^{-3}. Yield strain was found to be dependent on anatomical location, with maximum difference of about 20% in compression and 12% in tension (Table 1.3). The bigger difference of compressive yield strain could be due to about 2 times higher density in the femoral neck in comparison to other locations and compressive yield strain has been shown to increase with density [Kopperdahl and Keaveny, 1998]. However, within one site, the difference in yield strain is only between 5 and 12 % and therefore can be considered as uniform [Morgan and Keaveny, 2001]. Due to the isotropy of yield strain, and small differences of yield strain within an anatomical location, it is easier to judge the severity of loading in bone by looking at the strain, rather than stress.

The yield strain and ultimate strain values reported in the literature for cancellous bone are summarized in Table 1.3. The yield and ultimate strains values measured in some studies [Lindahl, 1976; Hansson *et al.*, 1987] are very high in comparison to other studies [Keaveny *et al.*, 1994a; Kopperdahl and Keaveny, 1998; Morgan and Keaveny, 2001]. The former tested the bone specimens between platens and strains are based on relative motion of the platens. This test method can cause artifactual errors due to damage at the specimen ends and friction at the specimen-platens interface [Keaveny *et al.*, 1994b]. It is suggested that the high failure strain exceeding 6 % reported in these studies may have too much experimental error to provide reliable failure strain data [Kopperdahl and Keaveny, 1998]. Studies that used waisted specimens [Keaveny *et al.*, 1994a; Kopperdahl and Keaveny, 1998; Morgan and Keaveny, 2001] removed the artifactual errors associated with platen test and generally measured yield strain of about 0.6 and 0.8% and ultimate strain of about 1.3 and 1.8%.

1.4.1.3 Damage to bone under repetitive loading

The Young's modulus, yield and ultimate stress of both cortical and cancellous bone are not constant under repetitive loading. Small, but consistent reductions in the elastic modulus of cancellous bone have been measured in specimens loaded to between 0.3 and 0.5 % strain [Keaveny *et al.*, 1994b; Keaveny *et al.*, 1999]. Keaveny *et al.* (1994b) suggested that this was caused by small cracks that developed in the bone. The reduction of modulus and strength of cortical and cancellous bone are also observed in reloading after loading beyond the yield limit in the first cycle (Figure 1.7) [Courtney *et al.*, 1996; Keaveny *et al.*, 1999]. Keaveny *et al.* (1999) reported that modulus and strength degradation is greater if the first cycle applied higher strain deformation.

Courtney *et al.* (1996) reported that significantly more cracks were observed in specimens from elderly people, but did not see significant changes among specimens from younger people, although the reduction in modulus was similar for both ages group. It is possible that the damage in the younger group had not developed as a visible crack as yet. Greater number of cracks can also be observed in cancellous bone that has been overloaded [Wachtel and Keaveny, 1997].

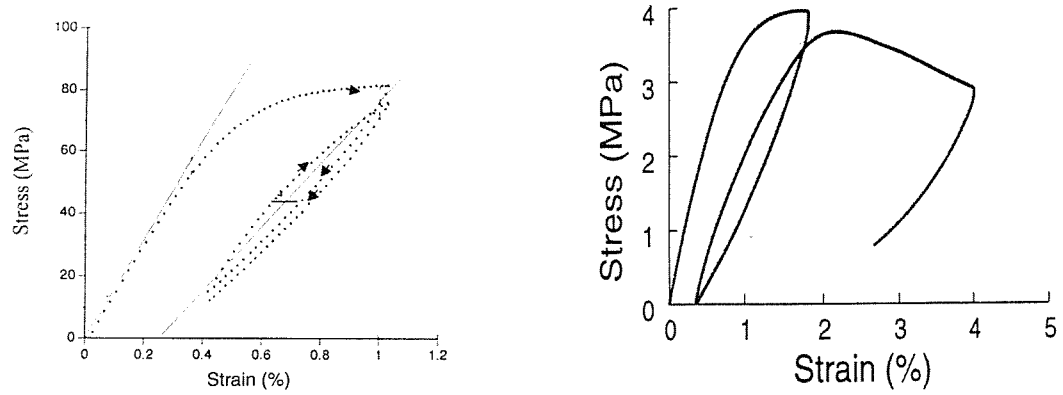

a b

Figure 1.7 Typical load-unload-load stress-strain curve of (a) Straight line is the Young's modulus of cortical bone [Courtney *et al.*, 1996]. The first slope is steeper than the second slope, which shows degradation of Young's modulus due to damage in cortical bone after it is loaded beyond yield limit. (b) Cancellous bone loaded beyond yield limit in the first load cycle [Keaveny *et al.*, 1999]. The second stress-strain line is more compliant than the first due to degradation of cancellous bone structure.

1.4.1.4 Density-Young's modulus relationship

Many researchers have relates the apparent Young's modulus of bone to its apparent density in the form

$$E = A+B\rho^{c} \text{ ---------- Equation 1.1}$$

Where E is the elastic modulus, ρ is the apparent density and c is the exponent. The value of c is still debated.

One of the most widely quoted relationships is by Carter and Hayes (1977). Carter and Hayes (1977) reported that compressive elastic modulus of bone is proportional to the cube of apparent density, in a study of human and bovine cancellous bone (Table 1.4). They assumed that the structure and material properties of human and bovine cancellous bone were similar and can be predicted by one equation. They also suggested that elastic modulus of cortical bone can be extrapolated from the results of experimental testing on cancellous bone, which implied that cancellous bone and cortical bone are similar engineering materials.

Rice *et al.* (1988) compared a quadratic exponent to a cubic exponent and proposed that the quadratic exponent explains the elastic modulus better (Table 1.4). The equation based on quadratic exponent explains the variance of elastic modulus slightly better than the cubic exponent (78% vs. 74% respectively). Rice *et al.* (1988) contradicted Carter and Hayes (1977) by suggesting that extrapolating elastic modulus of cortical bone from cancellous bone data will result in underestimation of the elastic modulus. Both studies did not consider exponent that is not an integer.

Authors	Anatomical location	Bone Type	Test method	Power law
Carter, 1977	Human proximal tibia and bovine femoral condyles	Cancellous bone	Uniaxial compression test	$E = 3790\dot{\varepsilon}^{0.06}\rho^3$
Keller, 1994	Human spine and femur	Cortical and cancellous bone (density = 0.05-1.89 g/cm^3)	Uniaxial compression test	$E = 2.61\rho^{2.58}$
Rice *et al.*, 1988	Pooled data of bone tests	Bovine cancellous bone	Regression analysis	$^tE = 0.07+2.46\rho^2$ $^cE = 0.07+3.29\rho^2$

[t] property under tensile loading
[c] property under compressive loading

Table 1.4 Density-Young's modulus relationship for cortical and cancellous bone.

Other studies have reported that the exponent is not necessary an integer [Keller, 1994]. Keller (1994) regression analysis did not assume any integer exponent and reported an equation with exponent of 2.58 (Table 1.4). This equation explained 93% of the variance of elastic modulus in the apparent density range of 0.05 to 1.89 gcm^{-3}, and suggests that there is no strong reason for the exponent to take an integer value.

The values predicted by Keller (1994) are compared to the values predicted by Carter and Hayes (1977) and Rice *et al.* (1988) (Figure 1.8) using data from Table 1.4. For Carter and Hayes (1977)'s equation, the physiological strain rate of 0.01 s^{-1} was used [Lanyon *et al.*, 1975]. The values predicted by these three studies are quite similar in the apparent density range smaller than 1 gcm^{-3}. At this point, the three curves diverged with Carter and Hayes (1977) predicting the highest bone elastic moduli for apparent density range greater than 1 gcm^{-3}. For the generally agreed highest apparent density of about 1.9 for cortical bone [Lotz *et al.*, 1991], the generally

agreed maximum elastic modulus is in the range of 20 GPa [Ashman *et al.*, 1984; Rho *et al.*, 1993]. Carter and Hayes (1977)'s prediction is about 20 GPa while Keller (1994) predicted 16 GPa, which is a bit lower than the generally accepted maximum elastic modulus of cortical bone. It is felt that the relationship used to predict the elastic modulus from apparent density should be comparable to experimental values reported in the literature. In this thesis, the cubic equation from Carter and Hayes (1977) is used as the prediction of cancellous bone property is similar to the other two studies but the maximum cortical bone elastic modulus is better predicted by the cubic equation.

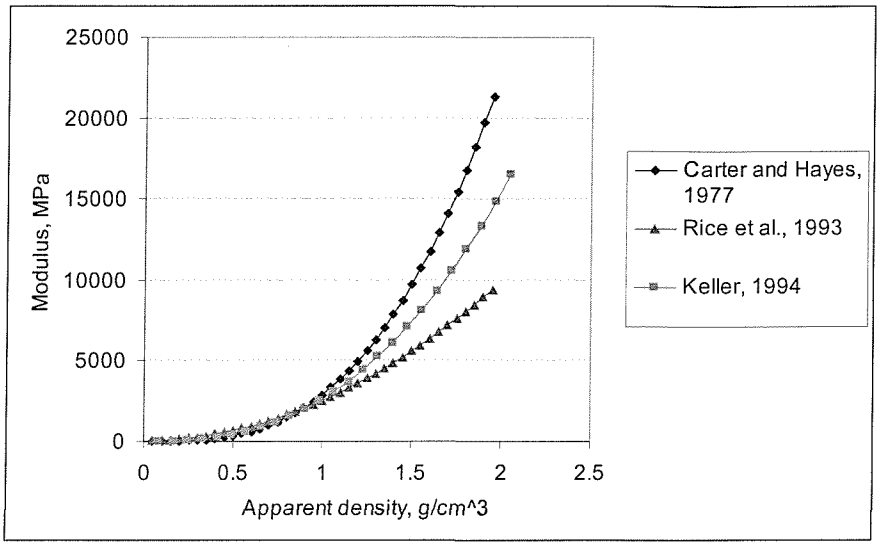

Figure 1.8 Elastic modulus predicted by three different studies [Carter, 1977; Rice *et al.*, 1988; Keller, 1994].

1.4.2 Creep deformation of bone

Both cancellous and cortical bone exhibit the three classical stages of creep [Fondrk *et al.*, 1988; Caler and Carter, 1989; Rimnac *et al.*, 1993; Bowman *et al.*, 1994; Bowman *et al.*, 1998] shown in Figure 1.9. The initial fast creep phase that slows down with time (primary) is followed by a long steady state creep phase (secondary), and the increasingly faster creep phase that leads to failure in the tertiary stage. Tensile creep testing of cortical bone [Fondrk *et al.*, 1988; Rimnac *et al.*, 1993] and compressive creep testing of cancellous bone [Bowman *et al.*, 1998] has shown that the creep strain rate during the second phase of both types of bone can be described by a power law relationship. If creep strain rate is a function of stress in the power law relationship, lower correlation has been reported [Fondrk *et al.*, 1988; Rimnac *et al.*, 1993]. Stronger correlation was reported if creep strain rate is a function of applied normalized stress (ratio of stress over elastic modulus) for tests using bovine cancellous bone [Bowman *et al.*, 1998]. The normalized stress is also equal to the strain in the linear elastic region of bone stress-strain curve and this suggests that bone creep is correlated to initial strain. Time to failure has also been used to study the creep of both cortical and cancellous bone. This parameter is also highly correlated to normalized stress

[Caler and Carter, 1989; Mauch *et al.*, 1992; Bowman *et al.*, 1994; Bowman *et al.*, 1998; Brown *et al.*, 2002].

Creep of cortical bone has been explained by both microstructural and ultrastructural creep mechanism. The microstructural creep mechanisms proposed for cortical bone include cracks within individual lamellar, delamination or shear of lamellae within the osteon and the shear between osteon and the surrounding interstitial bone [Lakes and Saha, 1979; Park and Lakes, 1986; Caler and Carter, 1989; Brown *et al.*, 2002]. In tensile creep, osteon pullout, separation between lamellae and stretched individual lamellae has been observed [Caler and Carter, 1989]. In compressive creep, individual lamellae have been drawn out and folded over [Caler and Carter, 1989]. During torsional creep test, cement line slippage occurred [Park and Lakes, 1986]. However, cement line slippage cannot explain a large portion of the observed creep strains, which suggest that ultrastructural mechanism is also involved in bone creep. The proposed ultrastructural creep mechanism includes dislocation generation or dislocation interaction of hydroxyapatite crystal [Rimnac *et al.*, 1993] and shear between collagen fibrils or separation of hydroxyapatite crystals and the collagen matrix [Fondrk *et al.*, 1988]. Fondrk *et al.* (1988) observed that since ratio of creep strain to permanent strain is highly correlated, this consistency in creep is more likely to be explain by ultrastructural mechanism than microstructural mechanism.

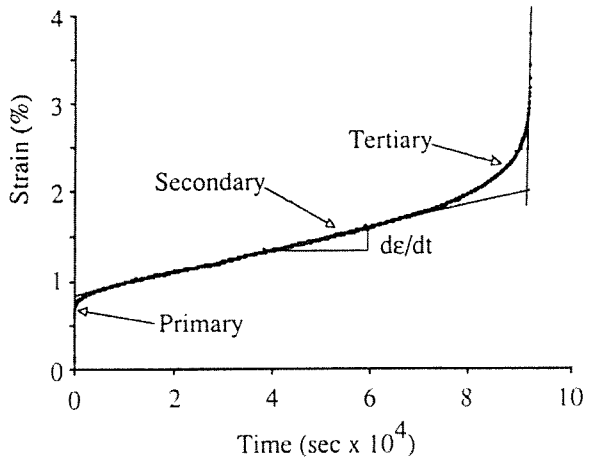

Figure 1.9 Three creep stages of bone – primary, secondary and tertiary. Both cancellous and cortical bones exhibit this behaviour [Bowman *et al.*, 1994].

Rimnac *et al.* (1993)'s suggestion that creep is caused by process involving hydroxyapatite crystal has been disputed by other investigators [Bowman *et al.*, 1999]. Bowman *et al.* (1999) suggest that the creep of bone (cortical and cancellous bone) involved the collagen fibre matrix. They dissolved the mineral phase of hydroxyapatite from bovine cortical bone to leave their specimen with only collagen fibre matrix. The creep test performed on the demineralised bone showed similar three stages creep and exponent in the power law relationship as the cortical and cancellous bone. They suggested that since collagen fibre denaturalised at about 56°C, at body temperature of 37°C, the homologous temperature T/T_{melt} is about 0.94 and it is highly likely to

creep. In comparison, hydroxyapatite which formed the other phase of bone at 37C is at a homologous temperature $T/T_{melt} \sim 0.17$. For a crystalline material, creep is unlikely to occur at this low homologous temperature.

1.4.3 Fatigue behaviour of bone

Repetitive loading of cortical and cancellous bone has been shown to fracture bone at stress below the ultimate strength [Carter *et al.*, 1981b; Carter and Caler, 1983; Bowman *et al.*, 1998]. Uniaxial fatigue test on human cortical bone (tension-compression) has found that human cortical bone has low fatigue strength [Carter *et al.*, 1981b]. The fatigue strength of cortical bone at 10 million cycles (predicted load cycles for ten years of normal activities) is about 7 MPa, assuming mean elastic modulus of 14.5 GPa. Carter *et al.* (1981) suggested that bone fatigue damage accumulation is physiological due to the low fatigue strength of bone and bone repair from remodelling activities is vital for maintaining bone integrity. The uniaxial fatigue damage accumulation is correlated better with strain range and independent of mean strain [Carter *et al.*, 1981a; Carter *et al.*, 1981b]. The uniaxial damage accumulation is less correlated with stress range [Carter *et al.*, 1981b].

A linear-life fraction model (inverse of the time to failure) to analyse fatigue life of cortical bone has been proposed [Carter and Caler, 1985]. This model consists of a time dependent component calculated from creep-fracture test and cycle-dependent component calculated from fully reversed fatigue tests [Carter and Caler, 1983; Carter and Caler, 1985]. The total damage is calculated from the superposition of the time dependent component and the cycle dependent component. A further study by Caler and Carter (1989) found that the life fraction for 0-tension fatigue test can be predicted from the result of tensile creep tests and this suggest that tensile fatigue accumulation is basically creep accumulation and time dependent. For the 0-compression fatigue test, the life-fraction can be primarily predicted by 0-compression cyclic loading data and this is cyclic dependent [Caler and Carter, 1989]. However, when the superposition of time dependent and cyclic dependent data is used to predict tension-compression cyclic loading, the damage is greater than the linear-life fraction model's prediction. This suggests more complicated interaction in tension-compression cyclic loading [Caler and Carter, 1989].

The creep contribution towards fatigue damage of bone has also been observed in bovine cancellous bone [Bowman *et al.*, 1998]. Bowman *et al.* (1998) observed that under uniaxial compressive fatigue test of cancellous bone, the stress-strain curve translated along the direction of increased strain as test progress, suggesting that creep is involved in the fatigue process. The products of creep strain rate and time to failure were constant for both fatigue and creep test and were equal to the measured creep strain to failure in creep and 0-compression tests. By manipulating the ratio of creep strain to failure from creep test and creep strain to failure from fatigue test, Bowman *et al.* (1998) found that the time to failure of the fatigue test can be predicted

from the creep test data. However, unlike 0-compression fatigue test of cortical bone which is largely cyclic dependent [Caler and Carter, 1989], fatigue strain accumulation of 0-compression fatigue of cancellous bone involved both creep components, cyclic crack growth component and possibly creep buckling [Bowman *et al.*, 1998]. This difference could be due to bending of trabeculae in cancellous bone which load the trabeculae in tension. Data for 0-tension fatigue test and its relationship with creep is unavailable at present.

1.4.4 Degradation of bone quality due to aging and abnormalities

The bone mass of human bone reaches its maximum at the age of about 30, and by the age of 70 less than 70% of peak bone mass remains [Cowin, 2001]. The reduction of bone mass affects the mechanical integrity of both cortical and cancellous bone [McCalden *et al.*, 1993; Ding *et al.*, 1997; McCalden *et al.*, 1997; Zioupos and Currey, 1998]. Zioupos and Currey (1998) reported 2.3% reduction of elastic modulus of cortical bone per decade while Ding *et al.* (1997) reported 40% drop in elastic modulus of cancellous bone between age 50 and 80 years. Ultimate strength of cancellous bone has also been reported to reduce by 8.5% per decade [McCalden *et al.*, 1997] in comparison to cortical bone which reduced by 5% per decade [McCalden *et al.*, 1993]. Cancellous bone seems to be affected more by aging than cortical bone probably due to higher remodelling rate in cancellous bone than cortical bone [Cowin, 2001].

The thinning of both cortical and cancellous bone occurred primarily at the surfaces adjacent to the marrow [Cowin, 2001]. There could be a small degree of gain of bone at the periosteal surface which partially offsets this loss. On the whole, there is a thinning of the cortex and expansion of the marrow cavity with enlargement of the bone circumference to a lesser degree. In cancellous bone, thinning of trabeculae, perforation of trabeculae plates and complete loss of connection between trabeculae cause a reduction in density and architectural integrity [Moselkilde, 2000; Cowin, 2001]. The changes in cancellous bone architecture due to aging is shown in Figure 1.10.

The changes in bone quality due to age has been shown to be different in men and women [Moselkilde, 2000]. Studies of vertebral bone have shown that men have higher peak bone mass and strength than women before the onset of bone loss. There is also a compensatory increase in bone size in men that was not found in women. During the postmenopausal period, women show a higher tendency than men for disconnection of the horizontal trabecular struts. In general, there is a greater deterioration of the trabecular network in women.

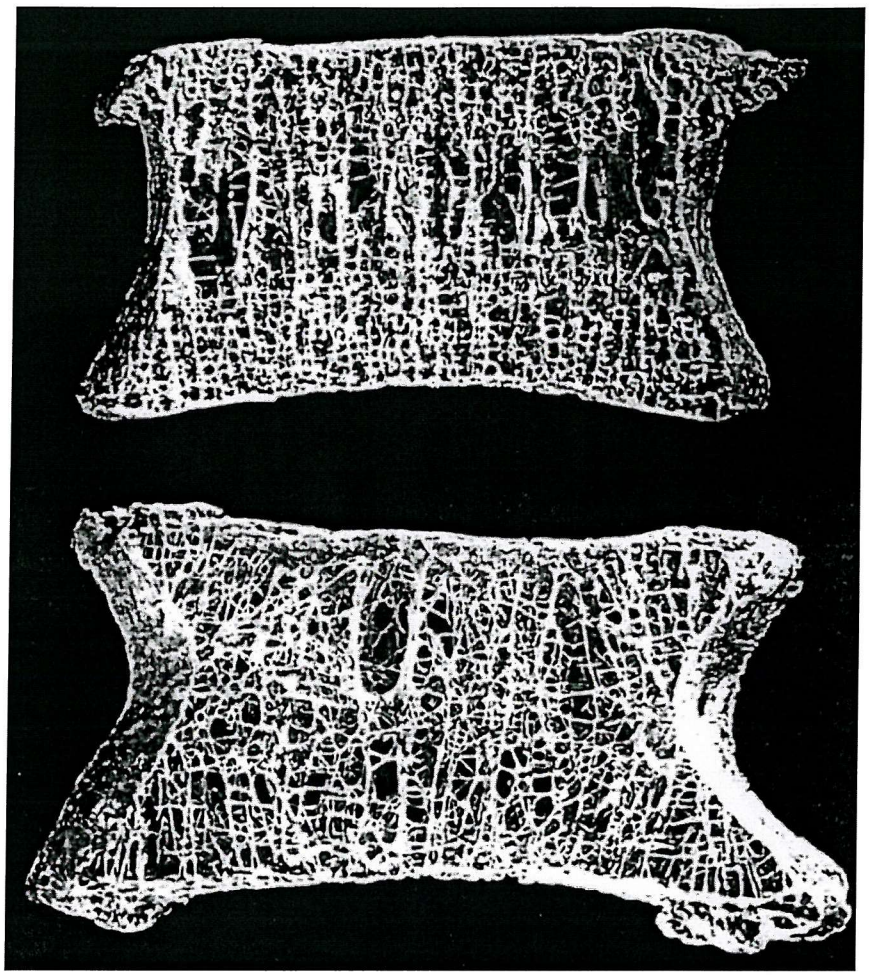

Figure 1.10 (Top) Vertebra from a young individual with denser central network. (Bottom) Vertebral from an elderly individual with reduced trabeculae density and more perforations. [Moselkilde, 2000]

Bone abnormalities like osteoarthritis and rheumatoid arthritis can also lead to changes in bone quality. Osteoarthritis is believed to cause reduction of quality of the subchondral bone [Zysset *et al.*, 1994; Ding *et al.*, 2001], although other studies have shown increase in stiffness over the femoral head and neck [Li and Aspden, 1997]. The mechanical properties of the bone with rheumatoid arthritis generally is much poorer than normal bone [Yang *et al.*, 1997; Bogoch and Moran, 1999]. Rheumatoid arthritis affects both cortical and cancellous bone with a loss in bone volume and strength due to a major increase in the rate of bone remodelling [Bogoch and Moran, 1999]. Yang *et al.* (1997) has reported a loss of 47% of cancellous bone elastic modulus in rheumatoid arthritis bone. Dalstra *et al.* (1996) have used 50% and 90% reduction of elastic modulus of cortical and cancellous bone respectively to model rheumatoid arthritic glenoid bone (one of the shoulder bone) based on measurements from Frich (1994). Like aging, loss of cancellous bone elastic modulus is faster than cortical bone.

Chapter 2 The Hip Joint – Anatomy And Forces Acting On The Hip Joint

2.1 Introduction

In this chapter, the basic anatomy of the hip and forces acting on the hip joint are discussed. Forces that act on the hip joint can be divided into joint contact force and muscles forces. The joint contact force is a direct contact reaction force between the two articular surfaces of the hip joint. The muscle forces are the forces that act on the pelvis and the femur (the thigh bone). The muscles act synchronously during locomotion to produce these forces.

The descriptions of the anatomical planes that are used in this thesis are shown in Figure 2.1 [Hall-Craggs, 1995]. Sagittal planes are all the vertical planes that are parallel to the Median plane, a plane passing from the front to the back of the body through the midline. Coronal planes are all the vertical planes that pass from side to side and are at right angles to the sagittal planes. Horizontal planes are at perpendicular to both coronal and sagittal planes.

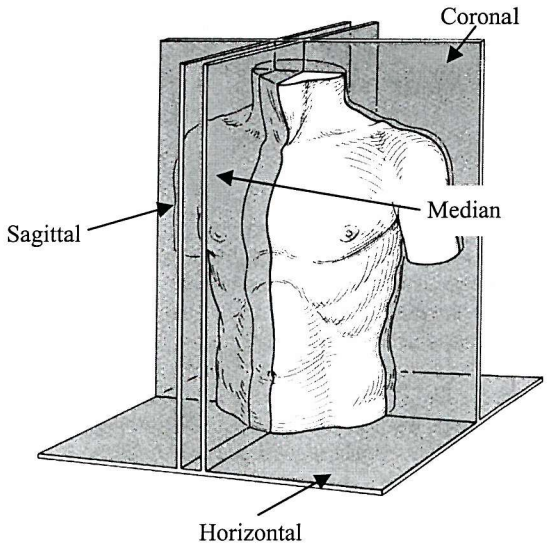

Figure 2.1 Anatomical planes of references [Hall-Craggs, 1995].

2.2 Anatomy of the hip joint

The hip joint is a ball and socket type of joint formed by the pelvis and femur [Hamilton, 1956] (Figure 2.2). A depression at the lateral side of the pelvis called the acetabulum (the socket) and the femoral head (the ball) are two comforming articulating surfaces with cartilage layer on both sides. A fibrous capsule encapsulates the joint, which is filled with synovial fluid. The femoral head is held in the socket by transverse ligament that encircles the acetabulum (Figure 2.2).

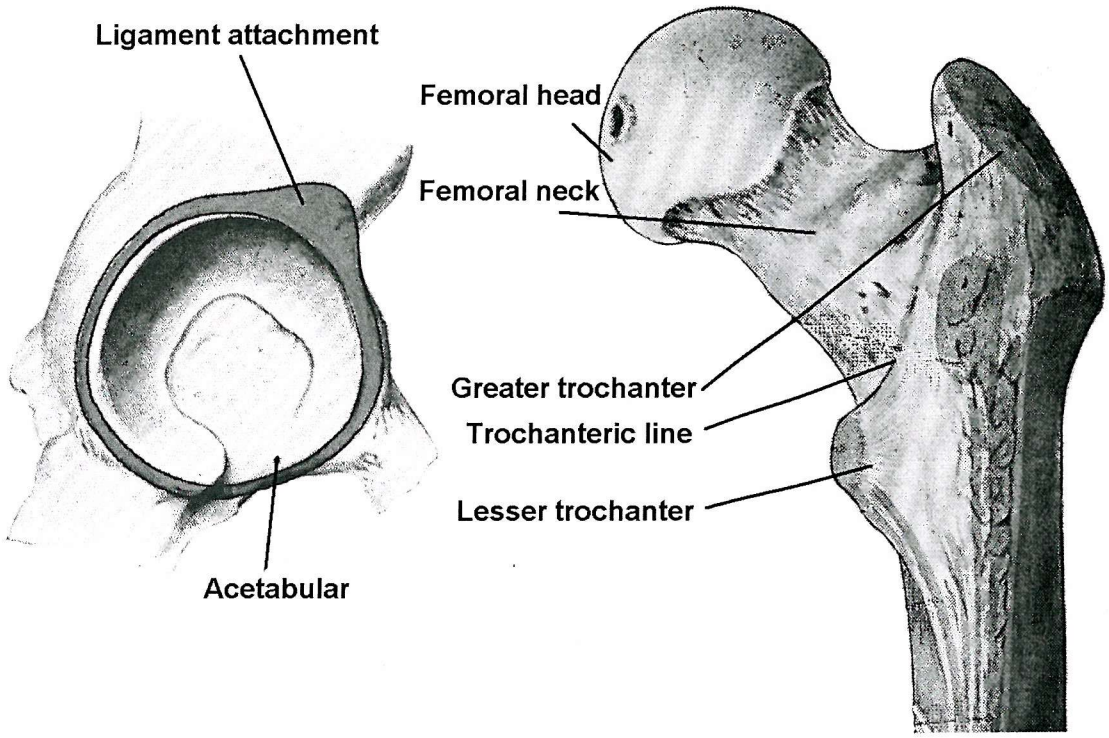

Figure 2.2 Anatomy of human hip joint. The femur head and the acetabulum formed a ball and socket joint. The hip joint ligaments are connected to the shaded region of the acetabulum to form the joint capsule. Most of the muscles attached to the femur originated from the pelvis. [Hamilton, 1956].

The femur is the longest bone in the body. It is a long shaft with two expanded ends. The prominent points on the proximal femur are the femoral head, femoral neck, greater trochanter and lesser trochanter. Near the base of the femoral neck where it meets the greater and smaller trochanter, ligaments (ilio-femoral, pubio-femoral and ischio-femoral) originating from around the rim of the acetabulum attached themselves here. The greater trochanter is a large prominence on the lateral side and the lesser trochanter is on the medial side. Both are areas of muscle attachments (Figure 2.2).

2.3 Movement of the hip joint and the muscles involved

The movement of hip joint can be described as below [Hamilton, 1956] : -

- Flexion – Forward movement of the femur relative to the pelvis. The flexion muscles are iliacus, psoas major, rectus femoris, pectineus and sartorius.
- Extension – Backward movement of the femur relative to the pelvis. Muscles involved are gluteus maximus, hamstring muscles, and lower part of adductor magnus.
- Abduction – Lateral movement of the femur. Muscles involved are gluteus medius and gluteus minimus.

- Adduction – Medial movement of the femur. Adductors muscles are adductores longus, brevis and magnus, and gracilis
- Medial rotation – Rotational movement where the anterior aspect of the knee is turned medially relative to the pelvis. Medial rotators are tensor fasciae latae and gluteus medius and minimus.
- Lateral rotation – Rotational movement where anterior aspect of the knee is turned laterally relative to the pelvis. Lateral rotators are obturator internus and gemelli, obturator externus, quadratus femoris and gluteus maximus.

Flexion is generally possible up to about 120°, limited by the contact between thigh and the abdominal wall. With the knee extended, flexion could be less due to tension in the hamstrings. The extension of hip is about 20°, varying between individuals. The hip rotation is about 90°, combining medial and lateral rotation together. Medial rotation is limited by short rotator muscles and lateral rotation is limited by tensor fasciae latae, gluteus medius and gluteus minimus muscles. Adduction and abduction is about 45° each [Palastanga *et al.*, 2002]. Adduction is limited by abductor muscles and abduction is limited by iliofemoral ligaments.

2.4 Gait cycle

Walking can be described as a sequence of events called the gait cycle. The phases of the gait cycle is normally described as the percentage of the gait cycle (Figure 2.3). The cycle starts at the moment the heel touches the floor, or the heel strike which corresponds to 0% of the gait cycle. The time the leg supported the weight is called the stance phase. The moment the toe leaves the floor is called toe off and corresponds to about 66% of the gait cycle. After toe off is the swing phase and the end of this phase corresponds to 100% of the gait cycle. The cycle restarts when the heel strikes the floor again. Figure 2.3b also showed the force acting on the hip joint during the gait cycle. This dynamic force changes with the progression of the cycle.

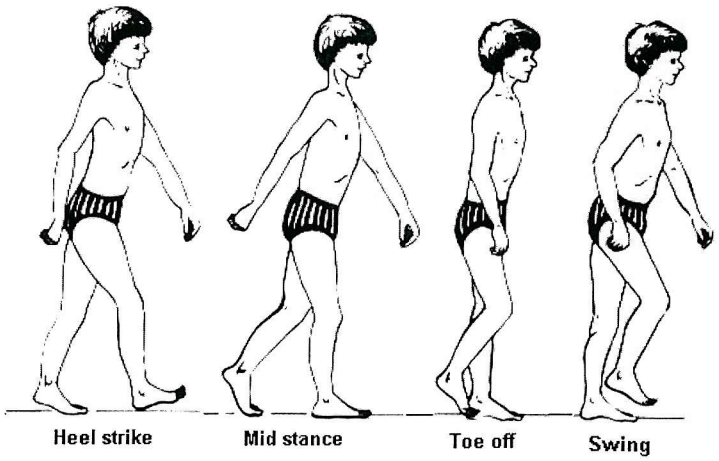

a

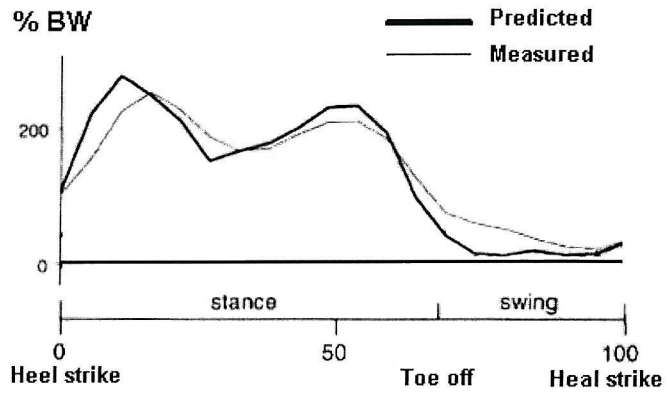

b

Figure 2.3 a) Gait cycle of human walking [Tyldesley and Grieve, 1996] (b) Joint contact force during the gait cycle [Heller *et al.*, 2001].

2.5 Hip joint contact and muscle forces

Hip joint contact and muscle forces of the hip joint have been studied analytically. Determination of joint contact and muscle forces is performed using an inverse dynamic method. The body is modelled as a system of rigid links. Each rigid link or segment is described by equilibrium equations that must satisfy the force and moment equilibrium. The reaction force at the foot is distributed to the joints and muscles by linear optimisation. The optimisation function is normally the minimum force in the muscles. The reaction force at the foot can be measured experimentally using force plate. The location histories of each segment can be derived from laboratory based kinematics studies (often in conjunction with force plate measurement).

Mathematical models of various ages and activities have been performed by a number of researchers [Paul, 1967; McLeish and Charnley, 1970; Seireg and Arvikar, 1975; Crowninshield *et al.*, 1978b; Rohrle *et al.*, 1984; Heller *et al.*, 2001]. Most of these analyses reported two maxima in the gait cycle for the joint reaction force - the first maximum occurs just after heel strike, and

second maximum occurs just before toe-off (Figure 2.3b). Some researchers have reported higher first maximum [Seireg and Arvikar, 1975; Crowninshield *et al.*, 1978b; Heller *et al.*, 2001], while others have reported higher second maximum [Paul, 1967; Rohrle *et al.*, 1984], as shown in Table 2.1. Heller *et al.* (2001) reported that the second maximum is not always present in patients who have undergone total hip arthroplasty.

Author and activity	Joint contact force	
	1st max.	2nd max.
Paul, 1967	4.25 BW	4.42 BW
McLeish and Charnley, 1970	2-3 BW	
Seireg and Arvikar, 1975	5.32 BW	4.64 BW
Crowninshield *et al.*, 1978a		
0.28 m/s old persons	3.31 ± 1.18 BW	
0.83 m/s old persons	3.81 ± 1.18 BW	
1.39 m/s old persons	4.42 ± 1.18 BW	
0.28 m/s young persons	3.44 ± 1.4 BW	
0.83 m/s young persons	4.29 ± 1.34 BW	
1.39 m/s young persons	5.85 ± 1.51 BW	
Crowninshield *et al.*, 1978b		
0.94 m/s	3.6 BW	1.9 BW
3.83 m/s	5.62 BW	2.92 BW
Rohrle *et al.*, 1984		
0.69 m/s	2.60 ± 1.65 BW	3.6 ± 1.65 BW
1.25 m/s	4.4 ± 1.65 BW	5.55 ± 1.65 BW
1.75 m/s	6.20 ± 1.65 BW	7.55 ± 1.65 BW
Heller *et al.*, 2001		
1.08 m/s, average patient,	2.61	2.41

Table 2.1 Calculated hip joint contact forces during walking and running.

The predicted values of joint contact force is quite different between studies. In studies that does not use force plate to measured the foot reaction force and kinematics data, peak joint contact force of 4.42 and 5.32 body weight (BW) has been predicted [Paul, 1967; Seireg and Arvikar, 1975] (Table 2.1). Studies with kinematics and force plate data have predicted higher peak joint contact force for higher walking speed [Crowninshield *et al.*, 1978a; Crowninshield *et al.*, 1978b; Rohrle *et al.*, 1984; Heller *et al.*, 2001] (Table 2.1). Heller *et al.* (2001) predicted much lower peak joint contact force in comparison to other studies [Crowninshield *et al.*, 1978a; Crowninshield *et al.*, 1978b; Rohrle *et al.*, 1984]. At the walking speed of 1.08 ms^{-1}, the predicted peak contact force was 2.61 BW while other studies predicted peak contact force higher than 3 BW at slower walking speeds. Crowninshield *et al.* (1978) and Rohrle *et al.* (1984) predicted peak contact force of 5.85 and 7.55 BW at walking speed of 1.39 and 1.75 ms^{-1} respectively.

Verification of predicted hip joint contact force is not easy to obtain as only instrumented prosthesis inserted into patients can provides this data. In comparison to analytical study, *in vivo* experiments measuring the hip joint contact force have shown that the first maximum is greater than the second maximum, or the second maximum was absent [Rydell, 1966; English and

Kilvington, 1979; Davy *et al.*, 1988; Kotzar *et al.*, 1991; Bergmann *et al.*, 1993; Bergmann *et al.*, 2001].

In vivo measurements consistently measure the joint contact force in the range of 2-3 body weight (BW) for slow and medium speed walking (Table 2.2). However, magnitude of peak contact force could be patient specific. In one of the study, one patient recorded contact force as high as 4.24 BW walking at the speed of 1.38 ms^{-1} [Bergmann *et al.*, 1993]. In comparison, for similar walking speed, the peak contact force was less than 3.3 BW in other studies [Rydell, 1966; Kotzar *et al.*, 1991; Bergmann *et al.*, 2001]. In comparison to older analytical studies at walking speed of about 1.3 ms^{-1} [Crowninshield *et al.*, 1978b; Rohrle *et al.*, 1984] which predicted contact force between 4.42 and 5.8 BW, the measured values are smaller. However, recent model Heller *et al.* (2001) showed that with accurate kinetic, inertia property and joint anatomic data, optimisation study can predict the joint contact force during walking within the 2-3 BW that is normally measured *in vivo* (Figure 2.3b). The subjects for the analysis also received instrumented hip prosthesis that measures the hip joint contact force [Bergmann *et al.*, 2001]. The maximum predicted and measured contact force differed by an average of only 12 %. This is the first verified optimisation model of the hip joint.

The hip joint contact force for ascending and descending stairs, standing on one leg, knee bend and standing and sitting down has been reported in the region of 1.4 to 2.6 BW (Table 2.2) [Bergmann *et al.*, 2001]. Fast jogging load was reported to be as high as 5 BW [Bergmann *et al.*, 1993]. However, the highest peak contact force has been measured to occur during uncontrolled activity. Stumbling produced the highest load between 7.2 and 8.7 BW [Bergmann *et al.*, 1993]. Subsequent efforts to reproduce this load through controlled activities failed.

The frontal angle (angle on the coronal plane between the vertical and direction of force) of joint contact force showed small variations for walking (Table 2.2). The angle has been reported to have a small variation between 15 and 25 degrees [Rydell, 1966; Bergmann *et al.*, 1993]. Even during stumbling of the patient, the frontal angle was in this range. The frontal angle of joint contact force remains small for other activities. Bergmann *et al.* (2001) measured 12-16 degrees for eight different activities (slow walking, normal walking, fast walking, up stairs, down stairs, standing up from sitting position, sitting down from standing position, and knee bend) and 7 degrees for one-legged stance.

For walking, the transverse angle (angle on the sagittal plane between vertical and the direction of force) measured by Bergmann *et al.* (1993) showed a much larger variation, -6.5 to 24 degrees (Table 2.2). Bergmann *et al.* (2001) showed a range of values from 1-46 degrees for nine different activities (slow walking, normal walking, fast walking, up stairs, down stairs, standing up from sitting position, sitting down from standing position, standing on two legs and then lift one leg and standing on two legs again, and knee bend).

The resultant joint contact forces for walking, standing, ascending and descending stair are similar but the anterior-posterior component of the contact force was higher in the stair climbing case and hence the greater torsional load on the hip implant [Bergmann *et al.*, 1993; Bergmann *et al.*, 2001]. The transverse angle of the joint contact force is different between stair-climbing and other activities. For standing, level and going down stairs, the angles of contact force vectors are in the range of 28-35°. The greatest angle of joint contact force vector is 46° during stair climbing. The more anterior-posteriorly directed joint contact force vector during stair climbing induced the highest rotational moment on the femoral head on the horizontal plane.

Up to now, it is still not possible to measure *in vivo* muscle forces directly. The various muscle forces applied in finite element models are calculated from optimisation models described earlier in this section. In Table 2.3, the muscle forces predicted by optimisation studies generally agreed that the abductors are active during walking. However, there are disagreements about other muscles that are active during the gait cycle. The magnitude of muscle forces also varies between studies. For example, Heller *et al.* (2001) and Seireg and Arvikar (1975) predicted abductor load of 1.04 BW and 2.15 BW respectively. The higher value predicted by Seireg and Arvikar (1975) could be due to failure to impose realistic upper bound constraints on the magnitudes of the muscle forces. Heller *et al.* (2001) imposed upper bound constraints for peak muscle force to below 85 % of a physiological muscle force. The force was calculated as the product of each muscle's physiological cross-sectional area (PCSA) and a physiological muscle stress of 1.0 Mpa [An *et al.*, 1989]. Prediction of muscle forces can be quite sensitive to certain changes. Rohrle *et al.* (1984) changes the muscle attachment of rectus femoris by 5 mm and this changes the predicted load of adductor longus by 55%, while hip contact force remained unchanged. In a study that use PCSA to constraint the magnitude and duration of muscle forces and activity, Brand *et al.* (1986) reported that predicted muscle forces varied by two to eight times in three analyses that used PCSA from three different sources. Inaccurate measurement of anatomic location during movement due to skin movement, prediction of inertia property, assumption of muscle forces act in straight lines and error in location of muscle attachment could potentially introduce errors to muscle force prediction.

Author	Activity	Peak joint contact force, body weight (BW)	Angle of force, Degree		Number of days post surgery	Patient age/sex (m/f)
			Sagittal plane	Coronal plane		
Rydell, 1966	Male					51
	Static one legged stance	2.5 BW		19		
	Walking					
	0.88 m/s	1.51		16		
	1.30 m/s	1.82		14		
	Female					56
	Walking					
	1.1 m/s	2.69 BW		21		
	1.4 m/s	3.27 BW		19		
English and Kilvington, 1979	Walking					59 years/f
	0.166 m/s (with stick)	1.85 BW			4 days	
	0.444 m/s	2.42 BW			12 days	
	0.730 m/s	2.70 BW			42 days	
Davy *et al.*, 1988	Static one legged stance	2.6 BW	$^{\alpha}$32	$^{\beta}$-15	31 days	67 years/f
	Walking with crutches- 0.5 m/s	2.64 BW	30-35	-15 – -25		
	Stair ascent	2.6 BW	20 - 90	-70 – -20		
Kotzar *et al.*, 1991	Static one legged	2.6 BW	$^{\alpha}$35	$^{\beta}$-18		
	Walking					
	0.9 m/s	2.5 BW				
	1.1 m/s	2.4 BW				
	1.3-1.4 m/s	2.8 BW				
	1.8 m/s	3.6 BW				
	Stair ascent	2.6 BW				
Bergmann *et al.*, 1993	Walking				30 months	82 years/m
	Patient EB, left side					
	0.28 m/s	2.73 BW	$^{\phi}$-6.5	$^{\gamma}$23		
	0.83 m/s	3.07 BW	9	25		
	1.38 m/s	3.69 BW	20	25		
	Patient EB, right side					
	0.28 m/s	2.82 BW	6.5	23		
	0.83 m/s	3.24 BW	18.5	23		
	1.38 m/s	4.24 BW	24	23		
	Jogging					
	Patient EB, left side					
	1.38 m/s	4.75 BW	19	26		
	1.94 m/s	4.91 BW	20	26		
	Patient EB, right side					
	1.38 m/s	4.84 BW	24.5	23		
	1.94 m/s	4.96 BW	26.5	22		
	Max. walking and jogging					
	left side	5.39 BW				
	right side	5.58 BW	15	19		
	Stumbling – 1.94 m/s	7.20 BW			12 months	
Bergmann *et al.*, 2001	Walking, slow, normal, fast				11-31 months	Typical patient. Values reported are the average of the results from a group of actual patients (51-76 years old).
	0.98 m/s	2.42	36	12		
	1.09 m/s	2.38	31	13		
	1.46 m/s	2.50 BW	30	12		
	Up stairs	2.51 BW	46	14		
	Down stairs	2.60 BW	35	12		
	Standing up	1.90 BW	16	14		
	Sitting down	1.56 BW	1	16		
	Standing on 2-1-2 legs	2.31 BW	28	7		
	Knee bend	1.43 BW	7	16		

α- Angle between the joint contact force and the plane of the prosthesis
β- Angle between the joint contact force and the neck axis
ϕ- Angle between joint contact force and the x-axis on the sagittal plane
γ- Angle between the joint contact force and the z-axis on the coronal plane

Table 2.2 Measured hip joint contact force for various activities.

Of all the optimisation studies reported in the literature, only Heller *et al.* (2001) result has been verified indirectly by comparing the predicted hip joint force and measured hip joint force [Bergmann *et al.*, 2001], which gave a good correlation. In comparison to other studies shown in Table 2.3, the predicted muscle forces are generally less than 1.1 BW while other studies have predicted muscle forces greater than 2 BW. Although it is not possible to measure directly the muscle forces predicted by Heller *et al.* (2001), the verification of the joint contact force at least gives more confidence to the magnitude of muscle forces predicted by this study in comparison to others. In this thesis, the muscle forces predicted by Heller *et al.* (2001) and the joint contact force measured by Bergmann *et al.* (2001) were used in the analysis.

Authors	Main muscle active during stance phase of gait (Magnitude*BW)	Percentage gait cycle at peak joint contact force, %
Seireg and Arvikar, 1975	Abductor Hamstrings (2.16) Quadriceps (1.09)	15%
Crowninshield *et al.*, 1978b	Gluteus maximus (2.0) Gluteus medius (2.0) Gluteus minimus (0.85) Vastus (2.0) Semitendinosus (0.42) Semimembranosus (0.8)	At maximun joint contact force, 20% cycle
Rohrle *et al.*, 1984	Rectus femoris (1.7) Obturatoris externus (1.1) Iliacus (0.56) Adductor longus (0.19)	30% (first maxima)
	Sartorius (0.5) Rectus femoris (3.17) Obturatoris externus (1.1) Adductor longus (0.96)	66% (peak)
Heller *et al.*, 2001	Abductors (1.04) Biceps femoris (0.041) Semimembranosus(0.342) Tensor fascia lata(0.19) Vastus lateralis(0.94)	20%

Table 2.3 Muscles forces acting on the hip joint predicted during peak joint contact load.

2.6 Comparison of measured and calculated forces with the loads used in finite element analysis of the human femur

Most finite element analysis applied the joint contact force and abductor muscle force as the loads on the femur [Yettram, 1989; Van Rietbergen *et al.*, 1993; Skinner *et al.*, 1994; Weinans *et al.*, 1994]. Some investigators considered other muscles loads as well [Rohlmann *et al.*, 1983; Cheal *et al.*, 1992; Ramaniraka *et al.*, 1996; Duda *et al.*, 1997; Duda *et al.*, 1998].

Assuming a patient who weights 700 N [Stolk *et al.*, 2001], the joint contact force measured by Bergmann *et al.* (2001) (value used in this thesis) during walking is about 1630 N. Hip contact force in the region of 1500 and 2000 N has been applied in some finite element models [Ramaniraka *et al.*, 1996; Turner *et al.*, 1997]. However hip contact force as high as 3000 N has

also been used [Weinans *et al.*, 1990; Skinner *et al.*, 1994]. It is felt that in the immediate postoperative period, a patient who received cementless hip stem is likely to have the support of crutches to lighten the joint contact force. It is reasonable to apply the joint contact load measured from the patients who are already walking without support. This is likely to be representative of the maximum load that patients in the immediate postoperative period is likely to encounter. For finite element analysis studying the longer term behaviour of the implanted proximal femur, the higher hip joint contact force of 3000 N could be representative. It has been measured that fast walking and jogging could load the hip joint to about 3.5 to 5 times BW [Bergmann *et al.*, 1993].

The muscle forces applied in finite element studies are very different from one study to another. The most common applied muscle force is the abductor muscle force. The highest values applied in finite element studies are in the region of 2000 and 2500 N [Rohlmann *et al.*, 1983; Skinner *et al.*, 1994; Mann *et al.*, 1995]. Mann *et al.* (1995) applied the abductor force taken from Paul (1967), which did not impose constraint on the maximum muscle stress or force and could lead to an unphysiological muscle force. In this thesis, the abductor muscle force during walking is about 717 N [Heller *et al.*, 2001], more similar in magnitude to some other finite element studies [Weinans *et al.*, 1994; Duda *et al.*, 1998; Stolk *et al.*, 2001]. At the gait cycle of 45% corresponding to peak joint contact force, Stolk *et al.* (2001) applied the forces of gluteus medius (anterior part), gluteus medius (posterior part), gluteus minimus and tensor fasciae latae of 95, 227, 145 and 96 N respectively. These are the abductor muscles forces acting at the greater trochanter. The forces were derived from optimisation study that imposed a constraint on how long muscle can be active given a certain muscle stress [Brand *et al.*, 1986]. It is possible that this optimisation criterion has reduced the muscle forces in order to maintain the muscle activity for a longer period of time. The magnitude of vastus lateralis applied here is 650 N. The magnitude applied by Stolk *et al.* (2001) is lower at 244 N, at gait cycle of 45%. It is generally acknowledged that it is difficult to be certain of the loads to be applied to finite element models due to uncertainty in optimisation model that calculates the muscle and hip joint contact forces. However, optimisation data from Heller *et al.* (2001) is at least verified for the magnitude and general trend of the joint contact force. It is felt that this is the best combination of muscles and hip joint force data available at the moment. Similar magnitudes of joint contact and muslce forces applied in this thesis have also been reported in other finite element studies.

Finite element studies have suggested that full set of muscle forces may not be necessary to study the mechanical environment of the femur up to the intertrochanteric level. In a finite element study by Duda *et al.* (1998) comparing the femoral strain at the intertrochanteric level, a full muscle model and a model with only joint contact, abductors and iliotibial band differs only by less than 3%. However, at subtrochanteric level, strain may change significantly in the absence of adductors force. In a similar study, Stolk *et al.* (2001) studied the effect of muscles forces on the strain distribution in the stem and the implanted femur. They concluded that small differences

existed from the proximal diaphyseal femur to the intertrochanteric region when a simple loadcase consisted of joint contact and abductors forces was compared with model that applied the full set of muscles forces acting on the femur.

Chapter 3 Cementless total hip arthroplasty

3.1 Total hip arthroplasty

Total hip arthroplasty (THA) is the most common form of joint replacement. Total hip arthroplasty is the replacement of the hip joint with an acetabular component and a femoral component. The femoral component is inserted into the femur to transfer load from the pelvis to the femur. The acetabular component is fixed to the acetabulum and provides the bearing for the femoral component head. The early development of total hip replacement can be traced back to pioneering work by Charnley (1960). His early conception of total hip arthroplasty was to provide 10 or more years of service for patients older than 65 years old. The restriction to older patients was to minimise the possibility of implant failure and the need of revision surgery. Activities were also limited to avoid high stresses that would lead to implant failure [Charnley, 1960]. This procedure is deemed to be unsuitable for younger or more active patients as failure of implant is more likely.

Charnley's concept of THA was a great success and patients gained tremendous relief of their hip disease. Implant survival was also much better than initially imagined. This led to more studies of the THA technique and eventually the procedure was extended to younger, physically active patients and for an ever-increasing variety of conditions [Tate Jr. and Sculco, 1998].

Initially, fixation of the acetabular and the femoral components was achieved using bone cement (polymethylmethacrylate or PMMA). This class of cemented femoral components is normally referred to as cemented hip stems. However, the low strength of cement made it vulnerable to high stress in the cement mantle and this led to cement mantle fracture and ultimately components loosening [Stauffer, 1982]. Cement failure is critical among physically active patients. However, over the years, improvement in cementing technique has also improved the long-term survival of the cement mantle [Stauffer, 1982; Tate Jr. and Sculco, 1998].

The early cementing technique has been shown to have a high rate of loosening [Stauffer, 1982; Neumann *et al.*, 1994], and this led to the search for alternative fixation techniques. This led to the development of a class of femoral components normally referred to as the cementless hip stems. The fixation is achieved by bone ingrowth onto the surface of the hip stems. Various surface finishes, coatings and amounts of coverage of the femoral stem with these materials have been employed in an attempt to improve ingrowth of bone into these stems. With some cementless stems, good clinical results have been reported while some stems give poor results [Neumann *et al.*, 1994]. However, clinical results with state of the art cementing technique have shown very good results as well [Mjoberg, 1991; Tate Jr. and Sculco, 1998]. This thesis is primarily on initial stability of cementless hip stems, and therefore, this review concentrates on cementless hip stems.

3.2 Clinical result of cementless femoral hip stem

The report from the Swedish National Hip Arthroplasty Registry [Malchau *et al.*, 2000] compared the performance of cemented and cementless hip stem between the period of 1979 to 1998. The report divided the study into the periods between 1979 to 1987, 1988 to 1998 and 1992 to 1998. The cemented stems implanted between 1979 and 1987 were considered to be using the first generation cementing technique while those implanted after 1987 were using modern cementing technique. For the cementless stem, the period between 1992 corresponding to introduction of modern uncemented technology, with the majority of the stems having hydroxyapatite (HA) coating or textured titanium surfaces. The performance of cemented stems is generally better than cementless stems. For stems implanted between 1979 to 1987 into osteoarthritic patients, the survivorship of cemented and cementless stems were 82.1 and 61.9 % respectively for follow-up period of 19 for the former and 15 years for the latter. For the period from 1992 to 1998, the survivorships were 98.0% for the former and 95.2% for the latter for follow-up period of 6 years. The performance of early cementless stems are clearly disappointing. However, improvement in cementless technology can be seen from the reduction in revision after 6 years postoperatively. The 1979 cohort reported revision rate of 8% and the 1991 cohort reported revision rate of 4% after 6 years. Longer follow-up is needed to judge the long-term performance of cementless hip stem. Improvement to cementless stems is needed to bring it on par with the success of cemented stems. However, in comparison to cemented stems in this study, more cementless stems were implanted into younger and more active patients, which could increase the risk of aseptic loosening.

Cementless hip stems can give good clinical results if proper stem design and surgical techniques are used [Engh *et al.*, 1990]. Engh *et al.* (1990) reported that for a ten years follow-up study involving 959 cases, the survivorship is 96.4% using revision as the measure of survivorship. Only 1% of these cases are due to mechanical failure like stem fracture (0.4%) and failure to achieve biological fixation stability (0.6%). Two-thirds of the stems that were revised due to fixation failure as a result of grossly undersizing stems, which are no longer used. The reason for other revisions were not mentioned, but it could be due to excessive pain. Using revision and failure to achieve biological implant stability (no biological fixation and no excessive subsidence or rotation of stem) as the survivorship criteria, the survivorship is down to 90.8%. This study also reported that the survivorship rate is 94.9 % in patients younger than 40 years old in a follow-up study between 2-7 years. The revisions that were due to failure of biological fixation were due to grossly undersized stems. In contrast, the revision rate of the stems in older patients (older than 65 years old) improved to 98.6 % in a follow-up between 2-8 years.

Engh *et al.* (1990) demonstrated the importance of proper sizing of stems and surgical technique. The importance of the size of implant was demonstrated in the comparison between

fully coated and partially coated stems. The partially coated stems were newer and different sizes were available. In comparison, some of the fully coated stems were only available with one size initially. The survivorship of the partially coated stems were 98.1% and the fully coated stem was 90.8% using revision and loosening as the failure criteria. Of the stems that achieved bone ingrowth at ten years, only 4 out of 849 cases were revised, and those revised were due to fractured stems. Out of the 110 stems that did not achieve bone ingrowth, 73% of the stems were stable due to bone-fibrous tissue encapsulation. The introduction of underreaming the canal also improved the bone ingrowth from 90.4% to 97.6% of the cases. This study demonstrated that with proper sizing of implants and surgical technique, cementless stem results can be very good. In another study, long-term revision rate at 12 years follow-up was reported to be 97 % and this is very encouraging [Engh and Culpepper, 1997]. Both studies used the anatomic medullary locking (AML) stems.

Martell *et al.* (1993)'s results are comparable to Engh *et al.* (1990) results for a series of fully coated hip that has some stems with less than optimal size, but inferior to another series of proximally coated stems which has different sizes for optimal fit and fill. Using Harris-Galante stem instead of AML stem, this study reported survivorship of 97% over a period of five years using revision as the failure criteria. However, during the corresponding period, survivorship was only 90% if revision and loosening is used as the failure criteria. Similar to Engh's *et al.* (1990) study, the loose stems have lower metaphyseal and diaphyseal fill than the stable stems. Higher limping rate was also associated with lower fill in this study. In addition to fill, better fit has also been associated with successful implants, in agreement with another study [Engh *et al.*, 1987]. Some of the loosening in this study was also associated with loosening of porous coating from the stem and femoral fracture. Of the 10 (8%) femurs fractured during surgery, 2 stems were loosed, although none was revised.

Hozack *et al.* (1993) compared two groups of patients implanted with similar stems, with one group having cement fixation (71 stems) and the other group having proximal porous coated surface for biological fixation (70 stems). The Charnley pain score was similar for both groups, but the Charnley function score was significantly higher for the cementless group. One revision was reported for the cemented group while none was reported for the cementless group. The period of observation was between 2 to 6 years postoperatively, and clinical performance of cementless and cemented stem were comparable. However, using the same design of a cementless stem may not be the best stem for cemented fixation. In another study, a consecutive series of 36 patients underwent primary cemented THA followed by primary cementless THA of the contralateral hip [Hearn *et al.*, 1995]. The patients reported similar pain scores in both hips. This comparison of results of this study eliminated the variability introduced by differences in sexes, weight, bone quality and activity level. Rorabeck *et al.* (1996) reported that in their study comparing cemented to cementless total hip arthroplasty, no statically significant difference in any of the health related

quality of life measures used when patients with cement were compared with patients without cement at mean follow-up period of 4.8 years. With good clinical practice and stem designs, cementless stem can give good clinical results.

The use of a smooth surface hip stem without hydroxyapatite or porous coating have been shown to perform inferiorly to porous-coated or HA coated stem [Freeman and Plante-Bordeneuve, 1994; Lombardi *et al.*, 1995; Donnelly *et al.*, 1997; Incavo *et al.*, 1998]. Incavo *et al.* (1998) reported better Harris hip scores with HA-coated stems in comparison to smooth stems. Donnelly *et al.* (1997) reported more radiolucent lines and higher migration were observed in smooth press-fit stems as compared to hydroxyapatite-coated stems. Freeman *et al.* (1994) reported that a smooth press-fit prosthesis has a high rate of migration and loosening in comparison to cemented or hydroxyapatite-coated stems, and has discontinued the use of smooth stems. Lombardi *et al.* (1995) reported poor survivorship of 78% in their series of smooth stems in a mean study period of 31 months, although the fill of the stem was good. The use of this stem has been discontinued.

3.3 Failure of cementiess hip stem

The long-term success of cementless total hip arthroplasty depends on a few factors: fixation of femoral component, fixation of acetabular component, wear of the bearing surface and prevention of infection. This section looks at the failure of fixation of the femoral component in cementless total hip arthroplasty.

Fixation of the femoral component can be defined as having achieved bone ingrowth or fibrous tissue ingrowth that will provide stability to the hip stem [Engh *et al.*, 1990]. Stable bony ingrowth is normally deduced from the absence of a radiolucent line on the radiograph. Radiographic features for stable fixation include either no implant migration or minimal initial subsidence that ceases after the first year of observation [Engh *et al.*, 1990; Mjoberg, 1991] and a stable radiolucent line that does not widen with time if fixation is achieved by stable fibrous tissue ingrowth [Engh *et al.*, 1990]. However, fixation by bony ingrowth is more likely to result in a totally pain-free hip [Engh *et al.*, 1987]

Failure of fixation of the cementless femoral hip stem can be caused be a number of factors: high implant relative micromotion [Pilliar *et al.*, 1981; Pilliar *et al.*, 1986; Aspenberg *et al.*, 1992; Soballe *et al.*, 1992b; Bragdon *et al.*, 1996], poor surgical fit and fill [Engh *et al.*, 1990; Cook, 1991; Martell *et al.*, 1993], osteolysis at the bone-stem interface due to wear debris [Schmalzried *et al.*, 1992; Wan and Dorr, 1996; Tate Jr. and Sculco, 1998], and the absence of porous-coating and/or hydroxyapatite coating for bone ingrowth [Lombardi *et al.*, 1995; D'Antonio *et al.*, 1997; Donnelly *et al.*, 1997; Incavo *et al.*, 1998; Tate Jr. and Sculco, 1998]. Failure of fixation due to

high implant relative micromotion and poor surgical fit and fill are discussed in more details in Section 3.8.

Osteolysis of bone-stem interface is normally caused by migration of polyethylene wear debris generated from the articular surface of the acetabular cup to the bone-stem interface and to a lesser extent wear of stem itself [Schmalzried *et al.*, 1992; Wan and Dorr, 1996; Tate Jr. and Sculco, 1998]. Wan and Dorr (1996) reported that osteolysis at the bone-stem interface is correlated to the amount of polyethylene wear from the acetabular component. Bone loss progress is slow in existing sites and faster in new osteolytic sites. Osteolysis can cause the lost of bone support and loosening of the implant. Debris has been seen on the surface of extracted prosthesis from femur with sign of osteolysis [Karrholm *et al.*, 1994a]. In areas of bone resorption, intra- and extracellular particles of polyethylene, metallic and polymethylmethacrylate or bone cement (only if the cup is cemented) debris was found in and around the macrophages [Schmalzried *et al.*, 1992].

Infection can cause serious problems in total hip arthroplasty. If the implanted femur has serious infection, it may need a revision surgery to remove the hip stem and disinfect the femur. This is a serious complication in the past, but with the use of antibiotic and laminar air flow in operating theatre, infection rarely occurs in modern day total hip arthroplasty [Tate Jr. and Sculco, 1998].

3.4 Migration of hip stem

Migration of hip stem refers to the permanent displacement of hip stem relative to the femur. The displacement can be permanent displacement in the proximal-distal direction, or rotation in the anterior-posterior and lateral-medial directions. Migration of hip stem has been observed in both cemented [Mjoberg *et al.*, 1986; Freeman and Plante-Bordeneuve, 1994; Kiss *et al.*, 1996; Alfaro-Adrian *et al.*, 1999] and cementless stems [Nistor *et al.*, 1991; Kroon and Freeman, 1992; Karrholm and Snorrason, 1993; Soballe *et al.*, 1993b; Freeman and Plante-Bordeneuve, 1994; Karrholm *et al.*, 1994b; Kiss *et al.*, 1996;.

Migration is fastest in the early postoperative period (about six months) [Mjoberg *et al.*, 1986; Nistor *et al.*, 1991; Freeman and Plante-Bordeneuve, 1994; Kiss *et al.*, 1996; Alfaro-Adrian *et al.*, 1999]. Mjoberg *et al.* (1986) reported most rapid migration occurred in the first 4 months postoperatively. Nistor *et al.* (1991) reported lower migration rate of 0.41 mm at 3 months postoperatively when patients were only partial weight bearing. Upon full weight bearing between 3 and 6 months postoperatively, migration was highest at 0.61 mm. Migration after 9, 12 and 15 months postoperatively decreased in each of the three month period (0.47, 0.35 and 0.24 mm). Lower linear migration after the initial 6 months postoperative period has been reported [Mjoberg

et al., 1986; Freeman and Plante-Bordeneuve, 1994]. Migration still occurs 8 years postoperatively [Freeman and Plante-Bordeneuve, 1994; Alfaro-Adrian *et al.*, 1999].

Some investigators have suggested that migration can be use as a predictor of future implant failure [Mjoberg, 1991; Freeman and Plante-Bordeneuve, 1994; Karrholm *et al.*, 1994a; Walker *et al.*, 1995]. In hip stems that failed and subsequently needed revision, higher migration rates were measured both in the early postoperative period and during longer-term observation [Nistor *et al.*, 1991; Karrholm and Snorrason, 1993; Freeman and Plante-Bordeneuve, 1994]. Mjoberg (1991) observed that stems with high migration rates may be loose from the early postoperative period and the consequence of the loose stem is high migration rate that will lead to revision surgery later on. Freeman suggested that beyond a migration threshold of 1.2 mm/year, a hip stem is likely to fail. Pain in the thigh is also more likely as total migration increases with time [Karrholm and Snorrason, 1993; Freeman and Plante-Bordeneuve, 1994]. A possible implication of a high rate of migration is that the stem has never achieved stable fixation [Mjoberg, 1991; Freeman and Plante-Bordeneuve, 1994].

A mechanism of hip stem migration in cemented and cementless hip stem has been proposed as the failure of the supporting interface cancellous bone [Taylor *et al.*, 1995; Taylor, 1997]. Finite element analysis of the Freeman stem has shown that interface cancellous bone stress correlated to *in vivo* stem migration data [Taylor *et al.*, 1995; Taylor, 1997]. Due to repeated load cycles *in vivo,* the failure of supporting cancellous bone may not be due to high stress plastic failure, but due fatigue failure of bone. If the repair of bone is slower than damage to bone due to fatigue, the stem would migrate slowly as the supporting interface bone fail. The correlation between interface bone stress and implant migration has also been shown at the tibia tray [Taylor *et al.*, 1998; Perillo-Marcone, 2001]. This study looked at the bone stress below the tibia tray in total knee arthroplasty using four patient specific tibia models. The *in vivo* migration data of the patients corresponds to the risk ratio calculated from the models. The risk ratio was defined as the ratio of stress over ultimate strength.

3.5 Fixation of femoral component with porous-coated stems and hydroxyapatite-coated stems

Cementless hip stems achieved fixation by having bone ingrowth at the bone-stem interface. Stem surface is coated with metallic beads to allow bone ingrowth. Bone grows into the pores on the surface of the stem and the stem is anchored to the bone mechanically. However, bone ingrowth on the stems was shown to be limited and some stems exhibited only fibrous tissue ingrowth [Cook, 1991; Engh *et al.*, 1993-1994].

To improve bone ingrowth, surface coatings like hydroxyapatite coating were applied on the surface of hip stem to enhance bone ingrowth [Sun *et al.*, 2001]. Chemically, hydroxyapatite is

similar to the mineral phase of bone. Hydroxyapatite is osteoconductive, a property which encourages bone already being formed to lie closely to or adhere to it. In the body, partial dissolution of hydroxyapatite coating releases calcium and phosphate ions, which encourages and speeds-up the formation of new bone on the surface of hydroxyapatite coating [Sun *et al.*, 2001].

The advantages of hydroxyapatite coated implants are (a) the faster initial fixation and stronger bonding between the host bone and the implant, and (b) more uniform bone ingrowth at the bone-stem interface [Sun *et al.*, 2001]. Hydroxyapatite coating was reported to enhance bone growth across a 1 mm gap at the bone-stem interface under stable and unstable mechanical conditions, capable of limiting formation of any fibrous membrane and converting a motion-induced fibrous membrane into a bony anchorage [Soballe *et al.*, 1992a; Soballe *et al.*, 1992b; Soballe *et al.*, 1993a]. Soballe and Overgaard (1996) also reported that hydroxyapatite coating around the proximal stem can reduce migration of wear debris from the articular surface to the bone-stem interface, which may reduce the incidence of osteolysis and the subsequent implant failure. Another important advantage of hydroxyapatite coating could be the effectiveness of hydroxyapatite coating to encourage bone growth which is improved under load [Mouzin *et al.*, 2001].

The use of hydroxyapatite coating has not been universally adopted due to concerns with its long-term stability [Dalton and Cook, 1995; Soballe and Overgaard, 1996] and threat of coating delamination that generates particulate debris [Bauer *et al.*, 1991]. One of the main concerns of the use of hydroxyapatite coating is the resorption and degradability of hydroxyapatite coating in a biological environment, which could lead to disintegration of the coating, resulting in the loss of both the coating-substrate bond strength and the implant fixation [Sun *et al.*, 2001].

Clinically, HA-coated implants has been reported to show higher bone ingrowth compared to porous coated stem (90% compared to 83%) [McPherson *et al.*, 1995]. Migration studies have also shown that HA-coated prostheses migrated the least, which seems to suggest it is superior to just porous-coated prostheses [Kroon and Freeman, 1992; Soballe *et al.*, 1993b; Freeman and Plante-Bordeneuve, 1994; Karrholm *et al.*, 1994b]. Up to a period of 10 years, some hydroxyapatite coated stems have been reported to have no aseptic loosening [Capello *et al.*, 1997; Donnelly *et al.*, 1997; McNally *et al.*, 2000].

3.6 Stress transfer from hip stems

The transfer of load from hip stem to the femur is one of the most important functions of a femoral hip stem. Depending on the type of hip stem, the load transfer pattern could be different. Huiskes (1990) looked at the stress patterns and load transfer mechanisms for four different kinds of hip stem fixation (cemented, fully porous coated, proximally porous coated and press-fit) and two types of materials with different stiffness (cobalt chromium molybdenum alloy and titanium).

The fully porous coated and proximally coated stems are considered to have perfect bonding at the bone-porous coating interface. The press-fit stem was considered to have no bone ingrowth. The FE models were two dimensional side-plates models.

In the cemented and fully porous coated (fully ingrown) stems, the stems were loaded in bending. The medial side was under compression and the lateral side was under tension (Figure 3.1). The maximum stress in the stem occurred at the proximal third of the cemented stem. The maximum stress in the stem in the fully coated stem was lower due to the bulkier size and occurred more distally at the midstem. The bending characteristics for both bonded cases were similar to a cantilever beam in bending.

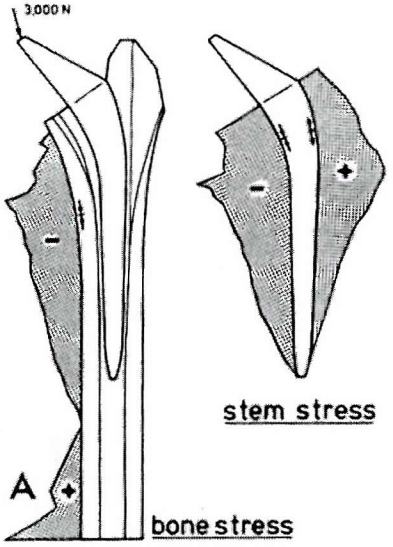

Figure 3.1 Bending stresses at the medial periosteal bone surface and at the medial and lateral faces of the stem for applied joint contact force of 3000N. Positive represents tensile and negative represents compressive stress. [Huiskes, 1990].

The interface stresses in the fully bonded models showed load transfer to the bone occurred proximally and distally (Figure 3.2). Stress was transferred through normal and shear stresses. The strongly tapered shape of the cemented stem gave a high proximal-medial stress concentration. The stiffer fully coated (fully ingrown) stem showed a similar stress distribution as the cemented stem, but the stiffer stem caused the proximal-medial stress to be lower and the distal-lateral stress to be much higher. Therefore, the stiffer stem transferred more load distally. This is also true for increase in stem stiffness due to the use of stiffer material in the stem.

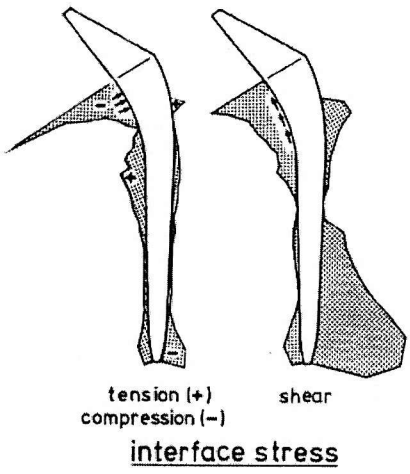

Figure 3.2 Stem-cement interface stresses of a cemented hip stem. The interface stresses are resolved into normal stress (tension and compression) and shear stress. [Huiskes, 1990].

The proximally coated stem transferred load at the distal end of the porous coating. This is in agreement with a finite element study by Skinner *et al.* (1994) and clinical study by Turner *et al.* (1986). The interface stress at the calcar was similar to the fully bonded models. The interface stress at the distal end of the porous coating and distal to the porous coating was similar to the cemented stem model. At the distal end, the interface stress was lower compared to the fully coated stem model.

Load transfer in a press-fit (no bone ingrowth) stem is different from the bonded stem. Press-fit stems can only transfer load through compression and shear (from friction). The press-fit stem has to transfer load through elastic subsidence into the femur, to generate compressive and shear stresses to equilibrate the axial load. The compressive component is likely to be much higher than the shear component. The bonded stem transfers load predominantly through shear at the interface. Huiskes (1990) assumed zero friction for smooth press-fit stem and therefore no load is transfered through shear at the interface. Therefore in the press-fit model, the compressive interface stresses were shown to be about 3 to 7 times greater than bonded models. The higher interface compressive stress has also been reported in a three-dimensional study using a physiological implanted femur model, which reported three times increases in minimum principal stress at the interface cancellous bone of the press-fit stem in comparison to the cemented or porous coated stems [Taylor *et al.*, 1995].

In the press-fit stem model, interface stresses no longer concentrated in the proximal and distal region (Figure 3.3a). The compressive interface stress is spread over regions of contact. Subsidence of the femur was resisted by the calcar, and therefore the lateral midstem was pushed towards the lateral endosteal bone (Figure 3.3c). The bending of the stem was similar to four point bending (Figure 3.3b). The cortical bone stress was found to be higher than those around the bonded stems. At the midstem, the cortical bone stress was 3 times greater than the cemented stem.

In reality, the loading and load transfer mechanism as described by Huiskes (1990) is a simplified version of reality. *In vivo*, the implanted femur would be loaded by other muscles as well. The joint contact force and the muscles forces do not act only in the frontal plane, but also out of plane to create a three-dimensional bending and also a torsional effect.

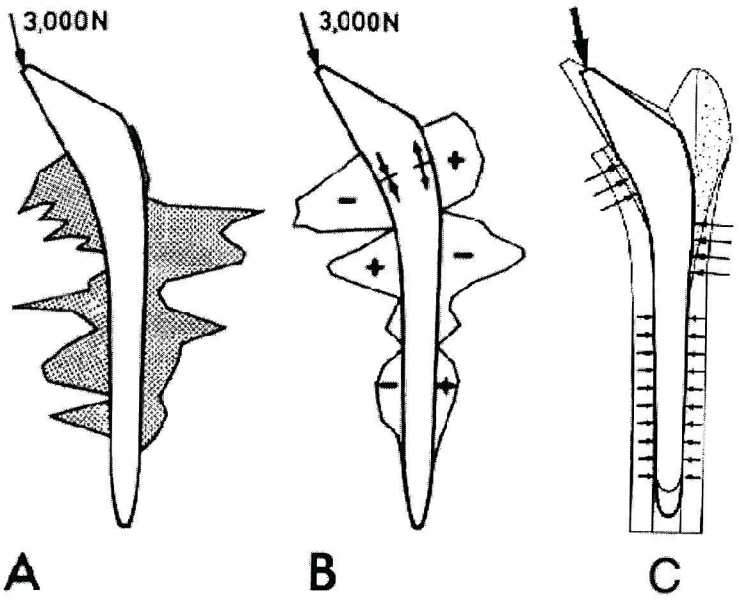

Figure 3.3 The press-fit stem loaded by joint contact force. (A) Compressive interface stresses. (B) Stem bending stresses. Positive represents tensile and negative represents compressive stresses. (C) Subsiding mechanism of the press-fit stem. Subsidence of the femur was resisted by the calcar, and the lateral midstem was pushed towards the lateral endosteal. This is the cause of the high compressive stress at the proximal medial and lateral midstem shown in A. [Huiskes, 1990].

3.7 Stress shielding and bone remodelling of the implanted proximal femur

As a result of the changed path of load transfer in the implanted femur, the stress distribution in the implanted femur after total hip arthroplasty is different from that of the intact femur. This can initiate adaptive bone remodelling which can lead to either bone resorption or bone hypertrophy, depending on the difference in the stress state of the implanted proximal femur relative to the intact femur [Beaupre *et al.*, 1990; Weinans *et al.*, 1993; Weinans *et al.*, 1994; Kerner *et al.*, 1999]. The sharing of load between femur and the hip stem leads to a state of lower femoral stress in comparison to the intact femur is called stress shielding. Stress shielding is more severe proximally than distally. Towards the more distal region, most or all load has been transferred to the femur, and therefore the stress state will be closer to the intact femur. Clinically, resorption and loss of density of the proximal cortex is seen on radiographs [Engh *et al.*, 1990; Engh *et al.*, 1992a; Toni *et al.*, 1996; Bugbee *et al.*, 1997].

Both finite element analysis and experimental studies have been used to study the periosteal strain or stress in intact and implanted femoral [Skinner *et al.*, 1994; McNamara *et al.*, 1997]. In a finite element analysis, Skinner *et al.* (1994) reported 80% reduction in compressive stress in the calcar region of the implanted femur in comparison to an intact femur. However, at the distal end

of the stem, the compressive stress was found to be similar in the intact femur and when implanted with a fully coated stem. The proximally coated stems were found to have much larger stresses, possibly due to rotation of the non-bonded tip causing high compressive stress. A combined experimental and finite element study also showed that periosteal stress shielding occurred along the entire length of the hip stem [McNamara *et al.*, 1997]. At the calcar region, 70% reduction in stress has been measured for a fully bonded stem both experimentally and using finite element techniques. This value is close to the value reported by Skinner *et al.* (1994). The reduction is less for non-bonded press-fit stems at about 40%. Stress shielding reduces in the proximal-distal direction for both press-fit and fully bonded stems. A proximally bonded model with loose distal fit showed stress shielding at the proximal 20% of the stem. In contrast, a proximally bonded stem with tight distal fit showed more extensive stress shielding than between the press-fit stem and the proximally bonded stem with a loose distal fit.

Patient specific adaptive finite element models have been used to study the stress shielding of the implanted femur obtained from autopsies of five patients [Kerner *et al.*, 1999]. The contralateral femur was assumed as the preoperative condition and difference in strain energy was used as the remodelling stimulus. The simulated radiographic images were compared with clinical radiographs. Kerner *et al.* (1999) has predicted proximal bone loss and retention of distal bone, in agreement to radiographic images of the same patients in which the models were derived from. Bone hypertrophy at the distal tip of the stem was also predicted, but was not seen in the radiographic image. The model, in agreement with clinical radiographs, also predicted densification of bone at the proximal lateral side of the stem. Similar to the radiographs, the region proximal to the porous coating and smooth surface border of the stem showed pronounced bone loss. It is found that bone-remodelling model can predict areas of bone loss and gain reasonably well, but the exact amount of remodelling is still overestimated in this model. The authors suggested that this overestimation could be due to our inadequate understanding of the remodelling law. The prediction of proximal periosteal bone loss in this study is consistent with the lower proximal periosteal bone stress measured in other studies [Skinner *et al.*, 1994; McNamara *et al.*, 1997].

The severity of stress shielding has been linked to stiffness of stems. Finite element analysis has shown that the stiffer stem transferred more load distally [Huiskes, 1990; Cheal *et al.*, 1992; Huiskes *et al.*, 1992]. Huiskes *et al.* (1992) predicted that a flexible stem which was five times more compliant than a titanium stem has 50% less bone loss due to stress shielding. However, the proximal interface stress is also higher in the more compliant stem, which may break the interface bond. Similar high proximal interface stress and periosteal stress shielding has been reported [Cheal *et al.*, 1992]. Periosteal stress has been reported to be lower in cemented stem in comparison to bulkier and more rigid cementless stem [Huiskes, 1990]. Animal experiment has shown that more compliant stems do cause less stress shielding [Bobyn *et al.*, 1990].

A situation that can lead to really bad stress shielding and dramatic proximal bone loss (up to 90%) is the jamming of distal stem within the diaphyseal femur [Weinans *et al.*, 1994]. In this case, the proximal contact between the stem and the femur is loose. This loose proximal fit and tight distal fit situation lead to most loads being transferred in the distal tip of the stem. This situation is called stress bypass [Weinans *et al.*, 1994]. Clinically, it has been observed that loose distal stems caused less proximal bone resorption in comparison with well fixed distal stems [Engh and Bobyn, 1988]

Although stress shielding appeared to be bad, there is no conclusive proof that it is detrimental to hip stem survivorship [Engh et al., 1990; Bugbee et al., 1997]. Clinically, some severely stress shielded femurs still support hip stems without problems, and did not seem to affect clinical pain rating [Engh *et al.*, 1987]. Bugbee *et al.* (1997) reported in their group of patients which showed stress shielding, have less revision surgery in comparison with the larger parent group of patients. However, there is concern that severe reduction of bone stock due to stress shielding will increase the risk of femoral fracture both *in vivo* and also if revision surgery is needed to replace a hip stem. A study has suggested that bone remodelling due to stress shielding stops after about two years [Engh *et al.*, 1987].

3.8 Relative motion at the bone-stem interface

Other than changes to bone density due to stress shielding, fibrous tissue formation at the bone-stem interface has been observed in clinical and animal studies (Section 3.8.1). This is not attributed to the stress changes after proximal implantation of the hip prosthesis, but is attributed to the relative motion between the bone and the hip stem. Formation of fibrous tissue instead of bone ingrowth has direct consequences on the long term stability of the hip stem.

3.8.1 Bone ingrowth or formation of fibrous tissue at the bone-stem interface: Clinical and animal studies

Clinical radiographic and histologic evaluation of retrieved human cementless porous coated stems revealed that 100 percent bone ingrowth into porous coating is not achieved clinically [Engh *et al.*, 1987; Cook *et al.*, 1988; Cook, 1991]. Most of the cementless hip stems have a combination of bone and fibrous tissue attachment on the porous coating. Radiographically, formation of fibrous tissue appears as a thin radiolucent line parallel to the surface of the stem [Engh *et al.*, 1987; Engh *et al.*, 1990]. However, the absence of radiolucent lines should not imply that bone ingrowth has occurred, although the chance of bone fixation is higher [Engh *et al.*, 1990].

Animal studies have been used to quantify the micromotion threshold that would lead to fibrous tissue formation [Pilliar *et al.*, 1981; Pilliar *et al.*, 1986; Aspenberg *et al.*, 1992; Soballe *et al.*, 1992b; Bragdon *et al.*, 1996]. These studies found that micromotion greater than 150 μm led to

tissue encapsulation of the prostheses. In a canine study, Bragdon *et al.* (1996) showed that micromotion below 20 μm still allowed bone ingrowth. Micromotion between 20 and 40 μm had a combination of bone and fibrous tissue ingrowth. The interface stiffness 6 weeks after the surgery is the same for implants that have 0 and 20 μm micromotion. The implant with 40 μm micromotion has interface stiffness that was about half the interface stiffness of the 0 and 20 μm implants. The 150 μm implants have the lowest stiffness.

Biological active coating like HA coating can change the amount of bone ingrowth and the property of fibrous tissue that grows onto the implant [Soballe *et al.*, 1992b]. Soballe *et al.* (1992b) implanted cylindrical porous and HA coated implants into dogs. The implants either have zero micromotion or 500 μm micromotion. Push out test showed that the HA coated stable implant has the highest shear strength, while the stable porous coated implant and the unstable HA coated implant have similar shear strength, but about 3 times lower than stable HA coated implant. The unstable porous coated implant has the lowest shear strength. The stable HA coated implant has five times more bony ingrowth than porous coated implant. In the unstable implants, no bony ingrowth was observed. The unstable HA coated implant was found to have more collagen fibres concentration than the unstable porous coated implant. The test was conducted four weeks after the surgery. Given a longer healing period, it is possible the push out test of the stable porous coated implant could show higher shear strength than the unstable HA coated implant as the interface bone matured.

Although excessive micromotion prevented bone ingrowth, stable fixation of the stem may also occur due to stable fibrous-tissue encapsulation [Engh *et al.*, 1987; Engh *et al.*, 1990]. It was reported that 72 % of the hips with no bone ingrowth achieved stable fixation [Engh *et al.*, 1990]. In an experiment involving implantation of a porous coated device in dogs, Pilliar *et al.* (1981) reported that orientation of fibrous tissue was oblique to the implant surface, which suggested load was transferred through the fibrous tissue layer. Progressive stem migration, subsidence, rotary instability, tilting or a combination of these characterizes unstable fibrous tissue fixation [Engh *et al.*, 1990].

3.8.2 Experimental micromotion study of the hip stem

Experimental measurement of the bone-stem interface relative motion in the implanted proximal femur is used to test the relative stability of different hip stem designs. It is hoped that this is translated to clinically meaningful estimates of their performance *in vivo*. Clinical verification of new designs requires a large patient sample and a bad design will impose considerable hardship on the patients. Therefore, it is desirable to have meaningful *in vitro* verification of stem design before a clinical trial is conducted. Various researchers have measured the micromotion in the implanted femur using cadaveric femurs [Walker *et al.*, 1987; Schneider *et*

al., 1989; Sugiyama *et al.*, 1989; Burke *et al.*, 1991; Phillips *et al.*, 1991; Callaghan *et al.*, 1992; Sugiyama *et al.*, 1992; Hua and Walker, 1994; Baleani *et al.*, 2000; Schneider *et al.*, 2001]. Most studies involved either axial or torsional loading conditions, or both.

Experimental micromotion studies have been performed to test stability of different designs [Schneider *et al.*, 1989; Callaghan *et al.*, 1992; Hua and Walker, 1994], methods of fixation (cemented or cementless) [Walker *et al.*, 1987; Schneider *et al.*, 1989; Sugiyama *et al.*, 1989; Baleani *et al.*, 2000] and surgical techniques [Sugiyama *et al.*, 1992]. The range of micromotion reported by these investigators varies over a wide range. Some of the values are shown in Table 3.1. Some values have been shown to be within the bone ingrowth threshold around 40-50 μm [Walker *et al.*, 1987; Schneider *et al.*, 1989; Callaghan *et al.*, 1992; Sugiyama *et al.*, 1992; Baleani *et al.*, 2000; Monti *et al.*, 2001], while some are in the order of 100-300 μm [Schneider *et al.*, 1989; Callaghan *et al.*, 1992; Sugiyama *et al.*, 1992].

Different design of cementless stem give very different micromotion values (Table 3.1). Schneider *et al.* (1989) measured the micromotion in four different cementless stem designs. The PCA stem with lateral bow has the lowest micromotion of between 9-12 μm, while two other straight stem designs with grooves have micromotions values below 56 μm. Another straight stem design has micromotion between 81 and 152 μm, which is much higher in relation to the rest. Sugiyama *et al.* (1992) tested different levels of coating and found that micromotion is not significantly affected. Hua and Walker (1994) tested a straight stem and two other stems with anterior flare, with one of them custom made to fill the femur it was implanted into. He found that the micromotions in these stems were not significantly different under walking load. However, under more torsional stair climbing load, the straight stem rotated considerably more in relation to the other two stems. Callaghan *et al.* (1992) compared a straight stem and an anatomic curved stem. Torsional load caused higher micromotion than axial load, a result similar to other investigators [Walker *et al.*, 1987; Hua and Walker, 1994]. The anatomic curved stem was found to be more resistance to torsional load in comparison with the straight stem design.

While the initial stability of cementless stems has been reported to vary across a wide range of micromotion, proper surgical procedure can reduce the micromotion. Sugiyama *et al.* (1992) reported that cementless implants inserted with an interference-fit at the femoral isthmus can reduce micromotion substantially in comparison with line-to-line fit (Table 3.1). The stems inserted with femoral isthmus underreamed were about four times more stable than stems inserted without underreaming. This showed that the technique employed by the surgeon to put in the hip stem is just as important as the shape of the stem.

Various studies have used different loading conditions, prostheses designs and variations in implantation techniques by different people, which make comparison between these studies very difficult. In Table 3.1, the test protocol shown is different from one researcher to another.

However, most studies simulated a single leg stance load and a stair-climbing load. The magnitudes and directions of these loads were different between different studies, and so were the experimental jigs. Simulated single leg stance load is normally used to study effect of axial load and stair climbing is used to study the effect of torsional load. However, most studies shared a common feature. The micromotion is measured from the displacement of a pin attached to the stem. A small hole is drilled in the femur to expose the stem and to allow the insertion of the pin into the stem. The micromotion measured is therefore not necessarily the slippage between bone and stem interface.

Sugiyama *et al.* (1989) applied rotational torque to the stem and measured the rotational stability of cemented and cementless hip stem. The torque was applied in 10 seconds and maintained for 5 seconds, before unloading that takes another 10 seconds. The micromotion was defined as the total displacement minus the residual displacement after unloading. At high torque, the subsidence (which is the final residual displacement) begins to increase rapidly and is much higher than the micromotion. The load regime is not physiological because loading rate should be much faster in bone. The non-linear rapid increase of subsidence after a certain load level in both the cementless and cemented stem suggest that bone is experiencing extensive creep deformation due to the slow loading. Therefore, the micromotion was measured from a loading that is not physiological. At low torque (5 to 10 Nm), the subsidence of the cementless and cemented stem was low. The micromotion of the cementless stem was below 20 μm at the load of 10 Nm. At about 20 Nm, the micromotion was about 60 μm. Micromotion was found to be higher than zero even at low loads for the cemented stems. This suggests that the cemented and cementless stem micromotion measured may not only be slippage at the interface, but some is due to elastic deformation of the interface bone. The micromotion of the cemented stem using second generation cementing techniques was also much lower than the stem using first generation cementing techniques. With greater penetration of cement into bone, the second generation cementing techniques is likely to create a more rigid interface, and thus lower micromotion due to elastic deformation.

For stair climbing loadcase, Walker *et al.* (1987) applied a 1000N load at 12° to vertical in the coronal plane and a 100N anterior-posterior directed load and measured the micromotion of the cemented and cementless stems. The resultant micromotion at the proximal medial stem was about 50 μm for the cementless stem and about 42 μm for the cemented stem. Upon unloading, the displacement returned close to zero, and Walker *et al.* (1987) suggested that the micromotion measured was not due entirely to slippage, but some part is due to elastic deformation of the interface bone. This suggestion is probably in agreement with the micromotion results of Sugiyama *et al.* (1989) at lower torque.

In comparison, in a micromotion study using retrieved implanted femurs, Engh *et al.* (1992b) reported that when midstance and stair climbing loads were applied to the implanted femur, micromotion was less than 40 μm for stems well fixed by bony ingrowth and was 150 μm for stems stabilized by fibrous tissue ingrowth. This is interesting as it shows that even the interface bone of stem well fixed by bony ingrowth deformed elastically when loaded.

Baleani *et al.* (2000) reported that stable micromotion with very small permanent displacement can be achieved after the cementless stem has been repeatedly loaded with 18.9 Nm torque to allow the stem to wedge in. Subsequently, the interface displacement is elastic and recoverable. This suggests that for a tight fit stem, it is possible that permanent displacement will not accumulate. However, it is difficult to say if there was slippage between stem and the femur in stable micromotion situation. Therefore, it is very difficult to compare a study that has achieved stable micromotion to studies that are not stable [Sugiyama *et al.*, 1989; Sugiyama *et al.*, 1992]. Instead of loading the stem repeatedly, some studies looked the first load cycle to calculate the micromotion [Callaghan *et al.*, 1992]. Callaghan *et al.* (1992) found that repeated loads did not change the micromotion by more that 5% and calculated the micromotion after 1 load cycle.

Author	Test note	Load	Stem type	Result		
				Anatomical location	Walking	Stair climbing
Monti *et al.*, 2001	Composite femur 1000 cycles	Axial = 1.68 kN Horizontal plane torque = 26.2 Nm Frontal plane torque = 23.2 Nm	Zimmer VerSys	Proximal-lateral Proximal medial Mid-medial		3 μm 2 μm 1 μm
Baleani *et al.*, 2000	Composite femur 100 cycles initial 1.7kN axial loads to press-fit	Torque = 0.1-18.9 Nm in 1000 cycles	Cementless (Ancafit)	Medial-proximal Medial-middle Medial-tip Anterior-proximal		56.2 ± 26.1 49.5 ± 25.6 39.5 ± 27.7 10.3 ± 9.6
			Cemented (Ancafit)	Medial-proximal Medial-middle Medial-tip Anterior-proximal		0.9 ± 0.2 0.6 ± 0.1 0.6 ± 0.1 0.7 ± 0.1
Hua and Walker, 1994	2500 cycles for walking loads and 500 cycles for stair-clinbing load.	1 kN for walking 150 N with 70° slant to femur for stair climbing	Symmetrical stem Asymmetrical stem Custom stem	20 mm distal to lesser trochanter	6 ± 6 19 ± 13 11 ± 12	0.063° ± 0.056° 0.018° ± 0.022° 0.009° ± 0.013°
Callaghan *et al.*, 1992	36 years mean age for donor	1.5 kN walking 1.2kN and 22 Nm stair climbing	Curved-stem (Zimmer)	Proximal/Distal Anterior-posterior Superior-inferior Medial-lateral	 14±21.5(1-61)/6±4.9(1-4) 14±11.9(2-33)/7±5(3-17) 24±19.2(5-61)/10±5.5(3-19)	 26±6.5(19-36)/33±19.6(9-59)
			Straight-stem Harris Galante (Zimmer)	Anterior-posterior Superior-inferior Medial-lateral	7±7.6(0-22)/3±2.1(1-7) 6±3.7(3-12)/12±10.7(6-36) 6±4(3-14)/5±4.5(2-15)	77±57.9(27-193)/ 34±117.2(37-379)
Sugiyama *et al.*, 1992	0.5-2 kgm torque applied in 0.25 kgm increment	2 kg/m or about 20 Nm	AML stem (DePuy) 4/5 coated/under-reamed 1/3 coated/under-reamed 4/5 coated/line-to-line	Medial-proximal		 65 60 270
Walker *et al.*, 1987	3 cycles of 666 N preconditioning load	1 kN axial load for walking 1 kN axial load and 100 N horizontal load for stair climbing	Exact-fit stem Cemented	Medial-proximal	18±3 30.8±3.5	52.5±5 42.5±1.3
Schneider *et al.*, 1989	1 preconditioning cycle equivalent to body weight 600 cycles/stage. 4 stages with 1,2,3 and 4 body weight applied giving a total of 2400 cycles	Loads depend on donor	CLS Muller85 Zweymuller PCA	4 sites on proximal femur	83-152 14-50 8-56 9-12	

Table 3.1 Micromotion values reported in experimental studies.

3.8.3 Evaluation of stem micromotion using finite element analysis

Finite element method has been used to study the micromotion at the bone-stem interface [Rubin *et al.*, 1993; Keaveny and Bartel, 1993c; Biegler *et al.*, 1995; Kuiper and Huiskes, 1996; Ramaniraka *et al.*, 1996; Ando *et al.*, 1999]. The advantage of using finite element analysis is the faster and easier implementation of this method to investigate different parameters. Finite element studies have looked into the designs of the stems [Keaveny and Bartel, 1993c; Biegler *et al.*, 1995; Ramaniraka *et al.*, 1996; Ando *et al.*, 1999], stiffness of stem [Kuiper and Huiskes, 1996] and different loadcases [Rubin *et al.*, 1993; Biegler *et al.*, 1995; Kuiper and Huiskes, 1996; Ramaniraka *et al.*, 1996]. In comparison to experimental measurement, finite element techniques can apply more physiological loads, measuring the true micromotion (rather than combination of micromotion and elastic displacement of the bone) over the entire bone-stem interface and is easier to change parameters to study different design ideas. However, finite element studies suffer from uncertainties over the assignment of material properties of the femur, boundary conditions at the bone-stem interface, assumption of continuum mechanics and validation of the results. Despite these limitations, finite element studies still provide valuable qualitative information when comparative studies of various designs are performed.

Ramaniraka *et al.* (1996) looked into the micromotion of straight and anatomic stem designs. Applying loads simulating the stance phase of the gait cycle, the straight stem was found to have smaller micromotions in comparison with an anatomic stem (approximately 42 μm difference at the maximum shear micromotion), as shown in Table 3.2. The anatomic stem has been reported to have higher micromotion in the single leg stance than straight stem in experimental studies as well, but lower micromotions were reported when higher torsional loads were applied [Callaghan *et al.*, 1992; Hua and Walker, 1994]. However, this study did not compare the stems under stair climbing load, which applied higher torsional load on the stem.

Ando *et al.* (1999) compared 5 different stem designs and measured the fit and fill of the stems (Table 3.2). Fit was defined as the percentage of the surface area of the stem within 1 mm of the inner cortex. Fill is defined in this study as the volume of stem over volume of femoral canal from distal end of lesser trochanter to the stem tip. The stems with better fit have been found to have lower micromotion in comparison with the stems with poor fit. Of the five stems, the Omniflex and Omnifit had the poorest fit. This is in agreement with experimental and clinical studies [Robertson *et al.*, 1988; Engh *et al.*, 1990; Cook, 1991]. Engh *et al.* (1990) reported that their early series of cementless hip stems had bad fit and fill due to the use of a single size stem for all patients and resulted in poor clincal results.

Keaveny *et al.* (1993c) studied the effect of the presence of a well supported collar on stem stability. The presence of a collar was found to reduce axial subsidence and rotational micromotion. In the model without collar, stem axial subsidence was found to be higher, in

agreement with experimental result comparing devices with and without collar [Schneider *et al.*, 1989].

In an investigation involving titanium alloy stem and isoelastic stem (made of material with a stiffness similar to cortical bone), Kuiper and Huiskes (1996) reported that the micromotion of the stiffer titanium stem was significantly less than the isoelastic stem. At the proximal medial region where the isoelastic stem generated the greatest micromotion (150 μm), the titanium stem generated approximately 50 μm micromotion. Subsidence of isoelastic stem was also found to be greater than the titanium stem, although the difference was quite small.

Friction affects the micromotion and hip stem subsidence under repeated load cycles [Kuiper and Huiskes, 1996]. The micromotion and subsidence of stem was reported to be the same in every cycle when the interface was assumed to be frictionless. However, when the friction interface was modelled, the stem gradually reached an equilibrium position and no further subsidence occurred as load cycles were repeated. The micromotion was evaluated after the stem had reached the equilibrium position. Kuiper and Huiskes (1996) suggested that finite element micromotion studies should apply repeated load cycles until the stem has wedged into an equilibrium position and subsides no further. The effect of subsidence has been observed experimentally [Hua and Walker, 1994; Baleani *et al.*, 2000]. However, three dimensional finite element micromotion study can be computationally expensive. Simulation of repeated cycles may be impractical. The zero friction condition in this study for the bone stem boundary is not very reasonable. Experiments have shown that bone-porous coated implant and bone-smooth metal interfaces have coefficients of friction of 0.6 and 0.4 respectively [Shirazi-Adl *et al.*, 1993]. Friction therefore played an important part in stability of cementless hip stem.

In comparison to experimental results, micromotion measured in finite element studies are normally between adjacent nodes at the bone stem interface. In comparison, the measurement of micromotion in experimental study is between the stem and the outer surface of the femur. This make it difficult to compare micromotion measured in experimental study to micromotion calculated in FE study. Keaveny *et al.* (1993c) compared the micromotion results calculated between adjacent nodes at the bone stem interface and results calculated between stem and surface femur nodes. It is found that the micromotion calculated in the former is insensitive to frictional characteristic at the bone stem interface because the elastic deformation of bone between the sampling points dominates the deformation. This is consistent with the suggestion that some of the micromotion measured in experimental study could be due to elastic deformation of bone instead of slippage at the interface [Walker *et al.*, 1987], and also micromotion is measured with cemented stems as well. It is therefore reasonable to assume that there is a lower limit (for example 10 μm) below which micromotion does not really occur.

Similar to experimental study, the applied loads were not uniform in finite element studies (Table 3.2). The joint contact force applied by various investigators varies from about 1000N to 3000N. The magnitude of applied load has been shown to affect the micromotion in a non-linear fashion [Ramaniraka *et al.*, 1996]. The magnitude of about 1500 N would be around two times body weights assuming the patient has 70 kg of mass. At 3000 N, the joint contact force would be about four times body weight. The former is closer to the average joint contact force during walking measured in four patients by Bergmann *et al.* (2001), although fast walking has been reported in the range of about four body weights [Kotzar *et al.*, 1991; Bergmann *et al.*, 1993]. During the early postoperative period, receiver of total hip joint replacement is not likely to walk very fast and will be weight protected by the used of crutches. Together with not standardized material properties and boundary conditions, it is very difficult to compare the results between studies. Most results will have to be compared qualitatively within the same study.

Finite element analyses of stem micromotion listed in Table 3.2 generally use of only one set of bone properties, i.e. the change of micromotion due to variation of bone properties was not studied. This could limit the risk assessment of hip stem to patients with bone quality similar to the property used in finite element analyses. As discussed in Section 1.4.4, bone quality changes due to aging and disease. A more representative assessment of hip stems may need to assess a greater range of bone quality.

Author	Stem type	Loadcase (Joint contact force)	Result		
			Anatomical location	Walking	Stair
Rubin *et al.*, 1993	CLS Spotorno	Single leg stance Ax, ML, AP, T = 1000N, 600N, 400N, 1160N Stair climbing Ax, ML, AP, T = 1220N, 550N, 470N, 1450N	Proximal	shear = 371 normal = 307	shear = 603 normal = 543
			Middle	Shear = 292 Normal = 60	Shear = 298 Normal = 139
			Distal	Shear = 298 Normal = 35	Shear = 341 Normal = 150
Biegler *et al.*, 1995	Model A (Mallory-Head) Model B (Harris-Galante) Both have medial flare, straight lateral, anterior and posterior sides. B bigger than A. Collarless	Single leg stance Ax, ML, AP =1401N FP = 417N Stair-climbing Ax, ML, AP = 1553N 709N, 600N SP moment = 123 Nm FP moment = 25 Nm	Calcar Upper quarter Lower quarter Distal tip	33, 14 ¦ 17, 14* 22, 19 ¦ 16, 14* 15, 13¦ 6, 4* 24, 22¦ 34, 32*	58, 56 ¦ 43, 41 8, 9 ¦ 14, 15 22, 18 ¦ 9, 11 14, 20 ¦ 43, 41
Keaveny and Bartel, 1993	AML Collared.	Single leg stance Ax, ML, AP = 2925N, 1492N , 915N	Proximal Smaller trochanter Lower quarter Distal tip	100 130 160 250	
Kuiper and Huiskes, 1996	2-D stem with medial flare. Titanium stem	Single leg stance 2317N at 24^0 to vertical	Proximal medial Proximal lateral Distal medial Distal lateral	60, 35Ψ 20, 2Ψ 80, 60Ψ 85, 70Ψ	
Ramaniraka *et al.*, 1996	Straight stem – distal fix Anatomical stem – proximal fix	Single leg stem = 1800N	Straight stem (max.) Anatomical stem (max.)	Shear = 140 Normal = 107 Shear = 182 Normal = 109	
Ando *et al.*, 1999	FMS FMS-anatomic Omniflex Omnifit IDS	Single leg stance Ax, ML, AP = 2714N, 1385N, 849N Stair-climbing Ax, ML, AP = 1553N, 709N, 600N SP moment = 123Nm FP moment = 25Nm	Proximal – average FMS-anatomical FMS Omniflex Omnifit IDS	26 47 144 109 16	14 15 57 47 10

* - results are arrange according to: Model A: uncoated, coated ¦ Model B: uncoated: coated

Ψ - results are arrange according to: $\mu = 0.15$, $\mu = 0.4$

Ax, FP, AP, T = axial, medial-lateral, anterior-posterior, total

FP, SP = frontal plane, sagittal plane

Table 3.2 Finite element micromotion studies by other investigators.

3.9 Interference-fit at the bone-stem interface

Cementless hip stem requires rigid initial fixation to achieve biological fixation (Section 3.8). Rigid fixation can be achieved through proper press fitting [Schwartz *et al.*, 1989; Engh *et al.*, 1990; Sugiyama *et al.*, 1992]. Engh *et al.* (1990) has suggested that clinical success has been improved with introduction of distal press-fit for AML stems. Distal press-fit is achieved by underreaming the femoral isthmus to have a small degree of interference-fit at the distal part of the hip stem. Better initial stability brought about by distal interference-fit has been confirmed in experimental micromotion study using human cadaver for the AML stem [Sugiyama *et al.*, 1992]. Interface micromotion is therefore affected by the amount of press-fit at the bone-stem interface.

In finite element studies of existing and new hip stem designs, little attention has been given to study the effect of interference-fit on the initial stability of hip stems. In comparative study of hip stem designs in Section 3.8.3, the interference-fit at the bone-stem interface has not been modelled. This does not reflect the true mechanical environment *in vivo*. While neglecting interference-fit in the modelling of hip stem can be considered as modelling line-to-line fit *in vivo*, most cementless stems are now implanted with interference-fit in mind [Schwartz *et al.*, 1989; Engh *et al.*, 1990; Jasty *et al.*, 1993].

Little is known about the optimal amount of interference-fit that should be introduced for optimal stability of hip stems. Studying the initial stability of hip stems in relation to implant stability has direct effect on the design of surgical instruments for cementless hip joint replacement. AML stem has been reported to be implanted into the femur with distal interference-fit of 0.5 mm [Engh *et al.*, 1990]. However, no studies have been done to examine if smaller interference-fits would have given the same clinical result. Measurement of the influence of interference-fit on stem micromotion has also been limited to only one degree of interference-fit [Sugiyama *et al.*, 1992].

Schwartz *et al.* (1989) has reported that most femoral fractures during insertion of AML stems occurred during preparation of femoral canal or during final impaction of the hip stem. Both proximal and distal fracture of the femur has been observed intraoperatively. Intertrochanteric fracture has been observed when the broach or the prosthesis has been driven too far down the femoral shaft or broach is slightly smaller than the stem. This lead to excessive wedging in the intertrochanteric area which lead to fracture [Schwartz *et al.*, 1989]. Higher incidence of intertrochanteric fracture has been reported to happen with bulkier, pyramidal proximal segment and a tapered stem that depend on tight proximal fit [Fitzgerald *et al.*, 1988]. Distal fracture of the femur during AML stem insertion is normally cause by impaction of tip of prosthesis against intramedullary canal [Schwartz *et al.*, 1989].

Most small fractures do not affect stability of cementless hip stem too much, but care has to be taken to slowly increase load bearing to allow healing of fracture [Schwartz *et al.*, 1989]. Experimental micromotion study has shown that a small fracture may only increase the initial micromotion slightly [Monti, 2000]. However, this study was performed using an artificial femur, may have different properties in comparison to a real femur. However, in cases where bone is completely displaced in a fracture, stabilization may be difficult to achieve and bone ingrowth may not occur [Schwartz *et al.*, 1989]. If fracture is not detected intraoperatively and postoperatively, steps to improve stabilization and special care with load bearing may not have been taken. Experimental study using a canine model has shown that in a fractured femur bone ingrowth is significantly lower even after stabilization of the fracture using cerclage wiring [Schutzer *et al.*, 1995]. They suggest this is due to lack of bone ingrowth deep to the fracture and increase femoral component micromotion.

Monti *et al.* (2001) implanted six composite femora with six Zimmer VerSys stems and cracked three of the composite bones during stem insertion and press-fit. This is a very high fracture rate and clearly points to the need for special care to be taken during the design process to limit femoral fracture due to excessive interference-fit. Clinically, femoral fracture has been reported to be in the range of 3-27.8 percent [Schwartz *et al.*, 1989]. The higher fracture rate has been associated with bad surgery technique, and with improved technique the rate of fracture has been reduced to about 2-3 percent [Schwartz *et al.*, 1989]. Recent study has also reported this fracture rate [Monti *et al.*, 2001]. It is likely that excessive interference-fit is responsible for these fractures. High assembly strains produced during insertion of cementless stem into femur have been shown to produce femoral fracture in a study using cadaver femur [Jasty *et al.*, 1993].

3.10 Objectives

In Chapter 4, the finite element model is described. A parametric study is performed to identify suitable parameters that provide stable results. Parameter identification has been reported to play an important role in contact analysis [Bernakiewicz and Viceconti, 2002].

Evaluations of hip stem designs reported in the literature were based on a single set of material properties [Rubin *et al.*, 1993; Keaveny and Bartel, 1993c; Biegler *et al.*, 1995; Kuiper and Huiskes, 1996; Ramaniraka *et al.*, 1996; Ando *et al.*, 1999]. As discussed in Section 1.4.4, mechanical properties of bone can change substantially throughout the life time of a person due to various factors. Cementless hip stems have been implanted into different individuals with different ages and complications [Engh *et al.*, 1990; McLaughlin and Lee, 2000]. The performance of hip implants in each individual will therefore be subjected to differences due to differences in bone quality. If significant changes in micromotion occur for different bone quality, it could be imperative to suggest a different postoperative care regime for patient with bad bone quality.

Chapter 5 examine the differences in initial micromotion and interface bone strain due to changes in bone quality and the implications on implant assessment.

Only a few finite element studies have modelled the interference-fit of the bone-stem interface of hip implant [Harrigan and Harris, 1991; Visnic *et al.*, 1994]. However, these studies were using simplified models of the implanted femur assembly. Harrigan and Harris (1991) used half cylindrical models to represent the stem and the femur to study the effect of different fit on the stress and contact distribution in the idealised femur. The stress distribution was much higher and different in the model simulated with interference fit. The contact area was also more than the model with line-to-line fit. Visnic *et al.* (1994) simulated the assembly strain due to interference-fit using a two-dimensional symmetrical model and found that equivalent strain was as high as 17.2%. Both studies agreed that interface stress and strain could be significantly increased with interference-fit. However, both studies did not report on the effect of interference-fit on initial micromotion. No finite element study has reported the effect of interference-fit on initial stability of hip stem, and simultaneously looked at the stress and strain field. Therefore, in Chapter 6, the effect of interference-fit on initial stability was studied using a finite element technique. The aim was to predict the improvement of initial stability due to interference-fit and the optimal amount of interference-fit needed in view of the femoral fracture risk brought about by high level of interference-fit. It is desirable to extend the use of finite element technique to preclinical analysis of surgical technique of cementless hip stem.

In Chapter 7, the study of interference-fit was extended to include modelling the plastic behaviour of bone in view of the high strain observed in Chapter 6. This is to model a more realistic material behaviour and to check if the results in Chapter 6 are influenced by plastic behaviour of bone.

There is considerable debate as to whether creep deformation in bone will render interference-fit ineffective in the first two to three months postoperatively. This is the critical period of healing and bone ingrowth where initial stability provided by the interference-fit provided the optimal condition for healing tissue to mineralise to become bone. A simplified model was created to study the creep behaviour of the femur in an interference-fit assembly in Chapter 8.

Chapter 4 A description of a finite element model of an implanted proximal femur with an IPS stem

4.1 Introduction

In this chapter, the generation of a finite element model of a cementless implanted proximal femur is described and the sensitivity of this model to mesh size and modelling parameters, particularly contact parameters will be assessed. The finite element study of the initial micromotion and interface strain of the cementless implanted proximal femur requires the implementation of contact procedures. In the immediate post-operative period, the cementless stem and the femur are two separate bodies that can slide relative to each other and the transfer of load between the two bodies is achieved through compressive and frictional forces. The surfaces of the stem and bone cannot transfer tensile load, and when subjected to tensile loads, the surfaces will separate.

Verification of finite element analysis of orthopaedic implants is difficult. Among the reasons for this difficulty include the complexity of loading *in vivo*, complexity of biological structure, biological activities and the practicalities of obtaining measurements *in vivo*. Most finite element analyses of orthopaedic implants make used of simplified loads, material properties and ignore biological activities all together. Although verification of finite element analysis may not be possible, it has been used for qualitative comparison of different parameters. For accurate comparison, the accuracy of finite element analysis should be assessed. The objective of this chapter is to assess the effect of various parameters that could affect the accuracy of the finite element model used in this thesis.

4.2 Model generation, material properties and boundary conditions

The generation of the model, assignment of material properties and boundary conditions are described in this section. The model generation follows the schematic diagram shown in Figure 4.1. The main steps and the software involved in the process are shown. The details of the steps are discuss in greater details in the subsections.

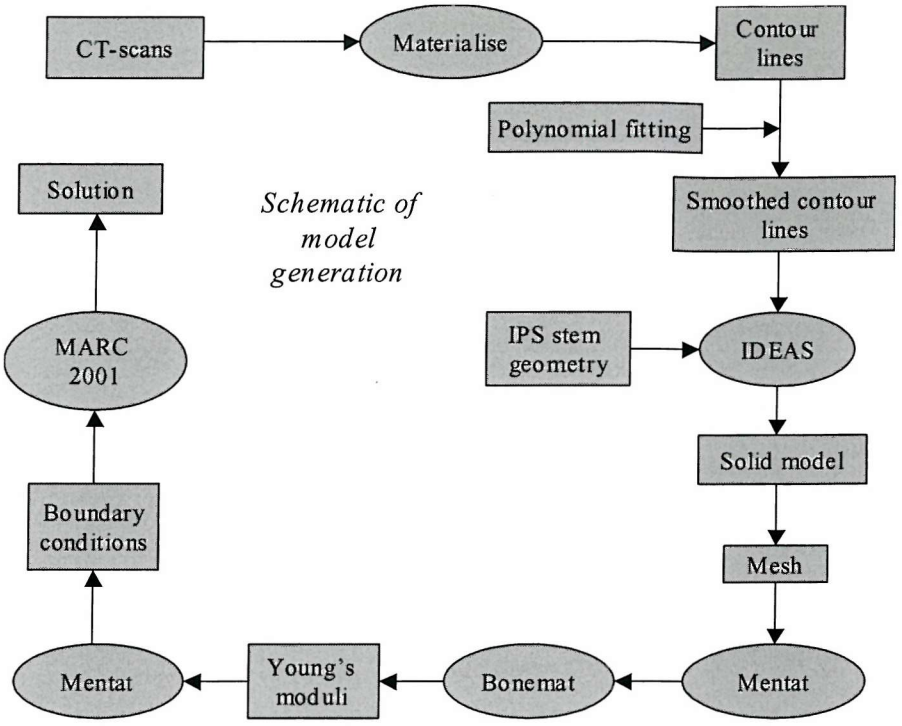

Figure 4.1 Schematic diagram of finite element model generation of the implanted proximal femur.

4.2.1 Generation of an anatomical model of the implanted femur

A set of Computed Tomography (CT) scan images of the intact human femur from Visible Human Project website (**http://www.nlm.nih.gov/research/visible/visible_human.html**) was obtained. Transverse CT scans of the left femur of a healthy 39 year old male subject were used. The cross-sectional images were taken at 1 mm interval and had a resolution of 512 pixels x 512 pixels, with each pixel made up of 16 bits of grey scale. The size of a pixel was 0.9375 mm x 0.9375 mm. An example of a slide of the CT-scan image is shown in Figure 4.2a.

The geometry of the femur model was acquired from the CT-scans. The outlines of the cross-sections of the femur were obtained using Materialise (Leuven, Belgium), a piece of virtual prototyping software. A thresholding procedure was performed to identify the outer bone surfaces. The program can automatically generate an outline of the cortical bone if an appropriate grey scale value for cortical bone is chosen for thresholding (Figure 4.2b).

Setting the threshold value of the cortical bone was done by inspection. A threshold value of 1278 was chosen. In certain areas where cortical bone was not well defined due to the low resolution of the images, manual corrections to the outlines created by the program were needed. This method of generating the outlines of the femur from CT-scan was also applied to generate the medullary cavity.

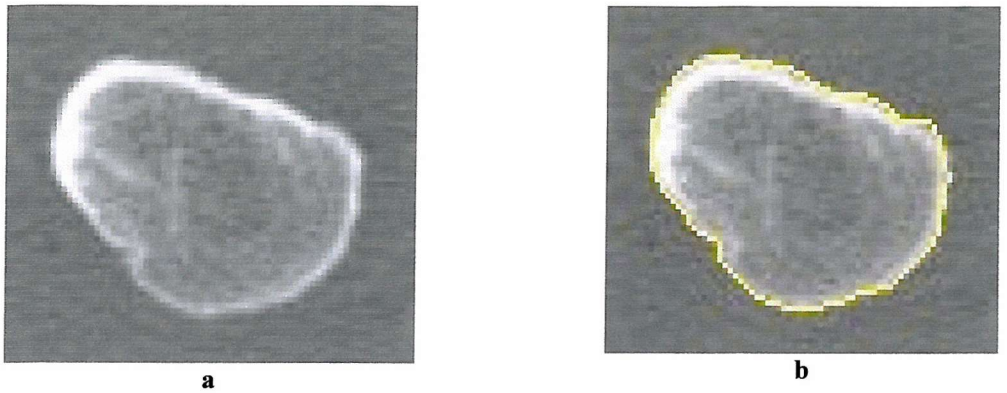

a b

Figure 4.2 (a) A CT-scan image from the male Visible Human CT-scans dataset (b) Contour automatically fitted to outer geometry of a femoral cross-section by Materialise.

After the thresholding operation, the outlines of the femur and the medullary cavity were jagged and were not ready to be manipulated to generate a solid model. These lines were smoothed using 4th order polynomials. The program automatically fitted smooth contours to the outlines. The contours were saved into separate IGES files for the outer femur geometry and the medullary cavity. The outer contours of the femur are shown in Figure 4.3.

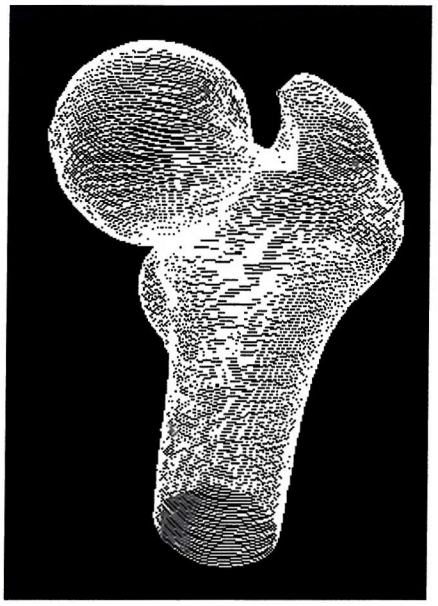

Figure 4.3 The smoothed outer contours of the femur. For clarity, the full geometry of the femur is not shown here.

The contour lines created from Materialise were imported in IGES format into IDEAS, a 3-D solid modelling and finite element package. Utilising the preprocessing tools in IDEAS (Texas, USA), the surface geometries of the femur and the medullary cavity were created using the LOFT function. Stitching the surfaces together, the solid volumes of the femur and medullary cavity were created. Cutting the solid volume of the femur with the medullary cavity created the solid model of the intact femur (Figure 4.4).

The stem used in this study is the new cementless IPS hip stem from DePuy International (Leeds, UK). It is proximally porous-coated with titanium beads. The beads are coated with

hydroxyapatite coating to enhance osseointegration. The surface geometry of the IPS stem was imported into IDEAS as an IGES file. The surfaces were stitched together to form a solid volume.

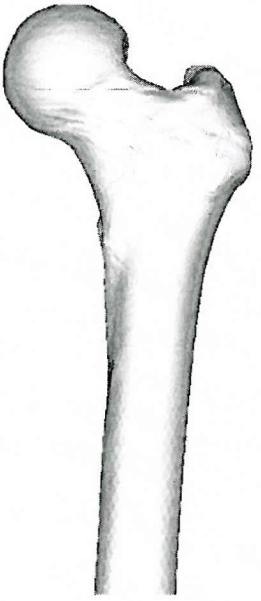

Figure 4.4 Solid model of the intact femur.

In IDEAS, the solid model of the hip stem was virtually implanted into the solid model of the femur according to the surgical manual. The solid model of the hip stem was used to partition the model of the femur to divide the model to different volumes representing the hip stem and the implanted femur. The hip stem and prepared femur were further partitioned into smaller volumes to enable selective meshing of different regions of interest.

The prepared femur and the hip stem were meshed with linear tetrahedral element in IDEAS. Due to partitioning of the femur and stem into different volumes, meshing with different element sizes for different regions of the femur was possible. Partitioning also allowed the generation of coincidental nodes at the bone-stem interface. This was done to simplify the calculation of micromotion at the bone-stem interface.

The finite element meshes of the implanted femur and the stem were separately imported into MARC as an IDEAS universal file. During each import, the elements and nodes were renumbered and defined as separate contact bodies. Two deformable contact bodies, the femur and the stem were created as a result (Figure 4.5).

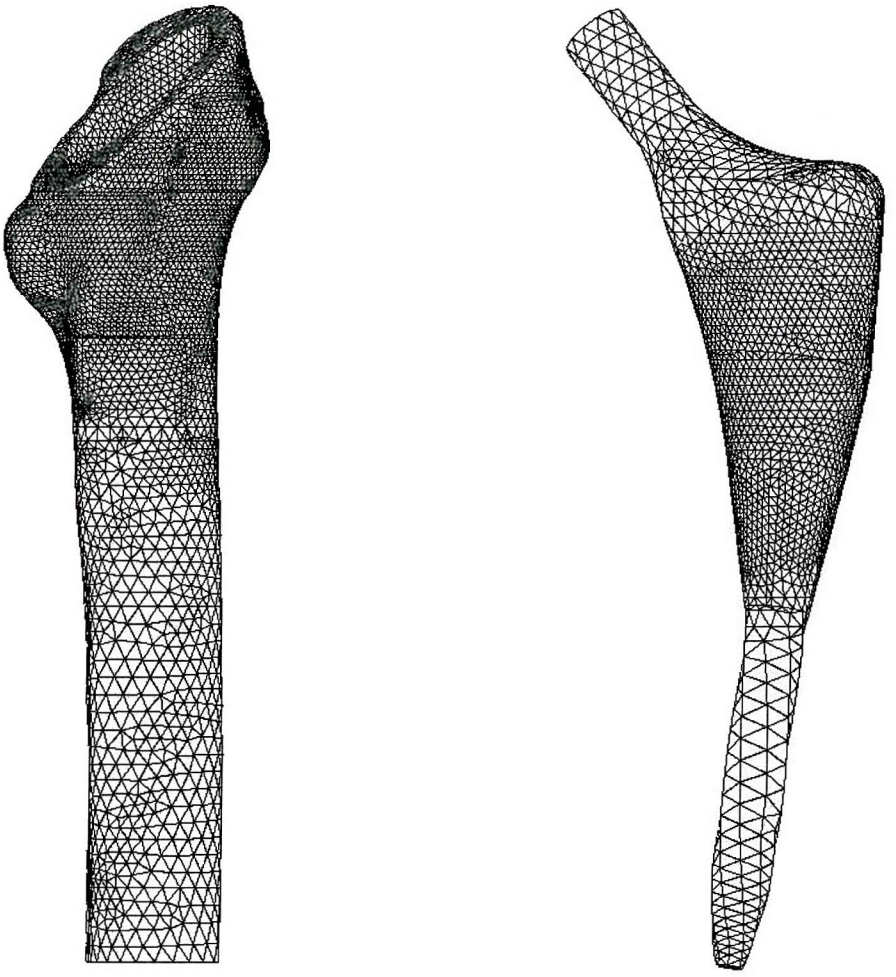

Figure 4.5 Finite element meshes of the implanted femur and IPS stem.

4.2.2 Material properties of the stem and femur

Elastic modulus of the femur varies from one anatomical location to another due to differences in the density and architecture of the bone. The different apparent densities of bone (ratio of bone mass to specimen volume including porosity) can be indirectly quantified based on properties of CT scans [Cann and Genant, 1980]. The Young's modulus of bone has been shown to be related to the apparent density of bone [Carter, 1977; Ashman and Rho, 1988; Rice *et al.*, 1988; Schaffler and Burr, 1988; Ashman, 1989; Hodgskinson and Currey, 1992; Keller, 1994; Keyak *et al.*, 1994]. Therefore, it is possible to assign the value of Young's modulus based on CT-scans. This method has been widely used in finite element analysis of bone and orthopaedic implants [Huiskes *et al.*, 1992; Skinner *et al.*, 1994; Keyak and Rossi, 2000; Weinans *et al.*, 2000]. However, up to now, normal CT scans are not able to capture the orthogonal properties of bone. As a result of this, the Young's modulus assigned is isotropic.

A group from Instituti Ortopedici Rizzoli, Bologna, Italy have developed a computer software (Bonemat) to automatically assign elastic moduli of bone to a finite element mesh based on data from a set of CT scans images [Zannoni *et al.*, 1998]. Bonemat reads the CT scans dataset

for information on the individual coordinates and Hounsfield Unit (HU) or the grey scale value of each pixel. Bonemat converts the values of HU of the CT scan voxels to apparent density values of bone. It was assumed in Bonemat that there is a linear relationship between HU and apparent density of bone. The density values are converted to elastic modulus using Equation 1.1.

Bonemat reads the coordinates of the nodes in the finite element model. From the nodal coordinates of the element, Bonemat forms a parallelepiped around the element and averages the sum of the HU of all the pixels in the parallelepiped. The elastic modulus of the element can therefore be derived from the averaged HU of the parallelepiped.

The density-modulus relationship in this study takes the form of

$$E = 2875\rho^3 \text{ ---------- Equation 4.1}$$

This relationship is taken from Carter (1977), as explained in Section 1.4.1.4. A number of finite element studies have used this relationship to assign material properties to bone [Huiskes *et al.*, 1992; Skinner *et al.*, 1994; Weinans *et al.*, 2000].

The CT-scan data set from VHP is not calibrated to a potassium phosphate (K_2HPO_4) phantom. The assumption made to convert HU to apparent density was to assume the minimum density of bone was 0.07 g/cm^3 [Hodgskinson and Currey, 1992; Keller, 1994; Weinans *et al.*, 1994] and this was equalled to the smallest HU and the maximum density of bone was 1.9 g/cm^3 [Keller, 1994] was equalled to the highest HU. The range of Young's modulus assigned to the mesh ranged between 94 and 19900 MPa.

A limitation of assigning material properties of bone based on normal CT scans data is that bone anisotropy is not taken into account. It is not possible to extract the 3-D structure of both cortical and cancellous bone. The anisotropy of cortical bone is dependent on the orientation of collagen fibres while orientation and structure of trabeculae determines the anisotropy of cancellous bone. However, it is only possible to extract the apparent density of bone and derive the Young's modulus in the direction normal to the plane of the CT-scans images. Within the state of the art in biomechanics finite element analysis, this limitation has yet to be overcome.

The Young's moduli assigned to the mesh were reasonable in comparison to values reported for the human femoral bone in the literature. The smallest Young modulus assigned was 94 MPa. This is in about the same order of magnitude as the values reported by Fazzalari *et al.* (1998) for the inter-trochanteric region of the femur, although 94 MPa is generally higher than the values reported by Fazzalari *et al.* (1998). In the mesh, the bone near the inter-trochanteric region was generally more compliant. In the greater trochanter, the values in the mesh range from about 140 to 600 MPa. This is the region similar to the anatomical location where bone specimens were cut out for mechanical testing by another study Morgan and Keaveny (2001). This study reported Young's modulus range between 300 and 900 MPa both in compression and tensile tests. The

values in the mesh fall within this range. However, Brown (1980) reported stiffer values for this region of around 1000 MPa. The region around the medial cortex just below the neck resection level has values between 7000 to 15000 MPa in the mesh. Brown (1980) reported 9700 MPa for the hard cancellous bone just beside the medial cortex in similar region. Tests of human femoral cortical bone gave a range between 13000 to 22000 MPa [Reilly and Burstein, 1975]. The Young's modulus in the medial cortex just below the neck resection level seems reasonable. The maximum Young's modulus in the mesh is 19900 MPa, which is also a reasonable value in comparison to values from mechanical test [Reilly and Burstein, 1975]. Since values derived from Equation 4.1 compare reasonably well with mechanical test results, this equation was used to assign values of Young's modulus.

4.2.3 *Interface boundary conditions*

All the finite element analyses in this thesis simulate the interface condition in the immediate post-operative period. Therefore, the bone-stem interface was assumed to be debonded and can only transfer compressive and shear loads. Shear load is transfer through friction at the interface.

The IPS stem is a proximally coated stem as shown in Figure 4.6. Contact was assumed in the porous coated region and also the smooth part in the mid-stem region. Distal to the smooth region, the stem was assumed not to be in contact with the diaphyseal femur as designed. The analyses in this chapter assumed line-to-line fit between the stem and the femoral canal.

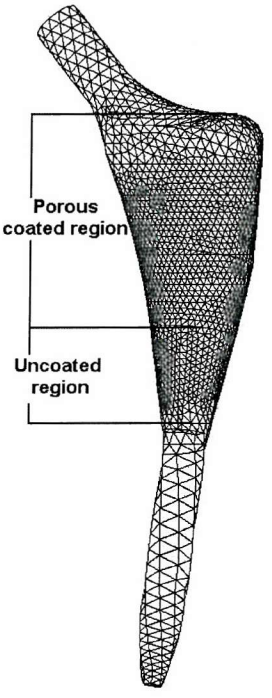

Figure 4.6 The porous coated and uncoated (smooth) region of the IPS hip stem. The contact area is defined for the area consists of both the coated and uncoated region. Distal to the uncoated region, the stem is not in contact with the diaphyseal femur.

Shirazi-Adl *et al.* (1993) measured the friction coefficient between cancellous bone and different implant surfaces (Table 4.1). The friction coefficient between cancellous bone and rough titanium porous bead surface is approximately 0.6. The friction coefficient between cancellous bone and smooth metal surfaces is approximately 0.4. The model implemented a stick-slip coulomb friction model employing coefficient of friction of 0.6 for the porous region and 0.4 for the smooth region. Previous finite element studies have used similar coefficients of friction [Biegler *et al.*, 1995; Ando *et al.*, 1999]. These values were used throughout the thesis unless otherwise stated.

Type of surface	Friction coefficient
Smooth metal	0.4
Titanium fibre mesh	0.6
Titanium porous beads	0.6
Vitalium porous beads	0.5

Table 4.1 Friction coefficient between cancellous bone and various metal surfaces [Shirazi-Adl *et al.*, 1993].

4.2.4 Joint contact and muscle forces acting on the implanted femur

In this study, the joint contact force was based on data obtained from *in vivo* measurement using an instrumented hip prosthesis [Bergmann *et al.*, 2001]. Gait data from Bergmann *et al.* (2001) was used by Heller *et al.* (2001) to calculate the muscle forces. Heller *et al.* (2001) used the measured hip contact force to validate the calculated muscle forces. Their data was made available in the compact disc 'Hip98' [Bergmann *et al.*, 2001; Heller *et al.*, 2001; Morlock *et al.*, 2001].

The coordinate system used in Hip98 is shown in Figure 4.7. The x-axis is parallel to the dorsal contour of femoral condyles in the lateral-medial direction. The y-axis is perpendicular to the x and z axes in the posterior-anterior direction. The z-axis is parallel to the idealised midline of femur.

The Bergmann *et al.* (2001) data showed that fast walking and stair climbing applied the most significant joint contact force and moment on the hip implant as compared to other common activities like standing up from a chair or knee flexion. During stair climbing, the average torque was reported to be 23 % greater than during normal walking. Therefore, it is important to include this loadcase in computer simulation to study the stability of a cementless hip stem.

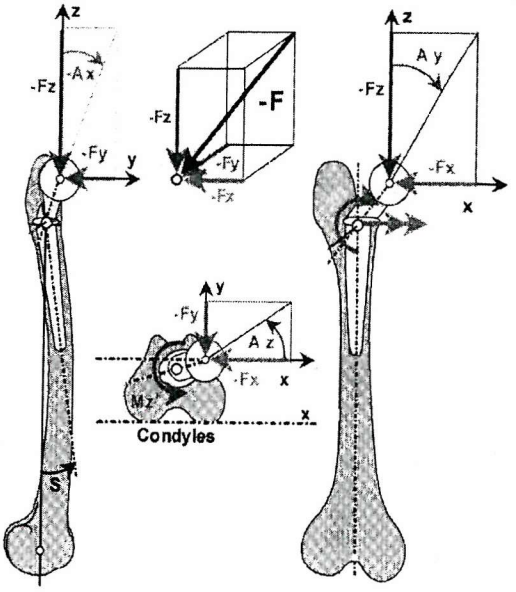

Figure 4.7 Hip coordinate system [Bergmann, 2002].

The loadcases suggested for implant testing from Hip98 dataset are shown in Table 4.2. The loads are applied to the implanted femur as shown in Figure 4.8. The distal end of the femur is constrained in all directions. When either walking or stair climbing loadcases are mentioned in this thesis, they refer to the normal walking and stair climbing loadcase shown in Table 4.2, unless otherwise stated.

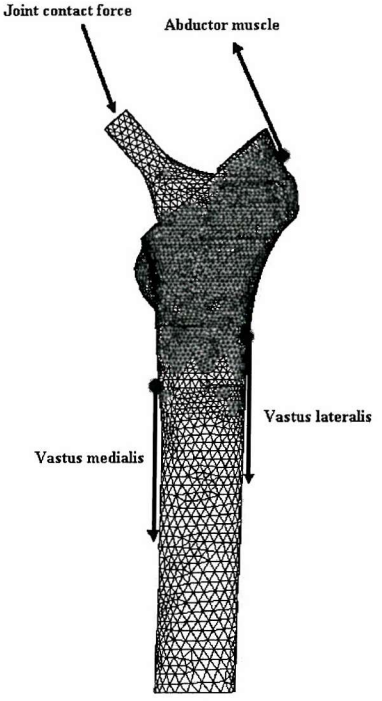

Figure 4.8 Joint contact and muscle loads applied to the implanted femur.

Activity	Applied loads	Force, % BW[a]			Force, N[b]			
		X	Y	Z	X	Y	Z	Resultant
Normal walking	Joint contact	54	32.8	-229.2	370	225	-1573	1631
	Abductor	-64.8	-15.2	80.7	-444	-104	554	717
	Vastus lateralis	0.9	-18.5	-92.9	6	-127	-638	650
Stair climbing	Joint contact	59.3	60.6	-236.3	407	416	-1622	1723
	Abductor	-83	-29.6	67.3	-570	-203	531	805
	Vastus lateralis	2.2	-22.4	-135.1	15	-154	-928	941
	Vastus medialis	8.8	-39.6	-267.1	60	-272	-1834	1855

[a] BW- Body Weight
[b] Body weight of 686.7 N was assumed

Table 4.2 Joint contact and muscle forces applied to the implanted femur model.

4.2.5 Solution using MARC 2001

All models were solved using MARC 2001 (Palo Alto, USA). This class of problem is a non-linear contact class problem. The femur and stem were considered as two separate deformable bodies in contact. The contact procedure was invoked through the CONTACT option in MARC. MARC automatically detects surfaces of a body that comes into contact with the surface nodes and appropriate kinematics constraints and nodal forces are applied. The loads were applied in an incremental procedure.

4.3 Sensitivity of model to mesh size and modelling parameters

The sensitivity of the model to mesh size and modelling parameters were evaluated based on the micromotion and equivalent strain parameters. Micromotion and strains are two relevant predictors of the performance of hip stem in the immediate postoperative period. Micromotion has been widely reported as a measure of the ability of hip stem to osseointergrate in evaluation of a cementless hip stem in both finite element and experimental methods [Walker *et al.*, 1987; Callaghan *et al.*, 1992; Sugiyama *et al.*, 1992; Keaveny and Bartel, 1993c; Hua and Walker, 1994; Biegler *et al.*, 1995; Ramaniraka *et al.*, 1996; Ando *et al.*, 1999]. On the other hand, stress/strain has been linked to bone-remodelling, stress-shielding and implant migration in hip joint replacement and other type of joint replacements [Cowin and Hegedus, 1976; Beaupre *et al.*, 1990; Huiskes, 1990; Cheal *et al.*, 1992; Weinans *et al.*, 1993; Skinner *et al.*, 1994; Keaveny and Bartel, 1994c; Taylor, 1997; Taylor *et al.*, 1998; Joshi *et al.*, 2000; Perillo-Marcone, 2001].

The micromotion reported in this thesis is the total micromotion, which is the resultant of all the components of micromotion, unless otherwise stated. The total micromotion between adjacent nodes was calculated as the resultant of the differences in the displacement components (in

directions of x, y and z axis as defined in the loading condition) between the two adjacent nodes. Spears *et al.* (2001) suggested that bone ingrowth is likely to depend on the combined effects of the normal and surface tangential micromotion, and therefore total micromotion is a suitable measure of implant stability.

Bone is a heterogeneous material with different Young's moduli in different anatomical locations. Thus the reporting of stress in isolation is not appropriate when analysing bone using a physiological distribution of bone stiffness. A more suitable measure of bone load is strain, as this give a clear idea of the deformation in bone regardless of the stiffness of bone as discussed in Section 1.4.1.2.

The equivalent strain is reported unless otherwise stated. The equivalent strain is a scalar value that represents an envelope of the direct and shear strain components and is based upon the classical von Mises failure criteria equation. The equivalent strain equation is shown below:

$$\varepsilon_E = [\varepsilon_X^2 + \varepsilon_Y^2 + \varepsilon_Z^2 - \varepsilon_X\varepsilon_Y - \varepsilon_Y\varepsilon_Z - \varepsilon_Z\varepsilon_X + 0.75*(\gamma_{XY}^2 + \gamma_{YZ}^2 + \gamma_{ZX}^2)]^{1/2} \text{ --Equation 4.2}$$

The sensitivity of the model to mesh size and modelling parameters was studied at the region of interest, which is the region of stem coated with porous beads. The micromotion and equivalent strain values at the bone-stem interface were reported at a cross section of the femur just below the neck resection level (Figure 4.9). This level is within the porous coating region of the stem and bone ingrowth is designed to occur here. For this chapter, only the normal walking loadcase was considered.

Figure 4.9 Micromotion and equivalent strain was sampled at the bone-stem interface at L1, just below the neck resection level.

4.3.1 Mesh refinement study

A mesh sensitivity study is performed to evaluate the sensitivity of the model to mesh size. Four different mesh sizes were created using linear tetrahedral elements. The edge length of the

elements in these four different meshes were 1.75, 1.6, 1.5 and 1.4 mm. The mesh refinement was performed in region of contact at the proximal femur while the mesh sizes in the greater trochanter, diaphyseal femur and part of the stem above the neck resection level were kept constant. The size of the meshes are shown in Table 4.3 and the increase in element number reflects the increase in mesh density in the region of contact.

Mesh	Element edge length, mm	Number of elements	Number of nodes
1	1.75	96560	22114
2	1.6	108346	24674
3	1.5	121706	27434
4	1.4	129823	29188

Table 4.3 Mesh sizes for mesh refinement study.

The convergence of micromotion and equivalent strain was studied by using a regression method as reported by Perillo-Marcone *et al.* (2003). The regression study for micromotion and equivalent strain between the coarser meshes and the finest mesh (1.4 mm mesh) were performed. The convergence of the meshes was evaluated using the slope of the regression line and the mean residual error (this is the distance of the values reported for the finest mesh (1.4 mm mesh) from the regression line). The micromotion around the cross section of level L1 is shown in Figure 4.10 for 1.75 and 1.4 mm models. A spline is fitted to the micromotion data to allow comparison of the micromotion in different mesh sizes at the same location, as the nodes are not in the same position. The micromotion of coarse meshes at different positions were plotted against the fine mesh. If both the slope of regression line and correlation coefficient are close to one, the coarse mesh converged to the values of the finest mesh. If plotted as in Figure 4.10, the micromotion values would be close to 1.4 mm model's curve. The mean residual error is a measure of the data spread from the regression line. Similarly, a spline is fitted for the equivalent strain values around cross section of Level 1 and regression analyses were performed between the coarser meshes and the finest mesh.

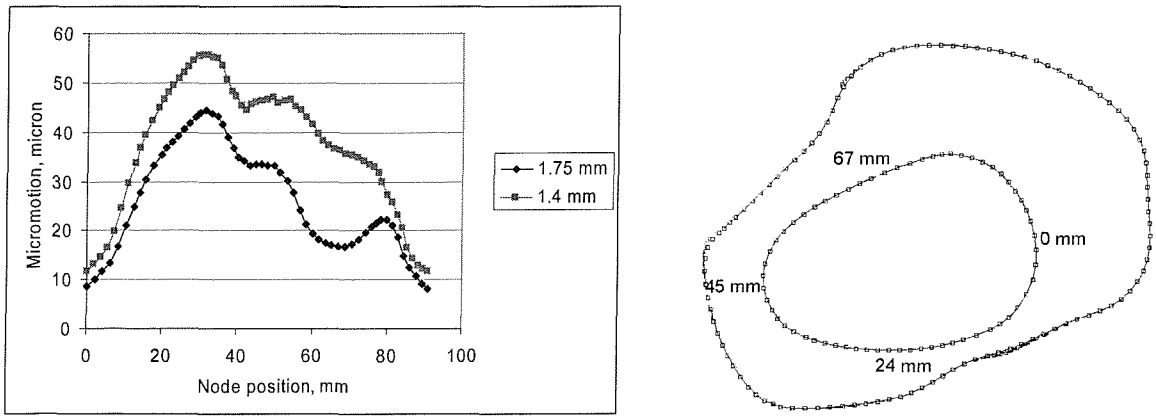

Figure 4.10 Micromotion of 1.75 and 1.4 mm models around the cross section of level L1. Nodal position is shown on the right. 0 mm is the lateral side while 24 mm is the anterior side.

In Figure 4.11, the micromotion and equivalent strain values of the coarser mesh were plotted against the values for the finest mesh. A linear regression was performed to find the slopes and the correlation coefficients of the data. The correlation coefficient r^2, slope and mean residual error are reported in Table 4.4.

For micromotion (Figure 4.11a), there was a good correlation for 1.5 and 1.6 mm meshes, with correlation coefficient r^2 greater than 0.99 (Table 4.4a). The regression slopes of these two meshes are 0.984 and 1.06 respectively, which is close to one. The relative error for these two meshes will be in the region of 2 and 6 %. Regression slope for the coarser 1.75 mm mesh is 0.701, which shows that this mesh will give a high relative error of about 30%. The mean residual error for the 1.75, 1.6 and 1.5 mm meshes are 7.77, 0.59 and 2.38 μm respectively (Table 4.4). The mean residual error in the 1.6 and 1.5 mm meshes are small as compared to the 50 μm micromotion normally regarded as the threshold for osseointegration [Engh *et al.*, 1992b; Fernandes *et al.*, 2002]. For this model, micromotion convergence was achieved for an element edge length less than 1.6 mm.

For the equivalent strain data (Figure 4.11b), the 1.6 and 1.5 mm meshes also have good correlation (Table 4.4b). The r^2 values for the 1.6 and 1.5 mm meshes are 0.974 and 0.956 respectively. The regression slopes for these two meshes are 0.974 and 1.012 respectively, which give relative errors of 2.6 and 1.2 % respectively. Regression slope for the coarser 1.75 mm mesh is 0.927, corresponds to relative error of 7.3%. The mean residual error for the 1.75, 1.6 and 1.5 mm meshes are 0.0125, 0.0048 and 0.0022 % strain respectively. These mean residual errors for the 1.6 and 1.5 mm meshes are relatively small in comparison to yield strains of bone, which have been reported in the literature in the range of 0.68 and 1.3% for cortical bone [Carter *et al.*, 1981b; Jepsen and Davy, 1997], and 0.61 and 0.85% for cancellous bone [Lindahl, 1976; Morgan and Keaveny, 2001]. Again for this model, equivalent strain convergence is achieved for mesh size of at least 1.6 mm.

On the basis of these results, for the remainder of the thesis, element edge lengths of at least 1.6 mm or lower were used.

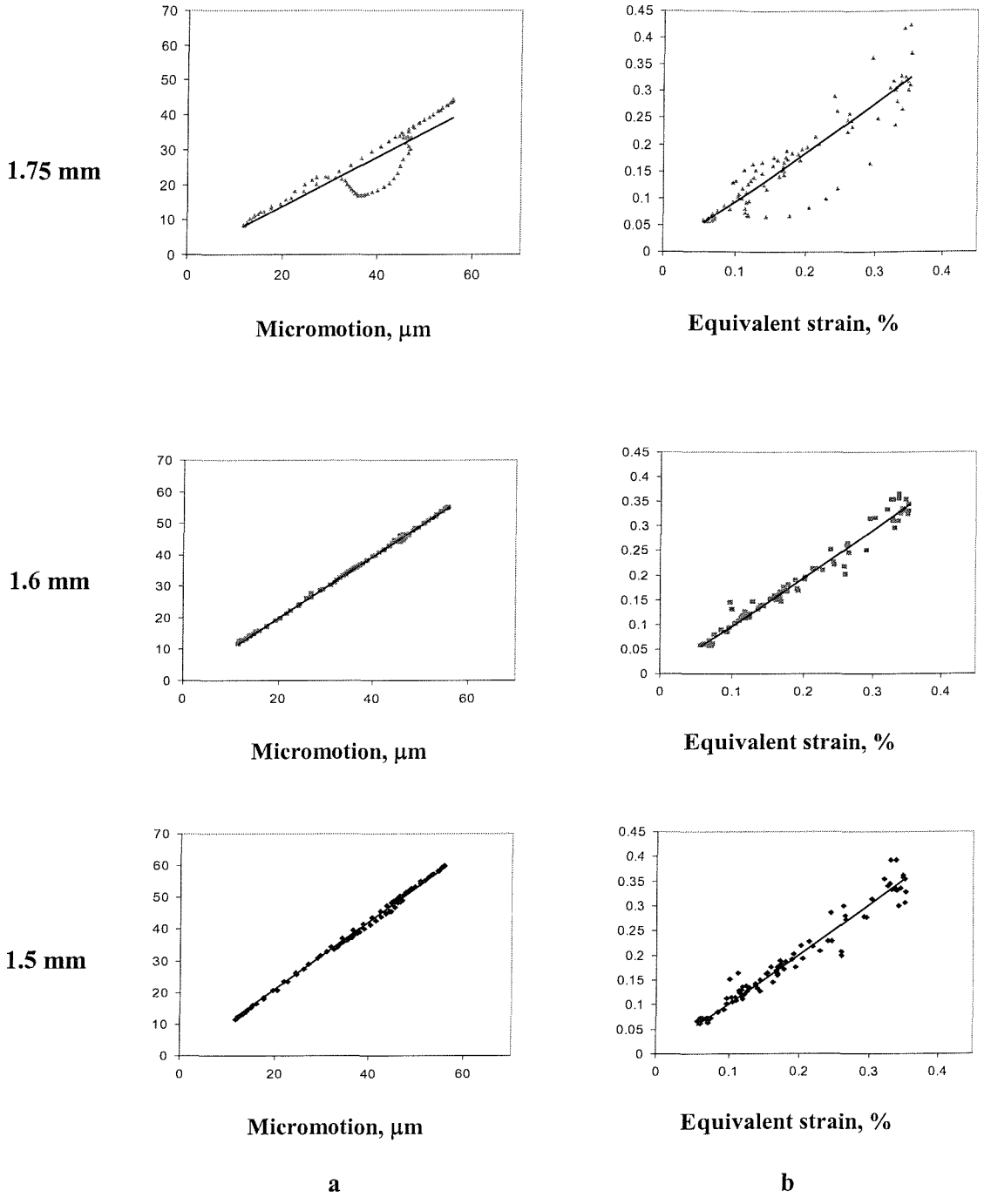

Figure 4.11 Micromotion (a) and strain (b) values of the coarser meshes were plotted against the values of the 1.4 mm mesh. A linear regression is performed for the plot and is shown here as a solid line.

Mesh	r^2	slope	Mean residual error (μm)
1.75 mm	0.8230	0.7012	7.7696
1.6 mm	0.9992	0.9842	0.5906
1.5 mm	0.9968	1.0637	2.3812
1.4 mm	-	-	-

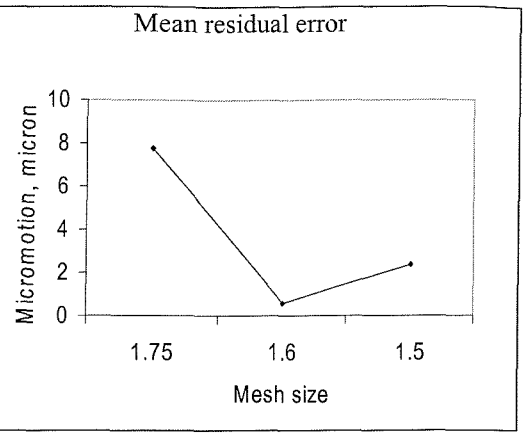

a

Mesh	r^2	slope	Mean residual error (%)
1.75 mm	0.8390	0.9273	0.0125
1.6 mm	0.9742	0.9741	0.0048
1.5 mm	0.9564	1.0121	0.0022
1.4 mm	-	-	-

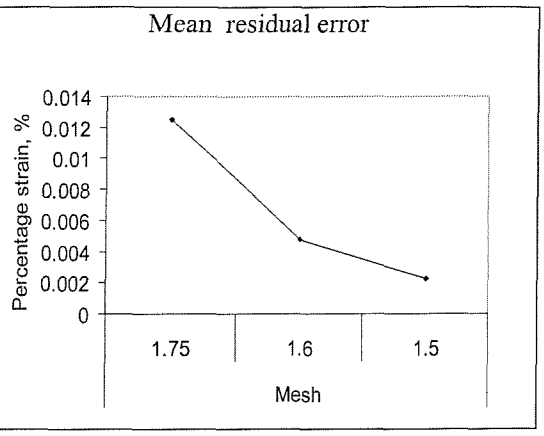

b

Table 4.4 The influence of mesh size on the convergence of (a) micromotion and (b) equivalent strain. The coefficient of correlation r^2 and slope were obtained from the linear regression of the plot of values of coarser meshes and 1.4 mm mesh.

4.3.2 Modelling parameters

The sensitivity of the model to modelling parameters was evaluated to check the robustness of the model. The parameters examined were convergence tolerance, contact separation force and contact tolerance. These three parameters were chosen because they affect the accuracy of the equilibrium of the model and accuracy of the contact detection.

4.3.2.1 Convergence tolerance

Convergence checking is used to check the accuracy of the equilibrium in the system during analysis. The convergence checking used for these analyses was the relative residual method, the default in MARC. In this method, the magnitude of the maximum residual force is compared to the magnitude of the maximum reaction force. Convergence is achieved if the ratio of these two forces is smaller than the tolerance set. Mathematically, a convergence criterion is satisfied if Equation 4.3 is satisfied.

$$\left\| \frac{F_{residual}}{F_{reaction}} \right\| < Tol \quad \text{---------- Equation 4.3}$$

$F_{residual}$ is the maximum absolute residual force and $F_{reaction}$ is the maximum absolute reaction force. Tol is the convergence tolerance.

The convergence tolerance was varied from 0.01 to 0.1. Similar to mesh convergence study in Section 4.3.1, the sensitivity of micromotion and equivalent strain to convergence tolerance was checked. The same regression method was used to quantify the error.

The micromotion and equivalent strain from the analysis with a tolerance value of 0.1 were plotted against values from analysis with a tolerance value of 0.01 (Figure 4.12a and b). The plot for the analysis with a tolerance value of 0.05 is not shown because it is very similar. The micromotion and equivalent strain values were not sensitive to the convergence tolerance for this model. In Table 4.5a, the slopes of the linear regressions for micromotion of the analyses with tolerance values of 0.1 and 0.05 relative to the tolerances of 0.01 are 1.006 and 1.004 respectively. Both the slopes of the linear regression for equivalent strain of the 0.1 and 0.05 tolerance values are 1.002 (Table 4.5b). The r^2 of micromotion and equivalent strain were 0.99 for tolerance values of 0.1 and 0.05. The mean residual error for micromotion is less than 0.1 μm and the mean residual error for equivalent strain is about 0.001% strain for tolerance values of 0.1 and 0.05. Therefore, convergence tolerance value of 0.1 did not introduce significant error relative to smaller convergence tolerance. From analysis run-time point of view, running the analysis with tolerance of 0.01 is likely to increase the run-time by more than two times the run-time of the analysis with tolerance of 0.1 (Figure 4.13). For the remainder of this thesis, a convergence tolerance of 0.1 was used.

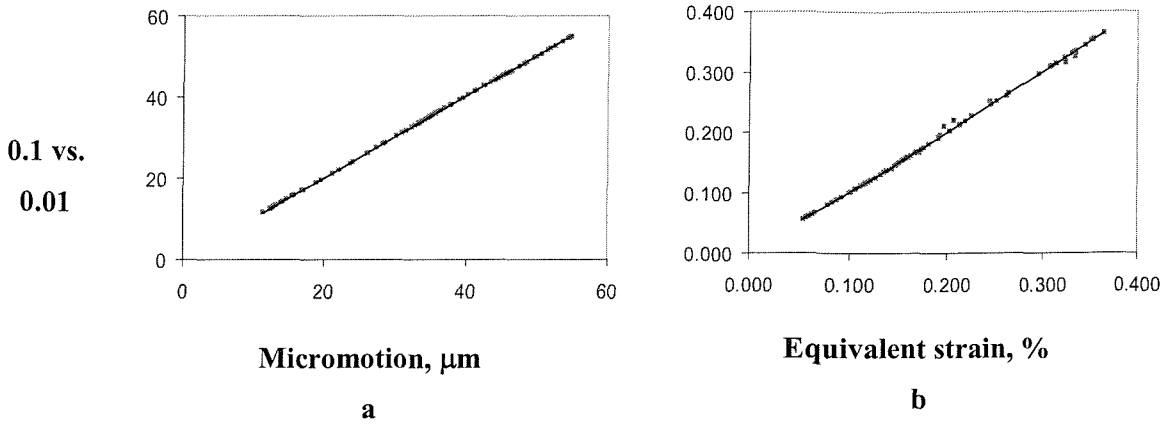

Figure 4.12 Micromotion and equivalent strain values from analyses with convergence tolerance of 0.1 and 0.01 were plotted. The analysis with convergence tolerance of 0.05 is not shown as the values are very similar. A linear regression was fitted and shown here as the solid line.

Micromotion, μm				Equivalent strain, %			
Convergence tolerance	**r^2**	**slope**	**Mean residual micromotion, μm**	**Convergence tolerance**	**r^2**	**slope**	**Mean residual strain, %**
0.1	0.99	1.006	0.072	0.1	0.99	1.002	0.00092
0.005	0.99	1.004	0.068	0.05	0.99	1.002	0.00106
0.01	-	-	-	0.01	-	-	-
a				b			

Table 4.5 The influence of convergence tolerance on (a) micromotion and (b) equivalent strain.

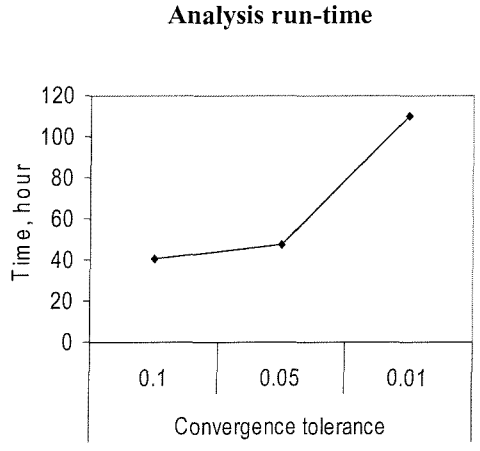

Figure 4.13 Analysis run-time for different convergence tolerance values. The run-time is almost identical for tolerance values of 0.1 and 0.05, but more than doubled when tolerance was set to 0.01.

4.3.2.2 Parameters influencing contact – Contact tolerance and contact separation force

Initially in the zero increment, the femur and the stem are in contact with each other. In increment one and subsequent increments, a small percentage of the loads are applied. When this happens, some nodes become separated and some nodes that have separated come into contact again. In MARC, this process of contact and separation is tracked by the direct constraint method. This procedure tracks the motion of the bodies and when they come into contact, direct constraints are placed on the motion using both kinematics constraints on nodal movement and nodal forces. The detection and separation of contact is described briefly below. A more detail description can be found in MARC 2001 reference manual Volume A (Theory and User information).

During the incremental procedure, MARC checks each potential contact node to see whether it is near a contact segment. In 3-D deformable bodies, the contact segments are the faces of the deformable bodies. The use of CONTACT TABLE option indicates the areas of contact and this reduces the amount of computation. The motion of each contact node is checked to see whether it has penetrated a surface by determining whether it has crossed a segment.

However, due to numerical consideration, it is unlikely that a node exactly contacts the surface of a segment. Therefore, a contact tolerance has to be set to define the distance from the segment where the node is considered to be in contact (Figure 4.14). MARC calculates the contact tolerance as 5% or the smallest element side. This value can be changed in the CONTACT TABLE option. During each increment, it is possible that a node can move beyond the contact tolerance. In this case, the node is considered to have penetrated the surface and the increment size will be reduced. Setting a very small contact tolerance can increase the computational cost due to difficulty in contact detection. However, a large contact tolerance will caused premature contact detection, which will give lower accuracy.

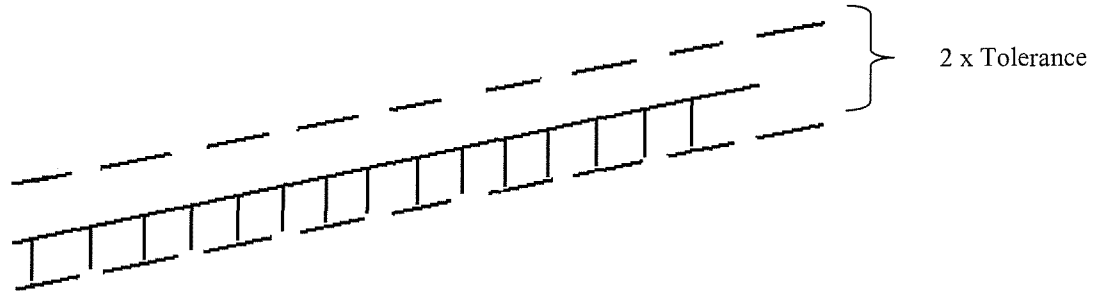

Figure 4.14 Contact zone within which node is considered to be in contact with a segment.

When a deformable body contacts another deformable body, a multipoint constraint is automatically imposed. For three-dimensional contact, five nodes – four from the patch and the

contacting node itself - are retained to form the constraint equation. The contacting node is able to slide on the contacted segment subjected to the friction conditions.

A node that has come into contact with a surface may separate from the surface during the subsequent iteration or increment. Separation occurs when the reaction force between the node and the surface becomes tensile or positive. This can be considered as a node should separate when the tensile force or normal stress exceeds the surface tension. However, a small positive reaction force might be due only to errors in equilibrium, the tensile force or stress required to cause separation can be entered by the user and this is known as the contact separation force. This avoids unnecessary separations.

4.3.2.3 Contact tolerance

Three analyses were run with the contact tolerance values set to 0.01, 0.0075 and 0.005 mm. The sensitivity of micromotion and equivalent strain to contact tolerance was evaluated using the same method described previously. If the model is not sensitive to these parameters, then the contact tolerance is sufficient to capture the moment of contact consistently.

The model was found to be insensitive to contact tolerance within the range of 0.01 and 0.005 mm. Micromotion and equivalent strain values of the analyses with contact tolerances of 0.01 and 0.0075 mm were plotted against the analysis with a contact tolerance of 0.005 mm. In Figure 4.15 only the plot between the 0.01 and 0.005 mm analyses is shown because of the similarity with the plot between the 0.0075 and 0.005 mm analyses. The slopes of the linear regressions for both plots are shown in Table 4.6a (micromotion) and b (equivalent strain). For linear regression of micromotion, the slopes for the 0.01 and 0.0075 mm analyses relative to the 0.005 mm analyses are 1.009 and 1.004 respectively (Table 4.6a), which are very close to 1 and showed small relative error. For linear regression of equivalent strain, the slope is 0.997 and 0.995 for contact tolerance of 0.01 and 0.0075 respectively. Again, the slopes are nearly one. The r^2 of micromotion and equivalent strain are 0.98 for contact tolerance of 0.01 and 0.0075. The mean residual micromotion for both analyses is less than 0.072 μm and the mean residual equivalent strain is less than 0.0011% strain, values which are small in comparison to micromotion threshold and yield strain of bone. As far as possible, the analyses in this thesis were performed with contact tolerance of about 0.01 mm.

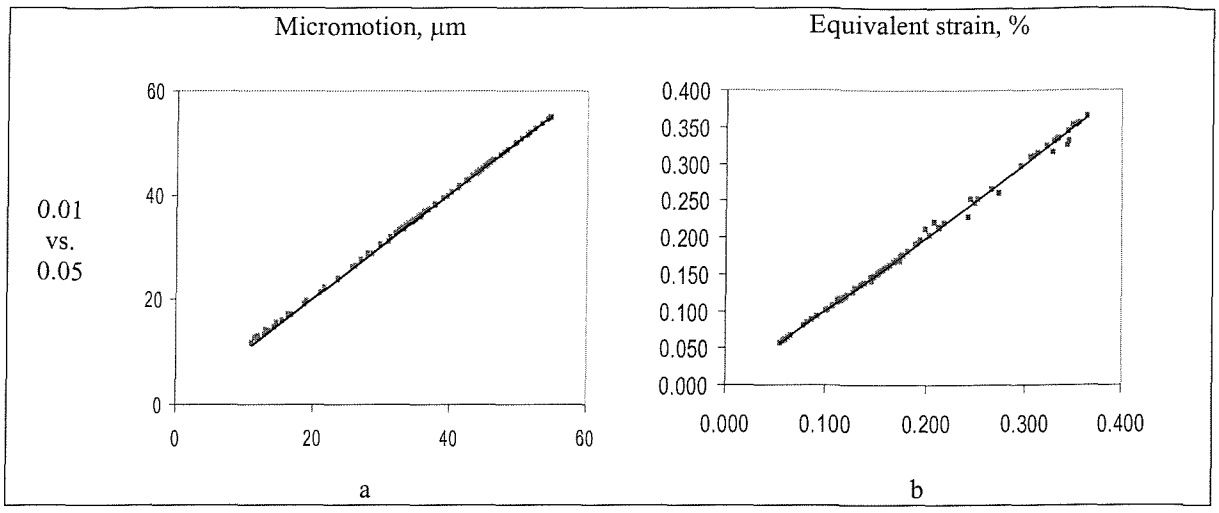

Figure 4.15 Micromotion and equivalent strain values from analyses with contact tolerance of 0.01 and 0.005 mm were plotted. The analysis with contact tolerance of 0.0075 mm is not shown as the values are very similar. A linear regression was fitted and shown here as the solid line.

Micromotion, μm				Equivalent strain, %			
Contact tolerance, mm	**r^2**	**slope**	**Mean residual micromotion, μm**	**Contact tolerance, mm**	**r^2**	**slope**	**Mean residual strain, %**
0.0100	0.98	1.009	0.221	0.0100	0.98	0.997	0.00203
0.0075	0.98	1.004	0.113	0.0075	0.98	0.995	0.00116
0.0050	-	-	-	0.0050	-	-	-
a				b			

Table 4.6 The influence of contact tolerance on (a) micromotion and (b) equivalent strain.

4.3.2.4 Contact separation force

The default contact separation force is the maximum residual force. Leaving this value to default, the contact separation force will vary during the analysis from increment to increment and also in different analyses. The effect of a variable contact separation force on micromotion and equivalent strain values will be hard to judge. In order to standardize this value for different analyses, the model sensitivity to this parameter was evaluated by running three analyses with contact separation forces of 0.05, 0.01 and 0.005.

The model is insensitive to the contact separation force between 0.05 and 0.005. In Figure 4.16,the micromotion and equivalent strain values of the analysis with contact separation force of 0.05 were plotted against the values from the analysis with contact separation force of 0.005. Similar plot with analysis with contact separation force of 0.01 is not shown because the plot is very similar. Table 4.7 shows the regression slopes for micromotion and equivalent strain for different values of contact separation force. For both micromotion and strain, the regression slopes are nearly 1 for both contact separation force of 0.05 and 0.01. The r^2 values of both micromotion

and equivalent strain are greater than 0.99 for both 0.05 and 0.01 contact separation force. The mean residual micromotions are 0.041 and 0.039 μm for the 0.05 and 0.01 analyses respectively. The mean residual equivalent strains are 0.0004% strain for the former and 0.00038% for the latter. Both the mean residual micromotion and equivalent strains are negligible in comparison to bone ingrowth threshold and bone yield strain. The contact separation force for the remainder of this thesis was kept at about 0.05.

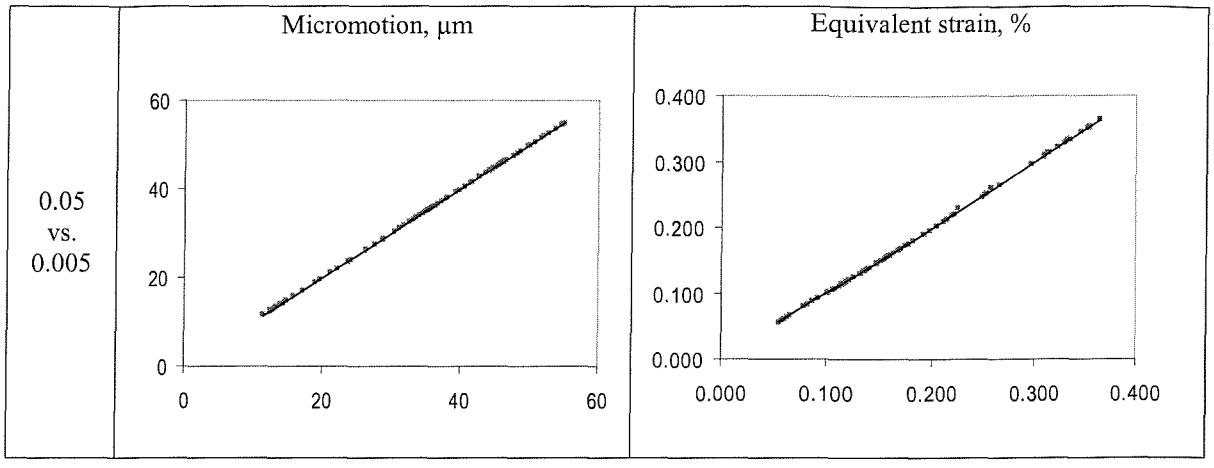

Figure 4.16 Micromotion and equivalent strain values from analyses with contact separation force of 0.05 and 0.005 were plotted. The analysis with contact separation force of 0.01 is not shown as the values are very similar. A linear regression was fitted and shown here as the solid line.

	Micromotion, μm				**Equivalent strain, %**		
Contact separation force	**r^2**	**Slope**	**Mean residual micromotion, μm**	**Contact separation force**	**r^2**	**Slope**	**Mean residual strain, %**
0.05	0.99	1.00001	0.041	0.05	0.99	1.00003	0.00040
0.01	0.99	1.00005	0.039	0.01	0.99	1.00135	0.00038
0.005	-	-	-	0.005	-	-	-
		a				b	

Table 4.7 The influence of contact separation force on (a) micromotion and (b) equivalent strain.

4.4 Summary

This is a robust model that has been shown to be insensitive to the following modelling parameters – convergence tolerance, contact tolerance and contact separation force. Bernakiewicz and Viceconti (2002) stresses on the importance of identifying parameters that affect the results of finite element contact analysis in orthopaedic biomechanics. Bernakiewicz and Viceconti (2002) suggested that the parameters evaluated in the previous section could have significant influence on the result of a contact study. The parameters were evaluated and did not introduce significant variability to the values of the predicted micromotion and equivalent strain. The values used in this thesis did not deviate much from the range of values evaluated in this chapter and therefore should not introduce significant errors on the predicted micromotion and equivalent strain.

Chapter 5 Effect of different bone material properties on initial stability of the IPS stem

5.1 Introduction

The Young's modulus and strength of bone vary between each individual due to differences in the degree of porosity, mineralization and architecture of bone. The differences between individuals can be significant depending on their diet [Cowin, 2001], activities [Cowin, 2001], age [McCalden *et al.*, 1993; Ding *et al.*, 1997; McCalden *et al.*, 1997; Zioupos and Currey, 1998; Moselkilde, 2000] and disease [Grynpas *et al.*, 1991; Zysset *et al.*, 1994; Li and Aspden, 1997; Yang *et al.*, 1997; Fazzalari *et al.*, 1998; Bogoch and Moran, 1999; Moselkilde, 2000; Ding *et al.*, 2001]. It is a well-known fact that active individuals normally have stronger bones due to higher degree of strain stimulus for their skeletal structure which leads to biological modelling of stronger bone structure.

After the age of 30 years, bone mass decreases slowly with age, which is thought to be caused by a small deficit of osteoblast deposition relative to osteoclast resorption [Ding *et al.*, 1997; Cowin, 2001; van der Linden *et al.*, 2001]. However, the loss of bone mass is different between individuals. For females, hormonal imbalance during the menopause causes an increase in bone resorption depth and activation frequency, leading to osteoporotic bone that is more susceptible to fracture [Mosley, 2000]. Although more prevalent among females, osteoporosis can also affect aging males [Cowin, 2001]. A diet riched in calcium may slow down the osteoporotic process among osteoporosis patient.

Among the patients undergoing total hip arthroplasty, the cause could be due to bone diseases like osteoporosis, osteoarthritis, rheumatoid arthritis and avascular necrosis [Mont *et al.*, 1992]. Bone diseases have been shown to affect the quality of bone like ultimate strength, Young's modulus and fracture energy [Grynpas *et al.*, 1991; Zysset *et al.*, 1994; Li and Aspden, 1997; Yang *et al.*, 1997; Fazzalari *et al.*, 1998; Moselkilde, 2000; Ding *et al.*, 2001]. The patients may have different bone quality, and yet they may have similar femur geometry and are implanted with hip stems of the same design and size. The performance of the hip stem in each patient is likely to be different due to differences in bone quality. Better quality bone provides better support for a hip implant and normally provides better fixation and greater satisfaction to the patient [Robertson *et al.*, 1988; Engh *et al.*, 1990].

Mechanical properties of bone change with age (Table 5.1). Zioupos and Currey (1998) reported reduction in Young's modulus of cortical bone in diaphyseal femur of about 2.3% per decade. One study reported that ultimate stress and strain of cortical bone reduced by 5 and 9% per decade respectively, but Young's modulus was unchanged by age [McCalden *et al.*, 1993].

Cortical bone specimens from elderly donors have been selectively taken from sites with thicker wall and this could have biased the selection towards bone with Young's modulus that has not changed significantly with age. Courtney *et al.* (1996) reported a more modest reduction in Young's modulus of cortical bone. They reported 6% reduction in Young's modulus between two groups of bone specimens with mean age of 26 and 72 years respectively. Ding *et al.* (1997) reported that tibia cancellous bone has the highest modulus between age 40 and 50 years; subsequently, reductions of as much as 40% between the age of 50 and 80 years old are possible. McCalden *et al.* (1997) reported 8.5% reduction of ultimate stress per decade in the distal femur cancellous bone. From these studies, cancellous bone seems to be losing its elasticity and strength faster with age than cortical bone. This is not surprising considering bone turnover of cancellous bone is much faster than cortical bone, and with every remodelling, some cancellous bone mass is lost [Cowin, 2001].

Bone quality changes in pathological bone is more complex (Table 5.1). Ding *et al.* (2001) reported that Young's modulus of cancellous bone during early-stage osteoarthritis in the proximal tibia is 42 % less than normal bone, while some studies showed that in late stage osteoarthritis, Young's moduli in cancellous bone is greater than normal bone [Li and Aspden, 1997]. Li and Aspden (1997) reported highest mean Young's modulus for osteoarthritic bone (14.8% more than normal bone), followed by normal bone and osteoporotic bone (20% less than normal. Zysset *et al.* (1994) reported that progression of osteoarthritis at the proximal tibia causes 65% reduction in stiffness of subchondral bone but not epiphyseal and metaphyseal bone. In comparison to normal and osteoarthritis bone, rheumatoid arthritis bone has been reported to be 47.5% and 39.5% less stiff respectively [Yang *et al.*, 1997].

Although it is known that bone quality affects the performance of cementless hip stems, it is difficult to quantify the bone quality of cadaveric femurs used in experimental studies of hip stems stability. Experimental studies normally report mean micromotion and the range of micromotion from a group of cadaveric femurs [Walker *et al.*, 1987; Schneider *et al.*, 1989; Burke *et al.*, 1991; Callaghan *et al.*, 1992; Sugiyama *et al.*, 1992; Hua and Walker, 1994]. In cadaveric studies, femur showing no pathologies are often used and therefore age is likely to be the only factor affecting bone quality. However, without a quantification of bone quality, it is not possible to predict the performance of the studied hip stems in relation to bone quality. It is therefore difficult to have an objective measure to decide whether a patient's bone is of sufficient quality to use cementless stem or the patient should receive cemented stem. Therefore during the design stage, consideration should be given to design a cementless stem that is able to give satisfactory performance even in patients with poor bone quality.

Finite element studies have been used extensively to study the stability of cementless hip stems [Rubin *et al.*, 1993; Keaveny and Bartel, 1993c; Kuiper and Huiskes, 1996; Ramaniraka *et al.*, 1996; Ando *et al.*, 1999; Viceconti *et al.*, 2000; Fernandes *et al.*, 2002]. A study by Viceconti

et al. (2000) which combined experimental and finite element study showed that finite element study can provide sufficient accuracy to predict the performance of a cementless stem. However, it has not been reported in the literature the effect of bone quality on the stability of hip stem. It is therefore easier to study the effect of bone quality on performance of cementless hip stem using finite element study.

In assessing the performance of hip stems, other studies have normally separately examined either implant micromotion or stress/strain. As discussed in Section 3.8, high micromotions can cause failure of bone ingrowth. However, as discussed in Section 3.4, high interface stress or strain could also cause fatigue failure of the supporting cancellous bone causing excessive migration. This could also lead to fixation failure. The evaluation of interface strain is therefore vital as part of the preclinical assessment of hip stem designs as this is a measure of the risk of implant migration. Fatigue life of supporting cancellous bone in the first few months postoperatively could be affected by a combination of the damage of bone due to weight bearing and also damage of bone during the insertion of the stem. Therefore, both the interface micromotion and strain should be examine together as part of the preclinical assessment of hip stem designs.

In this study, the effect of bone and stem quality on stability of the IPS stem was examined. The objectives were to look at :-

1) the sensitivity of cementless stem's stability as a result of variation in bone quality.
2) the sensitivity of the interface bone strain as a result of changes in bone quality.
3) is the assessment of implant stability based on one set of bone CT scan data adequate?

Author	Bone type	Location	Factor of change	Properties change	Note on changes of properties
Ding *et al.*, 1997	TB	Proximal tibia	Age	E = - 40% σ_{ult} = -50%	Reduction between 50-80 years old
Courtney *et al.*, 1996	CB	Diaphyseal femur	Age	E = -6%	Reduction between 26-72 years old
McCalden *et al.*, 1993	CB	Diaphyseal femur	Age	σ_{ult} = -5% ε_{ult} = - 9%	Reduction between 20-102 years old
McCalden *et al.*, 1997	TB	Distal femur	Age	σ_{ult} = -8.5 %/decade	Reduction between 20-102 years old
Zioupos and Currey, 1998	CB	Mid diaphyseal femur	Age	E = -2.3 %/decade	Reduction between 35-92 years old
Ding *et al.*, 2001	SB	Proximal tibia	Osteoarthritis	E = - 42 %	Early stage osteoarthritis
Zysset *et al.*, 1994	TB	Proximal tibia - subchondral	Osteoarthritis Medial Lateral	 E = - 58.6% E = -69.0%	Increment of osteoarthritis stages from 1 to 3
		- Epiphyseal		E = 0 %	
		- Metaphyseal		E = 0 %	
Yang *et al.*, 1997	TB	Proximal tibia	Normal	E = 1287 N/mm	Data of normal and osteoarthritis bone from another study.
			Osteoarthritis	E = 1116 N/mm	
			Rheumatoid arthritis	E = 675 N/mm	
Li and Aspden, 1997	TB	Femoral head	Normal	E =310 MPa	Mean values of regions in femoral head and neck.
			Osteoarthritis	E = 356 MPa	
			Osteoporosis	E = 247 MPa	

Table 5.1 Changes to mechanical properties of bone due to aging and diseases reported in the literature. E = Young's modulus, σ_{ult} = ultimate stress, ε_{ult} = ultimate strain, TB = cancellous bone, CB = cortical bone, SB = subchondral bone.

5.2 Modification to material properties of bone

The generation and assessment of the finite element model has been discussed in Chapter 4. In this study, the same model was used but the material properties of the femur were systematically reduced. The reduction of bone quality was achieved by scaling the density-elastic modulus relationship with a constant. Using Equation 4.1 (Section 4.2.2), the Young's modulus of each individual element was systematically reduced by 10%, 20%, 30% and 40%. The reduction was performed by multiplying the coefficient in Equation 4.1 by the appropriate factor (Table 5.2). The result of this action to the density-elastic modulus relationship is shown in Figure 5.1. Reduction of 40% of Young's modulus in cancellous bone can be expected due to changes in bone density with age [Ding *et al.*, 1997] or disease [Yang *et al.*, 1997]. These five models will be referred to as the **Bone-0**, **Bone-10**, **Bone-20**, **Bone-30** and **Bone-40** models to correspond to the reduction of modulus by 0, 10, 20, 30 and 40% respectively.

Reduction in Young's moduli	0 %	10 %	20 %	30 %	40 %
Coefficient	2875.0	2587.5	2300.0	2012.5	1725.0

Table 5.2 Modified coefficients of Equation 4.1, $E = 2875\rho^3$. The bone's Young's moduli have been reduced by 10 and 40 %.

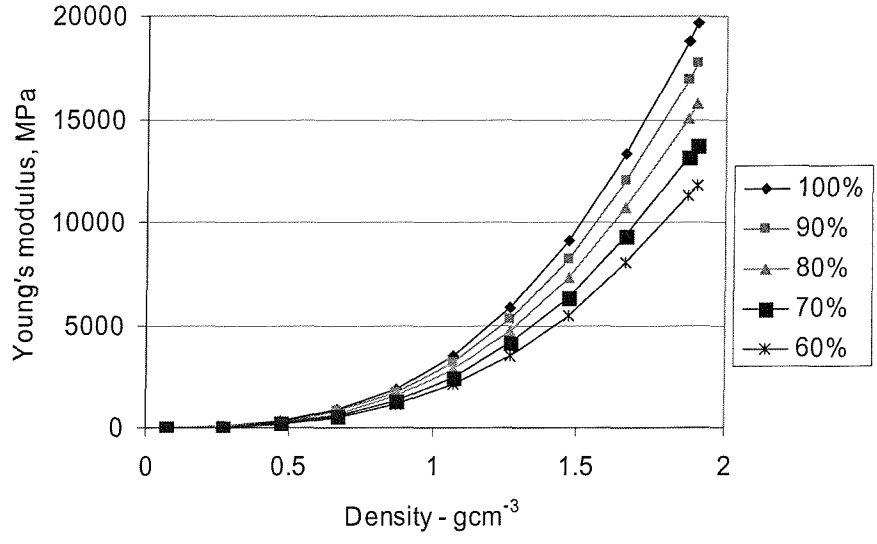

Figure 5.1 Systematic reduction of density-elastic modulus relationship by 10%, 20%, 30% and 40%. This could be seen as reduction of bone quality cause by aging or disease.

However, bone remodelling in cortical bone is slower than cancellous bone [Cowin, 2001]. The rate of Young's modulus change with age for cortical bone has also been reported to be lower at 2.3% per decade [Zioupos and Currey, 1998]. The reduction of cortical bone Young's modulus will be about 11.5 % from the age of 30 to 80 years old, according to this study. In order to account for a slower reduction of cortical bone Young's modulus in relation to cancellous bone,

two more analyses were performed with 0 and 20% reduction in cortical bone Young's modulus. However Cowin (2001) reported that humans lost at least 30% of the bone mass by age of 70. Since 80% of human bone mass comes from cortical bone, the thickness of cortical bone will also reduce with age [McCalden *et al.*, 1993; Cowin, 2001]. The reduction of cortical bone Young's modulus greater than the reduction reported by Zioupos and Currey (1998) can be seen as simulating the reduction of thickness of cortical bone as well as reduction of Young's modulus, as has been reported in another finite element analysis of a shoulder joint prosthesis [Lacroix *et al.*, 2000]. The cancellous bone Young's modulus was assumed to reduce by 40% in both cases and in the original femur, the Young's modulus of cancellous bone was assumed to be less than 1500 MPa. Brown (1980) reported cancellous bone values of less than 1400 MPa in the intertrochanteric region and greater trochanter. In finite element studies, 1500 MPa is about the highest value assigned for cancellous bone stiffness [Duda *et al.*, 1998]. These two analyses looked at the individual effect of cancellous and cortical bones qualities on the initial micromotion and strain. These two models will be referred to as the **40TB-0CB** (the moduli of cancellous and cortical bone are reduced by 40% and 0% respectively) and **40TB-20CB** (the moduli of cancellous and cortical bone are reduced by 40% and 20% respectively) models.

The total micromotion and equivalent strain at the implanted femur are reported here. Only the walking loadcase was analysed for this study (Section 4.2.4). Micromotion and equivalent strain are sampled in three different cross-sectional levels as shown in Figure 5.2. L1 is just below the neck resection level, L2 at the intertrochanteric region and L3 is at the distal end of the porous coating of the stem.

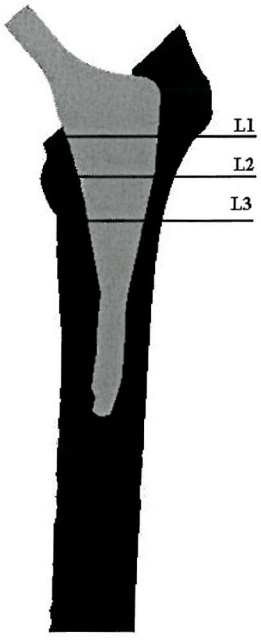

Figure 5.2 Results are sampled from cross-sectional levels L1, L2 and L3.

To compare the effect of material property on contact area, the percentage area under 50 μm micromotion at the bone-stem interface was measured. This is the ratio of length between nodes with micromotion less than 50 μm over the total length of the perimeter of the bone-implant interface at each level (Figure 5.3). This gives a measure of the of predicted area of bone ingrowth in each reported cross-section. 50 μm is considered as a reasonable threshold value that allows osseointegration [Engh *et al.*, 1992b; Bragdon *et al.*, 1996; Fernandes *et al.*, 2002] as discussed in Section 3.8.1.

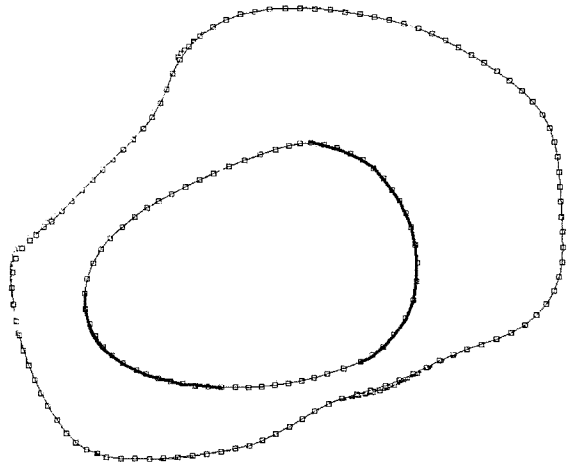

Figure 5.3 Area under 50 μm is defined as the ratio of the length of thick line (nodes with micromotion less than 50 μm) over the bone-stem interface perimeter.

5.3 Influence of Young's modulus on stem micromotion and femoral strain

5.3.1 Effect of reducing Young's modulus of cancellous and cortical bone by the same percentage

Initial stability of IPS stem is sensitive to changes in Young's modulus of bone. Reduction in Young's modulus of bone increases the micromotion of the hip stem. Figure 5.4 illustrates the changes in micromotion and area of bone ingrowth due to changes in Young's moduli.

Generally, predicted area under 50 μm decreases to correspond with reduction of Young's modulus as shown in Figure 5.4. The reduction in bone ingrowth area with Young's modulus is higher at L1 than at L2 and L3. The predicted area of bone ingrowth also reduces by a smaller amount at the more distal level. At level L1, the area of bone ingrowth is predicted to be highest in the Bone-0 model and lowest in Bone-40 model with values of 88% and 28% respectively. At level L2 and L3, areas of bone ingrowth remain high in Bone-0 model with values of 97% and 87% respectively. Predicted areas of bone ingrowth is still smallest in Bone-40 model, but with values of 56 and 76% at L2 and L3 respectively, are considerably higher than at L1. Overall, predicted bone ingrowth of the stiffest femur is highest. Bone-0 model showed good initial stability with bone ingrowth higher than 80% at all levels. The greater reduction in bone ingrowth

proximally could be due to a softer cortical bone envelope and a thicker layer of cancellous bone, which imposed less constraint to the stem. Distally, the stem is closer to the cortical bone envelope and hence the bone is stiffer.

Generally, the peak micromotions are higher at L1 and L3 than at L2, but the values of each model are in a narrow range. The peak micromotion showed a non-linear increment with reduction of Young's modulus as shown in Figure 5.4. In the Bone-0 model, peak micromotion is between 50-55 μm at L1, L2 and L3. This is just over the 50 μm bone ingrowth threshold value. On the other hand, in Bone-40 model the peak micromotion is between 80-91 μm. This is much higher than the 50 μm bone ingrowth threshold. Comparing Bone-0 and Bone-40, peak micromotion has increased significantly.

Figure 5.5 shows the distribution of micromotion at levels L1, L2 and L3. At level L1, peak micromotion consistently occurred at the anterior side in every model. The lateral micromotion is consistently the lowest in every model. The medial section retained high level of micromotion. At level L2, the medial side has the highest micromotion, with lowest micromotion at the posterior-lateral side. Level L3 also showed highest micromotion at the medial side. The lowest micromotion is at the posterior-lateral side.

Figure 5.6 shows the micromotion component in the anterior-posterior (AP), superior-inferior (SI) and medial-lateral (ML) directions for selected medial and lateral nodes at L1 and L3. Rotational micromotions on the horizontal plane increase with reduction of Young's modulus, which can be seen from the higher micromotions in the AP direction on the medial and lateral nodes. The directions are opposite for the medial and lateral nodes. The higher micromotion in the SI direction shows that the axial micromotion is also higher with reduction of Young's modulus. Reduction of Young's modulus increases both rotational and axial micromotions.

Poor bone quality in the femur also lead to higher strain in the interface bone. Figure 5.7 shows consistent increase in equivalent strain in the interface bone as the Young's modulus decreased. The maximum equivalent strain is also shown to be increasing in a non-linear fashion; with a gradually increasing gradient as the Young's modulus decreased. The mean equivalent strains are between 0.14 and 0.19% and maximum equivalent strains are between 0.28 and 0.36% for Bone-0 model. In comparison, the mean equivalent strains are between 0.23 and 0.31% and maximum equivalent strains are between 0.45 and 0.6% for Bone-40 model. In comparison to Bone-0 model, the equivalent strain is significantly higher for the Bone-40 model. The maximum equivalent strains in the Bone-40 model are close to the yield strain value of cancellous bone, which is about 0.7% strain.

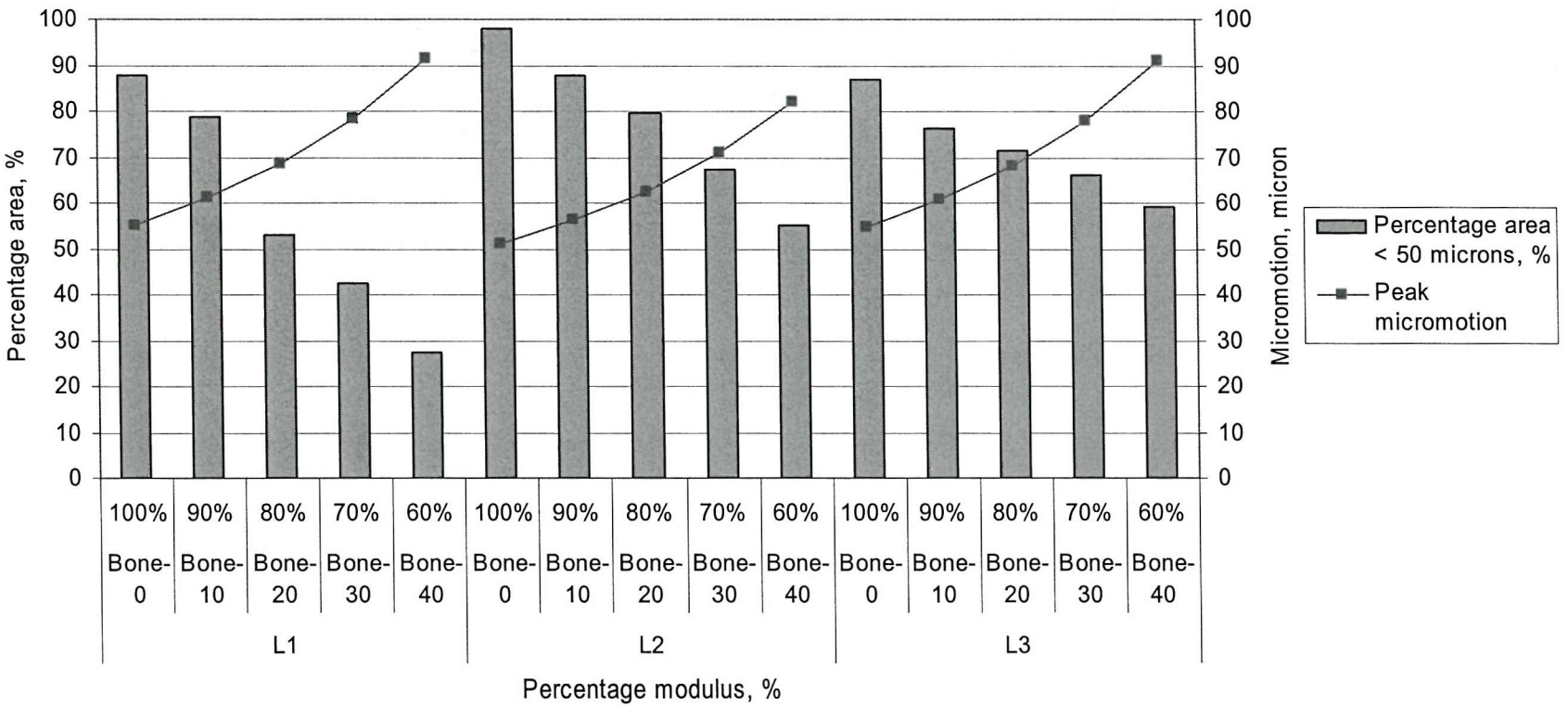

Figure 5.4 Micromotion at level L1, L2 and L3. The bar chart shows the percentage area at the particular level with micromotion less than 50 μm. The line chart shows the maximum micromotion in that particular level. Maximum micromotion increases as the Young's modulus of bone decreases, shown as the percentage Young's modulus of the normal bone in the horizontal axis. The increase is non-linear, with the gradient being steeper as the Young's modulus decreases. There is also a significant reduction in areas with micromotion under 50 μm. Level 1 is just below the resection level, Level 3 is at the distal end of the porous coating.

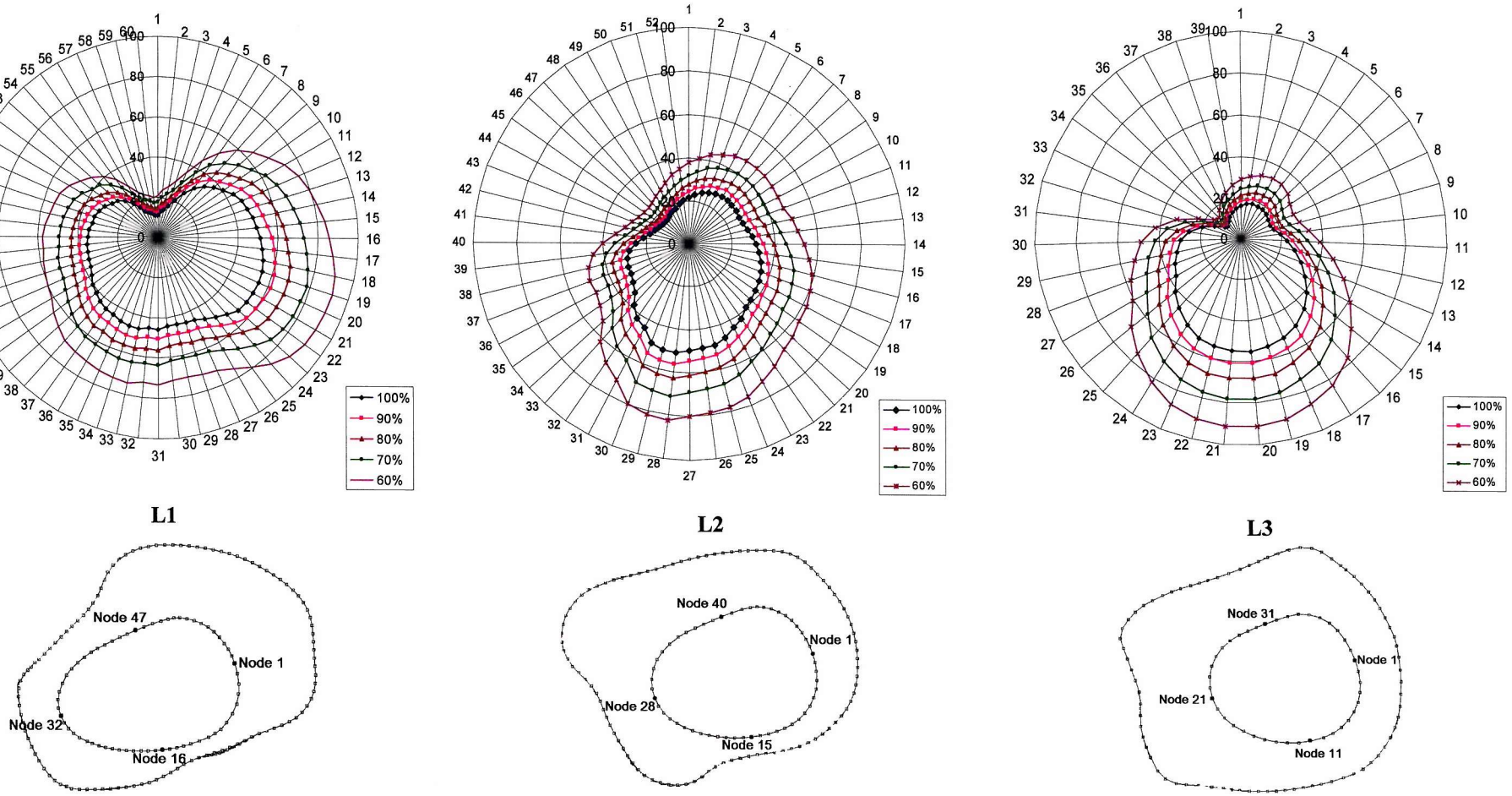

Figure 5.5 Distribution of total micromotion at level L1, L2 and L3. The outer perimeter of the chart showed node numbers corresponding to the numbers shown on the bottom figures. The radial scale displays the micromotion (μm). The lines represent the micromotion distribution for the Bone-0 (100%), Bone-10 (90%), Bone-20 (80%), Bone-30 (70%) and Bone-40 (60%) models.

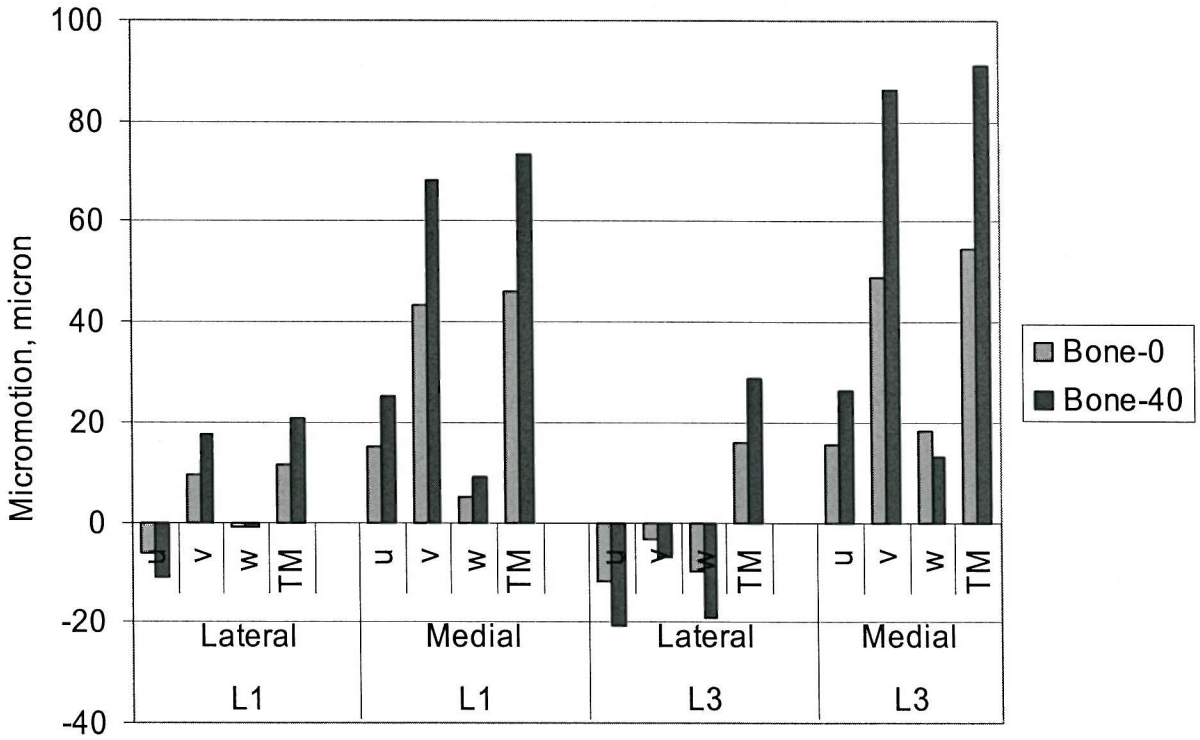

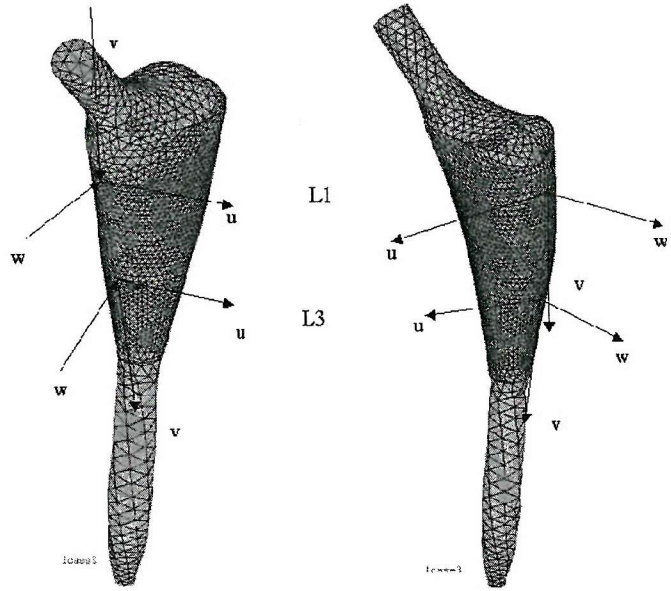

u: A-P = +ve, P-A = -ve
v: S-I = +ve, I-S = -ve
w: M-L = +ve, L-M = -ve
A = anterior, P = posterior, S = Superior, I = inferior,
M = medial, L = lateral, TM = total micromotion

Figure 5.6 Micromotion at the lateral and medial nodes at level L1 and L3 as shown on the right. With reduction of Young's modulus, micromotion increased in all directions. Bone-40 has higher axial micromotion (**v**) on both medial and lateral sides. Rotation of stem neck in the Bone-40 model is also higher with higher medial A-P motion(+ve **u**) and lateral P-A motion (-ve **u**).

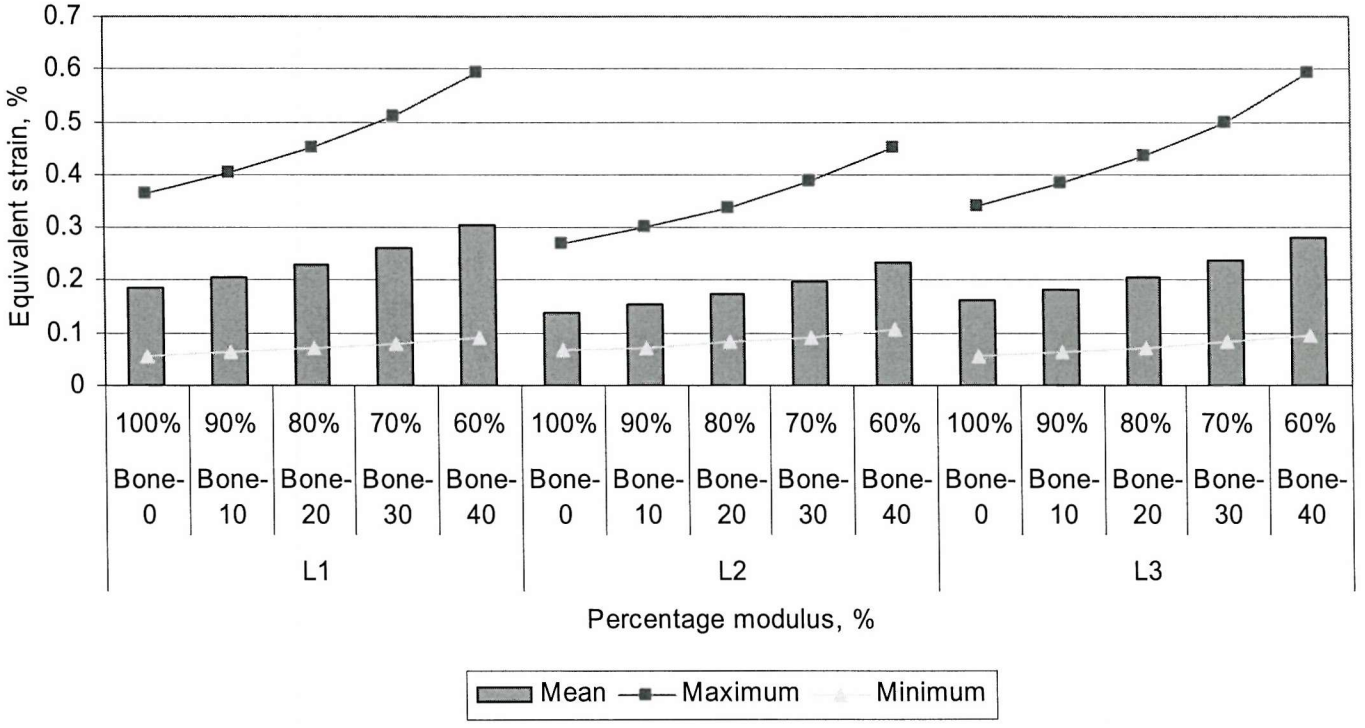

Figure 5.7 Equivalent strain at the bone-implant interface at level L1, L2 and L3. Mean strain at each level is shown as the bar chart. The line chart represents the maximum and minimum strain in each level. Maximum strain increases nonlinearly with reduction in bone Young's modulus, shown as the percentage of the normal bone at the horizontal axis.

5.3.2 Effect of reducing Young's modulus of cortical bone independent of cancellous bone

Figure 5.8 compares the average and maximum micromotion of Bone-0, Bone-40, 40TB-0CB and 40TB-20CB. Generally, there is a greater micromotion increase proximally than distally when only the cancellous bone modulus is reduced. The average and maximum micromotions of 40TB-0CB and 40TB-20CB fall between the values of Bone-0 and Bone-40. Reducing only the Young's modulus of cancellous bone by 40% (40TB-0CB), the average micromotion increased by less than 22% and the peak micromotion increased by less than 25% at L1, L2 and L3 in comparison to Bone-0. The highest micromotion increase occurred at L1, while L2 is higher than L3. The average micromotion increased by 15 and 13% in L2 and L3 respectively. Therefore, percentage micromotion increase is greater proximally when cancellous bone Young's modulus is reduced independently of cortical bone.

Generally, reducing cortical bone modulus increases distal micromotion more than proximal micromotion. When the cancellous bone Young's modulus was reduced by 40%, and cortical bone Young's modulus was reduced by 20% (40TB-20CB) and 40% (Bone-40) respectively, the increase in micromotion is greatest at L2 and L3 for both models in comparison to Bone-0. At L2, average micromotion in 40TB-20CB and Bone-40 increased by 35 and 66% respectively. In comparison, average micromotion increased only by 15% in 40TB-0CB. The increase of average micromotion at L2 is about 4 times greater in model Bone-40 than 40TB-0CB, in comparison to Bone-0. At L3, average micromotion increased by 13, 35 and 69% in models 40TB-0CB, 40TB-20CB and Bone-40 respectively. The increase of average micromotion at L3 is five times greater in model Bone-40 than 40TB-0CB, in comparison to Bone-0. At L1, average micromotion increased by 22, 39 and 64% in 40TB-0CB, 40TB-20CB and Bone-40 respectively. The increase of average micromotion at L1 is only three times greater in model Bone-40 than model 40-TB-0CB, in comparison to Bone-0. The comparison of micromotion change at level L1, L2 and L3 shows that the percentage micromotion change is greater distally when Young's modulus of cortical bone is reduced. This is most likely to be due to thinner layer of cancellous bone and thicker layer of cortical bone distally. Therefore, reducing the Young's modulus of cortical bone has a greater effect on micromotion distally.

Similar to micromotion, the reduction of cortical bone modulus affects the more distal equivalent strain more than the more proximal equivalent strain. Figure 5.9 shows the minimum, peak and mean equivalent strain in Bone-0, Bone-40, 40TB-0CB and 40TB-20CB. Reducing the Young's modulus of cancellous bone only (model 40TB-0CB), average equivalent strain increase by 37, 21 and 22% at L1, L2 and L3 respectively in comparison to Bone-0. Proximal strain increase is more than distal strain increase. Reducing the Young's modulus of cortical bone by 20% and cancellous bone by 40% (40TB-20CB), average equivalent strain increase by 49, 39 and

42% at L1, L2 and L3 respectively. Comparing model 40TB-20CB and 40TB-0CB, there is a higher percentage equivalent strain increase in the former at level L2 and L3 than L1. Since there is thicker layer of cancellous bone in L1 than the more distal L2 and L3, reducing the Young's modulus of cortical bone has greater effect on the stiffness of the femur in L2 and L3. Therefore, reducing Young's modulus of cortical bone increases the equivalent strain more distally than proximally. The maximum equivalent strain also increases with decreasing Young's modulus.

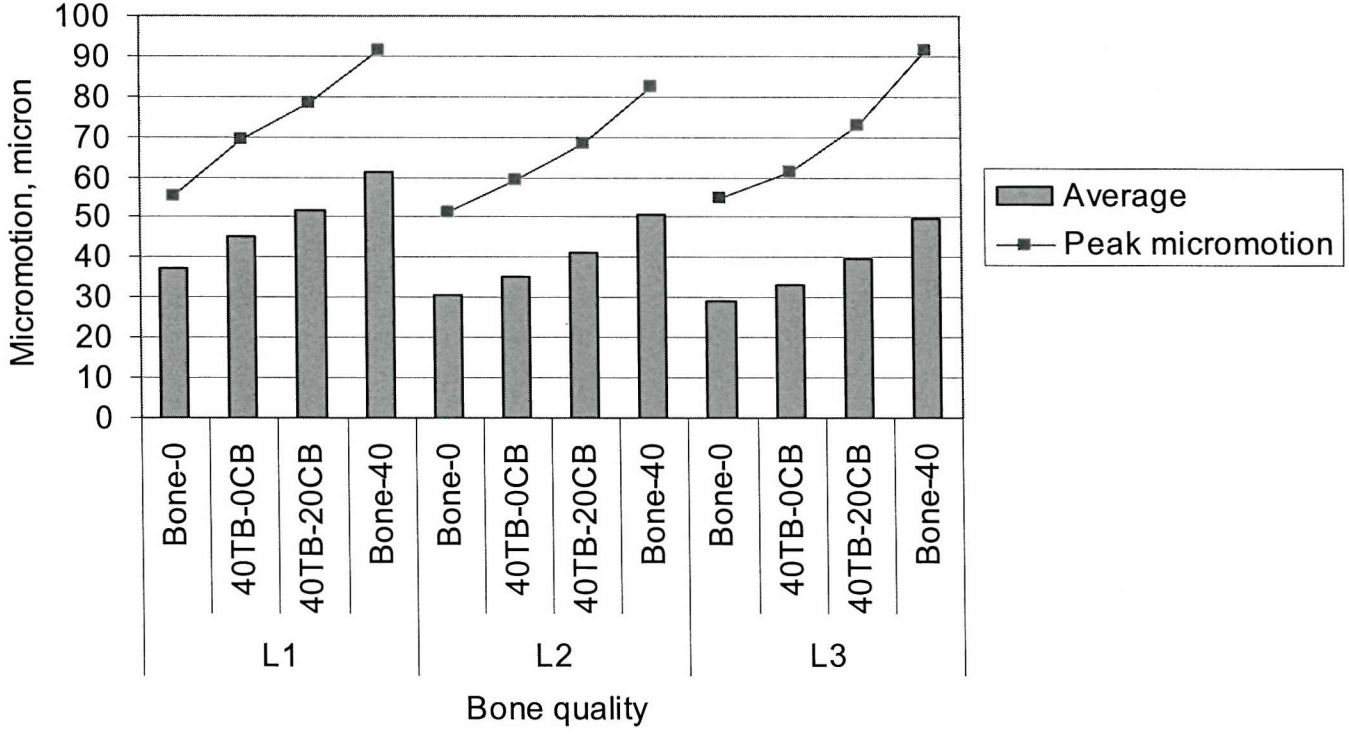

Figure 5.8 Comparing the effect of reducing Young's modulus of cortical and cancellous bones independently on micromotion. Looking at the effect of reducing stiffness of cancellous bone only (model 40TB-0CB), the effect is greater proximally in L1 and L2. The increased in average micromotion is 22, 15 and 13% in L1, L2 and L3 respectively. Reducing Young's modulus of cortical and cancellous bone by 20 (40TB-20CB) and 40% (Bone-40) respectively, average micromotion increased by 39, 35 and 35% in L1, L2 and L3 respectively. The effect of reducing Young's modulus of cancellous bone is greater proximally while effect of reducing Young's modulus of cortical bone is greater distally.

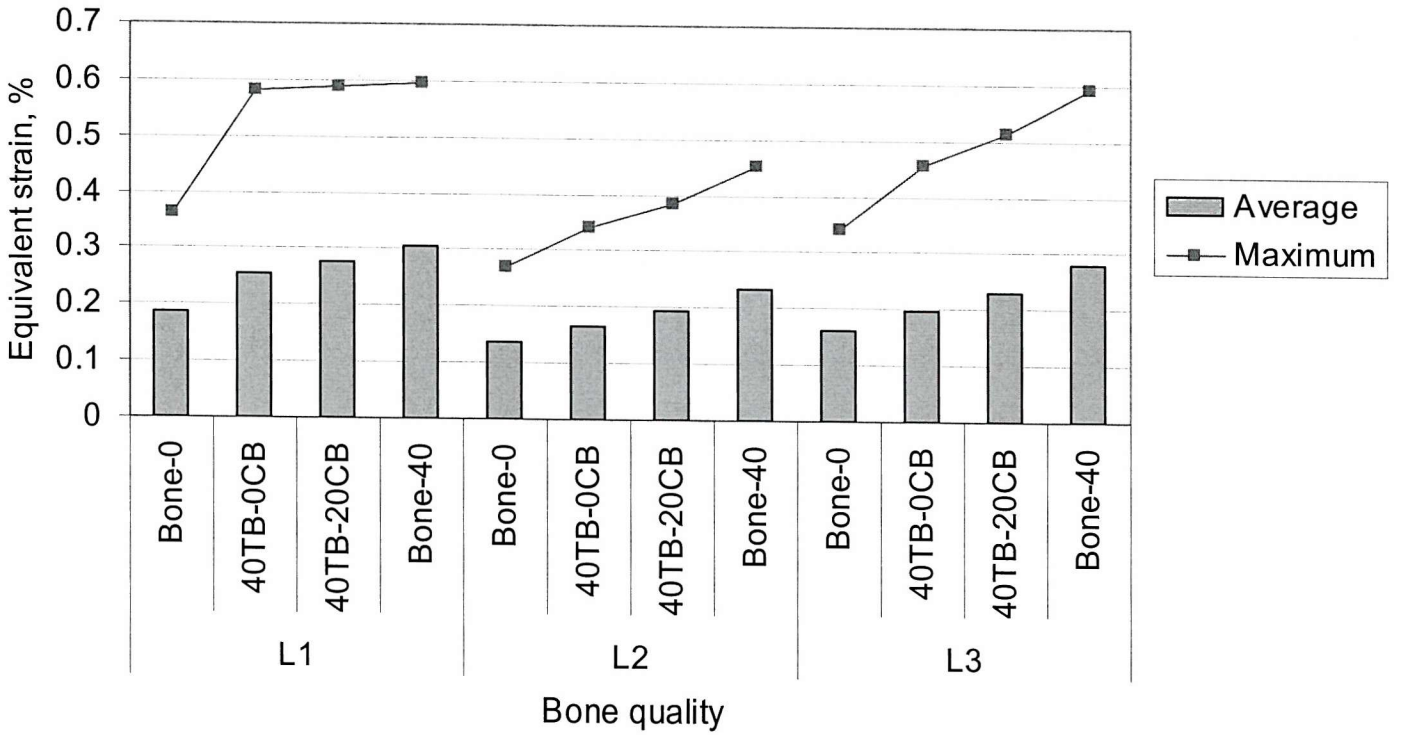

Figure 5.9 Comparing the effect of reducing Young's modulus of cortical and cancellous bone independently on strain. Similar to micromotion, the effect of reducing stiffness of cancellous bone only (40TB-0CB) increase the proximal equivalent strain (L1) more than distal equivalent strain (L2 and L3). Reducing Young's modulus of cortical bone has greater effect on equivalent strain in L2 and L3.

5.4 Discussion

Initial stability of the hip stem is affected by bone Young's modulus. The results showed that reduction in the modulus of bone leads to corresponding increase in interface micromotion. When Young's modulus of cortical and cancellous bones is reduced by 40%, there was 65% increase in the predicted peak micromotion. The increase in micromotion is not confine to any direction. All the components of micromotion on the medial and lateral nodes showed increase in micromotion when Young's modulus of bone was reduced.

The increase in interface micromotion also reduced the area of bone ingrowth. This is perhaps a significant quantity that should be given more attention. Increase in maximum micromotion without corresponding serious reduction in area of bone ingrowth is not as important. The result in this study has shown that with 40% reduction in bone stiffness, the predicted area of bone ingrowth has reduced to 28% at the proximal L1 region, to about 55-60% at L2 and L3. In normal bone (Bone-0), the predicted area of bone ingrowth is well over 80% in all these regions. The range of micromotion in each level is quite wide for the IPS stem. For example, at L1, micromotion ranged from 11 to 55 μm. If the range of micromotion is narrower, say 40-50 μm, reduction in stiffness by 40% is more likely to cause most of the interface area to exceed 50 μm micromotion. A stem design with a narrower range of micromotion and the average micromotion is near the bone ingrowth threshold in normal bone is more likely to fail to achieve significant fixation in poorer quality bone.

With aging, the modulus of cancellous bone reduces faster than modulus of cortical bone [Courtney *et al.*, 1996; Ding *et al.*, 1997; Zioupos and Currey, 1998]. The effect of reducing Young's modulus of cortical and cancellous bone was studied. Reducing only the Young's modulus of cancellous bone increases the interface micromotion, but not as much as the micromotion increase that was calculated when Young's modulus of cortical bone was reduced as well. Reducing Young's modulus of cancellous bone only has greater effect on micromotion proximally than distally. The thickness of cortical bone is less proximally than distally. The thickness of cancellous bone is significantly more proximally than distally. Therefore, cancellous bone has greater influence on the stiffness of the femur proximally than distally. Likewise, reducing the Young's modulus of cortical bone has greater effect on the micromotion distally.

This study has shown that that the overall stiffness of the femur dictates the interface micromotion rather than just the stiffness of interface bone. The effect of femoral stiffness on initial stability has not been reported in the literature before. Presently, more emphasis is given to modifying design of stems to improve performance of hip stem. However, assessing the variability of performance of new designs due to different quality of femurs is important to provide more meaningful risk assessment in different patients.

Reduction of cortical and cancellous bone by 40% in this study is reasonable to account for stiffness loss of the femur due to disease and age. Although Young's modulus of cortical bone is reported to decrease by only about 11.5% over five decades [Zioupos and Currey, 1998], it is not unreasonable to reduce the Young's modulus cortical bone by 40% in this micromotion study in order to simulate the corresponding reduction of thickness of cortical bone that also occurs with age. Cowin (2001) reported that human bone loses at least 30% of bone mass by the age of 70 years. Thickness of cortical bone reduced with aging and porosity also increases. Therefore, although Young's modulus of cortical bone does not reduce by 40%, the reduction in cortical bone thickness reduces the overall contribution of cortical bone to the stiffness of the femur. Since human cortical bone makes up 80% of bone mass, it must have lost quite a high percentage of its mass. In a finite element study of glenoid replacement prosthesis, Lacroix *et al.* (2000) reduced the Young's modulus of cortical bone by 50% to simulate both the change of stiffness and thickness of cortical bone due to rheumatoid arthritis. Therefore, the values used in this study are within the values reported in the literature.

It is difficult to compare the results of this study with result of previous finite element studies. Table 3.2 (Section 3.8.3) showed some of the results and loading conditions in other finite element studies. These studies have used a wide range of loading, different geometry and material properties of the femur, and different stem designs. The majority of the studies have reported range of micromotion of less than 100 μm and this is in the range of the present study [Biegler *et al.*, 1995; Kuiper and Huiskes, 1996; Ando *et al.*, 1999]. However, stems with poor fit and fill have been reported to have micromotions in the range of 150 μm [Ando *et al.*, 1999]. The results reported by Rubin *et al.* (1993) are much higher, but this study reported extensive plastic deformation (up to 400 times plastic yield criteria) of the interface bone. The amount of plastic deformation is not physiological, probably due to very low stiffness of cancellous bone in the model. The results reported by Keaveny *et al.* (1993c) are quite high as well, but the joint contact load in their study was about twice the value used in this study. However, for the collarless stem, Keaveny *et al.* (1993c) also reported lower proximal lateral micromotion and higher medial micromotion, similar to this study. In contrast Ramaniraka *et al.* (1996) reported high micromotion at both proximal lateral and proximal medial region of the stem. Their results were quite high, although the joint contact force is quite similar to the load used in the present study and those reported by two other studies [Biegler *et al.*, 1995; Ando *et al.*, 1999]. However the stiffness of the bone is not mentioned. The higher micromotion could be due to lower bone stiffness or stem design.

Besides affecting the micromotion, Young's modulus reduction also influences the strain at the interface bone. Reducing the Young's modulus of bone increases the interface strain. Maximum strain in L1 increases from about 0.36 to 0.6 % strain when the Young's modulus of both cortical and cancellous bone was reduced by 40%. 0.6 % strain is quite high and is

approaching the yield strain of cancellous bone (Table 1.3, Section 1.4.1.2). Similar to micromotion, proximal strain (L1) increase more with reduction of cancellous bone stiffness than more distal L2 and L3. Reduction of cortical bone stiffness will therefore affect the more distal L2 and L3 more than L1.

Similar to initial micromotion, this study has also shown that the interface strain is dependent on the overall stiffness of the femur rather than just the interface bone. Compressive fatigue tests of bovine cancellous bone showed that the transition to rapid creep accumulation occurred at about 0.6 % strain [Bowman *et al.*, 1998]. Bowman's *et al.* (1998) study showed that creep strain accumulation explained a significant part of the total permanent strain in bovine cancellous bone during fatigue testing, while crack growth and accumulation could possibly explain the remaining permanent strain. Before bone ingrowth occurs, if the strain is greater than the rapid creep rate regime, permanent creep deformation can accumulate rapidly due to repeated loading. This can cause rapid subsidence of stem and result in failure of fixation. High initial migration rate has been associated with failure of implant fixation [Freeman and Plante-Bordeneuve, 1994]. High interface cancellous bone stresses have been linked to high implant migration rates in the implanted proximal femur [Taylor *et al.*, 1995; Taylor, 1997]. The Freeman stem as either cemented, HA coated and smooth press-fit stems have been modelled and the maximum interface cancellous bone stress in the models has been found to follow the trend of the stem migration measured *in vivo*. The risk of excessive migration before fixation occurs is therefore higher in poorer quality bone.

This study has shown that the initial stability of IPS stem is affected by reduction in bone quality particularly at the proximal femur. The reduction in area under 50 μm in the model Bone-0 where Young's modulus is reduced by 40% is greatest at the proximal region. The degree of bone ingrowth in this critical region is therefore lower due to reduction of bone quality. The newer anatomic cementless hip stems are designed with proximal load transfer in mind to reduce stress shielding in the proximal cortex. Proximal fixation failure will increase the load transfer in the more distal region causing stress bypass. This will increase the chances of resorption of the proximal calcar. In this analysis of the IPS stem, it is observed that the micromotion at the proximal anterior-medial region is much higher than 50 μm when bone stiffness is reduced by 40%. Fixation in this area is especially important to prevent stress shielding to the proximal medial calcar.

Clinically, the effect of bone quality on performance of hip implant is rarely reported. A study reported that the incidence of pain is significantly higher in patients with poorer quality bone, but no significant difference in measurable influence on radiographic likelihood of bone ingrowth [Engh *et al.*, 1987]. However, the same study also reported 3 fold lower incidence of pain with hip that showed bone ingrowth in comparison to hip with fibrous tissue ingrowth. This does suggest that poorer quality bone may have lower incidence of bone ingrowth. The report from

the Swedish Hip Registry suggests that in patients younger than 55 years, patients with osteoarthritis (OA) and rheumatoid arthritis (RA) may have higher incidence of aseptic loosening than normal patients [Malchau *et al.*, 2000]. Between 1988 and 1998, the ten years survivorship from 1988 to 1998 for male OA, female OA and female RA patients were 81.2, 79.9 and 80.9% respectively. For normal female patients, the survivorship is 90.5%. However, this study did not differentiate cementless from cemented stems, but does suggest that patients with OA and RA may have higher risk of aseptic loosening. Although the report spanned the period between 1979 to 1987 as well, the immature technology of both cemented and cementless hip stem during this period may be the biggest cause of aseptic loosening and therefore it is hard to judge the effect of disease on implant performance.

This study has a few limitations. This study uses a single femur geometry and bone distribution. Therefore, it is not possible to capture the effect of femoral geometry on initial micromotion. The relative distribution of bone Young's modulus is also constant due to the availability of CT scan data for only one femur. However, if more sets of CT scan data are available, it is possible to study the effect of bone Young's modulus in different regions of the bone on initial stability. Figure 5.5 shows that in this study, the distributions of micromotion is similar in all the different models due to same relative variation of Young's modulus between models. With more CT scans based models, how this variation in elastic modulus in different region of the femur can be studied.

Ideally, a collection of CT scan data will have CT scans from patients of various age group, both sexes and different stages of diseases. Patient specific modelling on four patients who have received total knee replacement has been reported and it was found that migration rate of the tibia plate correlated with the risk ratio of cancellous bone failure below the tibia plate (defined as stress/yield stress) [Perillo-Marcone, 2001]. This clearly points to the advantage of being able to do preclinical testing on more than one set of CT scan. This enables the possibility to correlate between stem design, patient's bone quality and the risk of implant failure. This will enable surgeons to compare radiographic scans from patients with scans from the preclinical analysis to decide on the suitability of the stem design for certain patients.

In this study, bone was assumed to be isotropic. Bone is known to be anisotropic [Reilly and Burstein, 1975; Ashman *et al.*, 1984; Ashman, 1989]. The orientation of CT-scan is mostly along the axial direction of the femur. Therefore, the hoop stiffness could be overestimated due to assumption of isotropic material property, and micromotion and interface strain could be underestimated. However, with this as a systematic error built into every model, as a comparative study, the results reported here are valid.

5.5 Conclusion

The results of this study suggest that:-

1) Micromotion is influenced by the quality of both cortical and cancellous bone. If bone quality decreases, the micromotion increases nonlinearly. Overall stiffness of the femur is influenced by the cortical and cancellous bone modulus. Therefore, the reduction in the overall stiffness of the femur increases micromotion.

2) Decreasing cancellous bone quality has a greater effect on proximal micromotion.

3) Decreasing cortical bone quality has a greater effect on distal micromotion.

4) Interface equivalent strain is also influenced by bone quality, and thus the overall stiffness of the femur. Equivalent strain increases nonlinearly with decrease in bone quality.

5) Decreasing cancellous bone quality has a greater effect on proximal interface strain.

6) Decreasing cortical bone quality has a greater effect on distal interface strain.

7) Preclinical assessment of implant design using one set of CT scan data is not adequate to assess the performance envelope of a design as both micromotion and interface strain were found to increase with decrease of bone quality.

Chapter 6 Influence of the degree of interference on the initial stability and strain of the implanted proximal femur

6.1 Introduction

The performance of cementless porous-coated femoral hip stems is influenced by the initial stability in the immediate post-operative period. Bone ingrowth is hindered by excessive micromotion at the bone-stem interface [Pilliar *et al.*, 1986; Engh *et al.*, 1992b; Bragdon *et al.*, 1996]. In order for cementless stems to achieve greater long-term stability through bone ingrowth, minimal micromotion in the immediate post-operative period is vital. Excessive micromotion prevents calcification of soft tissue within the pores, and as a result, only fibrous tissue ingrowth occurs.

The clinical performance of a cementless porous-coated femoral hip prosthesis (AML, DePuy) has been shown to improve if a distal interference-fit at the femoral isthmus is created during the surgery [Engh *et al.*, 1990]. This is supported by experimental micromotion studies comparing the micromotion of the AML stem in the implanted femur employing either tight distal fit or line-to-line fit [Sugiyama *et al.*, 1992]. A tight distal fit is reported to result in much lower micromotion as compared to the line-to-line fit. All the stems were implanted with proximal anterior and posterior interference-fit of 1 mm. In one group, the stem was implanted with 0.25 mm interference-fit at the femoral shaft and another group was implanted without distal interference-fit. Micromotion in the first group with distal interference-fit was lower by about four times. The femur is thought to be left with a residual compressive stress, which is anticipated to reduce micromotion through greater friction force at the bone-stem interface and hence encourage bone ingrowth. Most experimental micromotion studies do not mentioned whether there is interference-fit in their studies, but presumably they are inserted according to the surgery guidelines [Walker *et al.*, 1987; Schneider *et al.*, 1989; Sugiyama *et al.*, 1989; Burke *et al.*, 1991; Phillips *et al.*, 1991; Callaghan *et al.*, 1992; Hua and Walker, 1994].

The initial stability of a hip stem may be affected by the presence an of interference-fit but this factor is given little attention in the literature. Most finite element studies of the initial micromotion of the hip stem neglect the effect that an interference-fit has on the initial micromotion between the stem and the bone [Rubin *et al.*, 1993; Keaveny and Bartel, 1993c; Kuiper and Huiskes, 1996; Ramaniraka *et al.*, 1996; Ando *et al.*, 1999; Viceconti *et al.*, 2000]. A few finite element studies using simplified models of the implanted femur assembly have reported the effect of interference-fit on the interface stress and contact area [Harrigan and Harris, 1991;

Visnic *et al.*, 1994]. However these studies did not use anatomical models and did not study the effect of interference-fit on the initial micromotion.

Studies examining the influence of interference-fit analysis have been performed for other joint replacement components such as the acetabulum component of a hip replacement [Spears *et al.*, 2001] and tibia component of a knee replacement [Dawson and Bartel, 1992]. These studies found that the highest interference-fit is not necessarily the best for optimal fixation of implants. For the acetabulum component, Spears *et al.* (2001) suggested that a moderate interference-fit of the acetabular cup gave the best initial stability due to good contact with surrounding bone but a higher interference-fit generates a large gap at the polar region of the cup. The additional surface-normal and frictional resistance of the moderate interference-fit model resists the load better and thus is more stable. Interference-fit at the peg of the tibia tray pushes the metal tray upwards and causes a loss of contact between the tray and the tibia bone [Dawson and Bartel, 1992]. Although the compressive stresses at the peg is conducive for bone ingrowth, the lack of contact at the tibia tray is detrimental to bone ingrowth and conducive to the formation of a layer of fibrous tissue.

Hip stem stability is thought to be better with an interference-fit, but this is associated with high interface bone and hoop stresses as well. The interference-fit in the implanted femur can be imagined as inserting a larger cone into a slightly smaller cone. Examples of interference-fit assembly have been reported in the literature where AML stems (DePuy, Warsaw, Indiana) have been inserted with interference-fit at the femoral isthmus [Schwartz *et al.*, 1989; Engh *et al.*, 1990; Sugiyama *et al.*, 1992]. A high degree of interference-fit can cause femoral fracture, due to high hoop stress during stem insertion and this has been reported clinically [Fitzgerald *et al.*, 1988; Schwartz *et al.*, 1989; Mont *et al.*, 1992]. Visnic *et al.* (1994) reported high stress at the interface bone in a two-dimensional finite element analysis which assessed the influence of an interference-fit. Experimental studies have shown that femoral fractures can occur at low hoop strain values [Jasty *et al.*, 1993]. In an experimental micromotion study using composite femurs, the investigators cracked three out of six femurs during insertion of the stems [Monti *et al.*, 2001]. A serious crack at the femur will defeat the purpose of having an interference-fit in the first place. Animal study has shown that cracks can be detrimental to bone ingrowth [Schutzer *et al.*, 1995].

The aims of this study were to investigate :-

a) the interaction between micromotion and strain with increasing level of interference-fit.

b) Is there an optimal interference-fit that minimises the micromotions, but also causes minimal bone damage.

Similar to Chapter 5, both the micromotion and interface strain are examined together to assess the implant stability and risk of implant migration.

6.2 Interference-fit at the bone-stem interface

The finite element model used in this chapter has been described in detail in Chapter 4. In this chapter, a modification has been made to the bone-stem interface boundary condition. An interference-fit is modelled at the bone-implant interface to model the surgical procedure where the femoral canal is undersized in comparison to the stem, as illustrated in Figure 6.1. The dotted line represents the size of the reamed canal and this is smaller than the stem size. The intersection between the canal and the stem forms the interference-fit. The friction coefficient at the interface remains similar.

Interference-fits of 0.1, 0.05 and 0.01 mm were modelled in this study. A control model with no interference-fit (0 mm interference) was modelled as a comparison. In MARC, the interference-fit can be modelled by specifying the overclosure parameter in the Contact Table option. This option pushes the contact surfaces away from each other perpendicular to the contact surface, according to the specified overclosure value. The interference-fit was modelled over the whole region of contact, which is the region with dotted line border shown in Figure 6.1. The models with 0.1, 0.05, 0.01 and 0 mm interference-fit will be referred to as the model **In-0.1**, **In-0.05**, **In-0.01** and **In-0** respectively.

Walking and stair climbing load cases were simulated in this study. These loadcases have been described in Section 4.2.4 (Table 4.2). In this analysis, loads are applied in three steps (Figure 6.2). The first step involved the simulation of interference-fit. The stem is constrained in the axial direction and the femur is constrained rigidly at the distal end. In the second step, the constraint on the stem is removed and the stem is allowed to springback. The third step is the application of either the walking and stair-climbing loadcases. Micromotion is calculated as the relative displacement between the adjacent nodes at the bone-implant interface after the third step in relation to the end of the second step. Equivalent strain at the end of the third step is reported here unless otherwise stated. In model In-0, the first and second loadsteps were not necessary. Results are reported at the three cross-sectional levels L1, L2 and L3, as reported in Chapter 5 (Section 5.2).

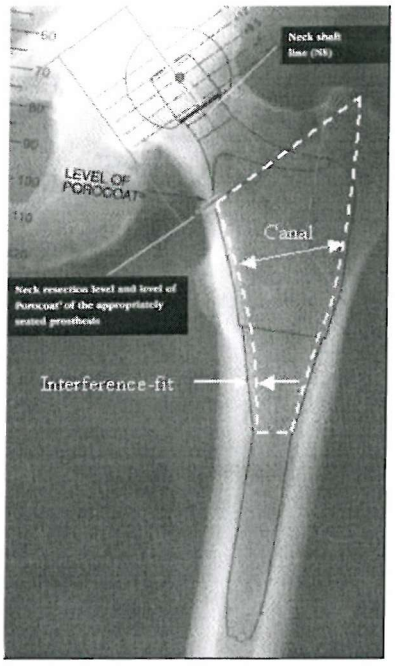

Figure 6.1 Interference-fit in the bone-stem assembly. The canal is reamed smaller than the size of the stem to creates an interference-fit during surgery.

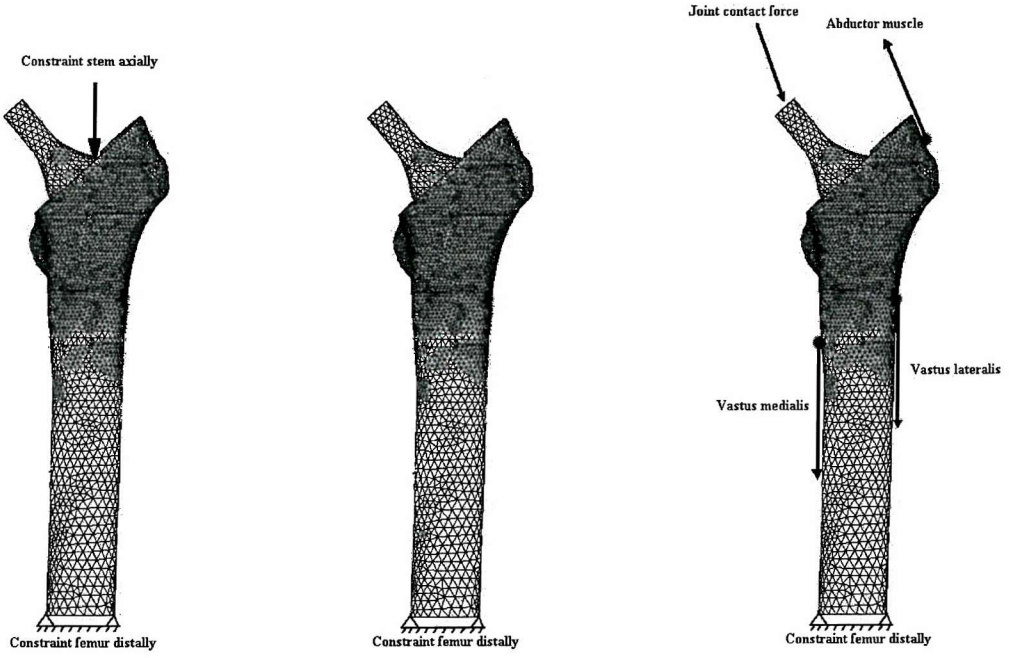

Figure 6.2 Three loadstep applied in the interference-fit analyses. Left: Stem is constrained axially. Middle: Stem allowed to springback by removing the axial constraint. Right: Loading for walking and stair climbing.

6.3 Influence of interference-fit on initial micromotion, equivalent strain and contact area

6.3.1 Micromotion

Figure 6.3 and Figure 6.4 show the micromotion at L1, L2 and L3 for different degrees of interference-fit during walking and stair climbing respectively. Generally, micromotion in the

interference-fit models (In-0.1, In-0.05 and In-0.01) are lower than in model In-0. The mean micromotions during walking at level L1, L2 and L3 are less than 5 μm in model In-0.1 and In-0.05, which are very low values. In model In-0.01, the mean micromotions at L1, L2 and L3 are between 8 and 13 μm. The mean micromotions in model In-0 are between 28 and 40 μm, which are significantly higher than model In-0.01. The peak micromotions in model In-0 exceed 50 μm (upper limit of micromotion that allows bone ingrowth [Engh *et al.*, 1992b; Bragdon *et al.*, 1996; Fernandes *et al.*, 2002]) at all three levels. Even with a slight interference-fit of 0.01 mm, peak micromotions have been reduced to below 25 μm in model In-0.01, which is conducive for osseointegration. The mean micromotions in model In-0.01 are about 2-4 times lower than values in model In-0.

The micromotions are higher during stair climbing (Figure 6.4) than during walking (Figure 6.3) because of the higher posteriorly directed force component during stair climbing and this is consistent with experimental micromotion studies [Walker *et al.*, 1987; Callaghan *et al.*, 1992]. In model In-0.01 and In-0, the proximal L1 level shows higher increase in micromotion during stair-climbing in comparison to the more distal L2 and L3 levels. It is likely that resistance to anterior-posterior rotation occurred in the bulkier and more oval proximal region of the stem, and therefore the higher increase in micromotion proximally. In model In-0.1 and In-0.05, the micromotion increase is minimal. The contact area and interface stress in these two models are greater and therefore provided better frictional resistance that reduces anterior-posterior rotation of the stem. The mean micromotions for model In-0.1 and In-0.05 are less than 5 μm during stair climbing, which is similar to the micromotion during walking. Micromotion in model In-0.01 is significantly lower than the 0 mm model. Again, the peak micromotion has been reduced to below 50 μm with a small interference-fit of 0.01 mm. In model In-0, the mean micromotion is greater than 50 μm in L1 and is approaching 50 μm in L2. This is much less conducive to osseointegration than model In-0.01.

Figure 6.5 shows the components of micromotion of the medial and lateral nodes at L1 and L3 for model In-0.01 and In-0 during stair climbing. Looking at the axial component v, model In-0 has higher axial micromotion than model In-0.01. The higher relative motion between the medial and the lateral nodes in model In-0 also showed that the rotational stability in the midplane of the stem is better in model In-0.01. The higher anterior-posterior component u in model In-0 also showed that the rotational stability in the anterior-posterior direction is better in model In-0.01. The smaller axial and anterior-posterior micromotion showed that interference-fit provides better axial and rotational stability.

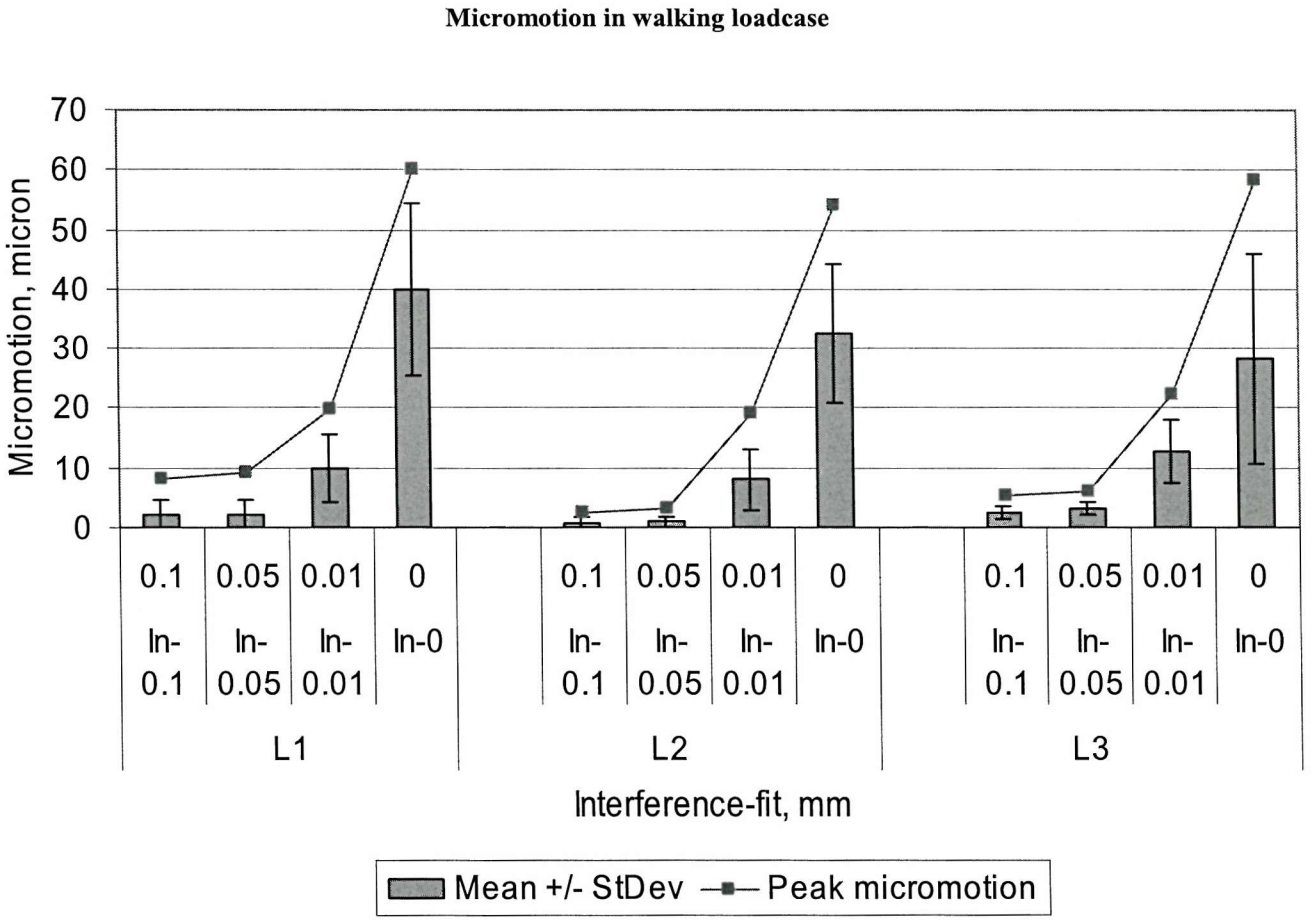

Figure 6.3 Micromotion at L1, L2 and L3 for walking loadcase. Bar chart shows mean micromotion ± standard deviation. Line chart shows the peak micromotion. Model In-0.1 and In-0.05 have very low micromotion and quite similar in magnitude. Model In-0.01 has micromotion values between model In-0 and model In-0.05. All the interference-fit models have peak micromotion below 50 μm. Significant reduction in initial micromotion can be achieved even with very small interference-fit of 0.01 mm.

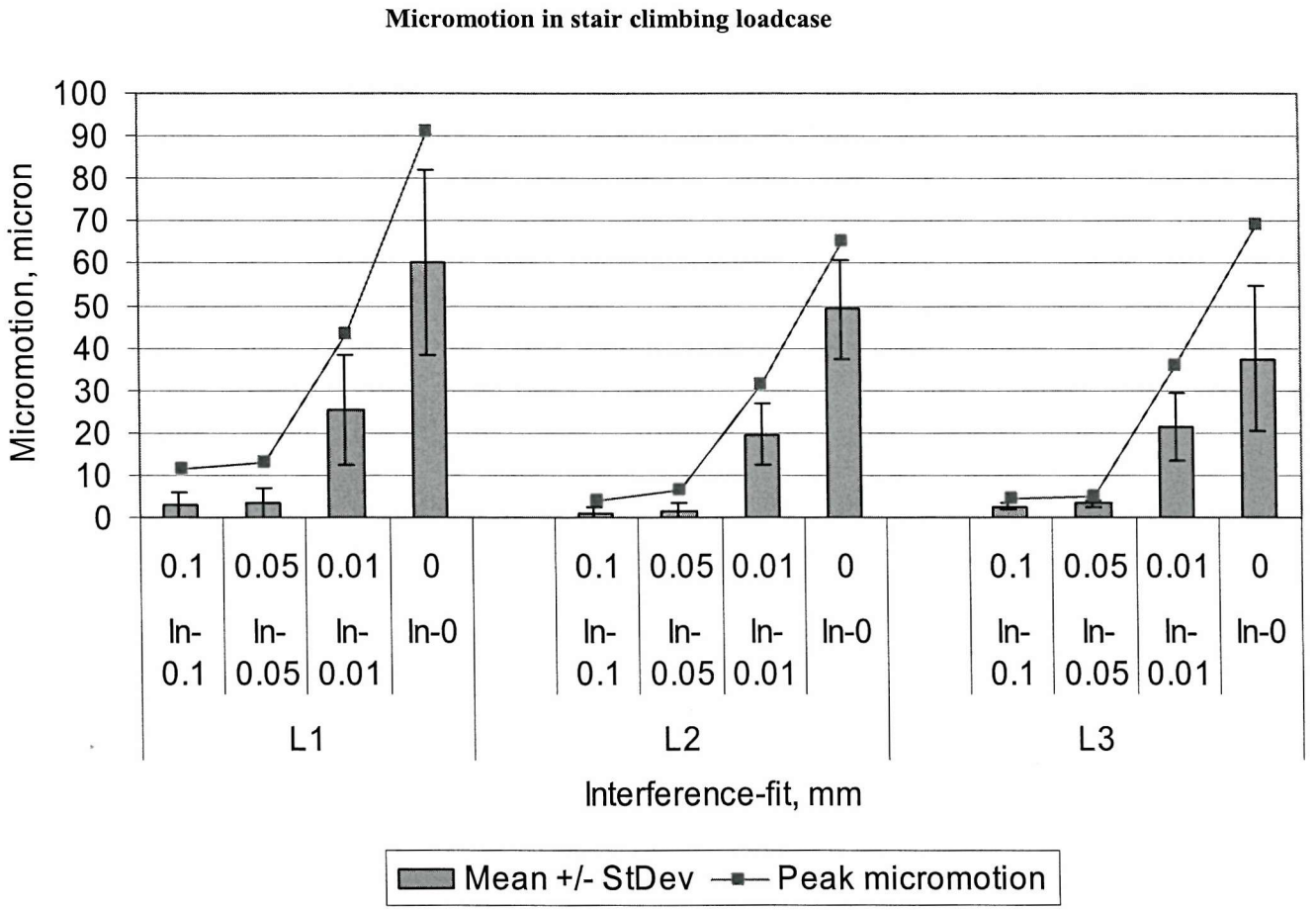

Figure 6.4 Micromotion at L1, L2 and L3 for stair climbing loadcase. Bar chart shows mean micromotion ± standard deviation. Line chart shows the peak micromotion. Similar to walking loadcase, the model In-0.1 and In-0.05 have very low micromotion. Again, significant reduction is seen in model In-0.01 as compared to model In-0. Maximum micromotion is greater in the stair climbing loadcase as compared to the walking loadcase especially proximally. Again very small interference of 0.01 mm reduced peak micromotion to below 50 μm.

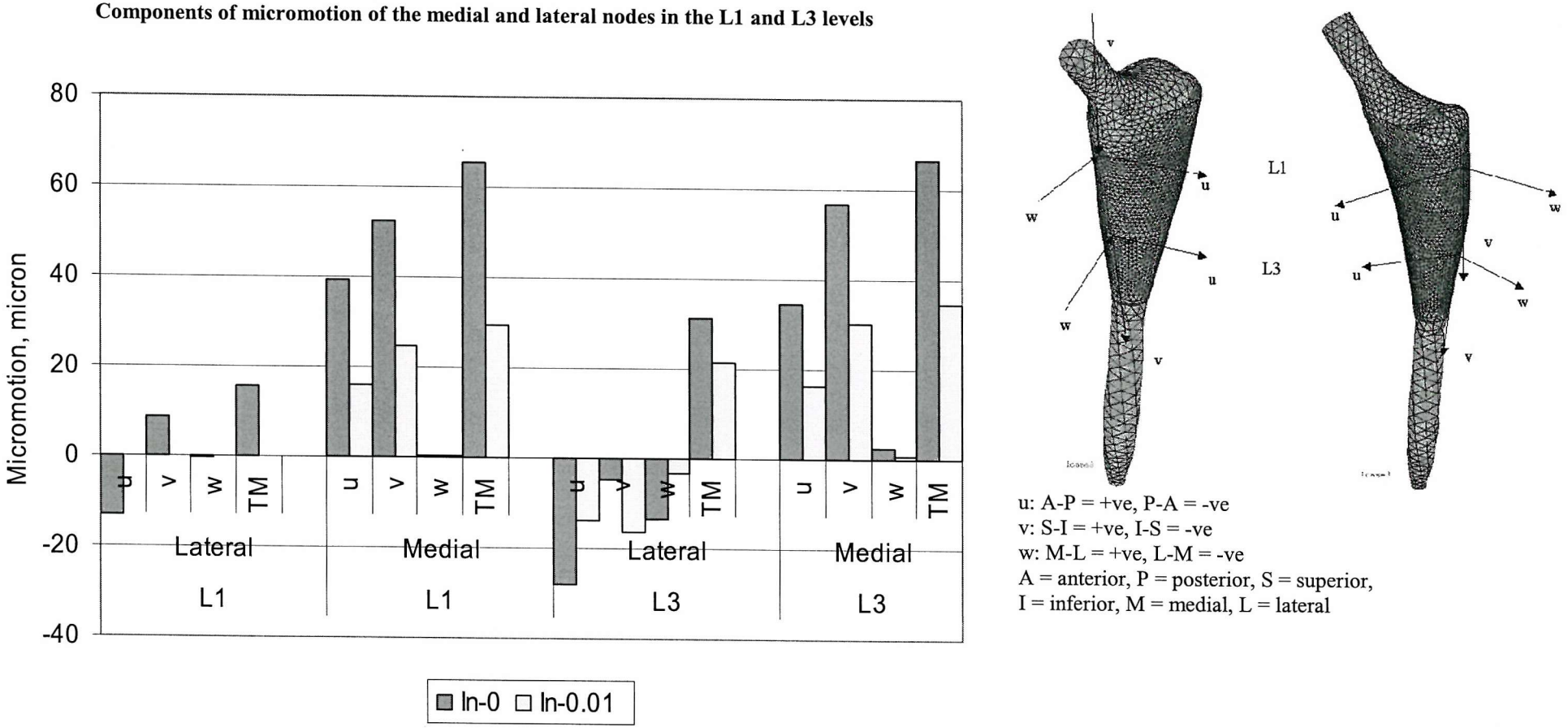

Figure 6.5 Components of micromotion of the lateral and medial interface nodes at L1 and L3 for model In-0.01 and In-0 for stair climbing loadcase. Comparing component v at L1 and L3, model In-0 has higher subsidence and rotation on the midplane of the stem. Comparing component u, model In-0 has higher rotation in the anterior-posterior direction.

6.3.2 Equivalent strain

Generally, equivalent strain increase with the degree of interference-fit. In the walking loadcase (Figure 6.6), model In-0.1 has the highest mean equivalent strains and these are about twice the mean equivalent strains in model In-0.05. Model In-0.01 and In-0 have similar mean equivalent strains. At the proximal L1 level, the mean equivalent strain in model In-0.01 and In-0 are about 4.5 times lower than in model In-0.1. At the more distal L3 level where the cross-section of the femur is smaller, the mean equivalent strain is about 7 times lower in model In-0.01 and In-0 than in model In-0.1. Model In-0.01 and In-0 have similar equivalent strains in L1, L2 and L3, but model In-0.1 and In-0.05 have increasing equivalent strain from L1 to L3 due to decreasing cross-sectional area of the femur from proximal to distal femur. The magnitude of equivalent strain in model In-0.01 and In-0 during stair climbing in each level is generally greater than during walking (Figure 6.6 and Figure 6.7). This is expected due to the higher joint contact force during stair climbing. In models In-0.1 and In-0.05 the magnitude of equivalent strain are similar between walking and stair climbing, and therefore the strains in the higher interference-fit models are dominated by the degree of interference-fit rather than the applied load.

The maximum equivalent strains in model In-0.1 are high and exceeded 1.5% strain at L2 and L3 (Figure 6.6 and Figure 6.7). Linde *et al.* (1992) has reported 1.5% strain as the ultimate strain of cancellous bone. The maximum equivalent strain in model In-0.05, In-0.01 and In-0 did not exceed 1.5% strain. However, the maximum equivalent strains in model In-0.05 are greater than 0.7 % strain, which is near or exceeded the yield strain of cancellous bone reported in the literature [Rohl *et al.*, 1991; Kopperdahl and Keaveny, 1998; Morgan and Keaveny, 2001]. However, the mean equivalent strain is generally below 0.5% strain except in model In-0.1 and L3 level of model In-0.05.

The equivalent strain on the periosteal bone surface is also dependent on the degree of interference-fit. The equivalent strain at the periosteal surface is concentrated at the proximal anterior and posterior regions, as shown in Figure 6.8. The equivalent strain is reported at the end of step two. In the anterior region, the maximum equivalent strains are 0.67 and 0.33 % strain in model In-0.1 and In-0.05 respectively. Posteriorly, the maximum equivalent strain is higher than the anterior region. The maximum equivalent strains are 0.97 and 0.48% in model In-0.1 and In-0.05 respectively. The periosteal equivalent strain is about twice as high in model In-0.1 relative to model In-0.05. Reilly and Burstein (1975) reported a value of 0.7% strain for the ultimate strain of cortical bone in the transverse direction and this value is either near or below the maximum equivalent strains at the anterior and posterior regions for model In-0.1. The fracture risk for model In-0.1 could be potentially high. Other than the proximal anterior and posterior regions, most regions are below 0.2% equivalent strain.

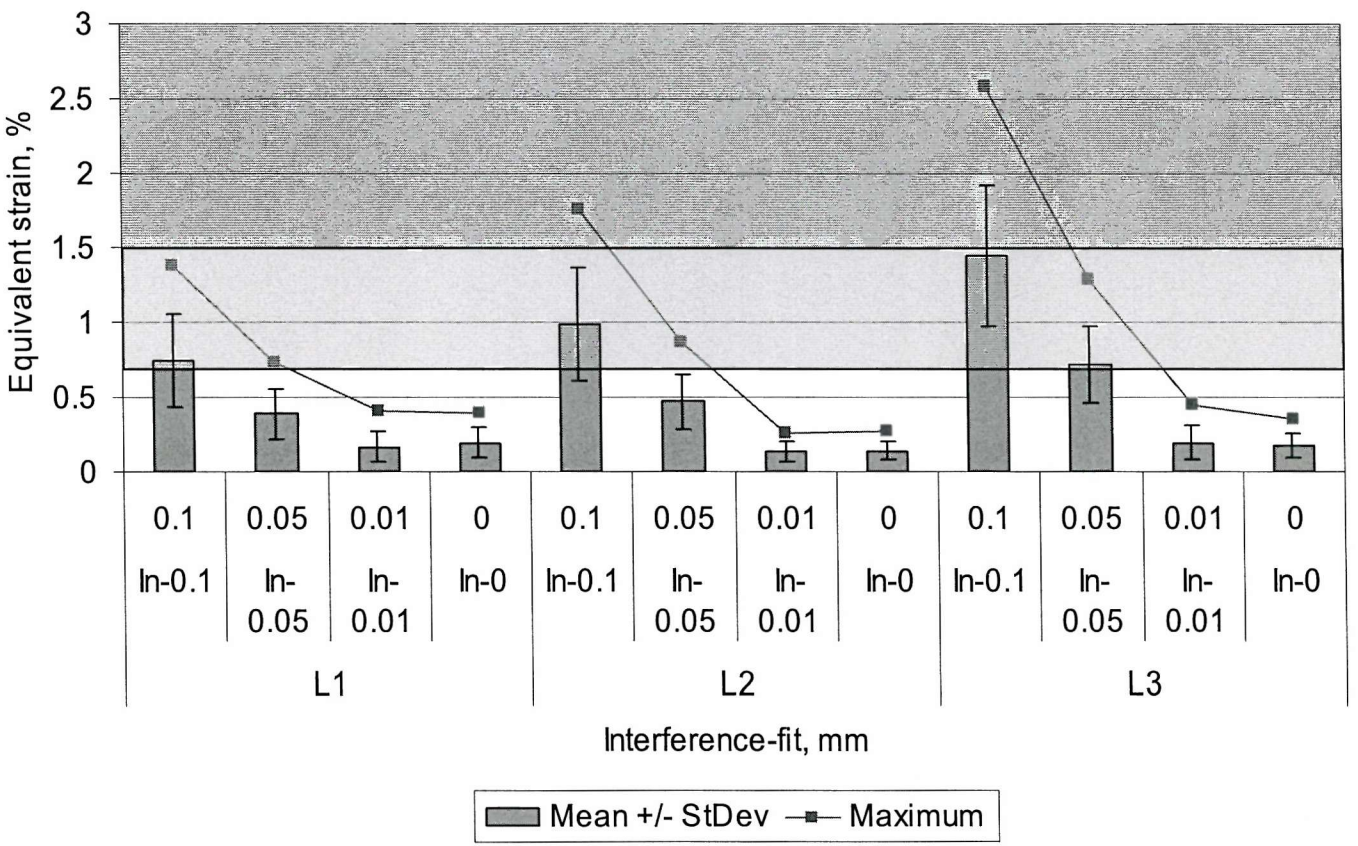

Figure 6.6 Equivalent strain at L1, L2 and L3 for walking loadcase. Bar chart shows the mean equivalent strain ± standard deviation. Line chart shows the maximum equivalent strain. The mean strains in model In-0.1 and In-0.05 are about three and two times the mean strain in model In-0 in the proximal level. At the distal level, the relative difference between model In-0.1 and In-0.05, and model In-0 is greater than at the proximal level. Model In-0.01 mm model has very similar mean and maximum equivalent strain value as compared to model In-0. The lighter shaded region is above yield strain and the darker shaded region is above the ultimate strain.

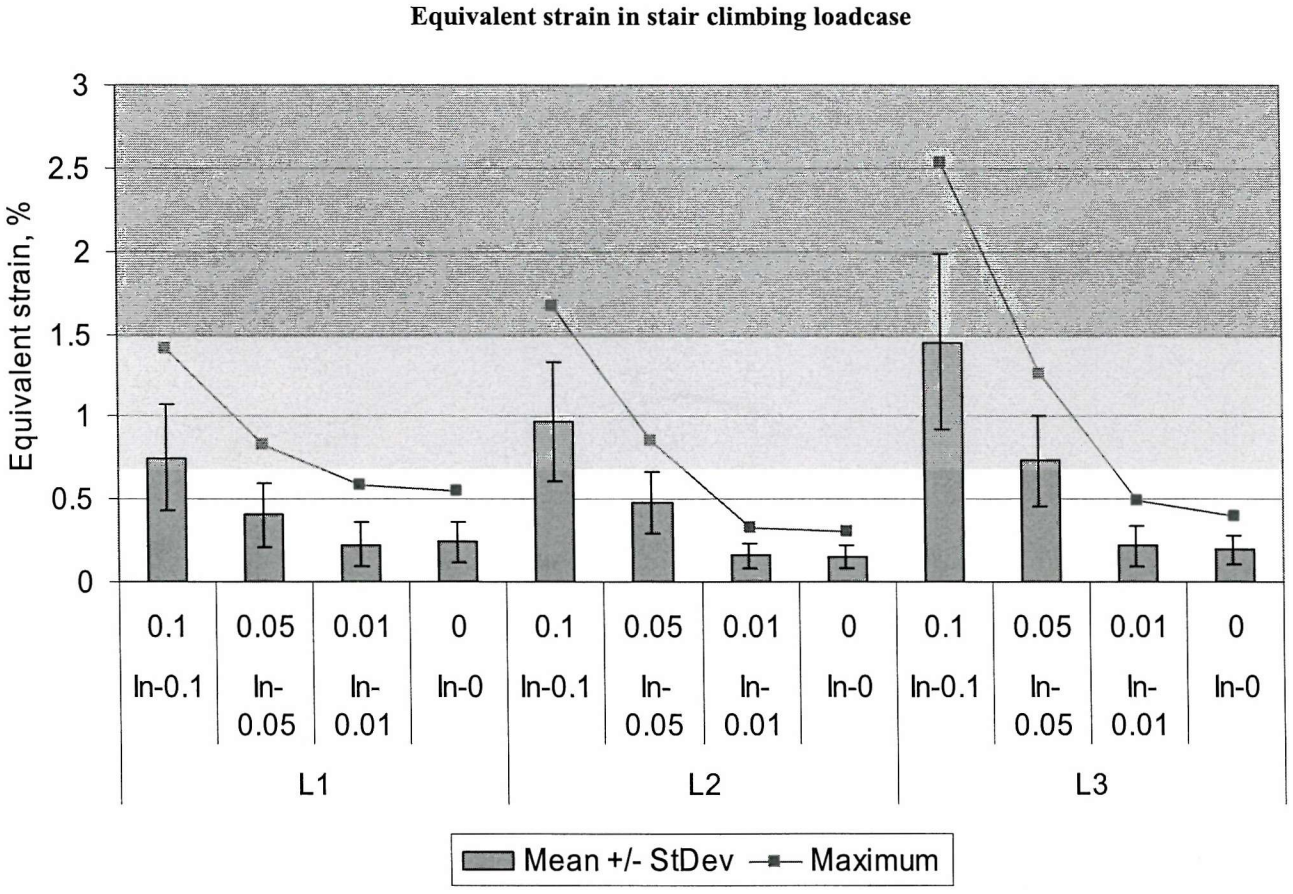

Figure 6.7 Equivalent strain at L1, L2 and L3 for stair climbing loadcase. Bar chart shows the mean equivalent strain ± standard deviation. Line chart shows the maximum equivalent strain. In term of relative strain between the interference models and the zero interference model, the strain ratio in the stair climbing loadcase is similar to the walking loadcase. However, the equivalent strain in the stair climbing loadcase is generally greater than the walking loadcase due to higher applied load. This is more clearly seen in model In-0.01 and In-0. The lighter shaded region is above yield strain and the darker shaded region is above the ultimate strain.

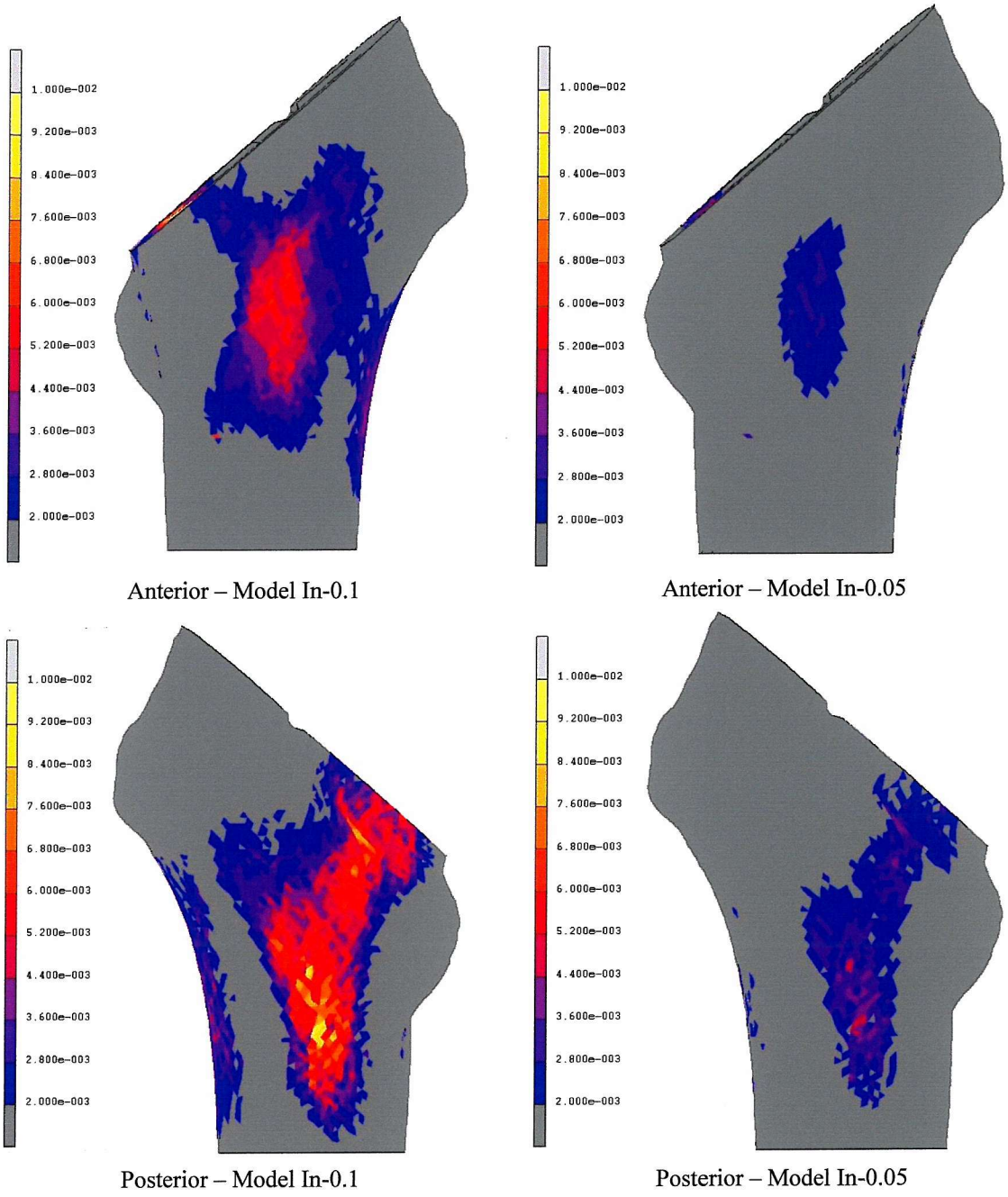

Figure 6.8 Periosteal equivalent strain in model In-0.1 and In-0.05. The proximal anterior and posterior sides have higher periosteal strain than other regions of the femur. Periosteal strain is higher in higher in model In-0.1.Generally, most regions are below the 0.2% strain.

6.3.3 Contact area

The effect of different degree of interference-fit on bone-implant contact area during walking is shown in Figure 6.9. Contact area is higher in the interference-fit models. Contact areas in models In-0.1 and In-0.05 are very good and identical in both models. In model In-0.01, contact area is less than models In-0.1 and In-0.05, but is better than model In-0. Model In-0.01 loses contact in the mid-lateral, proximal-anterior, and distal medial contact. Model In-0 loses more contact in the same region and in addition loses contact in the proximal-posterior region as well.

In comparison to walking, the contact area during stair-climbing is lower but the distribution is similar. Some of the area under contact during walking is not in contact during stair-climbing. This is more obvious in models In-0.01 and In-0 as the loss of contact is more. In models In-0.1 and In-0.05, the contact area is slightly less than during walking. Therefore, contact areas in models In-0.1 and In-0.05 are still very good.

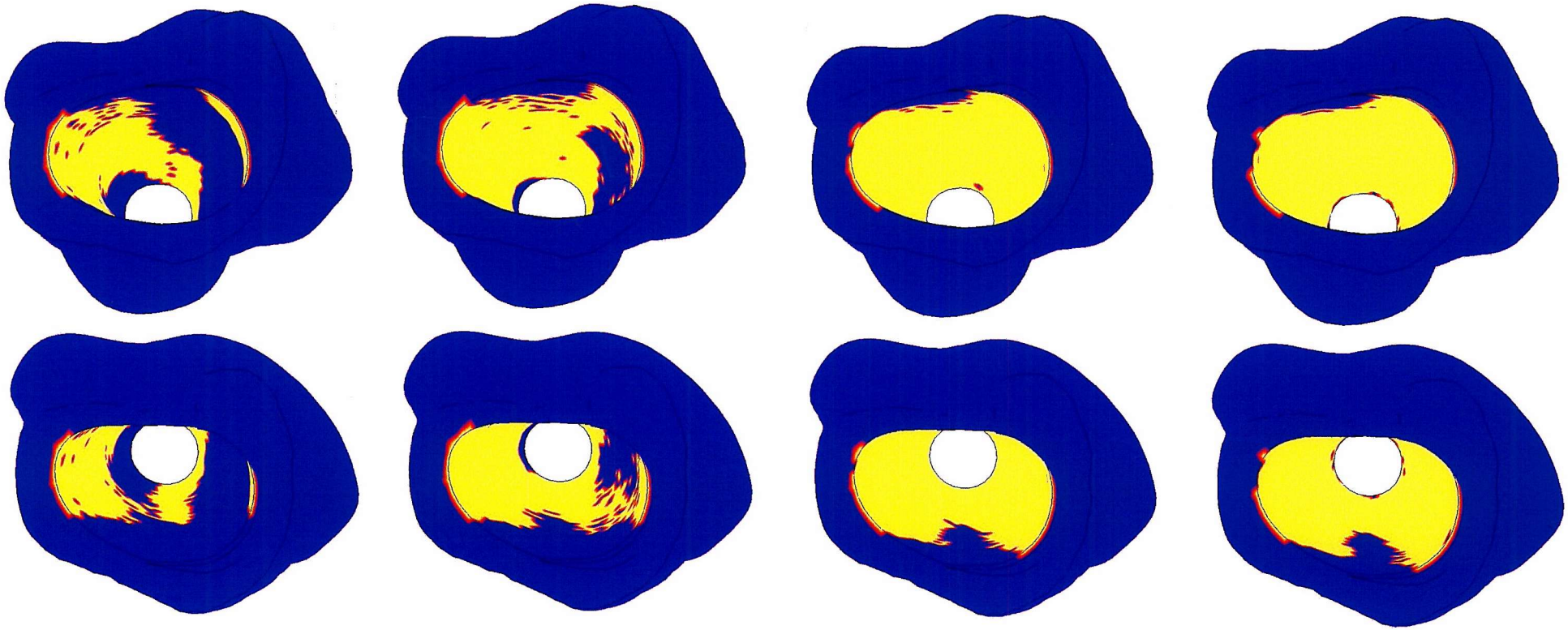

In-0 **In-0.01** **In-0.05** **In-0.1**

Figure 6.9 Contact area in four different models. Top row: A slightly more posterior view. Bottom row: A slightly more anterior view. From left to right: Model In-0, In-0.01, In-0.05 and In-0.1. High level of contact is observed in model In-0.1 and In-0.05. Model In-0.01 has less contact area than model In-0.1 and In-0.05 but more than model In-0.

6.4 Discussion

One of the objectives of this study was to determine the effect of interference-fit on the initial stability of the cementless hip stem. The result of this study shows that interference-fit plays a significant role in the initial stability of hip prosthesis. A comparison of the micromotion between all the different degrees of interference-fit shows that even for a small interference-fit of 0.01 mm, a significant reduction in initial micromotion is achievable. The benefit of having a small interference-fit is that the reduction in micromotion is achieved without the penalty of higher bone strain at the bone-implant interface. In contrast, higher degrees of interference-fit give better initial stability but at the same time, the bone strain at the bone-implant interface increases significantly. However, the similarity in initial stability between the 0.1 mm and 0.05 mm models suggest that there is a degree of interference-fit where optimal initial stability is reached. The highest degree of interference-fit is not necessarily the best for initial fixation, as high hoop strain can lead to development of femoral fracture [Schwartz *et al.*, 1989; Jasty *et al.*, 1993].

The significantly better performance of model In-0.01 in comparison to model In-0 can be explained by the fact that interface friction already exists without the need for the stem to wedge into the canal. The bone-stem interface in the interference-fit models was already under compressive stress without the need for the stem to subside further into the femur. Therefore, when model In-0.01 is loaded, friction is readily available to resist part of the axial load without the need to subside like model In-0 to generate compressive and friction stresses. As a result of the initial residual force at the interface, model In-0.01 subsided less and the contact area is greater than model In-0 (Figure 6.5 and Figure 6.9). Similarly, the friction force cause by the interface interference-fit enable model In-0.01 to resist anterior-posteriorly directed force better than model In-0. As a result the anterior-posterior micromotion is lower in model In-0.01 in comparison to model In-0 (Figure 6.5).

Some researchers have expressed concern that cementless hip stems cannot resist anterior-posteriorly directed load well [Walker *et al.*, 1987; Callaghan *et al.*, 1992; Biegler *et al.*, 1995], leading to high rotational micromotion. However, this study has shown that with proper surgical technique to introduce interference-fit, rotational micromotion can be minimized.

There are a few limitations to the current model that should be mentioned here. First of all, the bone has been modelled as an elastic isotropic material. It is well known that bone exhibits viscoelastic behaviour [Zilch *et al.*, 1980; Rimnac *et al.*, 1993; Bowman *et al.*, 1998; Bowman *et al.*, 1999; Brown *et al.*, 2001]. In high stress conditions, stress relaxation has been shown to occur in bone [Zilch *et al.*, 1980; Deligianni *et al.*, 1994]. Zilch *et al.* (1980) reported that the arithmetic mean stress relaxation in cancellous bone specimens from two human femurs were a reduction of 17.3 % and 15.8 % in the initial compressive stresses and stress relaxation reached equilibrium in matter of minutes. Deligianni *et al.* (1994) reported that stress relaxation in the range of 15 to 45%

has been measured for cancellous bone from the human femoral head and no significant changes occur after 24 hours. However, both experiments have been conducted as compression test between flat platens, which has been reported in the literature to introduce significant experimental artefact [Keaveny *et al.*, 1994b]. It is therefore unclear if the stress relaxation test is conducted using necked specimens, higher stress relaxation will occur. Therefore it is possible that the stability reported here for the 0.1 mm and 0.05 mm models could have been overestimated because stress relaxation of the femur is not accounted for.

Secondly, it should also be noted that plasticity was not modelled in this study, which again may reduce the interface stress and increase the initial micromotion. The ultimate strain of cancellous bone has been reported in the region of 1.5% strain in both tension and compression [Rohl *et al.*, 1991; Linde *et al.*, 1992; Kopperdahl and Keaveny, 1998]. In this study, the equivalent strains in some regions of model In-0.1 exceeded this value. Interface stresses in certain region are therefore overestimated. This could lead to overestimation of the initial stability in the interference-fit models.

This study modelled uniform interference-fit over the whole initial contacting surface. However in surgery, it is difficult to achieve this kind of uniformity, especially for a stem like IPS with quite complex geometry. The final degree of interference-fit is dependent on how far the surgeon pushed the stem into the canal and the nature of the surface of the stem. The proximal region of the IPS stem is coated with titanium beads, which act like a rasp when the stem is inserted into the canal. Although the stem is designed to be inserted with 0.375 mm interference-fit, the actual interference-fit could be much smaller due to the cutting of interface bone by the porous coating during the insertion of the stem. In reality, it is likely that the stem will be pushed more towards regions with softer bone, i.e. the insertion path of least resistance.

An examination of the results of experimental micromotion studies does suggest that uniform interference-fit is difficult to achieve in surgery. Table 3.1 showed the results of experimental micromotion studies by other researchers. The micromotion reported can vary from a few microns to hundreds of microns for both walking and stair-climbing loadcase. Sugiyama *et al.* (1992) reported that interference-fit of 0.25 mm in the femoral isthmus significantly reduces micromotion by about four times as compared to a line-to-line-fit prosthesis in stair-climbing loadcase. They reported micromotion below 20 μm for applied torque of 10 Nm, but micromotions increased to about 60 μm for an applied torque of 20 Nm. Other studies have reported lower micromotion values [Callaghan *et al.*, 1992; Hua and Walker, 1994; Monti *et al.*, 2001]. Callaghan *et al.* (1992) has reported values as low as a 1 μm to values as high as 60 μm for walking loadcase. For stair climbing loadcase, the curved stem has micromotion in the region of 9-59 μm. Hua and Walker (1994) has also reported micromotion as low as a few microns and as high as 33 μm. The lower values are closer to the values in the 0.1 and 0.05 mm interference-fit models (model In-0.1 and

In-0.05) while the higher values are closer to the 0.01 mm interference-fit model. Monti *et al.* (2001) reported very low micromotion values in their test using composite femur. They reported micromotion values less than 5 microns, very similar to the values in this study. However, this study used composite femur instead of cadaveric femur and the stem has a side fin to reduce rotation of the stem. The high degree of variation measured in most studies do suggest that a varying amount of interference-fit is achieved in reality. The variation can also be caused by femur quality in these studies. Since low micromotion is measured in some of the experimental studies, the greatest concern is probably to improve the surgery technique to ensure that a good interference-fit is achieved to set up an environment with residual stress so that the stem can be stabilized by friction.

It has also been discussed in Section 3.8.2 and 3.8.3 that the micromotion measurement is different between finite element studies and experimental micromotion studies. In experimental studies, micromotion is measured relative to the outer surface of the femur, and therefore may have included elastic bone deformation instead of just interface slippage. The actual interface slippage could therefore be lower than the micromotion reported in experimental studies. It has also been reported by finite element study that elastic deformation of bone between the interface bone and the periosteal bone could dominates the deformation and overestimate the actual slippage at the bone-stem interface [Keaveny and Bartel, 1993c]. Therefore, the micromotion values reported for model In-0.1 and In-0.05 are not unrealistic.

With interference-fit of 0.1 and 0.05 mm, the initial stability is lower than values that have been reported in other finite element studies (Table 3.2, Section 3.8.3). Other finite element studies in the literature did not model the interference-fit at the bone-stem interface. As a result, the micromotion reported in the literature is closer to the values reported for the zero interference-fit model in this study. It is therefore not possible to compare the stability of IPS stem modelled with interference-fit in comparison to other designs.

Significant strain can damage the interface bone by creating microcracks [Wachtel and Keaveny, 1997; Keaveny *et al.*, 1999]. As a result of damage, cancellous bone becomes more compliant [Keaveny *et al.*, 1994d; Keaveny *et al.*, 1999]. Keaveny *et al.* (1999) reported degradation of cancellous bone modulus by about 85% after overloading human vertebral cancellous bone to 1.75% total strain and above in uniaxial compression test. The interface strain is much higher if stem is inserted with 0.1 mm interference-fit instead of 0.05 mm interference-fit. In model In-0.1, some of the interface bones at the more distal region of the porous coating have been shown to have strain exceeding 1.5 % strain, which suggests that substantial modulus degradation should occur in these bones. At the distal L3 region in model In-0.1, the mean equivalent strain for the interface bone is about 1.5% strain, which would suggest quite a significant volume of the interface bone in this region will have significant modulus degradation. The degradation of interface cancellous bone stiffness may increase the initial micromotion as

suggested by the results in Chapter 5. The result of this study showed that there could be an optimum degree of interference-fit, where additional increase in interference-fit does not improve the initial stability of the stem. A study to find the optimum interference-fit should be performed to avoid loading the interface bone beyond its ultimate strain.

Intraoperative femoral fractures is one of the factor associated with hip stem loosening [Martell *et al.*, 1993] and an animal study has reported lower stability and lack of bone ingrowth [Schutzer *et al.*, 1995]. Schwartz *et al.* (1989) reported that about 3 % of the total hip replacement resulted in fracture of the femur. Monti *et al.* (2001) reported that similar fracture rate has been reported in other studies as well. Higher fracture rate of 10% has also been reported [Martell *et al.*, 1993]. High assembly strain has been measured in femur inserted with hip stem that is broader than the femoral cavity [Jasty *et al.*, 1993]. In this study, equivalent strain as high as 0.97 % strain has been calculated on the surface of the femur when a stem is inserted with an interference-fit of 0.1 mm. Maximum periosteal equivalent strain doubles as interference-fit increased from 0.05 mm to 0.1 mm. Jasty *et al.* (1993) has measured hoop strain as high as 0.6 % strain when straight stems were inserted with 0.25 mm interference-fit and fractured the femurs. This strain was measured in femurs inserted with larger stem than the optimum stem size recommended for the particular femur size. In femur inserted with the optimum stem with the same interference-fit, the measured maximum hoop strain is 0.24 % strain, a smaller value. Therefore, the size of the stem and degree of interference-fit determine the hoop strain in the femur. However, the hoop strain measured is not at the exact time the fracture had occurred and not at the location of fracture. It is possible that fractures occurred at a higher strain. Ultimate strain of cortical bone in the transverse direction has been reported in the region of 0.7 % strain in uniaxial tensile test [Reilly and Burstein, 1975]. The equivalent strain of 0.97 % equivalent strain calculated in this study can therefore be considered as high strain. When finite element result showed high strain values, it is probably useful to test the fracture risk on cadaveric femur. The areas of high strain in this study are in the anterior and posterior aspect of the femur. Femoral cracks during insertion of cementless stem have been reported in these regions [Schwartz *et al.*, 1989; Monti *et al.*, 2001].

6.5 Conclusion

The results of this study suggest that :-

1) Interference-fit plays an important part in improving the initial stability of the cementless press-fit prosthesis. Both the axial and rotational micromotion decrease with the introduction of an interference-fit.

2) The micromotion results suggest that there is a diminishing returns through further increase in interference-fit as less and less reduction of micromotion will be achieve. This suggests that there is an optimum amount of interference-fit that should be incorporated during the implantation of the stem. The degree of interference-fit should be design to give maximum initial stability and minimal femoral strain. In this study, a stem inserted with 0.05 mm interference-fit has similar stem stability in comparison to a stem inserted with 0.1 mm interference-fit but with lower femoral strain and therefore lower fracture risk. The former is probably the more optimum degree of interference-fit.

3) The results suggest that low interference-fit does not increase the interface bone strain significantly in comparison to zero interference-fit. However, at moderate and higher interference-fit, increasing interference-fit increases the interface strain substantially. High interface strain could increase the compliance of interface bone and increase interface micromotion. With diminishing reduction in micromotion due to further increase in interference-fit, higher degree of interference-fit may be counter-productive in term of maintaining interface bone integrity.

4) Doubling the interference-fit from 0.05 to 0.1 mm increases the maximum anterior and posterior periosteal strain by two times. This increases the risk of bone fracture significantly without the benefit of further decrease in micromotion. Therefore, above the optimal degree of interference-fit, higher interference-fit will only increase the risk of bone fracture without much benefit.

5) Contact area improved with interference-fit. This could reduce the gap between stem and interface bone, and facilitate bone ingrowth.

Chapter 7 The effect of modelling plasticity on the initial micromotion of the IPS stem and strain of the femur

7.1 Introduction

In Chapter 6, one of the main limitations of the models was neglecting to model the elastic-plastic behaviour of bone. This may have affected the prediction of the micromotion of the stem and strain of the femur, especially when an interference-fit was modelled. High interface strains have been calculated in the 0.05 and 0.1 mm interference-fit models. The equivalent total strain has exceeded 1.5% strain in the 0.1 mm interference-fit model, especially at the more distal L2 and L3 regions. The ultimate strain of cancellous bone has been reported in the region of 1.5 % strain [Rohl *et al.*, 1991; Linde *et al.*, 1992; Kopperdahl and Keaveny, 1998; Keaveny *et al.*, 1999]. The equivalent strains in the 0.05 mm model exceeded 0.7 % strain, which is in the region of yield strain reported in the literature [Rohl *et al.*, 1991; Kopperdahl and Keaveny, 1998; Morgan and Keaveny, 2001]. Failure to model the plastic yielding of bone may underestimate the interface strain and deformation of the interface bone. This could have underestimated the micromotion and strain in the implanted proximal femur.

Most finite element studies of the implanted proximal femur ignored modelling of plasticity in bone [Huiskes, 1990; Cheal *et al.*, 1992; Keaveny and Bartel, 1993c; Skinner *et al.*, 1994; Kuiper and Huiskes, 1996; Ramaniraka *et al.*, 1996; Ando *et al.*, 1999; Joshi *et al.*, 2000]. A few studies have modelled bone as elastic-perfectly plastic material [Rubin *et al.*, 1993; Visnic *et al.*, 1994; Taylor *et al.*, 1995]. Taylor *et al.* (1995) reported significant plastic strain can develop within cancellous bone of the femur implanted with a press-fit prosthesis. A two-dimensional model by Visnic *et al.* (1994) reported considerable plastic deformation in their simulation of insertion of press-fit prostheses. However, these two studies only examined the stress/strain distribution and did not report the predicted micromotion. Rubin *et al.* (1993) examined the micromotion and stress at the interface of the implanted femur. They reported plastic yielding up to 400 times the plastic yield criterion and suggested that this is probably due to very low stiffness assigned to the bone. The micromotion reported by Rubin *et al.* (1993) is very high, and most likely this is due to significant plastic deformation in the interface bone. However, modelling bone as elastic-perfectly plastic material in a model of the implanted proximal femur with interference-fit has not been studied. High interface strain can potentially reduce the integrity of the interface bone. High implant migration in the immediate postoperative period has been attributed to fatigue damage of necrotic interface bone [Taylor, 1997]. Loading interface bone beyond plastic limit of

bone may potentially reduce the fatigue life of interface bone in the immediate postoperative period.

The objective of this study is to look at the :-

1) The effect of modelling bone as an elastic-perfectly plastic material on the initial micromotion of the IPS stem and strain of the femur predicted in a finite element analysis.

2) The extent of plastic deformation of the interface bone.

7.2 Elastic-perfectly plastic analysis of the physiological model of the implanted proximal femur

This model has been described in Chapter 4 and 6. In this study, changes were made to the model by assigning yield stress to the bone. Bonemat [Zannoni *et al.*, 1998] was modified to allow it to assign yield stress to bone. Bone was assumed to behave as an elastic-perfectly plastic material and yield at 1.0, 1.25 and 1.5 % strain. The assumption of elastic-perfectly plastic behaviour is a reasonable assumption when compared with experimental data [Carter *et al.*, 1980; Keaveny *et al.*, 1994b]. In compression, typical bone stress-strain curve looked like Figure 7.1, with a long plateau region after ultimate strength has been reached. The elastic-perfectly plastic material has been used in previous finite element studies [Taylor *et al.*, 1995].

Linde *et al.* (1992) reported that compressive strength of cancellous bone can be calculated as

$$\sigma_{ultimate} = 0.015E + 0.193 \text{ ---------- Equation 7.1}$$

where $\sigma_{ultimate}$ is the compressive strength (MPa) and E is the elastic modulus (MPa). Assuming that for an elastic-perfectly plastic material the yield stress is equal to the ultimate stress, the yield strain can be calculated as

$$\sigma_y = E\varepsilon_y \text{ ---------- Equation 7.2}$$

where ε_y is yield strain, σ_y is yield stress (MPa) and E is Young's modulus (MPa). Comparing Equation 7.1 and Equation 7.2, the yield strain can be approximated to 0.015, which is 1.5 % strain. This yield strain value has been used before in a finite element analysis of the implanted proximal femur [Taylor *et al.*, 1995]. Other experimental studies have also reported the ultimate strain for cancellous bone of between 1.1 and 1.5% strain [Rohl *et al.*, 1991; Kopperdahl and Keaveny, 1998; Keaveny *et al.*, 1999]. Based on experimental data of cancellous bone, ultimate yield strain of 1 % is probably on the lower boundary of ultimate strain measured and between 1.25% and 1.5 % strain is the mean value of ultimate strain measured. The yield stresses assigned to the bone were the product of the elastic moduli of bone and the yield strains. An underlying assumption of this study is that only cancellous bone yields due to the much higher stiffness of

cortical bone. This is a reasonable assumption as the stem is mostly in contact with cancellous bone and yielding of cortical bone is likely to lead to fracture of the femur.

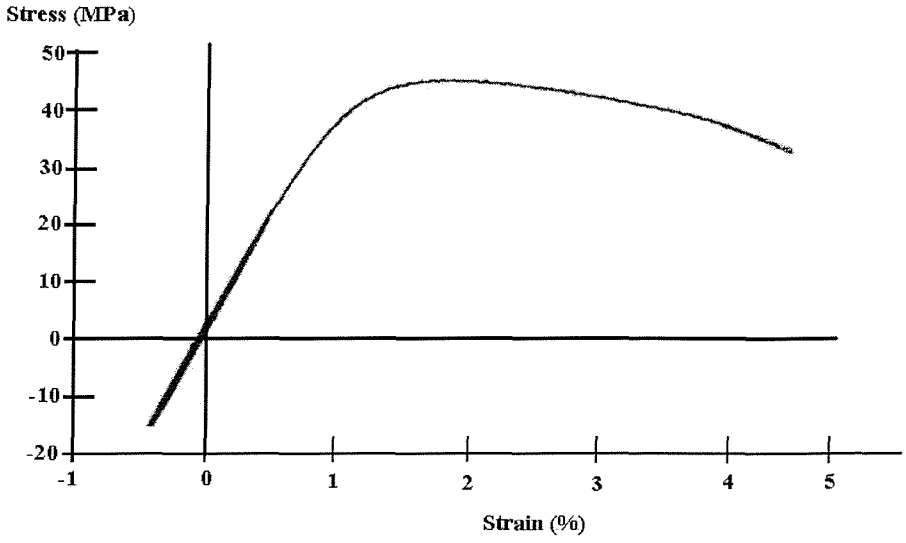

Figure 7.1 Stress-strain curve of cancellous bone in uniaxial test. Bone is linear elastic prior to yield. Post-yield behaviour showed long plateau region which can be reasonably approximated by elastic-perfectly plastic material model [Keaveny *et al.*, 1994b].

In MARC2001, the von Mises yield criteria was implemented. The three load steps in this study were similar to load steps used in the previous interference-fit study in Chapter 6. Four models, simulating an interference-fit of 0.1 mm, were analysed using the walking loadcase described in Chapter 4. Implementation of the interference-fit boundary condition was explained in Chapter 6. These four models simulated a linear elastic material model and elastic-perfectly plastic models with yield strains of 1.5, 1.25 and 1.0 % strain. They were referred to as model **In-0.1**, **In-0.1(P1.5)**, **In-0.1(P1.25)** and **In-0.1(P1.0)** respectively. Two models without interference-fit simulating linear elastic material model and elastic-perfectly plastic material model (1.5 % yield strain) were modelled as well. They will be referred to as model **In-0** and **In-0(P1.5)** respectively. Results were reported at level L1, L2 and L3, similar to the location reported in Chapter 6.

7.3 Effect of plasticity on initial micromotion, strain and stress

7.3.1 Micromotion

Figure 7.2 shows the micromotion at L1, L2 and L3 for model In-0.1, In-0.1(P1.5), In-0.1(P1.25) and In-0.1(P1.0). Comparison between linear elastic and the elastic-perfectly plastic interference-fit models shows that modelling of the plastic behaviour of bone does not significantly affect the predicted micromotion. The biggest difference in peak micromotion was seen at level L1, where model In-0.1(P1.0) was higher than model In-0.1 by 3 μm. This was not significant and hardly changes the conclusion of the linear elastic model. The average micromotion remains similar for all four models at level L1. At L2 and L3, both the peak and mean micromotions for all the models were similar. This result was quite surprising as significantly higher micromotions were expected from the elastic-perfectly plastic material models.

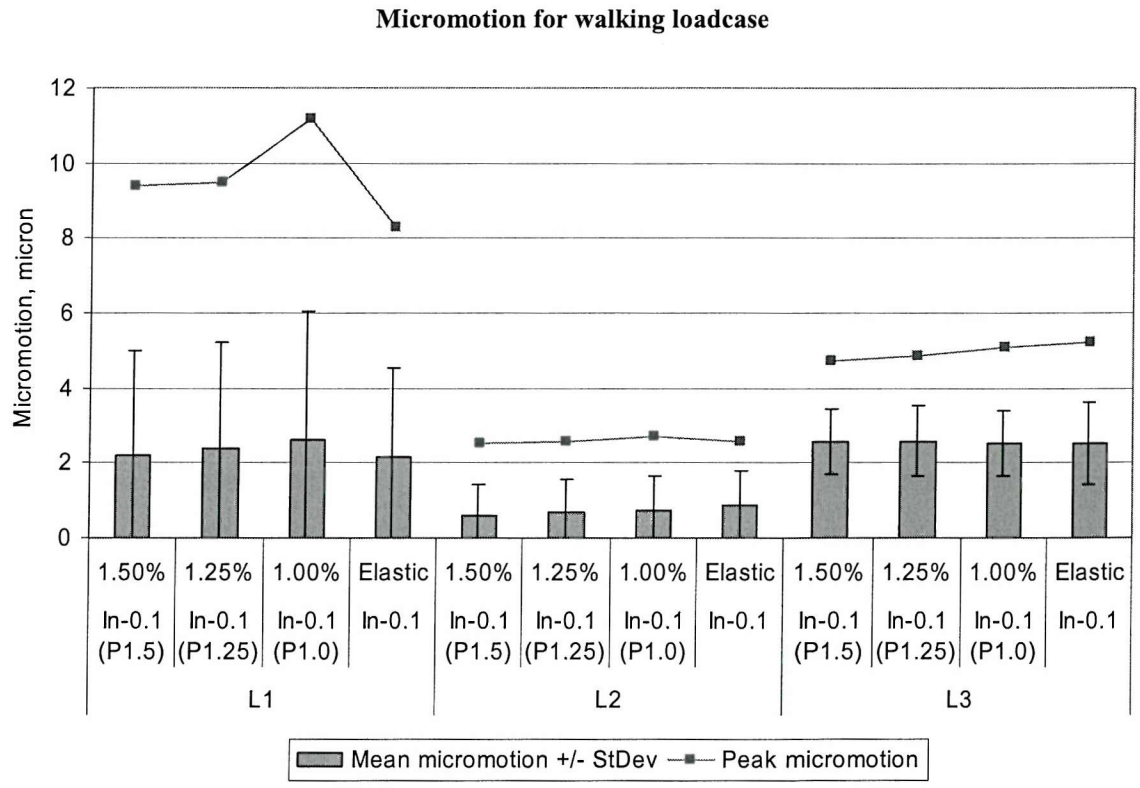

Figure 7.2 Comparison of micromotion at L1,L2 and L3 for model In-0.1, In-0.1(P1.5), In-0.1(P1.25) and In-0.1(P1.0). Mean micromotion ± standard deviation and maximum micromotion is shown here. Both mean and maximum micromotion is not significantly different between the elastic and the elastic-perfectly plastic models. Model In-0.1(P1.0) showed slightly higher peak micromotion, but does not change the conclusion of the linear elastic model (model In-0.1).

In Figure 7.3, the comparison of the micromotions in the model In-0 and In-0(P1.5) are shown. Model In-0 and In-0(P1.5) did not simulate the interference-fit at the bone-stem interface.

They have similar micromotions as virtually no plastic deformation was observed in model In-0(P1.5). The load was not high enough to deform the interface bone plastically.

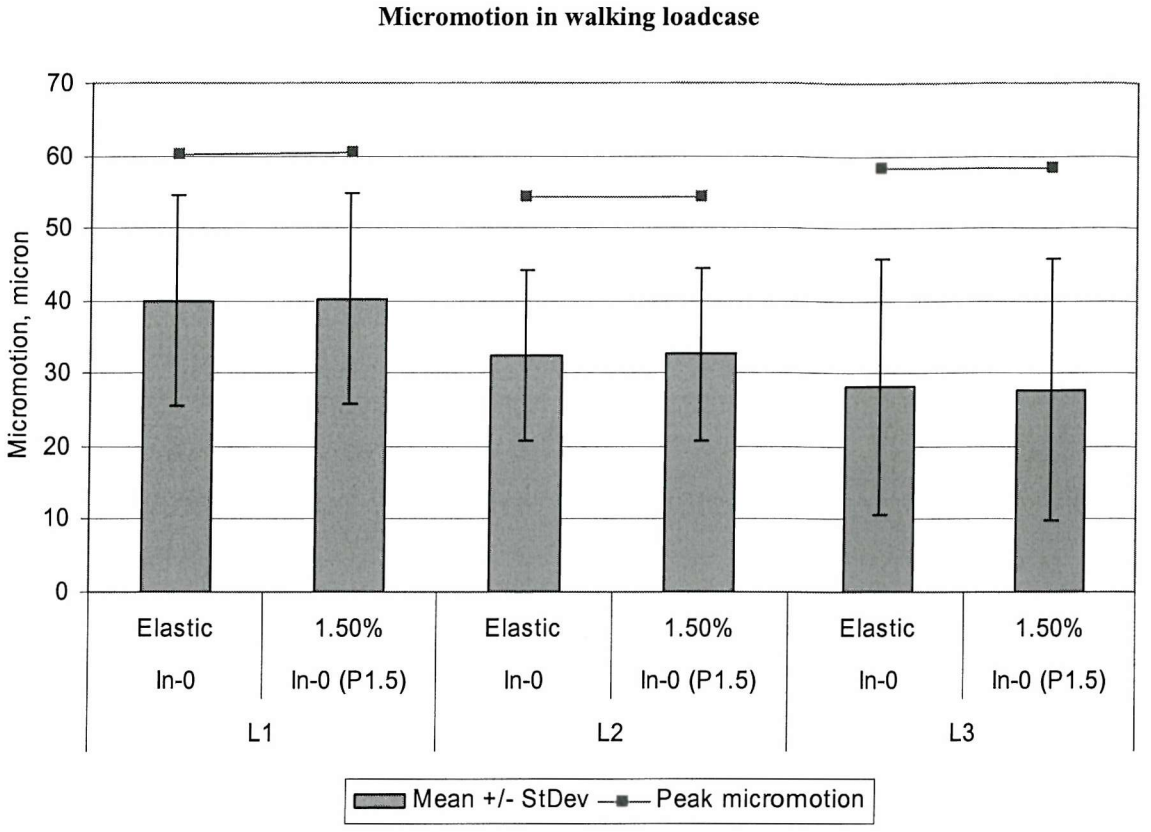

Figure 7.3 Comparison of the micromotion at L1, L2 and L3 for model In-0 and In-0(P1.5). Micromotion is not significantly different between them.

7.3.2 Strain

A comparison of equivalent total strain and equivalent plastic strain after loadstep 3 for model In-0.1, In-0.1(P1.5), In-0.1(P1.25) and In-0.1(P1.0) are shown in Figure 7.4. The elastic-perfectly plastic interference-fit models have nearly similar mean equivalent total strains in comparison to the elastic model. This is likely to be due to the interference-fit exerting similar radial displacement in all the models, regardless of the constitutive material law for bone. Although mean equivalent total strains are nearly similar in the elastic- perfectly plastic models, the mean equivalent plastic strains at L1, L2 and L3 are higher in the models with lower yield strain, i.e. the mean equivalent plastic strains are highest in model In-0.1(P1.0). The interface bone area that deformed plastically is also greater in model In-0.1(P1.0) as compared to model In-0.1(P1.5) and In-0.1(P1.25). The mean equivalent plastic strains increase proximally to distally in all the elastic-perfectly plastic models. Interference-fit induced higher strain in the smaller femoral cross-sectional area distally.

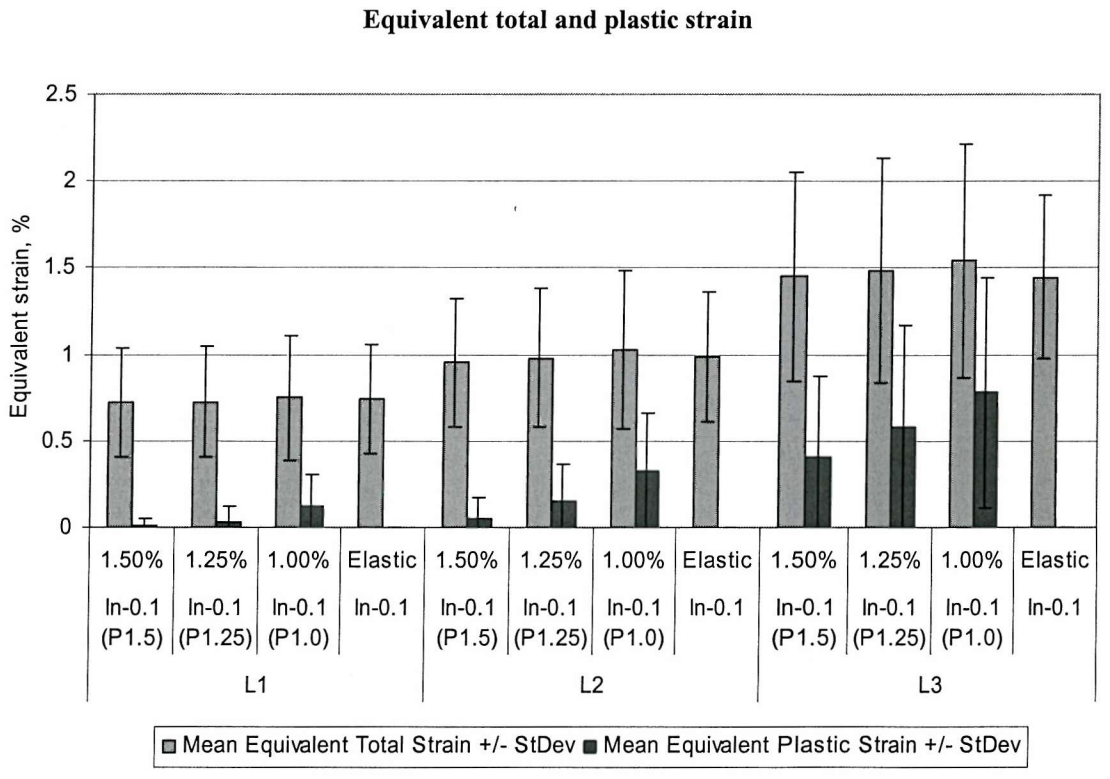

Figure 7.4 Mean equivalent total and equivalent plastic strain ± standard deviation at L1, L2 and L3 for model In-0.1, In-0.1(P1.5), In-0.1(P1.25) and In-0.1(P1.0) are shown here. A comparison of equivalent total strains shows similar values in all models. However, the equivalent plastic strains are different in the plastic models, depending on the yield strains of bones in the models.

In Figure 7.5, the distributions of equivalent plastic strains and Young's modulus in relation to their location on the bone-implant interface at L1, L2 and L3 in model In-0.1(P1.0) are shown. The regions that yield plastically correspond to the lower Young's modulus bone regions. The

higher Young's modulus regions do not yield. This is true as well in model In-0.1(P1.5) and In-0.1(P1.25), which are not shown here. Model In-0.1(P1.0) has higher equivalent plastic strains for the corresponding nodes than the higher yield strains models. There are also more nodes that deformed plastically in model In-0.1(P1.0) on all the cross-sections, and this leads to a larger area on the interface that yields plastically. Interface bone plastic deformation due to interference-fit is therefore not uniform. Plastic deformation is greater in the bone with lower Young's modulus.

Table 7.1 showed the volume of elements that deformed plastically after the first and third loadstep for model In-0.1(P1.5), In-0.1(P1.25) and In-0.1(P1.0). The volumes of bone that deformed plastically during the first load step simulating press-fit were 2425, 4172 and 6288 mm^3 in model In-0.1(P1.5), In-0.1(P1.25) and In-0.1(P1.0) respectively. The plastic deformation of the interface bone is quite extensive around the stem. In comparison to model In-0.1(P1.0), the deformation is less extensive proximally for model In-0.1(P1.5). In the third loadstep simulating walking, the plastic volumes increase by 442, 465 and 671 mm^3 in model In-0.1(P1.5), In-0.1(P1.25) and In-0.1(P1.0) respectively. The most extensive plastic deformation and highest increase in plastic deformation after simulating walking were observed in model In-0.1(P1.0) due to its lowest yield strain. Although the increase in volume of element that deforms plastically is highest in model In-0.1(P1.0), the volume that deforms plastically after the third loadstep is only 11 % higher than in the first loadcase. Therefore, most of the plastic deformation occurred in the first load step.

Model	**Element volume, mm^3**		**Increase in plastic volume, mm^3**	**Percentage difference, %**
	Loadstep			
	1	**3**		
In-0.1(P1.5)	2425	2867	442	18.2
In-0.1(P1.25)	4172	4637	465	11.1
In-0.1(P1.0)	6288	6959	671	10.7

Table 7.1 Volume of bone that deform plastically after loadstep 1 and 3 for model In-0.1(P1.0). After loadstep 3, the plastic volume in the bone increased by 10.7 %. Thus, the first loadstep is responsible for most of the plastic deformation in bone.

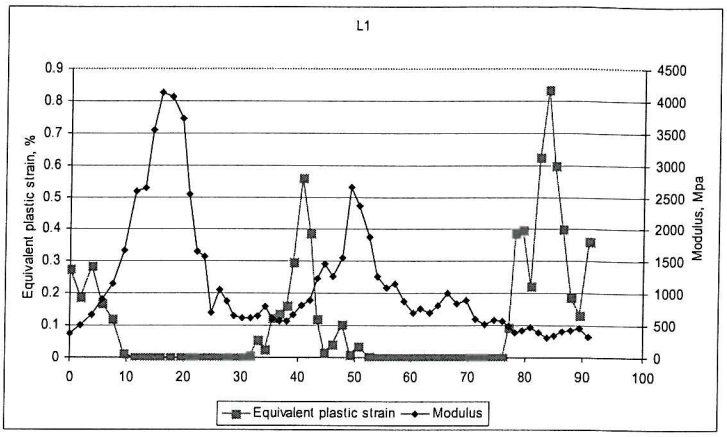

0 = lateral; 23 = Anterior; 43 = Medial; 65 = Posterior

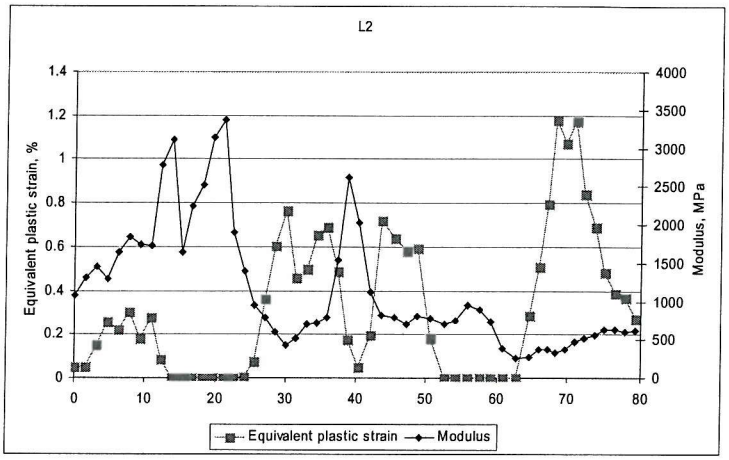

0 = Lateral; 20 = Anterior; 40 = Medial; 63 = Posterior

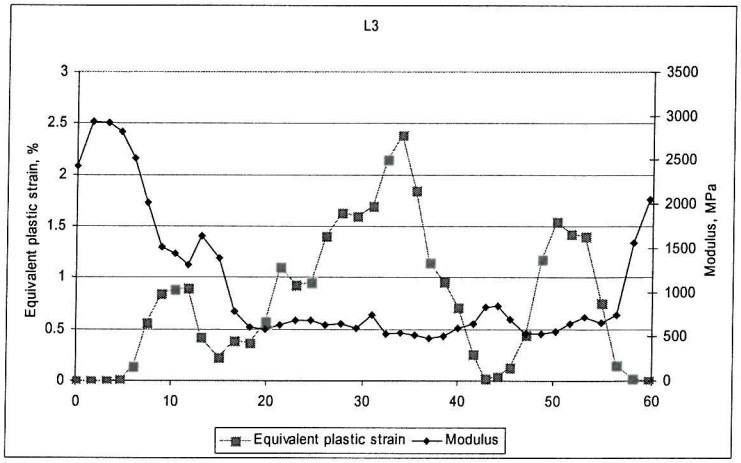

0 = Lateral; 15 = Anterior; 31 = Medial; 45 = Posterior

Figure 7.5 Distribution of equivalent plastic strain and Young's modulus at L1, L2 and L3 in model In-0.1(P1.0). X-axis refers to the length along the circumference of the bone-implant interface at the respective levels. The location on the bone is indicated below the graph. Yielding generally occurred at the region of low modulus.

Figure 7.6 shows the relative percentage volume of elements that fall into different equivalent plastic strain ranges for model In-0.1(P1.0). The percentage volume of elements that fall into different strain ranges in loadstep 1 and 3 are nearly the same. The load applied for simulating walking did not increase plastic strain in the bone significantly and shifted more elements toward the higher strain range region. The small increase in volume of elements that deformed plastically and nearly similar equivalent plastic strain distributions in different strain ranges after the third loadstep show that most of the plastic deformation is accumulated during the press-fit process. During the second loadstep, the stem's head displaced axially by 32 μm and the stress in the femur relaxed slightly. The maximum von Mises stress in the proximal femur reduced from 58.76 MPa to 57.81 MPa. This stress relaxation probably allows some of the bone that deformed plastically in the first load step to take some elastic load in the third loadstep. Therefore, the deformation in the third loadstep does not increase the plastic strain significantly and could be mostly elastic. The small increase in plastic strain probably explained the similarity in micromotion between the elastic and the elastic-perfectly plastic models.

The strain values in model In-0(P1.5) (without interference-fit) showed that the majority of the interface area is below 0.2 % equivalent strain and a few regions with equivalent strain between 0.2 and 0.4 % equivalent strain (Figure 7.7). There were only two small spots in the distal and proximal region where plastic deformation occurred. The low strain values in the majority of the area is in agreement to the small increase in volume of elements that deformed plastically after the third loadstep in Model In-0.1(P1.0).

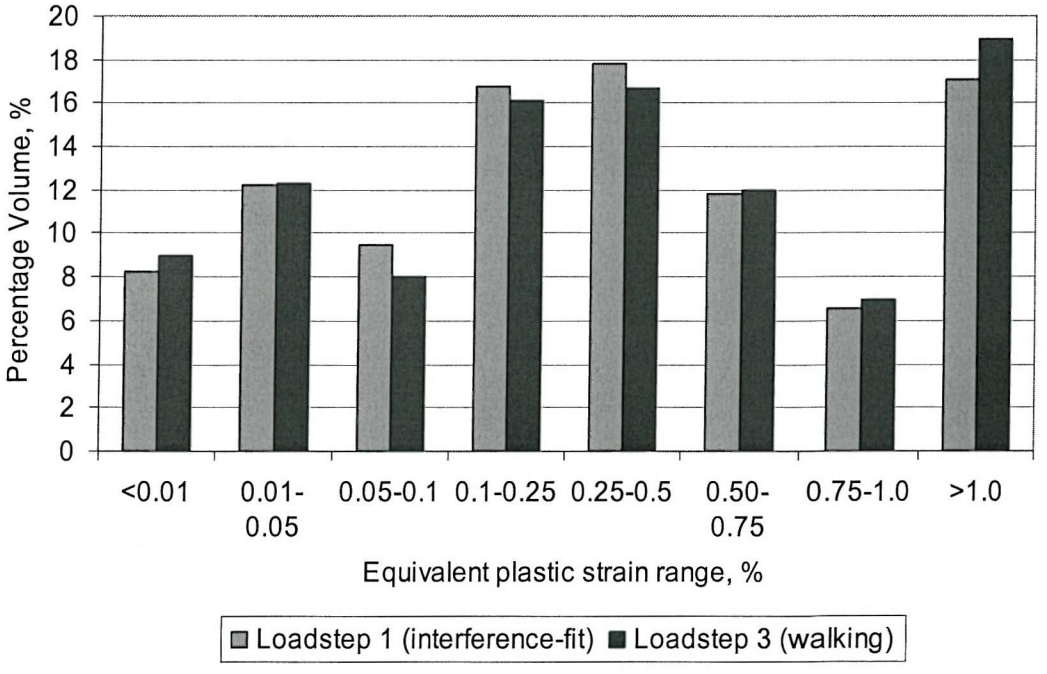

Figure 7.6 Ratio of the volume of elements within certain equivalent plastic strain range relative to the total volume of element that deformed plastically for model In-0.1(P1.0). The ratios in loadstep 1 and 3 are nearly identical.

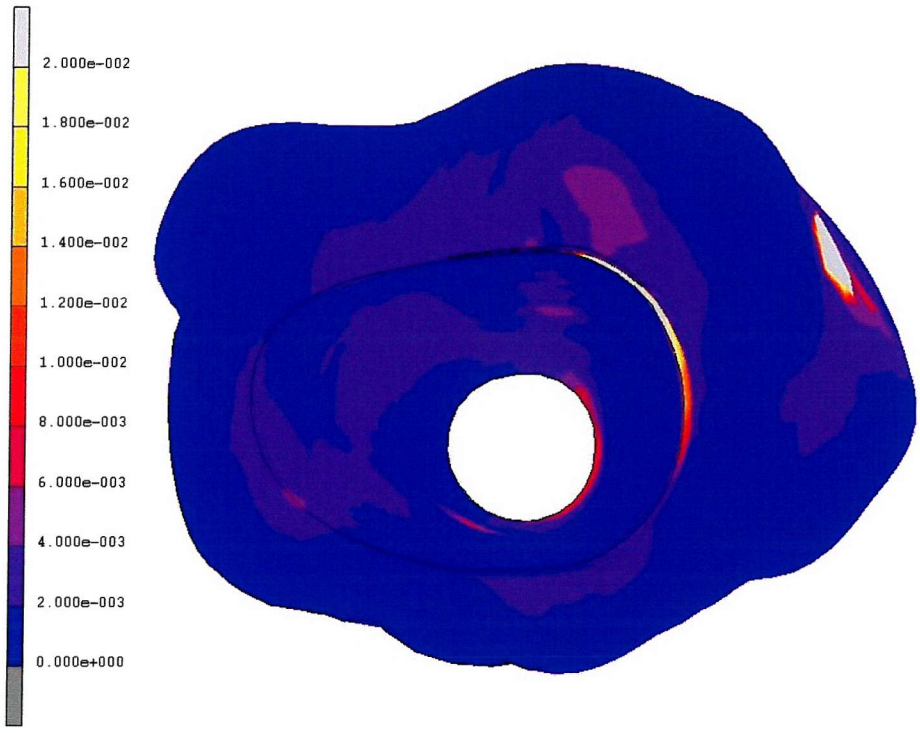

Figure 7.7 Equivalent total strain in model In-0(P1.5). In the interface bone, the majority of the area is less than 0.2 % strain. In some area, the strain is between 0.2 and 0.4 % strain. Overall, interface strain is quite low.

7.3.3 Stress

Von Mises stresses at level L3 for three different models were compared in Figure 7.8. Model In-0.1(P1.0) and model In-0.1 are from this chapter. Model In-0.05 is the linear elastic model with interference-fit of 0.05 mm from Chapter 6. A comparison of the von Mises stress between model In-0.1(P1.0) and In-0.1 showed that von Mises stress is slightly lower in model In-0.1(P1.0) due to plastic deformation. However, the von Mises stress in model In-0.1(P1.0) is still much higher than model In-0.05. The micromotions predicted for model In-0.1 and In-0.05 were quite similar. Since the residual stress of model In-0.1(P1.0) is much higher than model In-0.05, the effective interference-fit of model In-0.1(P1.0) is also much higher. This could further explain the similarity between the predicted micromotions of linear elastic and elastic-perfectly plastic model in this study.

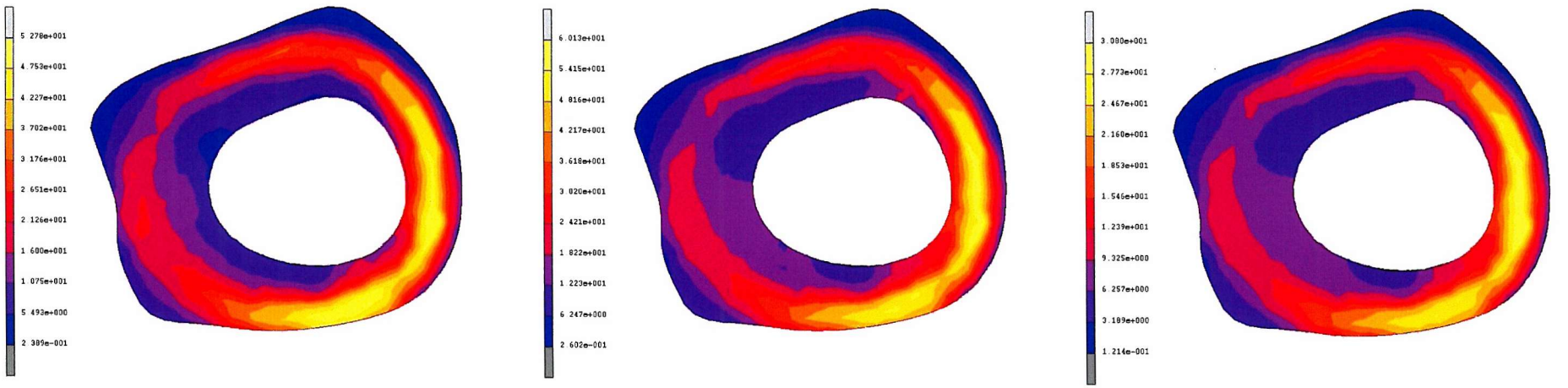

Model In-0.1(P1.0) Model In-0.1 Model In-0.05 (from Chapter 6)

Figure 7.8 von Mises stresses at level L3 from 3 different models. (Left) Elastic-perfectly plastic model with 0.1 mm interference-fit (model In-0.1(P1.0)). (Middle) Linear elastic model with 0.1 mm interference-fit (model In-0.1). (Right) Linear elastic model with 0.05 mm interference-fit (model In-0.05 from Chapter 6).

7.4 Discussion

The finite element models with interference-fit in Chapter 6 have shown very high interface strain when modelled with 0.1 mm interference-fit. The objective of this study was to evaluate if modelling bone as an elastic-perfectly plastic material has any influence on the predicted initial micromotion and strain of the interference-fit model. The result of this study has shown that the modelling of the elastic-perfectly plastic behaviour does not have significant effect on the predicted initial micromotion in the models with and without an interference-fit. The predicted initial micromotions in Chapter 6 are therefore not affected by the treatment of bone as a linear elastic material in Chapter 6. Model In-0.1(P1.0) has higher micromotion than model In-0.1, but is not significantly higher to change the conclusion of the linear elastic model In-0.1. Model In-0.1(P1.0) that has the lowest yield strain of 1.0% has a higher peak micromotion in comparison to other models, but the peak difference in micromotion of 3 μm is insignificant in comparison to the reported threshold of bone ingrowth of 50 μm [Engh *et al.*, 1992b; Bragdon *et al.*, 1996; Fernandes *et al.*, 2002]. In the models without interference-fit, the micromotion was identical because the load is not high enough to cause significant plastic deformation.

In the interference-fit models, significant plastic deformation of the interface bone was predicted. Most of the plastic deformation occurred during the loadstep simulating the establishment of interference-fit. In the loadstep simulating walking, a small increase in plastic deformation was seen. Overall, the total plastic deformation in the third loadstep is similar to the first loadstep. Since most plastic deformation was accumulated during the interference-fit step, the micromotion in the plastic interference-fit models were only slightly higher than the elastic model. The interface bone strain in the model without interference-fit showed low strain in most of the interface area. The small increase in plasticity in the third loadstep in the interference-fit model and the low interface bone strain in the model without interference-fit suggests that most of the deformation in the third loadstep is elastic in nature. This explains the nearly identical micromotion predicted by the elastic and elastic-perfectly plastic models. Clinically, the similarity in initial stability of the elastic and elastic-perfectly plastic model is important as this means that the initial micromotion of the IPS stem is not sensitive to some plastic deformation of bone, which is likely to occur during insertion of the stem.

The residual stress within model In-0.1(P1.0) decreased in comparison to model In-0.1 due to plastic deformation. However, in comparison to the elastic model with 0.05 mm interference-fit (model In-0.05), model In-0.1(P1.0) still has higher residual stress, which suggests that the effective interference-fit is higher in model In-0.1(P1.0). Since model In-0.1 and In-0.05 has similar micromotion, the higher residual stress of model In-0.1(P1.0) in comparison to model In-0.05 suggests that micromotion of model In-0.1(P1.0) will also be similar to model In-0.1 and In-

0.05. This could partly explain the similarity of micromotion of the elastic and elastic-plastic models.

Although the interface bone strain of the implanted proximal femur using the IPS stem in the model without interference is not high, studies have shown that interface contact stresses can vary widely either in distribution or magnitude in different stem designs [Ando *et al.*, 1999]. Different stems design also may cause higher strain at the interface bone. In a finite element analysis of a Freeman stem, Taylor *et al.* (1995) has shown that press-fit stem can cause high interface bone stress and cause significant plastic deformation of the interface bone, even without modelling an interference-fit. In models without an interference-fit, very high micromotions have been predicted when significant plastic deformation of the interface bone was modelled [Rubin *et al.*, 1993]. Therefore, for a stem that can generate high interface stress, modelling plasticity may give higher micromotion due to the possible greater deformation of the interface bone. The effect of plastic deformation of interface bone on the stability of press-fit stems with interference-fit in other stem designs should not be extrapolated from the results of this study.

Although under-reaming the femoral canal has become standard in cementless total hip replacement, little attention has been given to the potentially damaging high strain in an interference-fit assembly. The present study has shown that even a moderate interference-fit of 0.1 mm can cause significant plastic deformation of the interface bone. The plastic deformation is most likely to occur in areas of low bone modulus. A higher interference-fit will cause a greater amount of plastic deformation at the interface bone and the integrity of interface bone may be significantly affected as a result of excessive interference-fit.

Mechanical properties of bone have been found to change after undergoing plastic deformation. Overloading of cancellous bone beyond the ultimate strain reduces the Young's modulus of cancellous bone, depending on the extent of overloading [Keaveny *et al.*, 1999]. A limitation of the present study is the reduction of Young's modulus of cancellous bone after overloading was not modelled. The lowering of cancellous bone stiffness may affect the micromotion at the bone-stem interface. However, the volume of bone that yields plastically is small relative to the overall volume of the proximal femur supporting the stem. In Chapter 5, it has been shown that overall stiffness of femur affects the micromotion rather than just the stiffness of cancellous bone. It is possible that the reduction of stiffness of interface cancellous bone will not affect the micromotion too much since its effect on overall stiffness of femur is small.

Other limitations of this model are similar to those outlined in Chapter 6. This model still neglected the viscoelastic effect of bone. If creep of bone is modelled, it is likely that some stress relaxation of the interface bone will occur before simulation of the walking load step and reduce the residual stress in the femur.

Besides increasing the compliance of the interface, plastic deformation of the interface bone may increase the risk of interface bone failure due to daily loading and increase the risk of implant migration. When bone is deformed plastically, cracks are suspected to develop [Keaveny *et al.*, 1994b; Keaveny *et al.*, 1994d; Wachtel and Keaveny, 1997; Keaveny *et al.*, 1999]. Wachtel and Keaveny (1997) observed an increase in the number of cracks in bone loaded beyond yield, which supported the theory that plastic deformation of bone causes crack formation. In a high interference-fit environment, interface cancellous bone has been shown to have yield regions and the cancellous bones in these regions are bound to have more cracks. In the immediate postoperative period, bone may not have time to repair the damage cause by the interference-fit. With these damages already present, bone may reach a fatigue limit faster as fatigue damages are also accumulated from daily routines. This could have implication on the early migration of the implant. Taylor (1997) suggested that in the immediate postoperative period, the implant is supported on a layer of necrotic bone caused during surgery. Since this layer cannot repair accumulated damage, there is a higher risk of trabeculae fractures and hence stem migration could occur more rapidly than in the actively remodelling cancellous bone. Therefore, higher interface bone damage during stem insertion could increase the risk of fatigue fracture of bone in the immediate postoperative period and lead to higher migration.

7.5 Conclusion

The main conclusions of this study are:-

1) Modelling of bone as an elastic-perfectly plastic material does not change the predicted micromotion of the IPS stem in Chapter 6.

2) Significant plastic deformation of the interface bone occurred when the IPS stem is inserted with 0.1 mm interference. However, limited plastic deformation is accumulated due to applied walking load. Therefore, micromotions did not change significantly from the linear elastic model.

3) The von Mises stresses within the femur reduces, and thus the effective interference-fit reduces. However the reduction is not significant enough to change the predicted micromotion of the IPS stem.

4) In the interference-fit model, bone should be modelled as elastic-perfectly plastic material to check the extent of bone damage due to interference-fit. Extensive plastic deformation may compromise interface bone integrity and increase the risk of migration.

Chapter 8 Effect of creep on the initial stability of the stem and strain in the implanted proximal femur

8.1 Introduction

In Chapter 6, the results showed that the implanted femur assembly showed high assembly strains with a moderate interference-fit of 0.1 mm. It has also been discussed in Section 1.4.2 that bone undergoes creep deformation [Zilch *et al.*, 1980; Fondrk *et al.*, 1988; Rimnac *et al.*, 1993; Bowman *et al.*, 1998; Bowman *et al.*, 1999; Fondrk *et al.*, 1999; Brown *et al.*, 2002]. In a high strain environment like the interference-fit assembly in an implanted proximal femur, creep is likely to occur. Therefore, it is conceivable that for a high initial interference-fit value, creep will effectively reduce the residual stresses and thus the effective amount of interference-fit. How creep affects the effective interference-fit and the initial stability of the implanted proximal femur has not been reported in the literature.

Both cortical and cancellous bone have been shown to exhibit the three classical stages of creep observed in many engineering materials [Rimnac *et al.*, 1993; Bowman *et al.*, 1994; Bowman *et al.*, 1998; Bowman *et al.*, 1999; Brown *et al.*, 2002]. The creep rate decreases during the primary phase, is constant during the secondary phase and increases during the tertiary phase. The steady state creep rate and time to failure in both cortical and cancellous bone are strongly correlated to normalized stress by a power law relationship [Caler and Carter, 1989; Rimnac *et al.*, 1993; Bowman *et al.*, 1994; Bowman *et al.*, 1998; Bowman *et al.*, 1999]. The creep behaviour of both cortical and cancellous bone have been observed in a temperature range that includes the *in vivo* temperature of 37 °C [Rimnac *et al.*, 1993; Bowman *et al.*, 1998]. Therefore, creep can happen *in vivo*. It is reasonable to assume that if bone creeps *in vivo*, then residual bone stress cause by an interference-fit can reduce *in vivo*.

Postoperatively, cementless hip joint replacement patients are normally advised to partially weight bear for at least a few weeks postoperatively to allow bone ingrowth to occur [Nistor *et al.*, 1991]. Bone ingrowth onto the surface of hip stem *in vivo* will take at least a few weeks to occur postoperatively. Lamellae bone ingrowth has been observed in rabbits 4 weeks postoperatively [Dhert *et al.*, 1998]. This study observed formation of callus after 7 days and woven bone after 14 days. However, bone formation is faster in rabbits than in humans. Callus formation has been observed in fracture healing and the differentiation of this tissue forms bone [Goodship and Kenwright, 1985; Gardner *et al.*, 2000]. Direct measurement of the time needed for ingrowth to occur in humans has not been reported in the literature. However, it has been reported that the first

formation of woven bone from soft connective tissue adjacent to the fracture site during fracture healing in humans takes about 8 weeks [Gardner *et al.*, 2000]. At this time, woven bone reached 25% maturation. The maturation of woven bone reached 60% after 16 weeks. Towards the peripheral of the fracture callus, dense fibrous tissue was observed after 8 weeks. After 16 weeks, the fibrous tissue has remodelled to become mature bone. If the healing process in the bone-implant interface and in fracture share a similar time frame, then it is vital that interference-fit should provide stability for at least 8 weeks for the early stabilization to occur.

Due to possible creep in the femur *in vivo*, this study investigated the influence of creep on the effective interference-fit and initial stem micromotion. This is to address one of the limitations of the models in the previous chapters. The relative effect of residual stresses in the cortical and cancellous bone on stem micromotions are also studied to better understand the interference-fit design for hip stems. The stress relaxation of bone is simulated using creep data of bone. As a first step to model creep of bone in an interference-fit assembly, a simplified model was chosen. It is easier to study the separate effect of the creep of cortical and cancellous bone on interference-fit with a simplified model.

The objectives of this study were: -

1) To study if the length of time the interference-fit can be maintained is long enough for bone ingrowth to occur?
2) To study if bone creep affects the micromotion of the stem?
3) To study the factors affecting the effective interference-fit?
4) To study if interference-fit is maintained postoperatively, what is the optimum degree of interference-fit?
5) To study how effective interference-fit and micromotion of the stem is affected by bone quality?

8.2 A simplified model of the implanted proximal femur

8.2.1 Simplified model of the stem and femur

The simplified model of the implanted proximal femur used in this study is shown in Figure 8.1 and this model was based on a simplified model reported in another study [Lu and McKellop, 1997]. The proximal femur is modelled as truncated hollow cones with two layers of bone: an outer shell of cortical bone and an inner layer of cancellous bone. The cortical bone is extruded distally as a hollow cylinder to form the femoral shaft. The simplified stem is modelled as a truncated cone joined to an oblique cylindrical neck. The dimensions are shown in Figure 8.1.

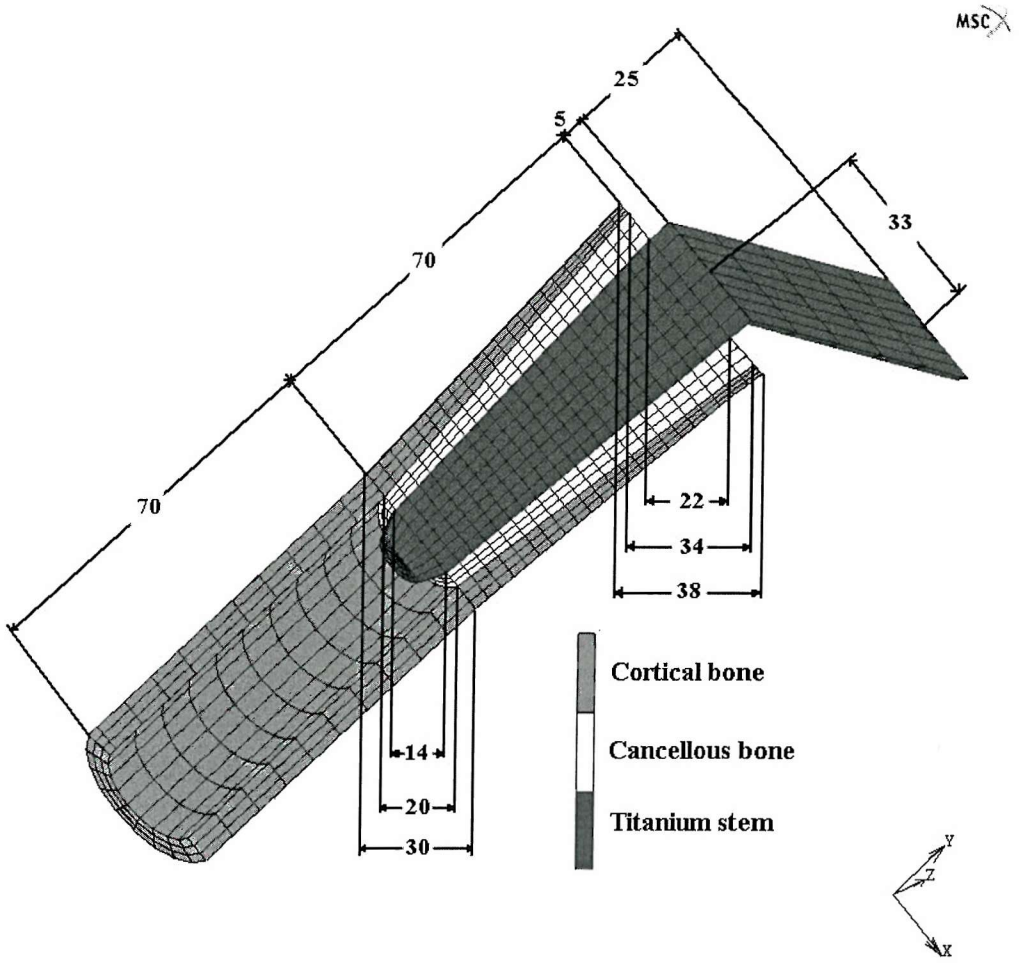

Figure 8.1 Simplified model of the implanted proximal femur. The midplane of the model is shown here. Dimensions are in millimetre.

8.2.2 Creep behaviour of bone

In the literature, creep parameters (steady state creep rate and time-to-failure) have been shown to be highly correlated to normalized stress (σ/E) defined as the ratio of stress over Young's modulus (Table 8.1). Bowman *et al.* (1999) suggested that collagen fibres could be responsible for creep behaviour of bone. Their results showed that demineralised bovine cortical bone (or collagen fibre) showed a similar exponent in the power-law relationship between steady state creep rate $d\varepsilon/dt$ and normalised stress σ/E to cortical and cancellous bone. The exponents for bovine cortical and cancellous bone obtained from tensile (the former) and compressive (the latter) creep test have been reported to take the values of 18.9 [Fondrk *et al.*, 1988] and 15.56 [Bowman *et al.*, 1998] respectively (Table 8.1). The exponent of the power law relationship between time-to-failure t_f and normalized stress σ/E of demineralised bovine cortical bone (or collagen fibre) has been reported to be -15.6 [Bowman *et al.*, 1999]. This is also similar to exponents of human cortical bone (tension = -15.81, compression = -17.76 [Caler and Carter, 1989], hoop = -13.64 [Brown *et al.*, 2002]), bovine cortical bone (tension = -16.7 [Mauch *et al.*, 1992]) and bovine cancellous bone (compression = -15.1 [Bowman *et al.*, 1998]), as shown in Table 8.1.

Demineralised bone also exhibits the usual three stages of creep observed in both cortical and cancellous bone. Like cortical and cancellous bone, creep behaviour of demineralised bone also has an Arrhenius temperature dependency. The demineralised bone creep activation energy of 113 kJ/mole [Bowman *et al.*, 1999] is within the range of creep activation energies for bovine cancellous and cortical bone (136 and 44 kJ/mole respectively) [Rimnac *et al.*, 1993; Bowman *et al.*, 1998], as shown in Table 8.1.

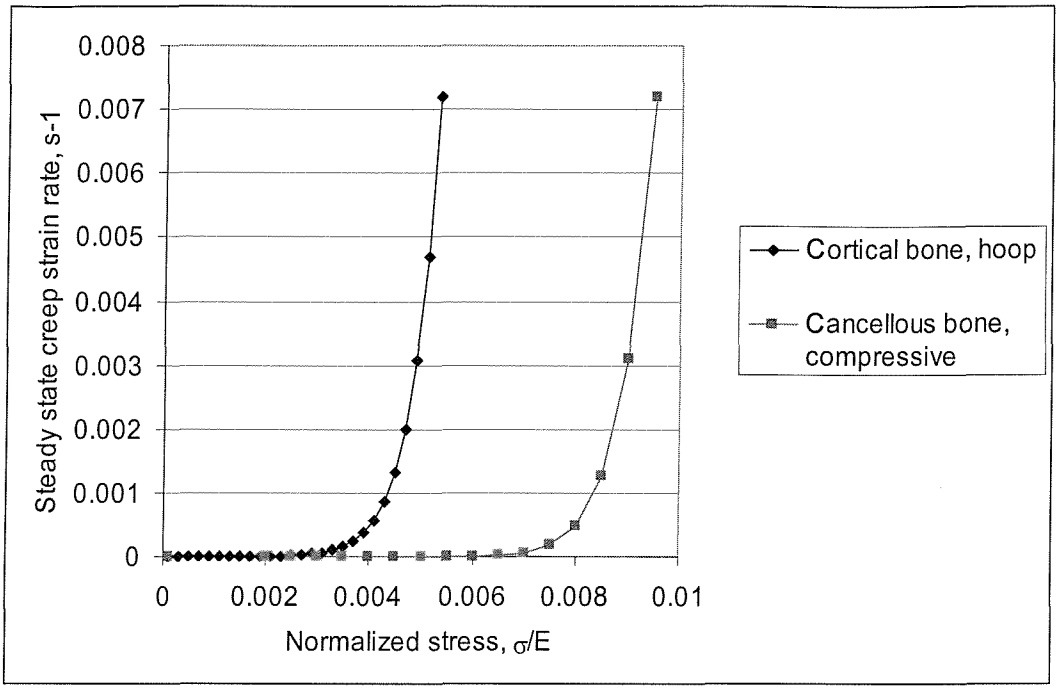

Figure 8.2 Plot of steady state creep strain rate against normalized stress. The cortical bone curve was obtained from hoop creep test of human cortical bone [Brown *et al.*, 2001; Brown *et al.*, 2002]. The cancellous bone curve was obtained from compression creep test of bovine cancellous bone [Bowman *et al.*, 1998].

In this study, the relationship between steady state creep strain rate $d\varepsilon/dt$ and normalised stress σ/E obtained from creep tests on bovine cancellous bone and human cortical bone was implemented [Bowman *et al.*, 1998; Brown *et al.*, 2001; Brown *et al.*, 2002], as shown in Figure 8.2. The relationship between steady state creep strain rate and normalized stress for human cancellous bone is unavailable in the literature. For bovine cancellous bone, only compressive creep test data is available [Bowman *et al.*, 1998]. The relationship between steady state creep strain rate and normalized stress for human cortical bone is only available from a hoop creep test [Brown *et al.*, 2001; Brown *et al.*, 2002]. In this test, a hollow cylinder of human cortical bone from the femur is internally pressurized and the circumferential hoop strain was measured for different locations on the surface of the cylinder. Similar relationships have not been reported for tensile and compressive creep of cortical bone.

The cancellous bone creep relationship was implemented at a body temperature of 310 °K (37 °C) and shown below [Bowman *et al.*, 1998] :-

$$\frac{d\varepsilon}{dt} = 2.1051\times10^{29}(\frac{\sigma}{E})^{15.56} \text{ ---------- Equation 8.1}$$

The cortical bone creep relationship obtained at 310 °K is shown below [Brown *et al.*, 2002]:-

$$\frac{d\varepsilon}{dt} = 9.02\times10^{-8}e^{2129.2(\frac{\sigma}{E})} \text{ ---------- Equation 8.2}$$

In Figure 8.2, the compressive creep strain rate of bovine cancellous bone is lower than the hoop creep of human cortical bone for the same normalized stress. To achieve a creep strain rate of 10 $\mu\varepsilon s^{-1}$, a normalized stress of 0.0062 is required for bovine cancellous bone whereas a normalized hoop stress of is 0.0022 is required for human cortical bone. Fondrk *et al.* (1988) reported similar creep strain rate from a tensile creep test of human cortical bone and reported that the stress to produce this creep strain rate is 73 MPa. The measured elastic modulus of the human cortical bone in Fondrk's et al. (1988) study was 13.1 GPa. The normalized stress is therefore 0.0055, which is higher than the normalized stress needed to produce similar creep strain rate in hoop creep test of human cortical bone. Therefore, the creep strain rate relationship of the bovine cancellous bone (Equation 8.1) can be considered as the upper bound and the creep strain relationship of the human cortical bone can be considered as the lower bound (Equation 8.2).

Two sets of analyses were performed with different creep conditions. The first set modelled the creep of cortical and cancellous bones with Equation 8.1 as the upper bound condition because of the lower creep strain rate at a given normalized stress in comparison to Equation 8.2. The second set of analyses modelled the creep of cortical bone with Equation 8.2 and cancellous bone with Equation 8.1 as a lower bound condition.

Creep behaviour in MARC 2001 is based on a von Mises creep potential with isotropic behaviour (MARC user's manual Volume A). Creep strain changes occur in the direction of outward normal to the current von Mises stress surface. Normalized stress is treated as the ratio of the current total equivalent stress and the Young's modulus of the bone.

Tissue	Author	Load[a]	Regression[b]	r^2	Q[c]
Human cortical bone	Caler and Carter, 1989	Tens.	$t_f = 1.45\times10^{-36}(\frac{\sigma}{E})^{-15.81}$	0.95	
		Comp.	$t_f = 4.07\times10^{-37}(\frac{\sigma}{E})^{-17.76}$	0.87	
	Brown *et al.*, 2002	Hoop	$t_f = 7.52\times10^{-36}(\frac{\sigma_H}{E_H})^{-13.64}$	0.71	
Bovine cortical bone	Fondrk *et al.*, 1988[d]	Tens.	$\frac{d\varepsilon}{dt} = 3.38\times10^{38}(\frac{\sigma}{E})^{18.9}$	0.56	
	Mauch *et al.*, 1992	Tens.	$t_f = 2.51\times10^{-35}(\frac{\sigma}{E})^{-16.7}$	0.51	
	Rimnac *et al.*, 1993	Tens.	$\frac{d\varepsilon}{dt} \approx e^{(\frac{-5330}{T})}$	0.41	44
			$t_f = 0.0042(\frac{d\varepsilon}{dt})^{-1.03}$ [e]	0.87	
Bovine cancellous bone	Bowman *et al.*, 1998	Comp.	$\frac{d\varepsilon}{dt} = 1.99\times10^{52}(\frac{\sigma}{E})^{15.6}e^{(\frac{-16400}{T})}$	0.84	136
			$t_f = 9.94\times10^{-53}(\frac{\sigma}{E})^{-15.1}e^{(\frac{15600}{T})}$	0.85	
			$t_f = 0.0218(\frac{d\varepsilon}{dt})^{-0.99}$	0.99	
Demineralised cortical bone	Bowman *et al.*, 1999	Tens.[f]	$\frac{d\varepsilon}{dt} = 6.74\times10^{12}(\frac{\sigma}{E})^{15.5}$	0.84	
			$t_f = 2.56\times10^{-15}(\frac{\sigma}{E})^{-15.6}$	0.79	
			$t_f = 0.0233(\frac{d\varepsilon}{dt})^{-0.99}$	0.92	
		Tens.[g]	$\frac{d\varepsilon}{dt} \approx e^{(\frac{-13600}{T})}$	0.91	113
			$t_f = 0.0059(\frac{d\varepsilon}{dt})^{-1.00}$	0.99	
		Tens.[h]	$t_f = 0.0293(\frac{d\varepsilon}{dt})^{-0.91}$	0.93	

[a] Tens.: Tensile; Comp.: Compression.
[b] units of dε/dt (steady state creep), t_f(time to failure), T (temperature) are s^{-1}, s and °K.
[c] Unit of Q (creep activation energy) is kJ/Mole.
[d] Bovine cortical bone modulus E of 23 GPa was assumed to manipulate Fondrk *et al.* (1988) original regression into the form presented here.
[e] Best-fit regression of the data presented in Rimnac *et al.* (1993) manuscript.
[f] Specimen from humeri. Creep test (21C).
[g] Specimen from tibiae. Creep activation energy test.
[h] Pooled data from humeri and tibiae.

Table 8.1 Review of creep relationships for human and bovine bone. Adapted from Bowman *et al.* (1999). However, human cancellous bone creep data is unavailable.

8.2.3 Elastic properties of bone and stem

Young's moduli of the cortical and cancellous bones were assumed to be 16000 MPa [Harrigan and Harris, 1991] and 500 MPa [Biegler *et al.*, 1995] respectively. The Young's modulus of the titanium alloy stem was assumed to be 116 000 MPa. Poisson ratio was assumed to be 0.3 for both bone and stem.

Both cortical and cancellous bones were assumed to yield at 1.0% strain and assumed to have perfectly plastic post-yield behaviour. Thus, the corresponding yield stresses of cortical and cancellous bone were 160 and 5 MPa respectively. Bone was not assumed to be linear elastic because it is unreasonable to assume that interface cancellous bone will not deformed plastically if the interference-fit is high. In Chapter 7, it has been explained that cancellous bone reaches the ultimate strain at about 1 and 1.5% strain in uniaxial test. With creep exponent of 15.56, the creep strain rate increases rapidly and the creep strain rate in equation 8.1 is about 8.77 εs^{-1} at 1.5% strain. Creep will quickly reduce the elastic stress. The creep test in Bowman *et al.* (1998) has also been performed within a strain range of 0.4 and 1% strain. It is therefore reasonable to assume bone to yield at 1% strain.

To study the effect of material properties on micromotions in models with an interference-fit, the stiffness of cortical and cancellous bone were reduced. Cancellous bone stiffness was reduced by 40% to 300 MPa. Stiffness of cortical bone was reduced by 20 and 40% to 12800 and 9600 MPa respectively. The yield strain remained as 1% and the yield stress adjusted accordingly. The reduction of stiffness of bone has been explained in detail in Chapter 5.

8.2.4 Boundary conditions and loads

Fourteen different analyses were performed with the boundary conditions shown in Table 8.2. Models In-0.05(0-Cr), In-0.03(0-Cr), In-0.01(0-Cr) and In-0(0-Cr) simulated the different degree of interference-fit of 0.05, 0.03, 0.01 and 0 mm. Creep is not simulated in these models (therefore 0-Cr) and they represented the condition at day 0. Models In-0.05(1-Cr), In-0.03(1-Cr), In-0.01(1-Cr) simulated creep using the upper bound condition (identical creep relationship for cortical and cancellous bone) as explained in Section 8.2.2. Models In-0.05(2-Cr), In-0.03(2-Cr) and In-0.01(2-Cr) simulated the lower bound conditions using different creep relationships for cortical and cancellous bone (2-Cr), as explained in Section 8.2.2. All the models in this paragraph have normal bone quality.

Models In-0.05(1-Cr)+40TB-0CB, In-0.05(1-Cr)+40TB-20CB and In-0.05(1-Cr)+40TB-40CB are models with cancellous bone modulus reduced by 40% (40TB) and cortical bone modulus reduced by 0, 20 and 40% (0CB, 20CB, 40CB) respectively. These models have an interference-fit of 0.05 mm. Model In-0.03(1-Cr)+40TB-0CB has interference-fit of 0.03 mm and

cancellous and cortical bones moduli reduced by 40 and 0% respectively. The models in this paragraph were simulated with the upper bound creep condition.

The implementation of the interference-fit in MARC2001 has been explained in Chapter 6. The friction coefficient between the bone and stem surfaces was 0.6, assuming contact between porous-coated stem and bone [Shirazi-adl *et al.*, 1993]. This friction condition has been used in the anatomical model used in previous chapters.

Bone quality, MPa	***Creep***	***Interference-fit, mm***			
		0.05	0.03	0.01	0
CB = 16000 TB = 500	1 creep law	In-0.05(1-Cr)	In-0.03(1-Cr)	In-0.01(1-Cr)	
	2 creep law	In-0.05(2-Cr)	In-0.03(2-Cr)	In-0.01(2-Cr)	
	No creep law	In-0.05(0-Cr)	In-0.03(0-Cr)	In-0.01(0-Cr)	In-0(0-Cr)
CB = 16000 TB = 300	1 creep law	In-0.05(1-Cr)+40TB-0CB	In-0.03(1-Cr)+40TB-0CB	-	-
CB = 12800 TB = 300	1 creep law	In-0.05(1-Cr)+40TB-20CB	-	-	-
CB = 9600 TB = 300	1 creep law	In-0.05(1-Cr)+40TB-40CB	-	-	-

CB = cortical bone, TB = cancellous bone
1-Cr = upper bound creep condition
0-Cr = creep was not simulated
2-Cr = lower bound creep condition

Table 8.2 Analyses with different interference-fit, creep condition and bone qualities.

The loadsteps (Figure 8.3) are similar to the study performed in Chapter 6. The first loadstep involves the simulation of the interference-fit. The second loadstep removes the axial stem constraint to allow elastic springback of the stem to occur. The third loadstep modelled the creep of bone. The simulated time frame was 28 days. In the fourth loadstep, the axial force of 3000 N was applied [Huiskes, 1990]. A load of 1500 N, similar in magnitude to the load described in Section 4.2.4 was initially applied. However, the load does not show clearly the differences in micromotion between different models. Therefore, a higher load of 3000 N was later used. In models In-0.05(0-CR), In-0.03(0-CR), and In-0.01(0-CR), the third loadstep was omitted because creep was not simulated.

It was discussed in the Introduction that bone ingrowth may take about 8 weeks to occur. The creep of bone should therefore be simulated for a period of 56 days to study if interference-fit can be maintain for this period of time. It is found that the differences in stress in the models between 14 and 28 days were small, as shown in the results in Section 8.3.1.3. Therefore between 28 and 56 days, the stress changes are not expected to be high. The stress relaxation simulation was therefore stopped after 28 days, and this is deemed a reasonable simulation time frame to study the effectiveness of interference-fit up to the point of bone ingrowth.

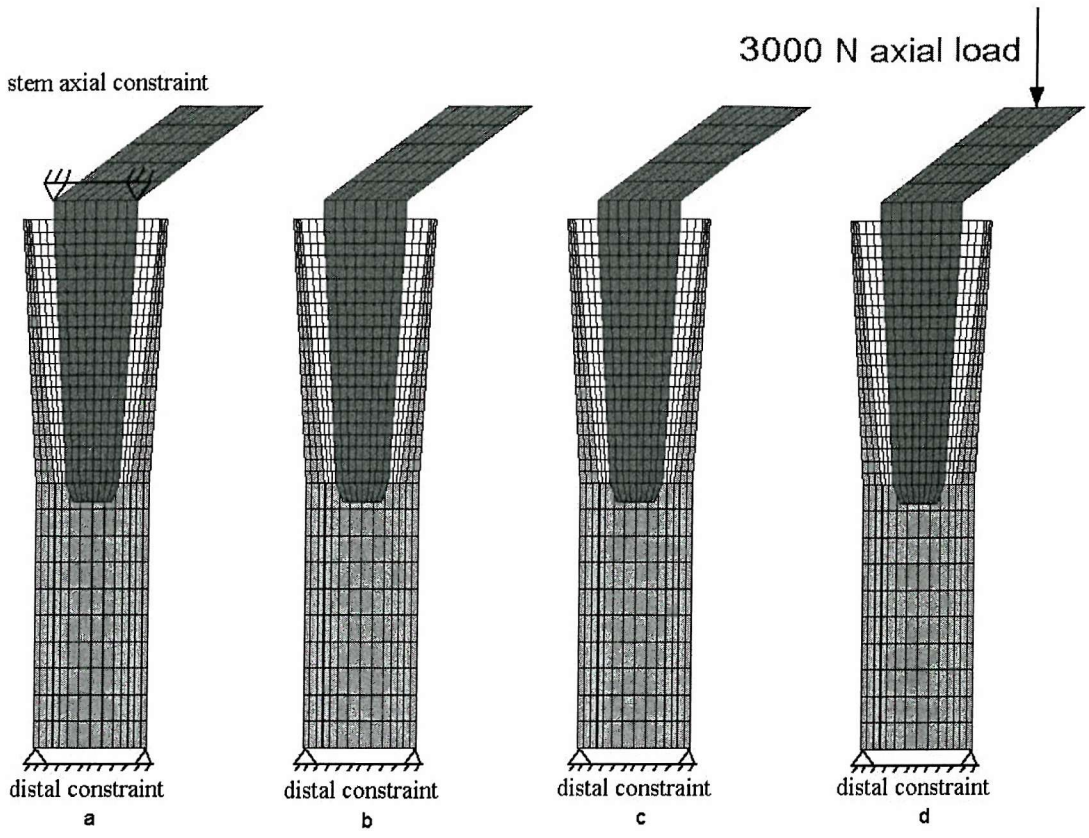

Figure 8.3 From left to right: (a) Interference-fit modelled (b) axial constraint removed for elastic springback (c) 28 days of simulated creep (d) axial load of 3000 N applied.

8.2.5 Mesh refinement study

The model was meshed in three different mesh sizes using an eight-node brick element (element 7) giving 3960, 4760 and 5560 elements (Figure 8.4) and are referred to as Mesh 1, Mesh 2 and Mesh 3. The mesh density differs only at the levels between the region of contact between the stem and the femur. A mesh refinement study was performed to ensure convergence in the model. Values of von Mises stress and micromotion were compared. Stress was compared because the effective interference-fit should be a related to the stress instead of the strain. Conditions for model In-0.05(1-Cr) was simulated for this convergence study. The four loadsteps described previously was simulated. The von Mises stresses reported for the convergence study was from the mid-medial endosteal and periosteal bone, at day 0 and 28 (Figure 8.4). The peak medial and lateral micromotions were compared at day 28. The medial micromotion was highest at the distal node while the lateral micromotion was highest at the proximal node.

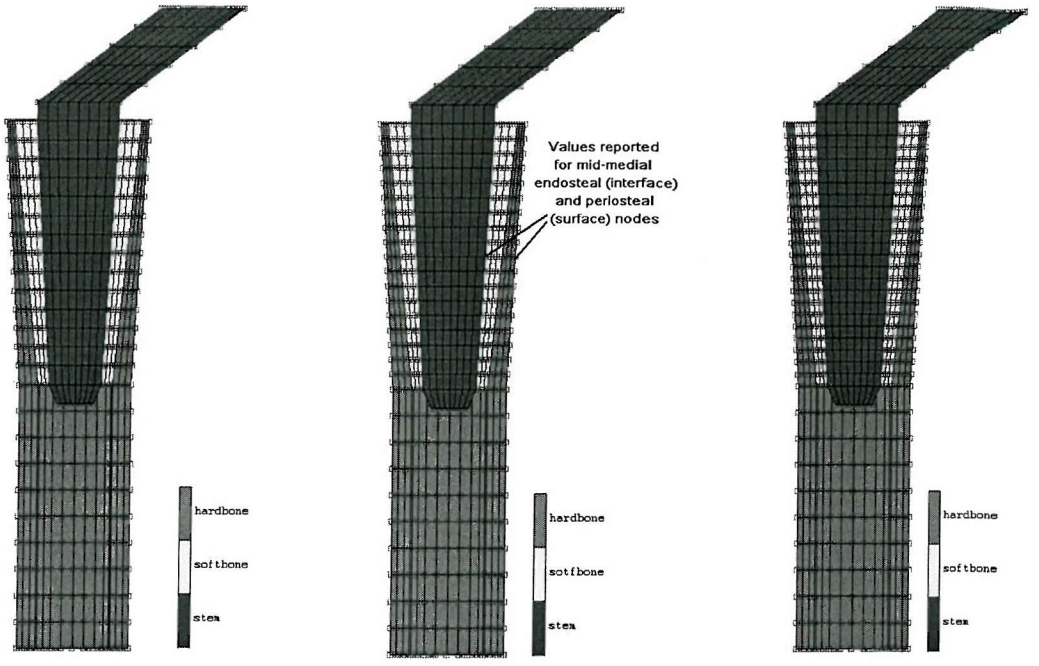

Figure 8.4 From left to right: Mesh 1, Mesh 2 and Mesh 3. The models from left to right have 3960, 4760 and 5560 elements respectively. The periosteal and endosteal stress were compared at the mid-medial nodes. Maximum micromotion at the medial and lateral side were compared.

8.2.5.1 Maximum micromotion and von Mises stress

The relative difference (error) of the peak medial and lateral micromotion between the coarser meshes (Mesh 1 and Mesh 2) and Mesh 3 is shown in Table 8.3. The percentage error of the peak medial micromotion is 7.86% and 1.87% for Mesh 1 and Mesh 2 respectively, and this shows convergence relative to Mesh 3. The respective absolute error is 4.55 and 1.07 μm respectively. The difference of peak medial micromotion between Mesh 2 and Mesh 3 is therefore quite small. The percentage error of the peak lateral micromotion is 41.97 and 7.17% for Mesh 1 and Mesh 2 and this shows convergence relative to Mesh 3. Although the lateral micromotion has a higher percentage difference between Mesh 2 and Mesh 3 than the medial micromotion, the absolute difference is only 1.25 μm.

	Error of peak micromotion, % (absolute, μm)	
	Mesh 1	**Mesh 2**
Medial	7.86 (4.55)	1.87 (1.07)
Lateral	41.97 (6.81)	7.17 (1.25)

Table 8.3 The relative and absolute difference of the maximum micromotion relative to Mesh 3.

The von Mises stresses at the midnodes on the endosteal and periosteal surfaces of Mesh 2 are shown to converge relative to Mesh 3 (Table 8.4). Before creep (day 0), the relative difference at the endosteal and periosteal bone between Mesh 2 and Mesh 3 are 2.97 and 3.26% respectively. At day 28 after stress relaxation, the endosteal and periosteal relative difference are 0.23 and 2.04 % respectively. The relative difference is therefore small between Mesh 2 and Mesh 3. The stress

convergence is achieved with Mesh 2 and Mesh 3. Mesh 3 was used for all the analyses in this study since it has been shown that both the micromotion and stress converged with this mesh size.

	Error of von Mises stress before stress relaxation and after stress relaxation, % (absolute, MPa)			
	Mesh 1		**Mesh 2**	
Time, day	0	28	0	28
Endosteal	17.2 (0.81)	0.07 (0.001)	2.97 (0.14)	0.23 (0.003)
Periosteal	3.86 (0.46)	7.38 (0.71)	3.26 (0.38)	2.04 (0.20)

Table 8.4 The relative and absolute difference of the von Mises stresses at the midnodes on the endosteal and periosteal surface of the femur between either Mesh 1 or 2 with Mesh 3. The von Mises at day 0 (before stress relaxation) and day 28 (after stress relaxation) shows convergence for mesh finer than Mesh 2.

8.3 Results

8.3.1 Comparing the micromotions, stresses and strains for the models with normal bone at day 0 and day 28

8.3.1.1 General micromotion distribution at day 0 and day 28 for different interference-fit models

The medial and lateral micromotion distributions at day 0 are shown in Figure 8.5. Generally, models with higher interference-fit have lower micromotions. Models with interference-fit of 0.05 and 0.03 mm have significantly lower micromotion distribution than the 0.01 mm interference-fit models. The peak micromotions of all the interference-fit models are 3 to 8 times lower than the model without interference-fit.

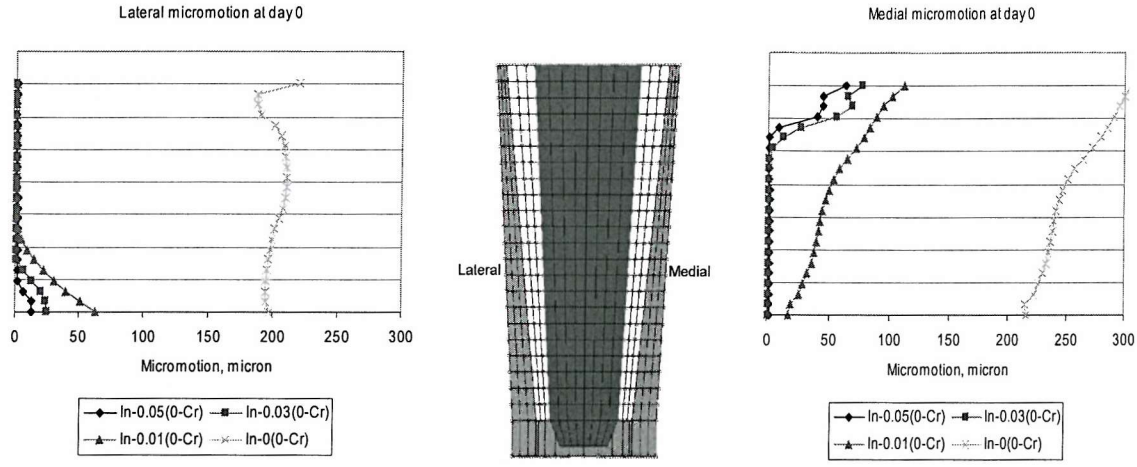

Figure 8.5 Medial and lateral micromotions at day 0 for models with different degree of interference-fit.

Generally, at day 28, the micromotions are higher because of bone creep. In Figure 8.6, the medial and lateral micromotions of model In-0.05(0-Cr) are compared with model In-0.05(1-Cr) and In-0.05(2-Cr). The medial and lateral micromotions are lowest in model In-0.05(0-Cr). On both the medial and lateral sides, model In-0.05(1-Cr) has slightly higher micromotion distributions than model In-0.05(0-Cr). In comparison, the micromotion distributions of model In-0.05(2-Cr) are much higher than model In-0.05(0-Cr) on both sides. The different creep laws used in models In-0.05(1-Cr) and In-0.05(2-Cr) has resulted in significantly different amount of stress relaxation, as will be discuss in later sections, and has a significant effect on the predicted micromotions.

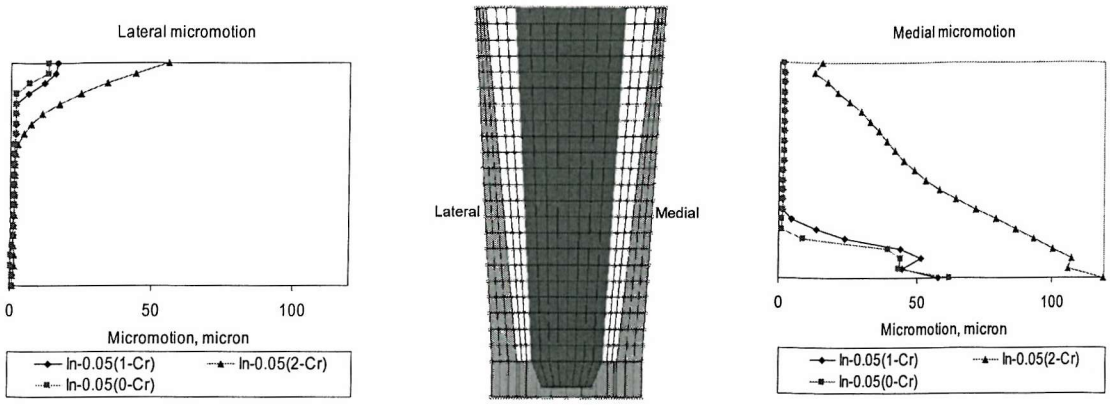

Figure 8.6 Medial and lateral micromotion of the models with interference-fit of 0.05 mm. Micromotions for model In-0.05(0-Cr) are at day 0, and for models In-0.05(1-Cr) and In-0.05(2-Cr) are at day 28.

8.3.1.2 Comparing micromotions at day 28 for different degrees of interference-fit

Bone creep was simulated for 28 days and the medial and lateral micromotions for models with various degrees of interference-fit are shown in Figure 8.7. The mean and peak micromotions for the models that simulated creep with one creep law for bone and models that simulated creep with separate creep law for cortical and cancellous bone are compared. Similar to day 0, at 28 day, the micromotions are lower for the models with higher interference-fits, provided these models have the same creep laws.

For models In-0.05(1-Cr), In-0.03(1-Cr) and In-0.01(1-Cr) shown in Figure 8.7, bone creep is simulated with a creep law obtained from uniaxial compressive test of bovine cancellous bone [Bowman *et al.*, 1998]. A moderate interference-fit of 0.01 mm (model In-0.01(1-Cr)) reduces the peak lateral and medial micromotion by 70% and 64% respectively, in comparison to model In-0(0-Cr). A greater reduction in peak micromotion is achieved with a higher interference-fit. As shown in model In-0.05(1-Cr), the peak lateral and medial micromotion were reduced by 92% and 81% respectively, in comparison to model In-0(0-Cr). Comparing the micromotion distributions of models In-0.05(1-Cr), In-0.03(1-Cr) and In-0.01(1-Cr) at day 28 and their distributions at day 0, the micromotions at day 28 are slightly higher. The effect of the creep model on the predicted micromotion is not very significant. The significant reduction in micromotion with a moderate interference-fit is consistent with the prediction of the anatomical model in Chapter 6. This creep model suggests that initial stability of the stem can be improved by a higher interference-fit.

For models In-0.05(2-Cr), In-0.03(2-Cr) and In-0.01(2-Cr) shown in Figure 8.7, the creep law used to simulated cortical bone creep is different from models In-0.05(1-Cr), In-0.03(1-Cr) and In-0.01(1-Cr). As explained in Section 8.2.2, cortical bone creep for the former models is expected to be higher than the latter models. In comparison to model In-0(0-Cr), model In-0.01(2-Cr) predicted a reduction of peak lateral and medial micromotion by 63 and 56% respectively. In comparison to model In-0.01(1-Cr), model In-0.01(2-Cr) has slightly higher peak lateral and

medial micromotion. However, models In-0.05(2-Cr) and In-0.03(2-Cr) have much higher peak lateral and medial micromotion in comparison to models In-0.05(1-Cr) and In-0.03(1-Cr). In fact, the micromotions for models In-0.05(2-Cr) and In-0.03(2-Cr) are only slightly lower than model In-0.01(2-Cr). In comparison to model In-0(0-Cr), the peak lateral micromotion was reduced by 73 and 71% for model In-0.05(2-Cr) and model In-0.03(2-Cr) respectively. The peak medial micromotion was reduced by 60% for both models. Comparing models In-0.05(2-Cr) and In-0.03(2-Cr) with model In-0.01(2-Cr), the reduction of peak lateral and medial micromotion is only about 10 and 4% more. Therefore, models In-0.05(2-Cr), In-0.03(2-Cr) and In-0.01(2-Cr) predict that a higher interference-fit does not improve the stem stability significantly, and shows that creep could affect the effective interference-fit significantly.

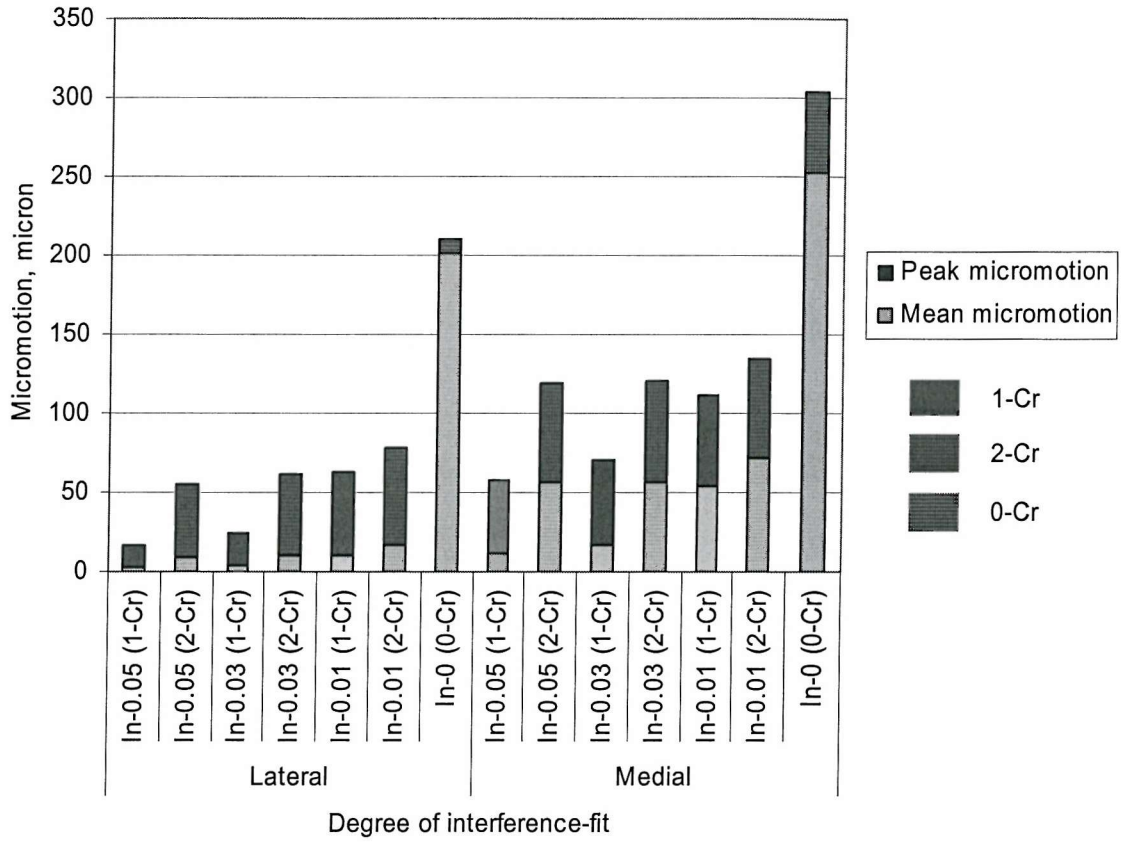

Figure 8.7 Medial and lateral micromotions for models with different degree of interference-fit after 28 days. Models with identical interference-fit but simulated with different creep laws are shown side by side.

8.3.1.3 Comparing midmedial endosteal, periosteal stresses and equivalent creep strain in different interference-fit models at day 0 and day 28

Figure 8.8 shows the typical stress relaxation curves at the medial endosteal and periosteal midnodes of model In-0.05(1-Cr). Stress relaxation curves of other models are similar and therefore not shown. Generally in all the models, the endosteal node has a lower stress than periosteal node. Rapid stress relaxation in the first day can be seen in all models. Subsequently, the stress relaxation in the models was minimal.

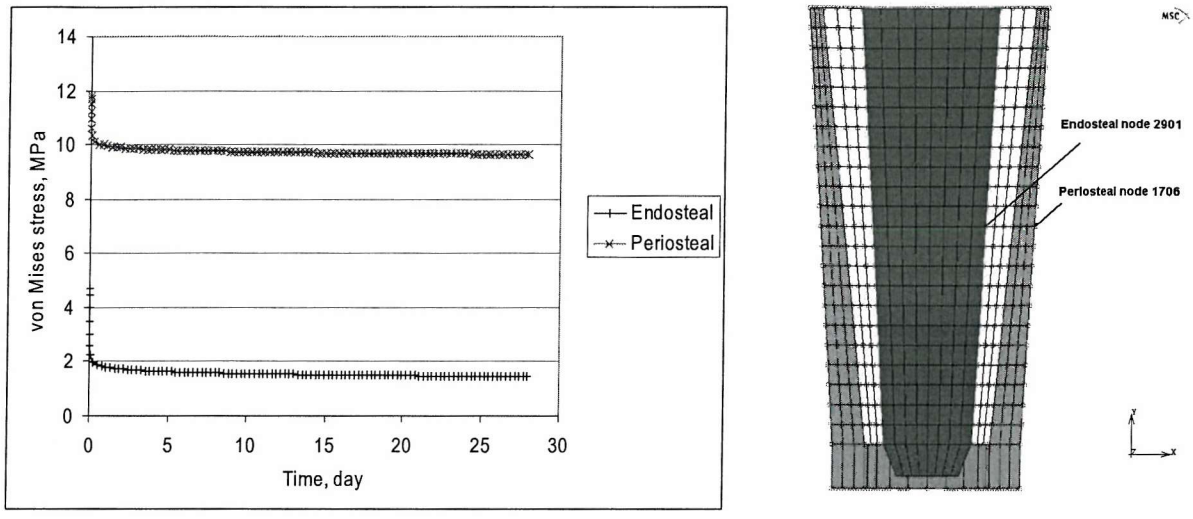

Figure 8.8 Endosteal and periosteal stress relaxation of model In-0.05(1-Cr). The values at the medial midnodes are shown here. The stress relaxation curves shown here is typical for other models as well.

The endosteal von Mises stresses of models In-0.05(1-Cr), In-0.03(1-Cr) and In-0.01(1-Cr) at day 0 and day 28 are shown in Figure 8.9. At day 0, higher stresses are seen in models with higher degree of interference-fit. However, because of creep, the endosteal stresses of model In-0.05(1-Cr) and In-0.03(1-Cr) are similar at about 1.5 MPa after 28 days. The initial endosteal stresses of models In-0.05(1-Cr) and In-0.03(1-Cr) reduced by 69 and 55% after 28 days. The endosteal stress of model In-0.01(1-Cr) did not change over the similar period due to the low initial endosteal stresses, which were below the creep threshold. For models In-0.05(1-Cr) and In-0.03(1-Cr), most of the stress relaxation in the endosteal bone occurred in the first day (Table 8.5). Between day 14 and 28, the absolute stress relaxation was about 0.07 MPa for both models In-0.05(1-Cr) and In-0.03(1-Cr) (Table 8.5). Subsequent stress relaxation after day 28 is therefore not expected to be high. If stress relaxation after day 28 is assumed to be linear and at the rate between day 14 and 28, the endosteal stress at the midnode will only relax by 0.14 MPa every four weeks. At the least, the final endosteal stress value will be about 1 MPa if simulated time is increased to a few months, similar to the stress in Model In-0.01(1-Cr). Maintaining this residual stress for a few months is vital to maintain stem stability until bone ingrowth has occurred.

Simulated Creep Time, day			0	1	14	28
Endosteal	In-0.05 (1-Cr)	Stress, MPa	4.71	1.81	1.52	1.45
		Percentage change from initial stress, %	0	61.6	67.7	69.2
	In-0.03 (1-Cr)	Stress, MPa	3.26	1.82	1.53	1.46
		Percentage change from initial stress, %	0	44.2	53.1	55.2
Periosteal	In-0.05 (1-Cr)	Stress, MPa	11.80	9.95	9.70	9.64
		Percentage change from initial stress, %	0	15.7	17.8	18.3
	In-0.03 (1-Cr)	Stress, MPa	7.45	6.83	6.60	6.54
		Percentage change from initial stress, %	0	8.3	11.4	12.2

Table 8.5 Stress and percentage drop from initial von Mises stress after 1, 14 and 28 days of simulated stress relaxation at the midnode on the endosteal and periosteal surfaces.

The stresses of the periosteal bone at the medial midnodes for models In-0.05(1-Cr), In-0.03(1-Cr) and In-0.01(1-Cr) are shown in Figure 8.10. At day 0, higher periosteal stresses are seen for models with a higher interference-fit. However, the periosteal cortical bone stresses for models In-0.05(1-Cr) and In-0.03(1-Cr) did not converge to the same value after 28 days, unlike the endosteal stresses. After 28 days, the higher interference-fit models still have higher periosteal stresses. Similar to the endosteal surfaces, most stress relaxation occurred in the first day (Table 8.5). The periosteal stress relaxations for model In-0.05(1-Cr) and In-0.03(1-Cr) are 18 and 12% respectively, and the percentage stress relaxation is lower than in the endosteal cancellous bone. Stress relaxation between day 14 and 28 is 0.5 and 0.8% of initial stress for In-0.05(1-Cr) and In-0.03(1-Cr) respectively (Table 8.5). Subsequent stress relaxation should not be too significant. Stress is lower than the creep threshold in model In-0.01(1-Cr), and therefore no stress relaxation occurred in this model. The periosteal stresses as a result of the interference-fit is not likely to reduce much in subsequent months.

Table 8.6 shows the equivalent creep strain for model In-0.05(1-Cr) and In-0.03(1-Cr). Since the stresses is below creep threshold for model In-0.01(1-Cr), this model has zero creep strain. The periosteal total equivalent creep strains for both models are negligible in comparison to endosteal equivalent total creep strains. Therefore, stress relaxation of the endosteal bone in both models is due to creep of the endosteal cancellous bone. From Figure 8.9, the stress of endosteal cancellous bone almost reached an equilibrium at about 1.5 MPa. The corresponding normalized stress (σ/E) is about 0.003. If the normalized stress in bone is lower than this value, creep will be very slow. Therefore, the creep threshold corresponds to normalized stress of about 0.003. The initial normalized stresses of the periosteal cortical bone are 0.00075 and 0.00047 for model A and B respectively (σ taken from day 0 values from Figure 8.10) and these values are much lower than the creep threshold value. Therefore, the creep is negligible at the periosteal bone and stress relaxation of the periosteal bone is not due to creep, but due to the creeping and deformation of the

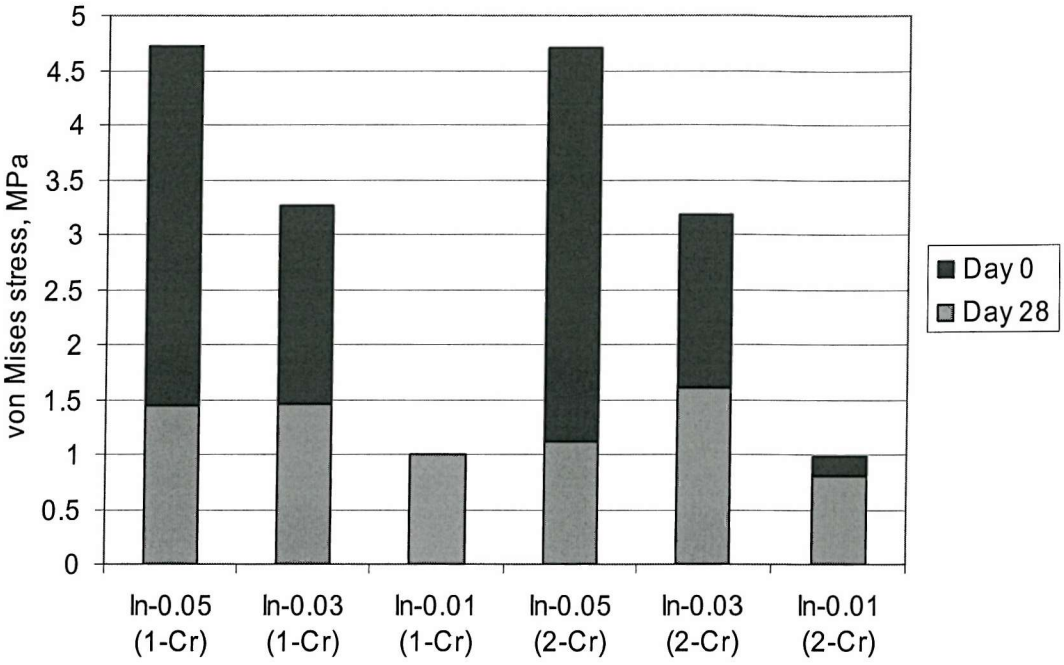

Medial endosteal bone

Figure 8.9 Stresses at day 0 and day 28 of the medial midnodes at the endosteal surface. Models In-0.05(1-Cr), In-0.03(1-Cr) and In-0.01(1-Cr) have a single creep law for cortical and cancellous bone. Models In-0.05(2-Cr), In-0.03(2-Cr) and In-0.01(2-Cr) have different creep laws for cortical and cancellous bone.

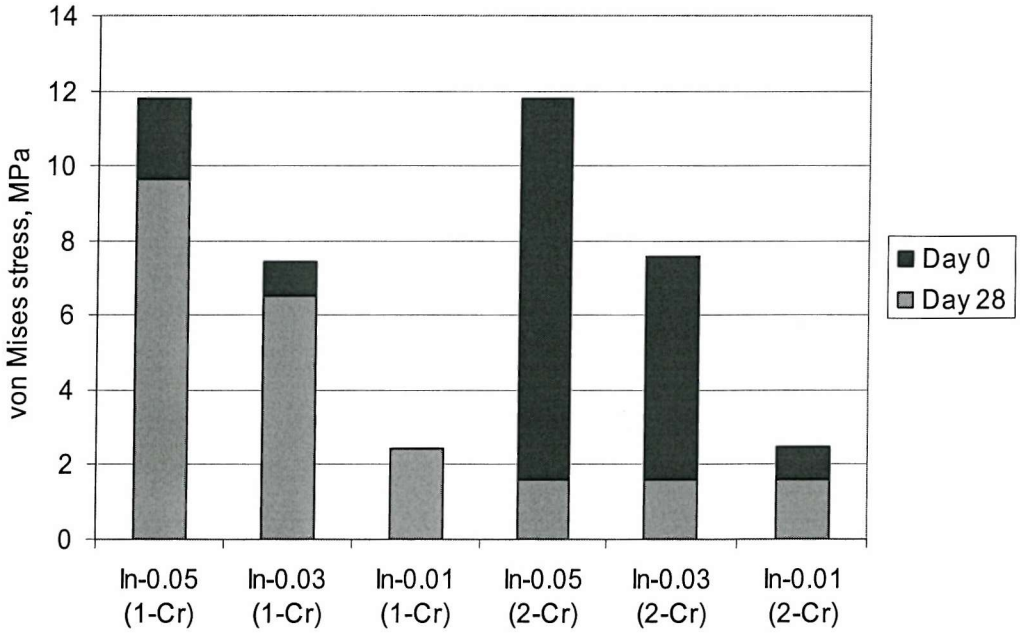

Medial periosteal bone

Figure 8.10 Stresses at day 0 and day 28 of the medial midnodes at the periosteal surface. Models In-0.05(1-Cr), In-0.03(1-Cr) and In-0.01(1-Cr) have a single creep law for cortical and cancellous bone. Models In-0.05(2-Cr), In-0.03(2-Cr) and In-0.01(2-Cr) have different creep laws for cortical and cancellous bone.

endosteal cancellous bone. As a result the periosteal bone stress does not converge to the same value for different degrees of interference-fit.

Model	**In-0.05(1-Cr)**		**In-0.03(1-Cr)**	
Node	Periosteal	Endosteal	Periosteal	Endosteal
Equivalent creep strain, %	6.15×10^{-13}	0.6335	9.74×10^{-16}	0.3713

Table 8.6 Equivalent creep strain at the midnode on the endosteal and periosteal surfaces. Periosteal creep strain is negligible in both model In-0.05(1-Cr) and In-0.03(1-Cr).

In Figure 8.9, the endosteal stresses for models In-0.05(2-Cr), In-0.03(2-Cr) and In-0.01(2-Cr) at day 0 and 28 are also shown. Initial stresses at day 0 in these models were identical to models In-0.05(1-Cr), In-0.03(1-Cr) and In-0.01(1-Cr). However, the endosteal stresses at day 28 are different. Endosteal stress of model In-0.05(2-Cr) at day 28 is 1.1 MPa, which is 0.4 MPa less than model In-0.05(1-Cr). Endosteal stress of model In-0.03(2-Cr) at day 28 is 1.6 MPa, which is similar to both model In-0.05(1-Cr) and In-0.03(1-Cr). Although at the endosteal midnode is higher in model In-0.03(2-Cr) than model In-0.05(2-Cr) due to slightly different stress redistribution in both models, generally femoral stress is higher in model In-0.05(2-Cr). The overall endosteal stress distribution are slightly lower for models In-0.05(2-Cr) and In-0.03(2-Cr) in comparison to models In-0.05(1-Cr) and In-0.03(1-Cr), for comparison between models with the same degree of interference-fit. Endosteal stress of In-0.01(2-Cr) reduced by 0.18 MPa after 28 days, but model In-0.01(1-Cr) did not creep at all. Similarly, creep in models In-0.05(2-Cr), In-0.03(2-Cr) and In-0.01(2-Cr) occurred mostly in the first day. Stresses also did not change significantly between day 14 and day 28. Therefore, residual endosteal stresses could be maintained for periods long enough for bone ingrowth to occur.

The stresses of the periosteal bone at the medial midnodes for models In-0.05(2-Cr), In-0.03(2-Cr) and In-0.01(2-Cr) are also shown in Figure 8.10. At day 28, periosteal stresses are much lower for models In-0.05(2-Cr) and In-0.03(2-Cr) than models In-0.05(1-Cr) and In-0.03(1-Cr) respectively. Periosteal stress for model In-0.01(2-Cr) is slightly lower than model In-0.01(1-Cr). Compared to the initial periosteal stresses, the periosteal stresses for models In-0.05(2-Cr), In-0.03(2-Cr) and In-0.01(2-Cr) reduced by 86, 79 and 35% respectively after 28 days. The residual stresses are similar for these three models and the stresses are about 1.6 MPa. This is almost the same as found in the cancellous bone stresses. The stresses for these models after 28 days are stable. Therefore, the creep model of cortical bone based on data from circumferential creep test of human cortical bone suggests that cortical bone cannot support high transverse residual stress. Even a moderate interference-fit of 0.01 mm can cause stress relaxation in model In-0.01(2-Cr). Similar to models In-0.05(1-Cr) and In-0.03(1-Cr), stress relaxation occurred mostly in the first day. No significant changes are expected to occur after 28 days.

Table 8.7 shows the endosteal and periosteal equivalent creep strain for models In-0.05(2-Cr), In-0.03(2-Cr) and In-0.01(2-Cr). The periosteal equivalent creep strains for models In-0.05(2-Cr), In-0.03(2-Cr) and In-0.01(2-Cr) are about 0.21, 0.08 and 0.02%, which in comparison to the periosteal creep strain for model In-0.05(1-Cr) and In-0.03(1-Cr) (Table 8.6) are significantly higher. The endosteal equivalent creep strains for models In-0.05(2-Cr) and In-0.03(2-Cr) are lower than models In-0.05(1-Cr) and In-0.03(1-Cr), although the endosteal stress relaxations were greater in model In-0.05(2-Cr) and similar in model In-0.03(2-Cr). The periosteal radius of models In-0.05(2-Cr) and In-0.03(2-Cr) was found to increase by 14 and 9 μm after stress relaxation. As a result of this, the cortical cancellous bone interface also expanded. In contrast, periosteal radius of models In-0.05(1-Cr) and In-0.03(1-Cr) shrunk by 2 and 1 μm. In models In-0.05(2-Cr) and In-0.03(2-Cr), a part of the cancellous bone stresses relaxed due to creep deformation of cortical bone, which results in expansion of cortical cancellous bone interface. Therefore, the endosteal equivalent creep strains in models In-0.05(2-Cr) and In-0.03(2-Cr) are less than in models In-0.05(1-Cr) and In-0.03(1-Cr). The greater expansion of the periosteal bone of models In-0.05(2-Cr) and In-0.03(2-Cr) also causes lower residual endosteal stress in the former in comparison with the latter. The periosteal cortical bone reaches equilibrium at about 1.6 MPa, which corresponds to a normalized stress of 0.0001. Due to this very low creep threshold, the effective interference-fit that can be supported by models In-0.05(2-Cr), In-0.03(2-Cr) and In-0.01(2-Cr) is very small. This explains the higher micromotion for models In-0.05(2-Cr) and In-0.03(2-Cr) in comparison to models In-0.05(1-Cr) and In-0.03(1-Cr).

Model	**In-0.05 (2-Cr)**		**In-0.03 (2-Cr)**		**In-0.01 (2-Cr)**	
Node	**Periosteal**	**Endosteal**	**Periosteal**	**Endosteal**	**Periosteal**	**Endosteal**
Equivalent creep strain, %	0.2094	0.3713	0.0839	0.1185	0.0171	1.37×10^{-7}

Table 8.7 Equivalent creep strain at the midnode on the endosteal and periosteal surfaces. Periosteal creep strain is not negligible in all the models.

8.3.2 Comparing micromotions and stresses at day 0 and 28 in models with same interference-fit but different Young's moduli

8.3.2.1 Micromotion

The effect of bone quality and interference-fit on initial micromotions were examined and Figure 8.11 shows the medial and lateral micromotion in the models with different Young's modulus and interference-fit of 0.05 mm. The micromotions are influenced by the overall stiffness of the femur. Lowest mean micromotions are observed in model In-0.05(1-Cr), which has the highest bone moduli, and model In-0.05(1-Cr)+40TB-40CB which has the lowest bone moduli has the highest mean micromotions. A reduction of cancellous bone Young's modulus by 40%, model In-0.05(1-Cr)+40TB-0CB has doubled the peak lateral micromotion and increased the peak medial micromotion by about two thirds in comparison to model In-0.05(1-Cr). The dependence of micromotions on the overall stiffness of the femur in this study is similar to the results of the anatomical femur model reported in Chapter 5, although interference-fit was not modelled by those models. The medial and axial movement of the stem head is highest in model In-0.05(1-Cr)+40CB-40TB, which has the lowest Young's moduli. Therefore, the greater bending is likely to be the cause of the greater micromotion. However, interference-fit still improved the initial lateral and medial stability of model In-0.05(1-Cr)+40CB-40TB in comparison to model In-0(0-Cr), which has the original stiffness but no interference-fit (Figure 8.7) by 84 and 43% respectively. Poorer bone quality increases micromotions, but with interference-fit, the stem stability in poorer quality bone is improved and the micromotions could be lower than the stem inserted with no interference into better quality bone.

Figure 8.12 compares the micromotions of two models with interference-fits of 0.05 and 0.03 mm, and modulus of cancellous bone reduced by 40% in both models (models In-0.05(1-Cr)+40TB-0CB and In-0.03(1-Cr)+40TB-0CB), with model In-0.03(1-Cr) which has the normal bone modulus. Model In-0.05(1-Cr)+40TB-0CB has lower mean and peak micromotions than model In-0.03(1-Cr)+40TB-0CB. However, model In-0.03(1-Cr) which has lower interference-fit than model In-0.05(1-Cr)+40TB-0CB has the lowest mean and peak micromotions. The lateral and medial peak micromotions of model In-0.05(1-Cr)+40TB-0CB are 46 and 42% higher than model In-0.05(1-Cr)+40TB-0CB. Therefore, stiffness of bone does influence significantly the micromotion of the stem. A higher interference-fit may not be able to compensate the lower stem stability because of poor bone quality.

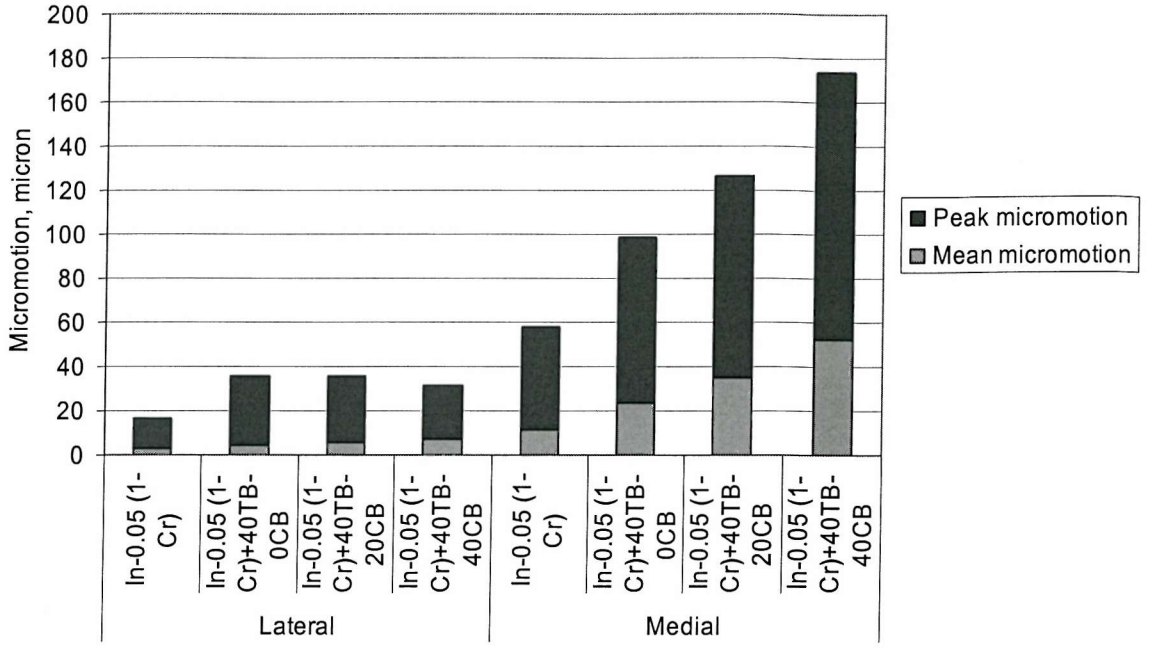

Figure 8.11 Comparing micromotion in models with different material properties. Interference-fit in the models was 0.05 mm.

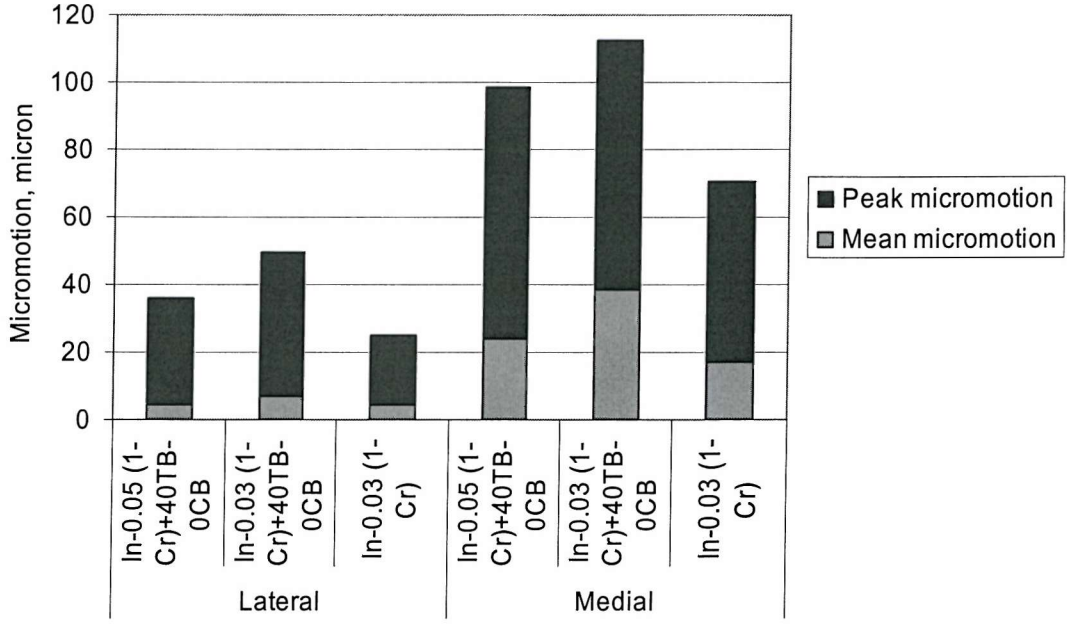

Figure 8.12 Comparing micromotion in models with reduced stiffness and different interference-fit of 0.05 and 0.03 mm, and a model with the normal stiffness and interference-fit of 0.03 mm. Stiffness of cancellous bone was reduced by 60% while stiffness of cortical bone was maintained in model In-0.05(1-Cr)+40TB-0CB and In-0.03B(1-Cr)+40TB-0CB.

8.3.2.2 Endosteal and periosteal stress

The effect of bone quality on bone stress is shown in (Figure 8.13). Generally, lower stress was observed in models with lower bone modulus. The endosteal bone stresses are similar for the models with reduced cancellous bone stiffness regardless of the cortical bone modulus, both before and after stress relaxation. The model with normal bone has the highest endosteal stress on day 28. The periosteal stresses are higher in models with higher cortical bone modulus. The periosteal stresses are slightly higher in model In-0.05(1-Cr)+40TB-20CB and In-0.05(1-Cr)+40TB-0CB in comparison to model In-0.05(1-Cr)+40TB-40CB, which has the lowest cortical bone modulus, at day 0 and 28. The periosteal stresses in all these three models are 30-40% lower in comparison to the model In-0.05(1-Cr), with the normal bone Young's modulus. The lower periosteal stresses could partly explain the higher micromotion in model In-0.05(1-Cr)+40TB-40CB, although bending of the femur could be the more significant contributor to the increase in micromotion.

The comparison between models In-0.03(1-Cr) and In-0.05(1-Cr)+40TB-0CB showed that the micromotion is higher in the latter model even though the interference-fit is higher. However the periosteal stresses for both models are quite similar after stress relaxation (Figure 8.10 and Figure 8.13). The endosteal stresses are lower in model In-0.05(1-Cr)+40TB-0CB and effectively, the residual stress is lower in this model. The medial movement of the stem head is also higher in this model relative to model In-0.03(1-Cr). It is possible as in the comparison of model In-0.05(1-Cr)+40TB-40CB, In-0.05(1-Cr)+40TB-20CB and In-0.05(1-Cr)+40TB-0CB that the combination of lower residual stress and reduced ability to resist bending due to the lower stiffness of bone contributed to higher micromotion in model In-0.05(1-Cr)+40TB-0CB in comparison to model In-0.03(1-Cr).

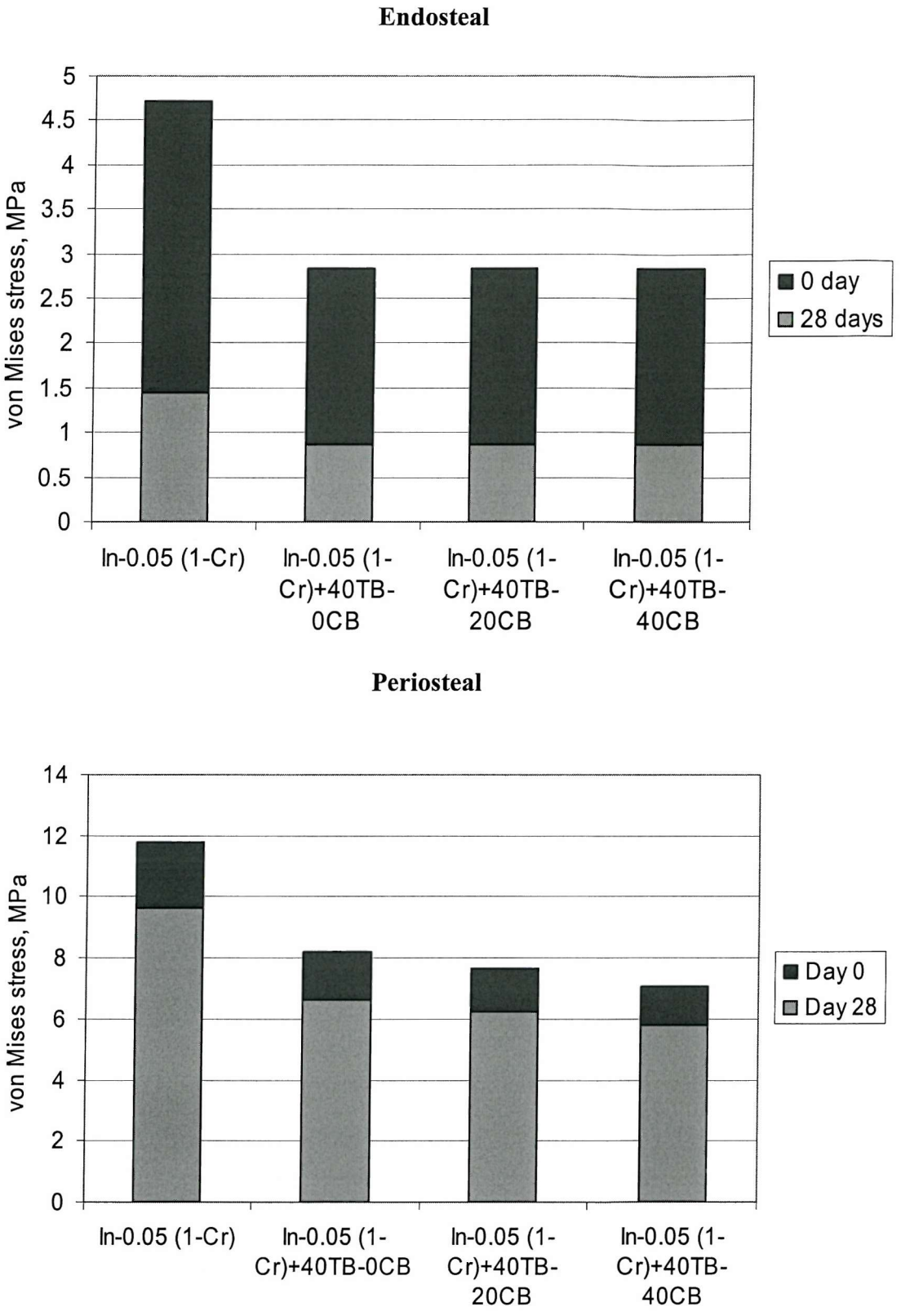

Figure 8.13 Stress relaxation at the endosteal (top) and periosteal (bottom) midnodes in models with different Young's moduli of bones.

8.4 Discussion

In this study, higher micromotion was found in the models that simulated the creep deformation of the bone in an interference-fit assembly in comparison to the models that neglected bone creep. This showed that as a result of creep, a degree of interference-fit is effectively lost and this tended to increase the micromotion of the stem. If the interference-fit models are compared to the model that did not simulate the interference-fit, it is clear that interference-fit can improve considerably the initial stability of the stem, even after creep has occurred. It has been shown that a small effective interference-fit reduces the stem micromotion by more than 50% in this simple model. However, it is only useful if the effective interference-fit in the bone is maintained over sufficiently long period of time to provide stability for the stem until osseointegration has occurred.

The stress relaxation in this study was simulated over a period of 28 days. This study showed that most of the relaxation in bone happens in the first day. Between day 14 and day 28, the changes in overall stresses in the whole femur are quite small. If the simulation time is increased to 8 weeks, even assuming linear loss after day 28, the stresses in the femur are not expected to change significantly. Therefore, assuming that the biological process does not change the interface condition significantly, the residual stress in the bone due to interference-fit is expected to last for at least 8 weeks. This is a meaningful simulation time as bone ingrowth will probably begin to occur after 8 weeks. Direct measurement of the time frame for osseointegration of the stem *in vivo* is not available. However, if the process of osseointegration is similar to fracture healing, after 8 weeks the beginning of formation of woven bone can be expected if suitable mechanical conditions exist [Gardner *et al.*, 2000]. In animal experiments involving rabbits and sheep, bone formation has been reported after a period of 4 and 10 weeks postoperatively [Goodship and Kenwright, 1985; Dhert *et al.*, 1998]. This agrees with clinical observation of the improved clinical result if an interference-fit is introduced during the preparation of the femoral canal [Engh *et al.*, 1990].

In this study, one set of analyses simulated creep using the same creep strain rate relationship for both the cancellous and cortical bones (upper bound condition). The endosteal cancellous bone stresses relaxed to a similar value of approximately 1.5 MPa, if the initial stresses were above this value. This stress value is the creep threshold of cancellous bone. If the interference-fit generates lower interface (endosteal bone) stress than the creep stress threshold, little creep will occur. The similarity of interface stress seems to suggest that different degrees of interference-fit that generate interface stress higher than the creep threshold will relax to the same effective interference-fit. However, the surface stress in the periosteal cortical bone for different degrees of interference-fit do not converge to the same stress as in the endosteal bone. After stress relaxation, the periosteal stress was higher if the degree of interference-fit was higher. The periosteal stress

was below the creep threshold for cortical bone and the stress relaxation of periosteal cortical bone was due to creep deformation of endosteal cancellous bone. Effectively, higher initial interference-fit will also have higher effective interference-fit, if the periosteal cortical stress does not exceed the creep threshold. In this situation where periosteal stress does not exceed the creep threshold, the effect of higher initial interference-fit is lower initial micromotion.

Another set of analyses simulated the creep of cortical and cancellous bone using different creep strain rate relationships for the two types of bones (lower bound condition). The endosteal stress is slightly lower than the models that simulated creep using only one creep law for both cortical and cancellous bone. However, the biggest difference is the significantly higher cortical bone creep deformation that is predicted when human cortical bone hoop creep data was used. As a result of this, the periosteal cortical bone creeps to very low stress of 1.6 MPa in models In-0.05(2-Cr), In-0.03(2-Cr) and In-0.01(2-Cr). In comparison, model In-0.01(1-Cr) has a higher periosteal cortical bone stress of about 2.5 MPa, despite lower interference-fit than model In-0.05(2-Cr) and In-0.03(2-Cr). As a result, the micromotion of models In-0.01(1-Cr), In-0.05(2-Cr) and In-0.03(2-Cr) are quite similar. Simulating bone creep using human cortical bone creep data therefore predicts a much lower effective interference-fit after creep deformation. Therefore, if the creep threshold of the periosteal cortical bone is exceeded, creep will reduce the effective interference-fit to the level where the normalized stress levels are the same as the creep threshold. The creep properties of cortical bone therefore play an important part in determining the effective interference-fit and hence stem micromotion. High cortical bone stresses are vital to maintain a high effective interference-fit.

One of the limitations of this study is the assumption that the creep behaviour of cancellous bone loaded in the hoop and radial direction can be predicted from data obtained from uniaxial compressive creep tests of bovine cancellous bone [Bowman *et al.*, 1998]. The creep strain rate of human cancellous bone may not be the same as bovine bone. Bovine bone has been shown to have higher compressive yield strain and similar tensile yield strain as human bone, and compressive yield strain is higher than tensile yield strain [Kopperdahl and Keaveny, 1998]. If yield strain of bone can be use to predict the creep behaviour of bone, then human cancellous bone will probably have higher compressive creep strain rate and similar tensile creep strain rate under the same normalized stress. The creep threshold could also be lower in human cancellous bone. Therefore, it is possible that the use of compressive creep data of bovine cancellous bone could have underestimated the degree of cancellous bone creep.

The hoop creep data for cortical bone seems to be suitable for this analysis as the loading in this study is mainly in the hoop and radial direction, similar to Brown's *et al.* (2002) experiment. The predicted creep threshold is very small and the simulations with this creep strain rate relationship suggests that cortical bone cannot support much residual hoop stress. Model In-0.05(2-Cr) and In-0.03(2-Cr) predicted that bone would creep extensively in an interference-fit

assembly over a few hours and there is a substantial increase in creep strain (Table 8.7). Brown *et al.* (2002)'s data seems to suggest that creep deformation will occur even at hoop strains as low as 100 με. This is not unreasonable, as stress relaxation at very low shear strain (10 με) has been reported in torsion test of human cortical bone [Lakes *et al.*, 1979].

For the models with 0.05 mm interference-fit, the periosteal cortical bone stress reduced by about 20% for the upper bound creep model and 85% for the model for the lower bound creep model after 28 days. However, no study has reported the stress reduction in an interference-fit assembly between an implant and cortical bone. *In vivo* measurements of axial stress of screws inserted into sheep tibia shaft have shown axial stress reduction with time [Blumlein *et al.*, 1977]. The stress was measured by a loadcell washer under the screw head. Blumbein et al. (1977) observed fast initial drop of axial stress during the first few days, and subsequently, the axial force decreased slowly. At 28 days, the axial stress was measured to have reduced between 30 and 60%, which is between the stress reduction of the upper and lower bound creep models. Bone is loaded differently by a screw than in an interference-fit assembly, but the smaller stress reduction in the screw could suggest that cortical bone can support higher residual stress than the prediction of the lower bound model. Further research will need to be done to verify the creep threshold of cortical bone for an interference-fit assembly and the level of residual stress that can be supported by cortical bone.

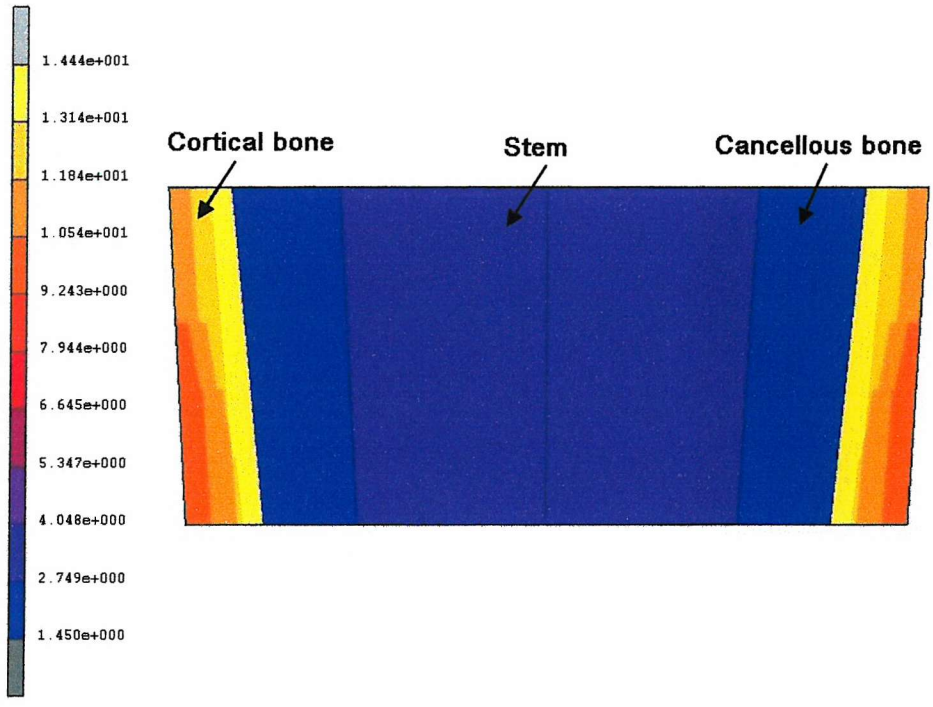

Figure 8.14 von Mises stress at the midsection of model In-0.05(1-Cr) after 28 days of simulated time. Cortical and cancellous bone acted like an elastic band around the stem. In this model, contribution of the cortical bone to the effective interference-fit is more than cancellous bone because of the higher stress supported by the cortical bone.

This study has provided some important insights. In this study, it is shown that higher reduction of micromotion is achieved with higher cortical bone stress, while cancellous bone

stress remains quite similar between different models. However, it is reasonable to assume that the combined residual stresses of cancellous and cortical bone both contribute to the effective interference-fit. Therefore, cortical and cancellous bone act like an elastic band that wrapped around the stem (Figure 8.14). This elastic band supports the stem when it is loaded and reduces micromotion. However, since cortical bone has much higher elastic modulus, it can be loaded at a much higher stress and contributes more to the stability of the stem. The effective interference-fit is greatly influenced by the cortical bone stress that can be maintained after creep deformation of bone. The cortical bone stress that can be maintained depends on the creep threshold. Below the creep threshold, cortical bone stress will increase with the degree of interference-fit as shown in models In-0.05(1-Cr), In-0.03(1-Cr) and In-0.01(1-Cr). However, above the creep threshold, further increase in interference-fit will not increase the cortical bone stress anymore, once creep has occurred as the bone stress will tend to relax to the creep threshold, as in models In-0.05(2-Cr) and In-0.03(2-Cr). Therefore, to ensure the maximum effective interference-fit, the cortical bone should be loaded to just above the creep threshold.

In this study, the effect of bone quality on the initial micromotion of the stem inserted with interference-fit was investigated. Reduction of bone quality was found to increase the micromotion of the stem significantly. This result is in agreement with the results in Chapter 5. However, the micromotion of the stem inserted into the femur with the poorest bone quality simulated in this study was still lower than the normal femur without interference-fit. Therefore, interference-fit still plays an important role in reducing stem micromotion regardless of the bone quality. The reduction of bone quality can probably be explained as a combination of reduced residual stress of the interference-fit assembly and lower resistance of the femur to bending. If bone quality is really poor, it is possible that the effect of poor bone quality cannot be compensated by improved stability due to the interference-fit assembly. In really poor quality bone, the risk of excessively high micromotion is possible even with proper interference-fit prepared during surgery.

8.5 Conclusion

The results of this study suggest that : -

1) Interference-fit can be maintained in the femur sufficiently long for osseointegration to occur.

2) Below the creep threshold of cortical bone, higher initial interference-fit is likely to increase the effective interference-fit in comparison to a lower initial interference-fit.

3) Interference-fit causes the bone to act like an elastic band wrapped around the stem. Therefore, bone with higher residual stress will wrap around the stem more strongly and improve the stem stability. The effective-interference-fit is therefore influenced by the residual stress in the bone, and the residual stress of both cortical and cancellous bones contributed to the effective interference-fit. The contribution of cortical bone to the total residual stress is potentially greater than cancellous bone due to the much higher modulus of cortical bone.

4) The optimum interference-fit is the degree of interference-fit that gives the maximum femoral stress achievable after creep.

5) Bone quality can influence the micromotion of the stem significantly in two ways. Better bone quality will have higher residual stress for a certain degree of interference-fit. Higher residual stress will improve the stem stability. Secondly, better bone quality will resist bending or deformation better and will reduce the stem micromotion.

6) The results of this study are based on a simplified model of the implanted proximal femur. Care must be exercised when extrapolating these results to an actual implanted femur, which has inhomogeneous material properties.

7) Depending on the degree of creep in the femur, the result in Chapter 6 could have overestimated the stability of the stem because creep was not modelled.

Chapter 9 Discussion

9.1 The role of present work in the preclinical analysis of cementless hip stem

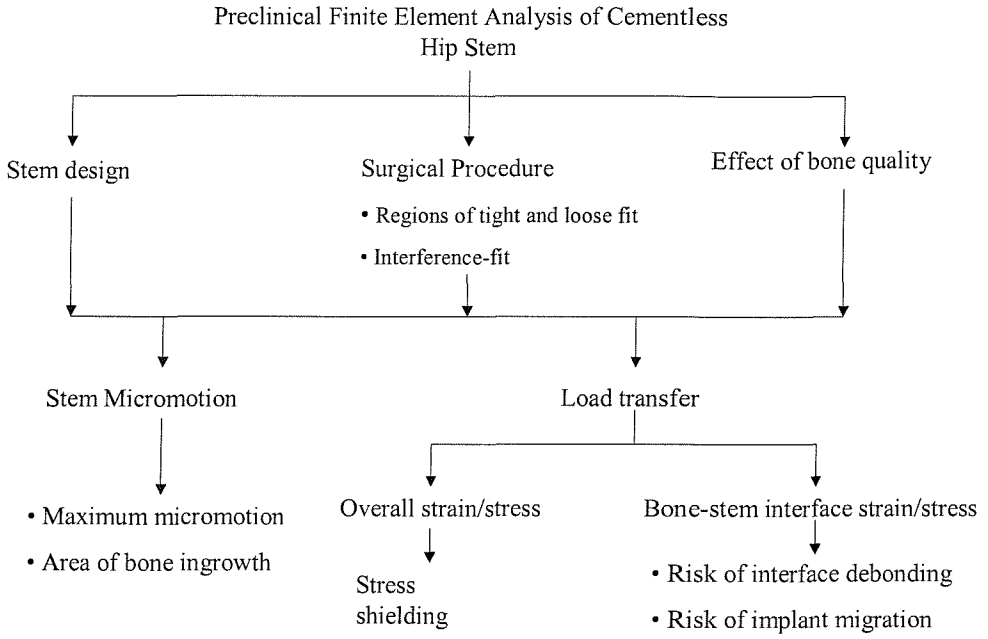

Figure 9.1 Schematic diagram of the role of preclinical finite element analysis of cementless hip stems.

The work of this thesis attempts to advance the preclinical analysis of cementless hip stem using the finite element method. The role of finite element analysis in preclinical analysis of cementless hip stem has been summarized in Figure 9.1. In general, finite element analysis can been use to compare various stem designs, surgical procedure and effect of bone quality on the relative micromotions of the stem and load transfer to the femur. These were reviewed in Chapter 3. Stem micromotion is of concern in the immediate postoperative period as it affects the chances of bone ingrowth (Section 3.8). Load transfer is both a concern in both the immediate postoperative period and for longer term implant survival (Section 3.6 and 3.7). In the shorter term, high interface shear stress can increase the risk of fracture of recent bone ingrowth [Huiskes, 1990; Cheal *et al.*, 1992; Viceconti *et al.*, 2002]. High cancellous bone stress in both the short and longer term may increase the risk of implant migration, which has been shown to be a predictor of implant failure [Taylor *et al.*, 1995; Taylor, 1997; Perillo-Marcone, 2001]. In the longer term, cementless stems have also been shown to cause stress shielding and reduce the density of the proximal cortex (Section 3.7).

Previous finite element studies [Rubin *et al.*, 1993; Keaveny and Bartel, 1993c; Kuiper and Huiskes, 1996; Ramaniraka *et al.*, 1996; Ando *et al.*, 1999; Viceconti *et al.*, 2000; Fernandes *et al.*, 2002] have not studied the effect of bone quality on the hip stem stability when assessing implant designs. Micromotion studies published in the literature looked at stem micromotion independent of interface bone strain. There are recent studies that suggest that interface bone strain is a predictor of implant migration [Taylor, 1997; Taylor *et al.*, 1998; Perillo-Marcone, 2001], which suggest that assessment of new implants should also look at interface bone strain. In this thesis, stem micromotion and bone strain were examined together.

In this thesis, two issues involving preclinical analysis of cementless hip stem were studied. In Chapter 5, the effect of bone quality on implant stability and femoral strain were examined. This section advances our understanding of the effect of bone quality on stem micromotion and interface bone strain, and the possible implication on analysis of hip stem designs.

In Chapter 6, 7 and 8, the effect of underreaming the femoral canal relative to the stem size to create an interference-fit were studied. This is a finite element study of the effects of surgical procedure on initial micromotion and interface strain. In clinical studies, interference-fit has been shown to improve the clinical results [Engh *et al.*, 1990], but also has the potential to cause femoral fracture (Section 3.9). In experimental micromotion studies, interference-fit has been been shown to reduce interface micromotion [Sugiyama *et al.*, 1992]. Despite the benefit of interference-fit in improving clinical results, very limited studies has been performed to improve the design of interference-fit for cementless hip stem. The contribution of these works are toward better understanding of the mechanical environment of the interference-fit assembly in the implanted proximal femur and the relationship with hip stem stability. The aims were to improve early fixation of cementless hip stem and to prevent femoral fracture due to excessive interference-fit.

9.2 The role of modelling different bone quality in preclinical assessment of new implant design

In the literature, the finite element studies on implant micromotion generally do not examine the influence of bone quality has on hip stem micromotion. The results of Chapter 5 suggested that this could be inadequate to assess the risk of hip stem fixation failure in various patients. With the IPS stem, the stem micromotion and interface bone strain have been shown to increase nonlinearly with reductions of bone modulus, and therefore the overall stiffness of the femur. Bone ingrowth can occur only below a certain micromotion threshold (generally assumed to be 50 μm). The results suggested that the area of bone ingrowth could fall rapidly in patients with poor bone quality. Above a certain interface strain, fatigue damage of interface bone can become critical.

Rapid accumulation of fatigue damage can lead to unstable implant migration and fixation failure. With a rapid fall of bone quality, the increase in interface bone strain is also increasing the risk of fatigue failure of interface bone. This could lead to higher implant migration [Taylor *et al.*, 1995; Taylor, 1997; Perillo-Marcone, 2001]. Finite element analyses of the Freeman stem implanted as cemented, HA coated and press-fit stem have reported that the maximum interface cancellous bone stresses in these models follows the same implant migration trend as reported *in vivo* [Taylor *et al.*, 1995; Taylor, 1997]. Perillo-Marcone (2001) looked at the bone stress below the tibia tray in total knee arthroplasty using four patient specific tibia models. The ratio of stress over ultimate strength was defined as the risk ratio. The risk ratio from four patients models and the corresponding rate of implant migration was compared. The risk ratio from the patient specific models was found to follow the same trend as the rate of implant migration *in vivo* for the patients.

It is also shown that the decline of cortical and cancellous bone Young's modulus affects stem micromotion differently in different regions of the femur. In regions where cancellous bone is thick and cortical bone is thin, reduction in the cancellous bone modulus will increase the stem micromotion the most. In more distal regions near the mid level of the lesser trochanter, the thickness of cortical bone increases and thickness of cancellous bone decreases. In this region, it is shown that decrease of cortical bone modulus plays a major role in increasing the stem micromotion. These findings suggest that certain patients suffering from very poor cancellous bone quality like patients with rheumatoid arthritis could benefit from more distal fixation, although this may cause further proximal stress shielding. Instead of designing a single level of porous or HA coating for all patients, there could be different levels of coating for patients with different needs. It is also possible to design a different stem geometry to improve stem stability and reduce the interface bone strain.

At present, most preclinical analysis is still comparative and cannot be verified with the true performance of the stem *in vivo*. Although it was shown that micromotion and interface strain increase with decreasing bone quality, it is not possible to quantify the relationship between the finite element results and bone quality that will constitute a high failure risk It is impractical to perform patient specific modelling for each patient to confirm the prediction of finite element study due to several reasons. Firstly, it is not possible to obtain detailed CT scans of each patients due to the high cost and ethical reasons. Secondly, it is time consuming to create the finite element models of each patient. Therefore, preclinical analysis has to contain information that surgeons can use as comparison to patient's data. If preclinical analysis can be performed with a set of CT-scans containing normal to very poor quality femurs, the corresponding dual-energy X-ray absorptiometry (DEXA) scans from this data set can then be use for comparison by surgeons. From comparison with follow-up studies on patients, it is then possible to relate finite element results to bone quality and then define the bone quality that can constitute as high risk. A more

predictive preclinical analysis may be useful to change the way new stems are designed and probably the postoperative care of the patients.

9.3 The effect of interference-fit on the mechanical environment of the implanted proximal femur

9.3.1 Stem micromotion

The presence of an interference-fit was found to reduce the stem micromotion significantly. The effect of interference-fit on initial stability of a hip stem has not been examined in anatomical finite element models before. In Chapter 6, the effect of interference-fit on the initial stability of an IPS hip stem was studied. The results showed that the initial stability of the hip stem is greatly influenced by the degree of interference-fit. In comparison to a stem inserted with line-to-line fitting, a moderate interference-fit has been shown to reduce the initial micromotion significantly. The results in Chapter 6 also suggest that there could be an optimum interference-fit where the micromotion can be reduced to minimum, without further increase to interference-fit. It is also found that a moderate interference-fit can improve significantly initial stability without increasing interface strain in comparison to a line-to-line fitting stem. Therefore, there is a diminishing reduction of micromotion with increasing degree of interference-fit.

The physiological model in Chapter 6 was extended to study the effect of interface plastic deformation on the predicted micromotion in Chapter 7. It is found that modelling the plastic deformation caused by interference-fit does not significantly affect the predicted micromotion in comparison to a linear elastic model. There could be two reasons for this. The first reason could be that the interface plastic deformation does not change the residual stress due to the interference-fit significantly in comparison to the elastic model. The bone stress was marginally lower, but not enough to alter the predicted micromotion. The second reason being the majority of the plastic deformation occurs when the interference-fit is established. The IPS stem does not impose high stress concentration at the interface bone. Therefore, during loading, the bone is still mostly working within the elastic range. The predicted micromotions in Chapter 6 are therefore not affected by plastic deformation at the interface bone.

However, the results in Chapter 6 and 7 do not take into account the possible creep deformation of bone. In Chapter 8, the effect of creep of cortical and cancellous bone on effective interference-fit was studied using a simplified model. In this study, it is shown that creep could influence the stem micromotion significantly. Comparison between models with and without creep showed higher stem micromotions in the creep models after a simulated 28 days period. Creep was shown to reduce the effective interference-fit. The amount of reduction of the interference-fit depends on the amount of creep. However, similar to results in Chapter 6, the higher effective interference-fit the better the stem stability. The creep deformation has also been simulated for a

clinically meaningful time of 28 days, and stress relaxation from creep was found to have stabilized. This is in agreement with clinical results, which have shown better rate of bone ingrowth in interference-fit stabilized stems [Engh *et al.*, 1990]. Again, the stem micromotion was also found to increase with reduction of Young's modulus with the same interference-fit. The dependence of stem stability on bone quality is similar to the results reported for line-to-line fit models in Chapter 5. Reduction of elastic modulus of cancellous bone only was shown to increase the stem micromotion.

9.3.2 The effect of residual stress on stem micromotion

Although linear elastic models in Chapter 6 predicted higher stability for higher degrees of interference-fit, in reality this may not be true. In Chapter 8, it is shown that the micromotion is higher if the residual stress within the femur is lower. The femur can be imagined as a composite of two shells, with outer cortical bone shell and inner cancellous bone shell (Figure 9.2). In an interference-fit assembly, the two shells can be imagined to be stressed like an elastic bands. The effective interference-fit can therefore be view as the residual femoral stress that the interference-fit can induce. The higher the residual stress in this elastic band, the greater stability the stem has. Depending on the creep threshold of bone, creep can reduce the residual stress of the interference-fit considerably in both the cancellous and cortical bone. If the normalized bone stress is above the creep threshold, the bone will creep and the residual stress will reduce close to the creep threshold value. The overall stress in the femur will depend on how much creep occurs in the cortical and cancellous bone shell. However, cortical bone has a higher elastic modulus in comparison to cancellous bone, and has been shown to generate higher stresses than cancellous bone before creep. Therefore, the contribution of cortical bone to the effective interference-fit is potentially greater than cancellous bone.

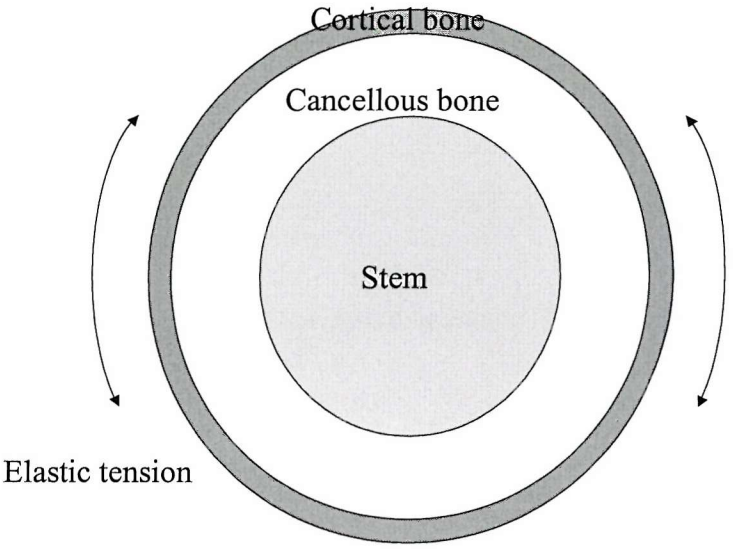

Figure 9.2 Effective interference-fit can be imagined as the residual stresses of an elastic band wrapping around the stem.

The results in Chapter 8 suggest that interface cancellous bone's normalized stress would be much higher than the normalized stress of cortical bone due to the lower elastic modulus of cancellous bone. Due to this, the normalized stress of cancellous bone is bound to be higher and creep is likely to occur in the cancellous bone. If the creep threshold of cortical bone is not exceeded, then increasing the interference-fit will increase the residual stress in the cortical bone without increasing residual stress of cancellous bone, as normalized stress of cancellous bone is likely to be higher than the creep threshold. However, as shown in chapter 8, if the creep threshold of cortical bone is exceeded, a higher degree of interference-fit is not going to increase residual stress because both the cortical and cancellous bone will creep. Therefore, higher interference-fit in this situation will not improve the stem stability.

The exact creep threshold of cancellous bone and cortical bone in a multiaxial stress state has yet to be determined. In Chapter 8, the compressive creep data of bovine cancellous bone has been used for cancellous bone. For cortical bone, the hoop creep data of human cortical bone has been used. For cancellous bone, the creep threshold in terms of normalized stress is about 0.003 or 0.3 % strain in a uniaxial test. The creep threshold of cortical bone based of hoop creep data has predicted normalized stress of about 0.0001, or 0.01% strain. This value is very low, and could mean that cortical bone cannot support much hoop stress. However, clinical experience seems to suggest that interference-fit at the femoral isthmus, which is mainly cortical bone, improved bone ingrowth significantly [Engh *et al.*, 1990]. The exact creep response of femur in an interference-fit assembly will need further study to predict the creep threshold of the femur.

9.3.3 Endosteal and periosteal strain

The femoral strain is affected by the degree of interference-fit. In Chapter 6, the femoral strain due to the modelling of the interference-fit also suggests that a small interference-fit like 0.1 mm can cause high periosteal strain in certain regions of the femur. For an anatomic stem like the IPS stem, the proximal anterior and proximal posterior regions of the femur are particularly vulnerable to high strain. The femoral wall in these regions can be quite thin. Therefore, the initiation of fracture could happen in these regions. Femoral fracture would have defeated the purpose of having interference-fit in the first place, although the fracture can be stabilized by the use of cerclage wire [Fitzgerald *et al.*, 1988; Schwartz *et al.*, 1989; Martell *et al.*, 1993; Schutzer *et al.*, 1995]. Repairing fracture during surgery with cerclage wire is also a time consuming process which can results in loss of blood and could be a potential source of soft tissue inflammation [Martell *et al.*, 1993]. Experimentally created femoral fractures in animal models showed lesser bone ingrowth even though the fractures have been stabilized by cerclage wire [Schutzer *et al.*, 1995]. It is therefore desirable for better design of interference-fit to avoid femoral fracture.

In Chapter 6 and 7, the endosteal strain can be very high even for an interference-fit of 0.1 mm. In Chapter 7, the interface bone was shown to have extensive plastic deformation. The crushing of endosteal bone due to interference-fit is not good, as this reduces the Young's modulus of the interface bone [Keaveny *et al.*, 1999]. It is shown in Chapter 5 and 8 that more compliant cancellous bone can increase micromotion. The crushing of endosteal bone could also reduce the fatigue life of the interface bone, resulting in higher migration risk [Taylor *et al.*, 1995; Taylor and Tanner, 1997; Perillo-Marcone, 2001]. With better understanding of the creep behaviour of the femur in the interference-fit assembly, it is perhaps not necessary to use excessive interference-fit, as the effective interference-fit is governed by the creep threshold of cortical bone.

9.4 Interference-fit design for hip stem

Finite element modelling of the implanted femur can play a role in the design of the interference-fit of the hip stem (Figure 9.3). Finite element analysis can play a role in early design analysis to identify regions of high fracture risk and the optimum interference-fit to prevent fracture and providing the best initial stability. In the design schematic shown in Figure 9.3, the prediction of finite element analysis can then be tested in experiments to verify the predicted strain and micromotion.

As shown in Chapter 6, the general periosteal strain is quite low except in certain regions. For the IPS stem, the anterior and posterior regions around the intertrochanteric region were shown to have high strains. These regions are at higher risk of fracture initiation. The degree of interference-fit can be varied in finite element models to assess the fracture risk. This gives a prediction of the degree of interference-fit that is safe without fracturing the femur. In region of high strain, the

surgical instruments can be designed so that the interference-fit in that particular region is smaller, while in other regions, the interference-fit can be design to be higher to maximise the residual stress. Finite element analysis also allows a check of the endosteal strain to ensure that interference-fit does not plastically deforms a huge region of the supporting cancellous bone.

It is also predicted in Chapter 6 that above a certain degree of interference-fit, improvement to stem stability with higher interference-fit is not significantly different. If finite element study predictions that a lower interference-fit can give similar implant stability in comparison to the interference-fit design for maximum residual stress, then the two different degrees of interference-fit should be tested experimentally. If the lower interference-fit can provide similar stem stability, then it should be the chosen interference-fit.

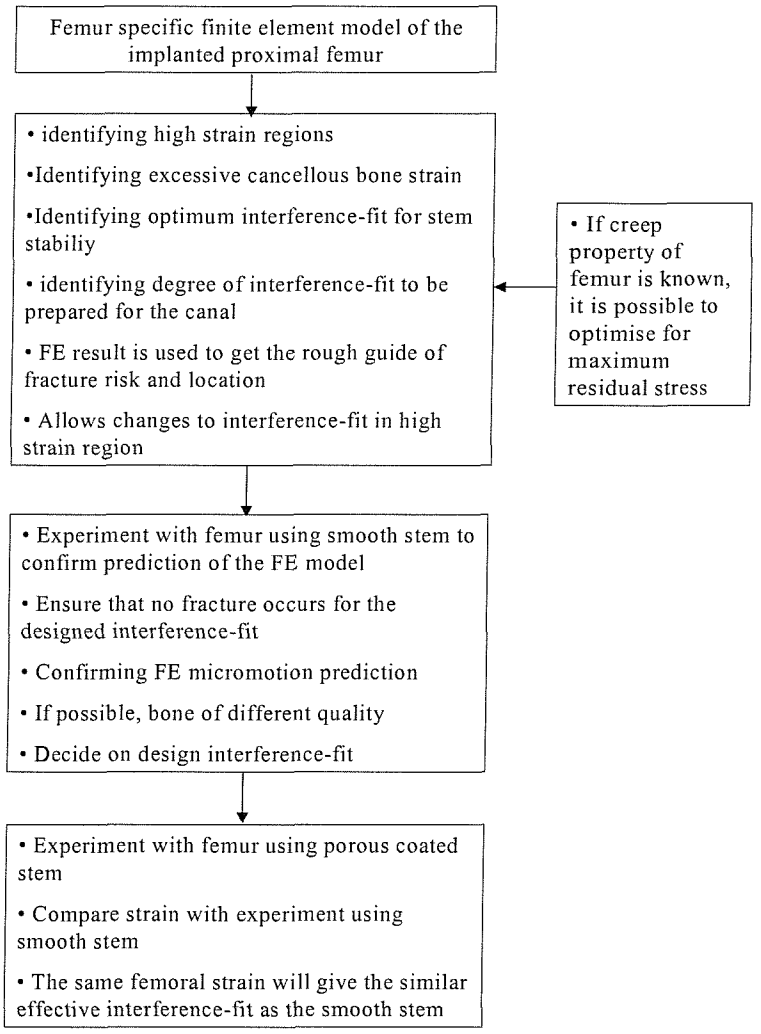

Figure 9.3 Schematic diagram of a proposed design scheme for interference-fit of hip stem.

However it is difficult to assess what constitutes a high fracture risk. Jasty *et al.* (1993) measured the assembly strain of the implanted proximal femur using the porous coated Harris Galante stem (Zimmer, US). The femurs were implanted with the optimum size stem with 0.25

mm interference-fit have maximum hoop strain of 0.24% strain, which was measured at the proximal cortex. One out of seven femurs was fractured. However, the strain at the fracture site prior to fracture was not measured. Another group of four stems were implanted with stems a size larger than optimum and implanted with the same interference-fit. The reported hoop strain in the proximal cortex was in the range of 0.24 and 0.6% strain. All the femurs fractured. The strain was measured prior to development of fracture. The ultimate strain of human cortical bone in the transverse direction has been reported to be about 0.7% strain [Reilly and Burstein, 1975]. This is very near to the hoop strain value of the femurs prior to fracture. The measured hoop strain in a hoop creep test has been reported to be typically less than 0.4% strain, but the maximum hoop strain measured was 0.51% strain [Brown *et al.*, 2002]. However, strain was not measured at the fractured site. It is possible that the hoop failure strain could be slightly higher than the measured strain. From the results of these studies, cortical bone ultimate hoop strain was found to be in the region of 0.5 and 0.7% strain. It is perhaps desirable to design the interference-fit so that the femoral hoop strain does not exceed 0.25 % hoop strain. This is at the level of strain measured by Jasty *et al.* (1993) for the optimum stem size implanted with interference-fit and about 2-3 times lower than the ultimate strain of cortical bone in the transverse direction [Reilly and Burstein, 1975; Jasty *et al.*, 1993; Brown *et al.*, 2002]. Further work on the prediction of bone fracture is necessary.

Based on current data on creep of bone, it is still not possible to predict the amount of creep in the interference-fit assembly. To be able to use finite element to design for maximum residual stress, more information on the creep of both cancellous and cortical bone is needed. If creep threshold information was available, it is more desirable to design the interference-fit so that the cortical bone strain is just above the creep threshold to ensure minimum damage to interface cancellous bone and avoid fracture. The stem micromotion has been shown to be lower for higher residual stress in the femur. Designing the interference-fit at the creep threshold will give the maximum residual stress and therefore maximum stability.

The finite element predictions will have to be confirmed by experiment (Figure 9.3). A smooth stem should be inserted into a femur with the designed interference-fit from finite element method to verify the finite element results. Strain gauges can be place in different areas, with greater emphasis in the high strain regions to ensure that strain is well below fracture strain. It is better if femurs of different quality can be obtained for the finite element models and to be use in the experiment. Verification of the hip stem micromotion should also be performed.

However, most cementless hip stems in the market are now coated with a layer of porous beads. The actual interference-fit of cementless hip stem with porous coating may be less due to shearing of interface bone during insertion of the stem and bone filling some of pores of the porous coating. After the confirmation that femur does not fracture for the periosteal strain measured in

the smooth stem experiment, porous coated stems can be design to give similar level of periosteal strain. This will give similar effective interference-fit.

9.5 Conclusion

The results of this thesis highlighted the need of preclinical analysis of the hip stem to look at the effect of patient variability and surgical procedure on the performance of hip stem. The following conclusions can be drawn from the results of this thesis :-

- The variability of the bone quality can have significant non-linear effect on the initial stability of a cementless stem. The initial stability of the stem is not just affected by the quality of the interface cancellous bone, but by the overall bone quality and thus the overall stiffness of the femur. The stiffness of the cortex is important in constraining the movement of the stem and therefore reducing stem micromotion.
- Variation in the overall stiffness of the femur also affects the interface cancellous bone strain non-linearly. Interface strain has been found to increase with lower overall bone stiffness. This increases the risk of fatigue failure of interface cancellous bone. Stem migration may increase with the failure of supporting interface cancellous bone.
- Quantifying the relative stability of the stem in different regions due to variation of bone quality highlights the need for variation of hip stem design such as different levels of porous coating for patients with different bone quality.
- Stem micromotion is greatly reduced by the presence of interference-fit. Increasing the degree of interference-fit results in a diminishing return, and therefore there is little value in increasing interference-fit further after a certain degree of interference-fit. Therefore, an optimal interference-fit exists, giving good initial stability but not at the expense of excessive bone strains.
- Bone strain increases much faster than the reduction of micromotion both at the interface bone and the surface of the femur. The increase in interface strain can load the interface bone beyond the ultimate strain and therefore increase the damage in the interface bone. This can reduce the fatigue life and stiffness of the interface bone. Increase in periosteal strain increases the risk of femoral fracture, which defeats the purpose of having an interference-fit.
- Creep reduces the residual stresses of an interference-fit and as a result the stem stability is reduced. The reduction of residual stresses reduces the effective interference-fit. Cortical bone stresses play a key role in maintenance of interference-fit. Therefore, the reduction of cortical bone stresses reduces the effective interference-fit significantly. If the residual stresses are higher than the creep threshold, stress relaxation will occur to the creep threshold value.

Chapter 10 Future Works

1) In Chapter 5, the influence of bone quality on stem micromotions and femoral strains has been performed by varying the bone modulus from one femur CT scans. A more realistic study of the performance envelope of a stem should be performed on multiple femurs CT scans to allow for more realistic variations in bone quality. Beside more realistic variations in bone quality, the use of multiple femurs CT scans also allows for study of the effect of femoral geometry on stem micromotion and femoral strain. Preclinical analyses performed with multiple femurs have the potential of allowing comparison between clinical performance and results of finite element analysis. Comparison like DEXA scans of the patients and of the femurs used for the finite element analyses can be used to correlate between the actual clinical performance and predictions of finite element analyses.

2) Experimental data is needed to confirm the results of finite element analyses in Chapter 6. Experimental verifications to confirm the diminishing reduction of micromotions with higher degree of interference-fit is needed to have more confidence in the results. Combined experimental and finite element studies will allow comparison between the results of experimental works and experimental specific finite element models.

3) The present understanding of the creep behaviour of both cortical and cancellous bone is still inadequate. Further research is needed to examine the creep behaviour of bone in multi-axial loading. This will enable development of more accurate finite element models to predict the maximum residual stress that can be induced in the bone due to the interference-fit and therefore, the optimal interference-fit for cementless orthopaedic implants. Experimental verification of the residual stress induced by an interference-fit that cortical bone can sustain is also necessary to have confidence in the finite element results.

4) Presently, bone ingrowth is predicted by the values of the stem micromotions. However, the differentiation of healing tissue at the interface to bone is dependent on the stress/strain history. The stress/strain history in the healing tissue can be influence by the surface texture of the implant and the amount of the stem micromotions. Incorporation of surface texture information into the model could improve the predictive power of finite element model. A two step calculation could then be performed. The first step evaluates the stem micromotion. In the second stem, the values of stem micromotion can be transferred to a model which incorporates soft tissue and surface texture. The stress/strain values can then be used as a more meaningful predictor of bone ingrowth.

References

1. Alfaro-Adrian, J., Gill, H. S. and Marks, B. E. (1999): Mid-term migration of a cemented total hip replacement assessed by radiostereometric analysis. *International Orthopaedics* **23**:140-144.

2. An, K. N., Kaufman, K. R. and Chao, E. Y. S. (1989): Physiological considerations of muscle force through the elbow joint. *Journal of Biomechanics* **22**:1249-1256.

3. Ando, M., Imura, S., Omori, H., Okumura, Y., Bo, A. and Baba, H. (1999): Non-linear three-dimensional finite element analysis of newly designed cementless total hip stems. *Artificial Organs* **23**:339-346.

4. Ashman, R. B., Rho, J.Y. , Turner, C.H. (1989): Anatomical variation of orthotropic elastic moduli of the proximal human tibia. *Journal of Biomechanics* **22**:895-900.

5. Ashman, R. B., Cowin, S. C., Vanbuskirk, W. C. and Rice, J. C. (1984): A Continuous Wave Technique For the Measurement of the Elastic Properties of Cortical Bone. *Journal of Biomechanics* **17**:349-361.

6. Ashman, R. B. and Rho, J. Y. (1988): Elastic-Modulus of Trabecular Bone Material. *Journal of Biomechanics* **21**:177-181.

7. Aspenberg, P., Goodman, S., Toksviglarsen, S., Ryd, L. and Albrektsson, T. (1992): Intermittent Micromotion Inhibits Bone Ingrowth - Titanium Implants in Rabbits. *Acta Orthopaedica Scandinavica* **63**:141-145.

8. Baleani, M., Cristofolini, L. and Toni, A. (2000): Initial stability of a new hybrid fixation hip stem: Experimental measurement of implant-bone micromotion under torsional load in comparison with cemented and cementless stems. *Journal of Biomedical Materials Research* **50**:605-615.

9. Bauer, T. W., Geesink, R. C. T., Zimmerman, R. and McMahon, J. T. (1991): Hydroxyapatite-Coated Femoral Stems - Histological Analysis of Components Retrieved At Autopsy. *Journal of Bone and Joint Surgery-American Volume* **73A**:1439-1452.

10. Beaupre, G. S., Orr, T. E. and Carter, D. R. (1990): An approach for time-dependent bone modeling and remodeling- Application: A preliminary remodeling simulation. *Journal of Orthopaedic Research* **8**:662-670.

11. Bergmann, G., Deuretzbacher, G., Heller, M., Graichen, F., Rohlmann, A., Strauss, J. and Duda, G. N. (2001): Hip contact forces and gait patterns from routine activities. *Journal of Biomechanics* **34**:859-71.

12. Bergmann, G., Graichen, F. and Rohlmann, A. (1993): Hip-Joint Loading During Walking and Running, Measured in 2 Patients. *Journal of Biomechanics* **26**:969-990.

13. Bernakiewicz, M. and Viceconti, M. (2002): The role of parameter identification in finite element contact analyses with reference to orthopaedic biomechanics applications. *Journal of Biomechanics* **35**:61-67.

14. Biegler, F. B., Reuben, J. D., Harrigan, T. P., Hou, F. J. and Akin, J. E. (1995): Effect of porous coating and loading conditions on total hip femoral stem stability. *Journal of Arthroplasty* **10**:839-847.

15. Blumlein, H., Cordey, J., Schneider, U. A., Rahn, B. A. and Perren, S. M. (1977): Long-term measurements of the axial force of bone screws *in vivo*. .

16. Bobyn, J. D., Glassman, A. H., Goto, H., Krygier, J. J., Miller, J. E. and Brooks, C. E. (1990): The Effect of Stem Stiffness On Femoral Bone-Resorption After Canine Porous-Coated Total Hip-Arthroplasty. *Clinical Orthopaedics and Related Research* **261**:196-213.

17. Bogoch, E. R. and Moran, E. L. (1999): Bone Abnormalities in the surgical treatment of patients with rheumatoid arthritis. *Clinical Orthopaedic and Related Research* **366**:8-21.

18. Bowman, S. M., Gibson, L. J., Hayes, W. C. and McMahon, T. A. (1999): Results from demineralized bone creep tests suggest that collagen is responsible for the creep behavior of bone. *Journal of Biomechanical Engineering-Transactions of the Asme* **121**:253-258.

19. Bowman, S. M., Guo, X. E., Cheng, D. W., Keaveny, T. M., Gibson, L. J., Hayes, W. C. and McMahon, T. A. (1998): Creep contributes to the fatigue behavior of bovine trabecular bone. *Journal of Biomechanical Engineering-Transactions of the Asme* **120**:647-654.

20. Bowman, S. M., Keaveny, T. M., Gibson, L. J., Hayes, W. C. and McMahon, T. A. (1994): Compressive creep behaviour of bovine trabecular bone. *Journal of Biomechanics* **27**:301-310.

21. Bragdon, C. R., Burke, D., Lowenstein, J. D., Oconnor, D. O., Ramamurti, B., Jasty, M. and Harris, W. H. (1996): Differences in stiffness of the interface between a cementless porous implant and cancellous bone in vivo in dogs due to varying amounts of implant motion. *Journal of Arthroplasty* **11**:945-951.

22. Brand, R. A., Pedersen, D. R. and Friederich, J. A. (1986): The Sensitivity of Muscle Force Predictions to Changes in Physiological Cross-Sectional Area. *Journal of Biomechanics* **19**:589-596.

23. Brown, C. U., Kish, V. L., Norman, T. L., Gruen, T. A. and Blaha, J. D. (2001): Circumferential creep of human cortical bone suggests threshold for press-fit stems. *47th Annual Meetin, Orthopaedic Research Society, Feb 25-28*.

24. Brown, C. U., Norman, T. L., Kish, V. L., Gruen, T. A. and Blaha, J. D. (2002): Time-dependent circumferential deformation of cortical bone upon internal radial loading. *Journal of Biomechanical Engineering-Transactions of the Asme* **124**:456-461.

25. Brown, T. D. (1980): Mechanical property distributions in the cancellous bone of the human proximal femur. *Acta Orthopaedica Scandinavica* **51**:429-437.

26. Bugbee, W. D., Culpepper, W. J. and Engh, C. A. (1997): Long-term clinical consequences of stress-shielding after total hip arthroplasty without cement. *Journal of Bone and Joint Surgery-American Volume* **79A**:1007-1012.

27. Burke, D. W., Oconnor, D. O., Zalenski, E. B., Jasty, M. and Harris, W. H. (1991): Micromotion of Cemented and Uncemented Femoral Components. *Journal of Bone and Joint Surgery-British Volume* **73**:33-37.

28. Burstein, A. H. and Frankel, V. H. (1968): The viscoelastic properties of some biological materials,. *Ann. N.Y. Acad. Sci.* **146**:158.

29. Caler, W. E. and Carter, D. R. (1989): Bone creep-fatigue damage accumulation. *Journal of Biomechanics* **22**:625-635.

30. Callaghan, J. J., Fulghum, C. S., Glisson, R. R. and Stranne, S. K. (1992): The Effect of Femoral Stem Geometry On Interface Motion in Uncemented Porous-Coated Total Hip Prostheses - Comparison of Straight-Stem and Curved-Stem Designs. *Journal of Bone and Joint Surgery-American Volume* **74A**:839-848.

31. Cann, C. E. and Genant, H. K. (1980): Precise measurement of vertebral mineral content using computed tomography. *J. Computed Assisted Tomography* **4**:493-500.

32. Capello, W. D., D'Antonio, J. A., Feinberg, J. R. and Manley, M. T. (1997): Hydroxyapatite-coated total hip femoral components in patients less than fifty years old. Clinical and radiographic results after five to eight years of follow-up. *Journal of Bone and Joint Surgery* **79A**:1023-1029.

33. Carter, D. R., Hayes, W.C. (1977): The compressive behaviour of bone as a two-phase porous structure. *Journal of Bone and Joint Surgery* **59A**:954-962.

34. Carter, D. R. (2000): Mechanobiology of skeletal tissue ingrowth and adaptation. *12th Conference European Society of Biomechanics, Dublin* **12**:7.

35. Carter, D. R. and Caler, W. E. (1983): Cycle-dependent and time-dependent bone fracture with repeated loading. *Journal of Biomechanical Engineering* **105**:166-170.

36. Carter, D. R. and Caler, W. E. (1985): A cumulative damage model for bone fracture. *Journal of Orthopaedics Research* **3**:84-90.

37. Carter, D. R., Caler, W. E., Spengler, D. M. and Frankel, V. H. (1981a): Fatigue behaviour of adult cortical bone - The influence of mean strain and strain range. *Acta Orthopaedica Scandinavica* **52**: 481-490.

38. Carter, D. R., Caler, W. E., Spengler, D. M. and Frankel, V. H. (1981b): Uniaxial Fatigue of Human Cortical Bone - the Influence of Tissue Physical Characteristics. *Journal of Biomechanics* **14**:461-470.

39. Carter, D. R. and Hayes, W. C. (1976): Bone compressive strength; the influence of density and strain rate. *Science* **194**:11-17.

40. Carter, D. R., Schwab, G. H. and Spengler, D. M. (1980): Tensile fracture of cancellous bone. *Acta Orthopaedica Scandinavica* **51**:733-741.

41. Cezayirlioglu, H., Bahniuk, E., Davy, D. T. and Heiple, K. G. (1985): Anisotropic Yield Behavior of Bone Under Combined Axial Force and Torque. *Journal of Biomechanics* **18**:61-69.

42. Chang, W. C. W., Christensen, T. M., Pinilla, T. P. and Keaveny, T. M. (1999): Uniaxial yield strains for bovine trabecular bone are isotropic and asymmetric. *Journal of Orthopaedic Research* **17**:582-585.

43. Charnley, J. (1960): Anchorage of the femoral head prosthesis to the shaft of the femur. *Journal of Bone and Joint Surgery-British Volume* **42B**:28-30.

44. Cheal, E. J., Spector, M. and Hayes, W. C. (1992): Role of Loads and Prosthesis Material Properties On the Mechanics of the Proximal Femur After Total Hip-Arthroplasty. *Journal of Orthopaedic Research* **10**:405-422.

45. Cook, S. D. (1991): Clinical radiographic, and histologic evaluation of retrieved human noncement porous coated implants. *Journal of Long-Term Effects of Medical Implants* **1**:11-51.

46. Cook, S. D., Thomas, K. A. and Haddad, R. J. (1988): Histologic Analysis of Retrieved Human Porous-Coated Total Joint Components. *Clinical Orthopaedics and Related Research* **234**:90-101.

47. Courtney, A. C., Hayes, W. C. and Gibson, L. J. (1996): Age-related differences in post-yield damage in human cortical bone. Experiment and model. *Journal of Biomechanics* **29**:1463-1471.

48. Cowin, S. C. (2001): Bone Mechanics Handbook Boca Raton, Florida: CRC Press.

49. Cowin, S. C. and Hegedus, D. H. (1976): Bone remodelling 1: theory of adaptive elasticity. *Journal of Elasticity* **12**:313-326.

50. Crowninshield, R. D., Brand, R. A. and Johnston, R. C. (1978a): The effect of walking velocity and age on hip kinematics and kinetics. *Clinical Orthopaedics and Clinical Research* **132**:140-144.

51. Crowninshield, R. D., Johnston, R. C., Andrews, J. G. and Brand, R. A. (1978b): A biomechanical investigation of the human hip. *Journal of Biomechanics* **11**:75-85.

52. Currey, J. D. (1975): The effect of strain rate, reconstruction, and mineral content on some mechanical properties of bovine bone. *Journal of Biomechanics* **8**:81.

53. Dalstra, M., Frich, L. H. and Sneppen, O. (1996): The loss of load-bearing capability in rheumatoid glenoids: "Proceedings 10th Conference of the ESB.", pp 178.

54. Dalstra, M., Huiskes, R., Odgaard, A. and van Erning, L. (1993): Mechanical and textural properties of pelvis trabecular bone. *Journal of Biomechanics* **26**:523-535.

55. Dalton, J. E. and Cook, S. D. (1995): In-Vivo Mechanical and Histological Characteristics of Ha- Coated Implants Vary With Coating Vendor. *Journal of Biomedical Materials Research* **29**:239-245.

56. D'Antonio, J. A., Capello, W. N., Manley, M. T. and Feinberg, J. (1997): Hydroxyapatite coated implants. Total hip arthroplasty in the young patient and patients with avascular necrosis. *Clinical Orthopaedics and Related Research* **344**:124-38.

57. Davy, D. T., Kotzar, G. M., Brown, R. H., Heiple, K. G., Goldberg, V. M., Berilla, J. and Burstein, A. H. (1988): Telemetric Force Measurements Across the Hip After Total Arthroplasty. *Journal of Bone and Joint Surgery-American Volume* **70A**:45-50.

58. Dawson, J. M. and Bartel, D. L. (1992): Consequences of an Interference Fit On the Fixation of Porous- Coated Tibia Components in Total Knee Replacement. *Journal of Bone and Joint Surgery-American Volume* **74A**:233-238.

59. Deligianni, D. D., Maris, A. and Missirlis, Y. F. (1994): Stress relaxation behaviour of trabecular bone specimens. *Journal of Biomechanics* **12**:1469-1476.

60. Dhert, W. J. A., Thomsen, P., Blomgren, A. K., Esposito, M., Ericson, L. E. and Verbout, A. J. (1998): Integration of press-fit implants in cortical bone: A study on interface kinetics. *Journal of Biomedical Materials Research* **41**:574-583.

61. Ding, M., Dalstra, M., Danielsen, C. C., Kabel, J., Hvid, I. and Linde, F. (1997): Age variations in the properties of human tibia trabecular bone. *Journal of Bone and Joint Surgery-British Volume* **79B**:995-1002.

62. Ding, M., Danielsen, C. C. and Hvid, I. (2001): Bone density does not reflect mechanical properties in early- stage arthrosis. *Acta Orthopaedica Scandinavica* **72**:181-185.

63. Donnelly, W. J., Kobayashi, A., Freeman, M. A., Chin, T. W., Yeo, H., West, M. and Scott, G. (1997): Radiological and survival comparison of four methods of fixation of a proximal femoral stem. *Journal of Bone and Joint Surgery-British Volume* **79B**:351-60.

64. Duda, G. N., Heller, M., Albinger, J., Schulz, O., Schneider, E. and Claes, L. (1998): Influence of muscle forces on femoral strain distribution. *Journal of Biomechanics* **31**:841-846.

65. Duda, G. N., Schneider, E. and Chao, E. Y. S. (1997): Internal forces and moments in the femur during walking. *Journal of Biomechanics* **30**:933-941.

66. Engh, C. A. and Bobyn, J. D. (1988): The Influence of Stem Size and Extent of Porous Coating On Femoral Bone-Resorption After Primary Cementless Hip Arthroplasty. *Clinical Orthopaedics and Related Research* **231**:7-28.

67. Engh, C. A., Bobyn, J. D. and Glassman, A. H. (1987): Porous-Coated Hip-Replacement - the Factors Governing Bone Ingrowth, Stress Shielding, and Clinical-Results. *Journal of Bone and Joint Surgery-British Volume* **69**:45-55.

68. Engh, C. A. and Culpepper, W. J. (1997): Long-term results of use of the anatomic medullary locking prosthesis in total hip arthroplasty. *Journal of Bone and Joint Surgery-American Volume* **79A**:177-184.

69. Engh, C. A., Glassman, A. H. and Suthers, K. E. (1990): The Case For Porous-Coated Hip Implants - the Femoral Side. *Clinical Orthopaedics and Related Research* **261**:63-81.

70. Engh, C. A., McGovern, T. F., Bobyn, J. D. and Harris, W. H. (1992a): A Quantitative-Evaluation of Periprosthetic Bone-Remodeling After Cementless Total Hip-Arthroplasty. *Journal of Bone and Joint Surgery-American Volume* **74A**:1009-1020.

71. Engh, C. A., McGovern, T. F., Zettl-Schaffer, K. F., Ghaffarpour, M. and Hooten, J. P. (1993-1994): Evaluation of bone ingrowth into proximally and entensively porous coated AML prostheses retrieved at autopsy. *Orthopedics Trans.* **17**:940.

72. Engh, C. A., Oconnor, D., Jasty, M., McGovern, T. F., Bobyn, J. D. and Harris, W. H. (1992b): Quantification of Implant Micromotion, Strain Shielding, and Bone-Resorption With Porous-Coated Anatomic Medullary Locking Femoral Prostheses. *Clinical Orthopaedics and Related Research* **285**:13-29.

73. English, T. A. and Kilvington, M. (1979): In vivo records of hip loads using a femoral implant with telemetric output. *Journal of Biomedical Engineering* **1**:111-115.

74. Fazzalari, N. L., Forwood, M. R., Smith, K., Manthey, B. A. and Herreen, P. (1998): Assessment of cancellous bone quality in severe osteoarthrosis: Bone mineral density, mechanics, and microdamage. *Bone* **22**:381-388.

75. Fernandes, P. R., Folgado, J., Jacobs, C. and Pellegrini, V. (2002): A contact model with ingrowth control for bone remodelling around cementless stems. *Journal of Biomechanics* **35**:167-176.

76. Fitzgerald, R. H., Bringley, G. W. and Kavanagh, B. F. (1988): The uncemented total hip arthroplasty: intraoperative femoral fractures. *Clinical Orthopaedic and Related Research* **235**:61.

77. Fondrk, M., Bahniuk, E., Davy, D. T. and Michaels, C. (1988): Some viscoelastic characteristics of bovine and human cortical bone. *Journal of Biomechanics* **21**:623-630.

78. Fondrk, M. T., Bahniuk, E. H. and Davy, D. T. (1999): Inelastic strain accumulation in cortical bone during rapid transient tensile loading. *Journal of Biomechanical Engineering-Transactions of the Asme* **121**:616-621.

79. Freeman, M. A. R. and Plante-Bordeneuve, P. (1994): Early migration and late aseptic failure of proximal femoral prosthesis. *Journal of Bone and Joint Surgery* **76B**:432-438.

80. Frich, L. H. (1994): Strength and structure of glenoid bone. PhD. Thesis, Arhus University, Denmark.

81. Fritton, S. P., McLeod, K. J. and Rubin, C. T. (2000): Quantifying the strain history of bone: spatial uniformity and self-similarity of low-magnitude strains. *Journal of Biomechanics* **33**:317-325.

82. Frost, H. M. (1997): Perspective, on our age related bone loss: insights from a new paradigm. *Journal of Bone Mineral Research* **12**:1539.

83. Gardner, T. N., Stoll, T., Marks, L., Mishra, S. and Tate, M. K. (2000): The influence of mechanical stimulus on the pattern of tissue differentiation in a long bone fracture - an FEM study. *Journal of Biomechanics* **33**:415-425.

84. Gibson, L. J. (1985): The mechanical behaviour of cancellous bone. *Journal of biomechanics* **18**:317-328.

85. Goldstein, S. A., Wilson, D. L., Sonstegard, D. A. and Matthews, L. S. (1983): The Mechanical-Properties of Human Tibia Trabecular Bone As a Function of Metaphyseal Location. *Journal of Biomechanics* **16**:965-969.

86. Goodship, A. E. and Kenwright, J. (1985): The influence of induced micromovement upon the healing of experimental tibia fractures. *Journal of Bone and Joint Surgery-British Volume* **67B**:650-655.

87. Goulet, R. W., Goldstein, S. A., Ciarelli, M. J., Kuhn, J. L., Brown, M. B. and Feldkamp, L. A. (1994): The Relationship Between the Structural and Orthogonal Compressive Properties of Trabecular Bone. *Journal of Biomechanics* **27**:375-389.

88. Grynpas, M. D., Alpert, B., Katz, I., Lieberman, I. and Pritzker, K. P. H. (1991): Subchondral bone in osteoarthritis. *Calcified Tissue International* **49**:20-26.

89. Hall-Craggs, E. C. B. (1995): "Anatomy as a basis for clinical medicine." London: Williams and Wilkins.

90. Hamilton, W. J. (1956): Textbook of human anatomy London: Macmillan and Company Ltd.

91. Hansson, T. H., Keller, T. S. and Panjabi, M. M. (1987): A Study of the Compressive Properties of Lumbar Vertebral Trabeculae - Effects of Tissue Characteristics. *Spine* **12**:56-62.

92. Harrigan, T. P. and Harris, W. H. (1991): A finite element study of the effect of diametral interface gaps on the contact areas and pressures in uncemented cylindrical femoral total hip components. *Journal of Biomechanics.* **24**:87-91.

93. Hearn, S. L., Bicalho, P. S., Eng, K., Booth, R. E., Hozack, W. J. and Rothman, R. H. (1995): Comparison of Cemented and Cementless Total Hip-Arthroplasty in Patients With Bilateral Hip Arthroplasties. *Journal of Arthroplasty* **10**:603-608.

94. Heller, M. O., Bergmann, G., Deuretzbacher, G., Durselen, L., Pohl, M., Claes, L., Haas, N. P. and Duda, G. N. (2001): Musculo-skeletal loading conditions at the hip during walking and stair climbing. *Journal of Biomechanics* **34**:883-93.

95. Hernandez, C. J., Beaupre, G. S. and Carter, D. R. (2000): A model of mechanobiologic and metabolic influences on bone adaptation. *Journal of Rehabilitation Research and Development* **37**:235-244.

96. Hodgskinson, R. and Currey, J. D. (1992): Young's modulus, density and material properties in cancellous bone over a large density range. *J. Mat. Science: Mat. in Med.* **3**:377-381.

97. Hozack, W. J., Rothman, R. H., Booth, R. E. and Balderston, R. A. (1993): Cemented Versus Cementless Total Hip-Arthroplasty - a Comparative-Study of Equivalent Patient Populations. *Clinical Orthopaedics and Related Research* **289**:161-165.

98. Hua, J. and Walker, P. S. (1994): Relative Motion of Hip Stems Under Load - an in-Vitro Study of Symmetrical, Asymmetrical, and Custom Asymmetrical Designs. *Journal of Bone and Joint Surgery-American Volume* **76A**:95-103.

99. Huiskes, R. (1990): The Various Stress Patterns of Press-Fit, Ingrown, and Cemented Femoral Stems. *Clinical Orthopaedics and Related Research* **261**:27-38.

100. Huiskes, R., Weinans, H. and Vanrietbergen, B. (1992): The Relationship Between Stress Shielding and Bone-Resorption Around Total Hip Stems and the Effects of Flexible Materials. *Clinical Orthopaedics and Related Research* **274**:124-134.

101. Incavo, S. J., Schneider, R. and Elting, J. (1998): The effect of surface coating of femoral prostheses implanted without cement: a 2- to 4-year follow-up study. *Am J Orthop* **27**:355-61.

102. Jasty, M., Henshaw, R. M., O'Connor, D. O. and Harris, W. H. (1993): High assembly strains and femoral fractures produced during insertion of uncemented femoral components. *Journal of Arthroplasty* **8**:479-487.

103. Jepsen, K. J. and Davy, D. T. (1997): Comparison of damage accumulation measures in human cortical bone. *Journal of Biomechanics* **30**:891-894.

104. Joshi, M. G., Advani, S. G., Miller, F. and Santare, M. H. (2000): Analysis of a femoral hip prosthesis designed to reduce stress shielding. *Journal of Biomechanics* **33**:1655-1662.

105. Kaplan, S. J., Hayes, W. C. and Stone, J. L. (1985): Tensile strength of bovine trabecular bone. *Journal of Biomechanics* **18**:723-727.

106. Karrholm, J., Borssen, B., Lowenhielm, G. and Snorrason, F. (1994a): Does early micromotion of femoral stem prosthesis matter? 4-7 year stereoradiographic follow-up of 84 cemented prostheses. *Journal of bone and joint surgery* **76B**:912-917.

107. Karrholm, J., Malchau, H., Snorrason, S. and Herbert, P. (1994b): Micromotion of femoral stems in total hip arthroplasty. *Journal of Bone and Joint Surgery* **76A**:1692-1705.

108. Karrholm, J. and Snorrason, F. (1993): Subsidence, tip and hump micromovement of noncoated ribbed femoral prostheses. *Clinical Orthopaedic and Related Research* **287**:50-60.

109. Keaveny, T. M. and Bartel, D. L. (1993c): Effects of Porous Coating, With and Without Collar Support, On Early Relative Motion For a Cementless Hip-Prosthesis. *Journal of Biomechanics* **26**:1355-1368.

110. Keaveny, T. M. and Bartel, D. L. (1994c): Fundamental Load-Transfer Patterns For Press-Fit, Surface- Treated Intramedullary Fixation Stems. *Journal of Biomechanics* **27**:1147-1157.

111. Keaveny, T. M., Guo, X. E., Wachtel, E. F., McMahon, T. A. and Hayes, W. C. (1994b): Trabecular Bone Exhibits Fully Linear Elastic Behavior and Yields At Low Strains. *Journal of Biomechanics* **27**:1127-1136.

112. Keaveny, T. M. and Hayes, W. C. (1993): A 20 year perspective on the mechanical properties of trabecular bone. *Transaction of the ASME* **115**:534-542.

113. Keaveny, T. M., Wachtel, E. F., Ford, C. M. and Hayes, W. C. (1994a): Differences Between the Tensile and Compressive Strengths of Bovine Tibia Trabecular Bone Depend On Modulus. *Journal of Biomechanics* **27**:1137-1146.

114. Keaveny, T. M., Wachtel, E. F., Guo, X. E. and Hayes, W. C. (1994d): Mechanical-Behavior of Damaged Trabecular Bone. *Journal of Biomechanics* **27**:1309-1318.

115. Keaveny, T. M., Wachtel, E. F. and Kopperdahl, D. L. (1999): Mechanical behavior of human trabecular bone after overloading. *Journal of Orthopaedic Research* **17**:346-353.

116. Keller, T. S. (1994): Predicting the compressive mechanical behaviour of bone. *Journal of Biomechanics* **27**:1159-1168.

117. Kerner, J., Huiskes, R., van Lenthe, G. H., Weinans, H., van Rietbergen, B., Engh, C. A. and Amis, A. A. (1999): Correlation between pre-operative periprosthetic bone density and post-operative bone loss in THA can be explained by strain- adaptive remodelling. *Journal of Biomechanics* **32**:695-703.

118. Keyak, J. H., Lee, I. Y. and Skinner, H. B. (1994): Correlations Between Orthogonal Mechanical-Properties and Density of Trabecular Bone - Use of Different Densitometric Measures. *Journal of Biomedical Materials Research* **28**:1329-1336.

119. Keyak, J. H. and Rossi, S. A. (2000): Prediction of femoral fracture load using finite element models: an examination of stress- and strain-based failure theories. *Journal of Biomechanics* **33**:209-214.

120. Kiss, J., Murray, D. W., Turner-Smith, A. R., Bithell, J. and Bulstrode, C. J. (1996): Migration of cemented femoral components after THR. *Journal of Bone and Joint Surgery* **78B**:796-801.

121. Kopperdahl, D. L. and Keaveny, T. M. (1998): Yield strain behavior of trabecular bone. *Journal of Biomechanics* **31**:601-608.

122. Kotzar, G. M., Davy, D. T., Goldberg, V. M., Heiple, K. G., Berilla, J., Brown, R. H. and Burstein, A. H. (1991): Telemeterized Invivo Hip-Joint Force Data - a Report On 2 Patients After Total Hip-Surgery. *Journal of Orthopaedic Research* **9**:621-633.

123. Kroon, P. O. and Freeman, M. A. R. (1992): Hydroxyapatite coating of hip implant. *Journal of Bone and Joint Surgery* **74B**:518-522.

124. Kuiper, J. H. and Huiskes, R. (1996): Friction and stem stiffness affect dynamic interface in total hip replacement. *Journal of Orthopaedic Research* **14**:36-43.

125. Lacroix, D., Murphy, L. A. and Prendergast, P. J. (2000): Three-dimensional finite element analysis of glenoid replacement prostheses: A comparison of keeled and pegged anchorage systems`. *Trans of the ASME- Journal of Biomechanical Engineering* **122**:430-436.

126. Lakes, R. S., Katz, J. L. and Sternsteins, S. S. (1979): Viscoelastic properties of wet cortical bone- I. Torsional and biaxial studies. *J. Biomech.* **12**:657-678.

127. Lakes, R. S. and Saha, S. (1979): Cement line motion in bone. *Science* **204**:501-503.

128. Lanyon, L. E., Hampson, W. G. J., Goodship, A. E. and Shah, J. S. (1975): Bone deformation recorded invivo from strain gauges attached to the human tibiat shaft. *Acta Orthopaedica Scandinavica* **46**:256-268.

129. Li, B. H. and Aspden, R. M. (1997): Composition and mechanical properties of cancellous bone from the femoral head of patients with osteoporosis or osteoarthritis. *Journal of Bone and Mineral Research* **12**:641-651.

130. Lindahl, O. (1976): Mechanical properties of dried defatted spongy bone. *Acta Orthopedica Scandinavia* **47**:11-19.

131. Linde, F., Hvid, I. and Madsen, F. (1992): The Effect of Specimen Geometry On the Mechanical-Behavior of Trabecular Bone Specimens. *Journal of Biomechanics* **25**:359-368.

132. Lombardi, A. V., Jr., Mallory, T. H., Eberle, R. W., Mitchell, M. B., Lefkowitz, M. S. and Williams, J. R. (1995): Failure of intraoperatively customized non-porous femoral components inserted without cement in total hip arthroplasty. *Journal of Bone and Joint Surgery - American Volume* **77A**:1836-44.

133. Lotz, J. C., Gerhart, T. N. and Hayes, W. C. (1991): Mechanical-Properties of Metaphyseal Bone in the Proximal Femur. *Journal of Biomechanics* **24**:317-329.

134. Lu, Z. and McKellop, H. (1997): Effects of cement creep on stem subsidence and stresses in the cement mantle of a total hip replacement. *Journal of Biomedical Materials Research* **34**:221-226.

135. Malchau, H., Herberts, P., Soderman, P. and Oden, A. (2000): Prognosis of total hip replacement: Update and validation of results from the Swedish National Hip Arthroplasty Registry 1979-1998: "67th Annual Meeting of the American Academy of Orthopaedic Surgeons." Orlando, USA:.

136. Mann, K. A., Bartel, D. L., Wright, T. M. and Burstein, A. H. (1995): Coulomb Frictional Interfaces in Modeling Cemented Total Hip Replacements - a More Realistic Model. *Journal of Biomechanics* **28**:1067-1078.

137. Marieb, E. (1998): "Human anatomy and physiology." Addison Wesley Longman, Inc.

138. Martell, J. M., Pierson, R. H., Jacobs, J. J., Rosenberg, A. G., Maley, M. and Galante, J. O. (1993): Primary Total Hip Reconstruction With a Titanium Fiber-Coated Prosthesis Inserted Without Cement. *Journal of Bone and Joint Surgery-American Volume* **75A**:554-571.

139. Martens, M., van Audekercke, R., Delport, P., de Meester, P. and Mulier, J. C. (1983): The mechanical characteristics of cancellous bone at the upper femoral region. *Journal of Biomechanics* **16**:971-983.

140. Mauch, M., Currey, J. D. and Sedman, A. J. (1992): Creep fractures in bones with different stiffnesses. *Journal of Biomechanics* **25**:11-16.

141. McCalden, R. W., McGeough, J. A., Barker, M. B. and Court-Brown, C. M. (1993): Age related changes in the tensile properties of cortical bone. *Journal of Bone and Joint Surgery* **75A**:1193-1205.

142. McCalden, R. W., McGeough, J. A. and Court-Brown, C. M. (1997): Age-related changes in the compressive strength of cancellous bone. The relative importance of changes in density and trabecular architecture. *Journal of Bone and Joint Surgery* **79**:421-427.

143. McLaughlin, J. R. and Lee, K. R. (2000): Total hip arthroplasty in young patients - 8-to 13-year results using an uncemented stern. *Clinical Orthopaedics and Related Research* **373**:153-163.

144. McLeish, R. D. and Charnley, J. (1970): Abduction forces in the one legged stance. *Journal of Biomechanics* **3**:191-209.

145. McNally, S. A., Shepperd, J. A. N., Mann, C. V. and Walczak, J. P. (2000): The results at nine to twelve years of the use of a hydroxyapatite-coated femoral stem. *Journal of Bone and Joint Surgery-British Volume* **82B**:378-382.

146. McNamara, B. P., Cristofolini, L., Toni, A. and Taylor, D. (1997): Relationship between bone-prosthesis bonding and load transfer in total hip reconstruction. *Journal of Biomechanics* **30**:621-630.

147. McPherson, E. J., Dorr, L. D., Gruen, T. A. and Saberi, M. T. (1995): Hydroxyapatite-Coated Proximal Ingrowth Femoral Stems - a Matched-Pair Control Study. *Clinical Orthopaedics and Related Research* **315**:223-230.

148. Mjoberg, B. (1991): Fixation and loosening of hip prostheses. *Acta Orthopedica Scandinavia* **62**:500-508.

149. Mjoberg, B., Selvik, G., Hansson, L. I., Rosenqvist, R. and Onnerfalt, R. (1986): Mechanical loosenign of total hip prostheses. A radiographic and roentgen stereophotogrammetric study. *Journal of Bone and Joint Surgery* **68B**:770-774.

150. Mont, M. A., Maar, D. C., Krackow, K. A. and Hungerford, D. S. (1992): Hoop stress fractures of the proximal femur during hip arthorplasty. *Journal of Bone and Joint Surgery* **74-B**:257-260.

151. Monti, L., Cristofolini, L., Toni, A. and Ceroni, R. G. (2001): In vitro testing of the primary stability of the VerSys enhanced taper stem: a comparative study in intact and intraoperatively cracked femora. *Proceedings of the Institution of Mechanical Engineers Part H- Journal of Engineering in Medicine* **215**:75-83.

152. Morgan, E. F. and Keaveny, T. M. (2001): Dependence of yield strain of human trabecular bone on anatomic site. *Journal of Biomechanics* **34**:569-577.

153. Morlock, M., Schneider, E., Bluhm, A., Vollmer, M., Bergmann, G., Muller, V. and Honl, M. (2001): Duration and frequency of every day activities in total hip patients. *Journal of Biomechanics* **34**:873-881.

154. Moselkilde (2000): Age-related changes in bone mass, structure, and strength - effect of loading. *Zeitschrift fur Rheumatologie* **59**:Suppl 1, 1-9.

155. Mosley, J. R. (2000): Osteoporosis and bone functional adaptation: Mechanobiological regulation of bone architecture in growing and adult bone, a review. *Journal of Rehabilitation Research and Development* **37:** 189-199.

156. Mouzin, O., Soballe, K. and Bechtold, J. E. (2001): Loading improves anchorage of hydroxyapatite implants more than titanium implants. *Journal of Biomedical Materials Research* **58**:61-68.

157. Neumann, L., Freund, K. G. and Sorenson, K. H. (1994): Long-term results of Charnley total hip replacement. *Journal of Bone and Joint Surgery* **76B**:245-251.

158. Nistor, L., Blaha, D., Kjellstrom, U. and Selvik, G. (1991): In vivo measurements of relative motion between an uncemented femoral total hip component and the femur by roentgen stereophotogrammetric analysis. *Clinical Orthopaedic and Related Research* **269**:220-227.

159. Palastanga, N., Field, D. and Soames, R. (2002): "Anatomy and Human Movement." Oxford: Butterworth Heinemann.

160. Park, H. C. and Lakes, R. S. (1986): Cosserat micromechanics of human bone: strain redistribution by a hydration sensitive constituent. *Journal of Biomechanics* **19**:385-397.

161. Paul, J. P. (1967): Forces at the human hip joint. PhD. Thesis, University of Glasgow:181-242.

162. Perillo-Marcone, A. (2001): Finite element analysis of the proximal implanted tibia in relation to implant loosening: PhD. Thesis, Faculty of Engineering and Applied Science, Southampton: University of Southampton, pp 175.

163. Perillo-Marcone, A., Alonso-Vazquez, A. and Taylor, M. (2003): Assessment of the effect of mesh density on the material property discretisation within QCT-based FE models:- a practical example using the implanted proximal tibia. *Computer Methods in Biomechanics and Biomedical Engineering* **6**:17-26.

164. Phillips, T. W., Nguyen, L. T. and Munro, S. D. (1991): Loosening of cementless femoral stems- A biomechanical analysis of immediate fixation with loading vertical, femur horizontal. *Journal of Biomechanics* **24**:37-48.

165. Pilliar, R. M., Cameron, H. U., Welsh, R. P. and Binnington, A. G. (1981): Radiographic and Morphologic Studies of Load-Bearing Porous- Surfaced Structured Implants. *Clinical Orthopaedics and Related Research* **156**:249-257.

166. Pilliar, R. M., Lee, J. M. and Maniatopoulos, C. (1986): Observations On the Effect of Movement On Bone Ingrowth Into Porous-Surfaced Implants. *Clinical Orthopaedics and Related Research* **208**:108-113.

167. Prendergast, P. J. and Taylor, D. (1994): Prediction of Bone Adaptation Using Damage Accumulation. *Journal of Biomechanics* **27**:1067-1076.

168. Ramaniraka, N. A., Leyvraz, P. F., Rakotomanana, L. R., Rubin, P. J. and Zysset, P. K. (1996): Micromotion at the bone-stem interface during the gait cycle after cementless total hip replacement: influence of stem design and loading level. *Hip International* **6**:51-58.

169. Reilly, D. T. and Burstein, A. H. (1975): The elastic and ultimate properties of compact bone tissue. *Journal of Biomechanics* **8**:393-405.

170. Rho, J. Y., Ashman, R. B. and Turner, C. H. (1993): Young's modulus of trabecular and cortical bone material :ultrasonic and microtensile measurements . *Journal of Biomechanics* **26**:111-119.

171. Rice, J. C., Cowin, S. C. and J.A., B. (1988): On the dependence of the elasticity and strength of cancellous bone on apparent density. *Journal of Biomechanics* **21**:155-168.

172. Rimnac, C. M., Petko, A. A., Santner, T. J. and Wright, T. M. (1993): The Effect of Temperature, Stress and Microstructure On the Creep of Compact Bovine Bone. *Journal of Biomechanics* **26**:219-228.

173. Robertson, D. D., Walker, P. S., Hirano, S. K., Zhou, X. M., Granholm, J. W. and Poss, R. (1988): Improving the fit of press-fit hip stems. *Clinical Orthop.* **228**:134-140.

174. Rohl, L., Larsen, E., Linde, F., Odgaard, A. and Jorgensen, J. (1991): Tensile and Compressive Properties of Cancellous Bone. *Journal of Biomechanics* **24**:1143-1149.

175. Rohlmann, A., Mossner, U., Bergmann, G. and Kolbel, R. (1983): Finite-Element-Analysis and Experimental Investigation in a Femur With Hip Endoprosthesis. *Journal of Biomechanics* **16**:727-742.

176. Rohrle, H., Scholten, R., Sigolotto, C., Sollbach, W. and Kellner, H. (1984): Joint forces in the human pelvis-leg skeleton during walking. *Journal of Biomechanics* **17**:409-424.

177. Rorabeck, C. H., Bourne, R. B., Mulliken, B. D., Nayak, N., Laupacis, A., Tugwell, P. and Feeney, D. (1996): The Nicolas Andry award - Comparative results of cemented and cementless total hip arthroplasty. *Clinical Orthopaedics and Related Research* **325**:330-344.

178. Rubin, P. J., Rakotomanana, R. L., Leyvraz, P. F., Zysset, P. K., Curnier, A. and Heegaard, J. H. (1993): Frictional Interface Micromotions and Anisotropic Stress-Distribution in a Femoral Total Hip Component. *Journal of Biomechanics* **26**:725-739.

179. Rydell, N. W. (1966): Forces acting on the femoral head prosthesis. *Acta Orthopedica Scandinavica Suppl.* **86, 93**:71-132.

180. Schaffler, M. B. and Burr, D. B. (1988): Stiffness of Compact-Bone - Effects of Porosity and Density. *Journal of Biomechanics* **21**:13-16.

181. Schmalzried, T. P., Jasty, M. and Harris, W. H. (1992): Periprosthetic Bone Loss in Total Hip-Arthroplasty - Polyethylene Wear Debris and the Concept of the Effective Joint Space. *Journal of Bone and Joint Surgery-American Volume* **74A**:849-863.

182. Schneider, E., Eulenberger, J., Steiner, W., Wyder, D., Friedman, R. J. and Perren, S. M. (1989): Experimental-Method For the Invitro Testing of the Initial Stability of Cementless Hip Prostheses. *Journal of Biomechanics* **22**:735-744.

183. Schneider, E., Michel, M. C., Genge, M., Zuber, K., Ganz, R. and Perren, S. M. (2001): Loads acting in an intramedullary nail during fracture healing in the human femur. *Journal of Biomechanics* **34**:849-857.

184. Schutzer, S. F., GradyBenson, J., Jasty, M., Oconnor, D. O., Bragdon, C. and Harris, W. H. (1995): Influence of intraoperative femoral fractures and cerclage wiring on bone ingrowth into canine porous-coated femoral components. *Journal of Arthroplasty* **10**:823-829.

185. Schwartz, J. T., Mayer, J. G. and Engh, C. A. (1989): Femoral fracture during non-cemented total hip arthroplasty. *Journal Bone Joint Surgery* **71A**:1135.

186. Seireg, A. and Arvikar, R. J. (1975): The prediction of muscular load sharing and joint forces in the lower extremities during walking. *Journal of Biomechanics* **8**:89-102.

187. Shirazi-Adl, A., Dammak, M. and Paiement, G. (1993): Experimental-Determination of Friction Characteristics At the Trabecular Bone Porous-Coated Metal Interface in Cementless Implants. *Journal of Biomedical Materials Research* **27**:167-175.

188. Skinner, H. B., Kim, A. S., Keyak, J. H. and Mote, C. D. (1994): Femoral Prosthesis Implantation Induces Changes in Bone Stress That Depend On the Extent of Porous Coating. *Journal of Orthopaedic Research* **12**:553-563.

189. Soballe, K., Brockstedtrasmussen, H., Hansen, E. S. and Bunger, C. (1992a): Hydroxyapatite Coating Modifies Implant Membrane Formation - Controlled Micromotion Studied in Dogs. *Acta Orthopaedica Scandinavica* **63**:128-140.

190. Soballe, K., Hansen, E. S., Brockstedtrasmussen, H. and Bunger, C. (1993a): Hydroxyapatite Coating Converts Fibrous Tissue to Bone Around Loaded Implants. *Journal of Bone and Joint Surgery-British Volume* **75**:270-278.

191. Soballe, K., Hansen, E. S., Rasmussen, H. B., Jorgensen, P. H. and Bunger, C. (1992b): Tissue Ingrowth Into Titanium and Hydroxyapatite-Coated Implants During Stable and Unstable Mechanical Conditions. *Journal of Orthopaedic Research* **10**:285-299.

192. Soballe, K. and Overgaard, S. (1996): The current status of hydroxyapatite coating of prostheses. *Journal of Bone and Joint Surgery-British Volume* **78B**:689-691.

193. Soballe, K., Toksvig-Larsen, S., Gelineck, J., Fruensagaard, S., Hansen, E. S., Ryd, L., Lucht, U. and Bunger, C. (1993b): Migration of hydroxyapatite coated femoral prostheses. *Journal of Bone and Joint Surgery* **75B**:681-687.

194. Spears, I. R., Pfleiderer, M., Schleider, E., Hille, E. and Morlock, M. M. (2001): The effect of interfacial parameters on cup-bone relative micromotions - A finite element investigation. *Journal of Biomechanics* **34**:113-120.

195. Stauffer, R. N. (1982): Ten-year follow-up study of total hip replacement. *Journal of Bone and Joint Surgery* **54A**:983-990.

196. Stolk, J., Verdonschot, N. and Huiskes, R. (2001): Hip-joint and abductor-muscle forces adequately represent in vivo loading of a cemented total hip reconstruction. *Journal of Biomechanics* **34**:917-926.

197. Stone, J. L., Beaupre, G. S. and Hayes, W. C. (1983): Multiaxial strength characteristics of trabecular bone. *Journal of Biomechanics* **16**:743-752.

198. Sugiyama, H., Whiteside, L. A. and Engh, C. A. (1992): Torsional fixation of the femoral component in total hip arthroplasty. The effect of surgical press-fit technique. *Clin Orthop* **275**:187-93.

199. Sugiyama, H., Whiteside, L. A. and Kaiser, A. D. (1989): Examination of Rotational Fixation of the Femoral Component in Total Hip-Arthroplasty - a Mechanical Study of Micromovement and Acoustic-Emission. *Clinical Orthopaedics and Related Research* **249**:122-128.

200. Sun, L., Berndt, C. C., Gross, K. A. and Kucuk, A. (2001): Material fundamentals and clinical performance of plasma-sprayed hydroxyapatite coatings: A review. *J Biomed Mater Res* **58**:570-92.

201. Tate Jr., D. and Sculco, T. P. (1998): Advances in total hip arthroplasty. *The American Journal of Orthopedics* **27**:274-282.

202. Taylor, M. (1997): Finite element analysis of cancellous bone stresses within an implanted proximal femur and their relationship to implant migration: PhD. Thesis, Queen's Mary College, London: University of London.

203. Taylor, M. and Tanner, K. E. (1997): Fatigue failure of cancellous bone: A possible cause of implant migration and loosening. *Journal of Bone and Joint Surgery-British Volume* **79B**:181-182.

204. Taylor, M., Tanner, K. E. and Freeman, M. A. R. (1998): Finite element analysis of the implanted proximal tibia: A relationship between the initial cancellous bone stresses and implant migration. *Journal of Biomechanics* **31**:303-310.

205. Taylor, M., Tanner, K. E., Freeman, M. A. R. and Yettram, A. L. (1995): Cancellous bone stresses surrounding the femoral component of a hip prosthesis: an elastic-plastic finite element analysis. *Medical Engineering and Physics* **17**:544-550.

206. Toni, A., McNamara, B., Viceconti, M., Sudanese, A., Baruffaldi, F. and Giunti, A. (1996): Bone remodelling after total hip arthroplasty. *Journal of Materials Science-Materials in Medicine* **7**:149-152.

207. Turner, C. H. (1989): Yield behaviour of bovine cancellous bone. *Journal of Biomechanical Engineering-Transactions of the Asme* **110**:256-260.

208. Turner, C. H., Anne, V. and Pidaparti, R. M. V. (1997): A uniform strain criterion for trabecular bone adaptation: Do continuum-level strain gradients drive adaptation? *Journal of Biomechanics* **30**:555-563.

209. Turner, C. H., Rho, J., Takano, Y., Tsui, T. Y. and Pharr, G. M. (1999): The elastic properties of trabecular and cortical bone tissues are similar: results from two microscopic measurement techniques. *Journal of Biomechanics* **32**:437-441.

210. Turner, T. M., Sumner, D. R., Urban, R. M., Rivero, D. P. and Galante, J. O. (1986): A comparative study of porous coatings in a weight-bearing total hip arthroplasty model. *Journal of Bone and Joint Surgery-American Volume* **68A**:1396.

211. Tyldesley, B. and Grieve, J. I. (1996): "Muscles, Nerves and Movement: Kinesiology in Daily Living." Oxford: Blackwell Science.

212. van der Linden, J. C., Homminga, J., Verhaar, J. A. and Weinans, H. (2001): Mechanical consequences of bone loss in cancellous bone. *J Bone Miner Res* **16**:457-65.

213. Van Rietbergen, B., Huiskes, R., Weinans, H., Sumner, D. R., Turner, T. M. and Galante, J. O. (1993): The Mechanism of Bone Remodeling and Resorption Around Press- Fitted Tha Stems. *Journal of Biomechanics* **26**:369-382.

214. Viceconti, M., Dotti, M., Pancati, A., Cristofolini, L. and Toni, A. (2002): A micromotion-based model of bone-implant interface remodelling: "4th World Congress of Biomechanics." Calgary, Canada:.

215. Viceconti, M., Muccini, R., Bernakiewicz, M., Baleani, M. and Cristofolini, L. (2000): Large-sliding contact elements accurately predict levels of bone-implant micromotion relevant to osseointegration. *Journal of Biomechanics* **33**:1611-1618.

216. Visnic, C. D., Reid, R. H., Ghattas, O., DiGioia III, A. M. and Jaramaz, B. (1994): Finite element pre-operative simulation of cementless hip replacement. *Proceedings of the 1994 Winter Simulation Conference*:856-860.

217. Wachtel, E. F. and Keaveny, T. M. (1997): Dependence of trabecular damage on mechanical strain. *Journal of Orthopaedic Research* **15**:781-787.

218. Walker, P. S., Mai, S. F., Cobb, A. G., Bentley, G. and Hua, J. (1995): Prediction of clinical outcome of THR from migration measurements on standard radiographs. A study of cemented Charnley and Stanmore femoral stems. *J Bone Joint Surg Br* **77**:705-14.

219. Walker, P. S., Schneeweis, D., Murphy, S. and Nelson, P. (1987): Strains and Micromotions of Press-Fit Femoral Stem Prostheses. *Journal of Biomechanics* **20**:693-702.

220. Wan, Z. and Dorr, L. D. (1996): Natural history of femoral focal osteolysis with proximal ingrowth smooth stem implant. *J Arthroplasty* **11**:718-25.

221. Weinans, H., Huiskes, R. and Grootenboer, H. J. (1990): Trends of Mechanical Consequences and Modeling of a Fibrous Membrane Around Femoral Hip Prostheses. *Journal of Biomechanics* **23**:991-1000.

222. Weinans, H., Huiskes, R. and Grootenboer, H. J. (1994): Effects of Fit and Banding Characteristics of Femoral Stems On Adaptive Bone Remodeling. *Journal of Biomechanical Engineering-Transactions of the Asme* **116**:393-400.

223. Weinans, H., Huiskes, R., Vanrietbergen, B., Sumner, D. R., Turner, T. M. and Galante, J. O. (1993): Adaptive Bone Remodeling Around Bonded Noncemented Total Hip-Arthroplasty - a Comparison Between Animal-Experiments and Computer-Simulation. *Journal of Orthopaedic Research* **11**:500-513.

224. Weinans, H., Sumner, D. R., Igloria, R. and Natarajan, R. N. (2000): Sensitivity of periprosthetic stress-shielding to load and the bone density-modulus relationship in subject-specific finite element models. *Journal of Biomechanics* **33**:809-817.

225. Yang, J. P., Bogoch, E. R., Woodside, T. D. and Hearn, T. C. (1997): Stiffness of trabecular bone of the tibia plateau in patients with rheumatoid arthritis of the knee. *Journal of Arthroplasty* **12**:798-803.

226. Yettram, A. L. (1989): Effect of Interface Conditions On the Behavior of a Freeman Hip Endoprosthesis. *Journal of Biomedical Engineering* **11**:520-524.

227. Zannoni, C., Mantovani, R. and Viceconti, M. (1998): Material properties assignment to finite element models of bone structures: a new method. *Medical Engineering & Physics* **20**:735-740.

228. Zilch, H., Rohlmann, A., Bergmann, G. and Kolbel, R. (1980): Material properties of femoral cancellous bone in axial loading. Part 2: Time dependent properties. *Arch. Orthop. Traumat. Surg.* **97**:257-262.

229. Zioupos, P. and Currey, J. D. (1998): Changes in the stiffness, strength, and toughness of human cortical bone with age. *Bone* **22**:57-66.

230. Zysset, P. K., Sonny, M. and Hayes, W. C. (1994): Morphology-mechanical property relations in trabecular bone of the osteoarthritic proximal tibia. *Journal of Arthroplasty* **9**:203-216.

Appendix

Presentations

Wong, A.S., New, A.M.R., Ritchie, A. and Taylor, M.: Influence of an interference-fit on the strains distribution in the implanted proximal femur. 18th Congress of International Society of Biomechanics, Zurich, Switzerland, July, 2001.

Wong, A.S., New, A.M.R., Isaacs, G. and Taylor, M.: Influence of an interference-fit on the initial stability of cementless proximal femoral stems. 4th World Congress of Biomechanics, Calgary, Canada, August 2002

Wong, A.S. New, A.M.R., Isaacs, G. and Taylor, M.: Influence of bone quality on the initial stability of hip stem in total hip arthroplasty. 2003 Summer Bioengineering Conference, Florida, USA, June 2003.